LEABHARLANN CHOLÁISTE NA TRÍONÓIDE, BAILE ÁTHA CLIATH
Ollscoil Átha Cliath

TRINITY COLLEGE LIBRARY DUBLIN
The University of Dublin

**Terms and Conditions of Use of Digitised Theses from Trinity College Library Dublin**

**Copyright statement**

All material supplied by Trinity College Library is protected by copyright (under the Copyright and Related Rights Act, 2000 as amended) and other relevant Intellectual Property Rights. By accessing and using a Digitised Thesis from Trinity College Library you acknowledge that all Intellectual Property Rights in any Works supplied are the sole and exclusive property of the copyright and/or other IPR holder. Specific copyright holders may not be explicitly identified. Use of materials from other sources within a thesis should not be construed as a claim over them.

A non-exclusive, non-transferable licence is hereby granted to those using or reproducing, in whole or in part, the material for valid purposes, providing the copyright owners are acknowledged using the normal conventions. Where specific permission to use material is required, this is identified and such permission must be sought from the copyright holder or agency cited.

**Liability statement**

By using a Digitised Thesis, I accept that Trinity College Dublin bears no legal responsibility for the accuracy, legality or comprehensiveness of materials contained within the thesis, and that Trinity College Dublin accepts no liability for indirect, consequential, or incidental, damages or losses arising from use of the thesis for whatever reason. Information located in a thesis may be subject to specific use constraints, details of which may not be explicitly described. It is the responsibility of potential and actual users to be aware of such constraints and to abide by them. By making use of material from a digitised thesis, you accept these copyright and disclaimer provisions. Where it is brought to the attention of Trinity College Library that there may be a breach of copyright or other restraint, it is the policy to withdraw or take down access to a thesis while the issue is being resolved.

**Access Agreement**

By using a Digitised Thesis from Trinity College Library you are bound by the following Terms & Conditions. Please read them carefully.

I have read and I understand the following statement: All material supplied via a Digitised Thesis from Trinity College Library is protected by copyright and other intellectual property rights, and duplication or sale of all or part of any of a thesis is not permitted, except that material may be duplicated by you for your research use or for educational purposes in electronic or print form providing the copyright owners are acknowledged using the normal conventions. You must obtain permission for any other use. Electronic or print copies may not be offered, whether for sale or otherwise to anyone. This copy has been supplied on the understanding that it is copyright material and that no quotation from the thesis may be published without proper acknowledgement.

# THERMAL ASPECTS OF THE GRINDING PROCESS

**A thesis submitted to the**
**University of Dublin**
**in accordance with the**
**requirements of the degree of**
**Doctor of Philosophy**
**in the**
**Faculty of Engineering**
**Department of Mechanical & Manufacturing Engineering**
**University of Dublin**
**Trinity College**

**October 1999**

**Darren Gerard Walsh BA,BAI,MSc**

# Abstract

Grinding is a commonly used process for material removal. It has been used for a long time mainly as a finishing process, although this situation is changing, with the development of creep feed grinding, and high efficiency deep grinding. In these processes, grinding is a stock removal, and finishing operation.

The quality of the finished component is usually assessed in terms of form, surface roughness, and thermal damage. In this thesis, thermal aspects of the grinding process are examined. These aspects include: the manner in which the workpiece geometry in form grinding influences the grinding temperatures; the identification of the temperature at which tensile thermal residual stresses manifest themselves in the workpiece; the ground plane temperature in deep cut grinding; the role of the coolant in creep feed grinding.

Analysis of the aforementioned topics illustrated that form is an important aspect of temperature prediction in form grinding, and the critical regions in forms are sharp corners. The critical temperature for thermally induced tensile residual stress formation can be identified using a simple method based on the workpiece material properties. A formula predicting the maximum ground plane temperature in deep cut grinding has been developed using numerical methods. The cutting fluid has been shown to be of primary importance, regarding workpiece temperatures, in deep cut grinding.

# DECLARATION

The accompanying dissertation entitled “Thermal Aspects of the Grinding Process” is submitted in support of an application for the degree of Doctor of Philosophy in Engineering at the University of Dublin, Trinity College.

The dissertation is based on independent work by the candidate, except where clearly referenced.

No portion of the work referred to in this dissertation has been submitted in support of an application for another degree or qualification in this, or any other university or other institute of learning.

The views and opinions expressed in this thesis are solely those of the author and not the University of Dublin.

I declare that the above statements are true,

Darren Gerard Walsh

October, 1999.

# Acknowledgements

This work has only been possible through the co-operation and support of a large number of people. In particular, I would like to express my sincere thanks to Prof. A.A. Torrance, for his guidance and wisdom, throughout the course of this research.

I would like to thank all the members of the Mechanical Engineering Workshop and Department staff , in particular Mr Paul Normoyle, and Mr. Tom Havernon. In addition I wish to thank Dr. Mike Morgan of Liverpool John Moores University for his good advice, and Mr. Peter Ward from Dormer Drills for accommodating the grinding trials.

The support and friendship of many others, who helped me enjoy three happy years, is fully appreciated.

Finally, I thank my family, for their patience and encouragement during the past three uncertain years.

# CONTENTS

# LIST OF FIGURES

# LIST OF TABLES

# Nomenclature List

| | |
|---|---|
| A | Area $m^2$ |
| B | Coefficient vector |
| c | Specific heat capacity J/kgK |
| d | Depth of cut m |
| E | error matrix |
| e | Specific energy $J/mm^3$ |
| E | Youngs modulus $N/m^2$ |
| f | Feed rate m/s |
| H | (2Kh/kV) Dimensionless convective heat transfer coefficient |
| h | Convective heat transfer coefficient $W/m^2K$ |
| $h_1$ | Distance m |
| $h_2$ | Distance m |
| $h_3$ | Distance m |
| k | Thermal conductivity W/mK |
| K | Thermal diffusivity $m^2/s$ |
| $l_c$ | Arc of cut length m |
| L | $Vl_c /2K$ Dimensionless length |
| $L_1$ | Distance m |
| $L_2$ | Distance m |
| $L_3$ | Distance m |
| n | Concentration factor |
| N | Data vector |

| | |
|---|---|
| Nu | Nusselt number |
| Pi | Dimensionless numbers |
| Pr | Prandtl number |
| $q$ | Heat flux $W/m^2$ |
| $r$ | Temperature ratio |
| $R,R'$ | radii m |
| R_ | Partition ratio |
| Re | Reynolds number |
| $r_o$ | Radius m |
| $T,\theta$ | Temperature, Temperature rise K |
| $V$ | velocity m/s |
| $X$ | $Vx/2K$ Dimensionless distance |
| $Z$ | $Vz/2K$ Dimensionless depth |
| $\alpha$ | Coefficient of thermal expansion / angle |
| $\beta$ | Heat conductivity $(k\rho c)^{1/2}$ $kg/sK^{2.5}$ |
| $\varepsilon$ | Strain |
| $\phi$ | Angle |
| $\phi_p$ | Predicted parameters vector |
| $\phi_x$ | Measured parameters vector |
| $\gamma$ | Angle |
| $\rho$ | Density $kg/m^3$ |
| $\sigma$ | Stress $N/m^2$ |
| $\psi$ | Angle |
| $Y$ | Yield stress $N/m^2$ |

| | |
|---|---|
| $\zeta$ | Variable |

## Subscripts

| | |
|---|---|
| c | cutting/grinding |
| cc | chip |
| f | Flat plane |
| g | Grain |
| i | inflexion point |
| m | maximum |
| p | apex |
| r | residual |
| s | wheel |
| w | workpiece |

# Chapter 1

# Introduction

## 1.1 Introduction

The grinding process is widely used in industry for both large and small production runs. Traditionally it has been used as a finishing process, where good surface finish and close dimensional accuracy are required. In recent times, particularly with the advent of deep cut grinding and high speed grinding, the grinding process has been used as a stock removal process. This type of operation allows roughing and finishing runs on the same machine, possibly in one pass, which has obvious economical advantages. The general aim of current research is to increase stock removal rates, whilst maintaining the required surface finish, and dimensional accuracy. Even small improvements in the grinding process will return relatively large savings, especially with large production runs. These savings arise from two aspects of the manufacturing process. Firstly, a higher efficiency in the grinding process reduces the unit cost of the manufactured component. Secondly, a fuller understanding of the process, and due application of this knowledge, prevents thermal damage of the workpiece. This is particularly important, since the grinding process is usually carried out near the end of the manufacturing cycle. Damage to the component at this stage of manufacture carries a far more severe financial penalty, than if it had occurred at the start of the operation.

## 1.2 Description of the main classes of grinding process:

There are several different types of grinding process, including surface grinding, cylindrical grinding, centerless grinding, abrasive cut-off, and deep cut grinding. In these processes, a wheel of bonded abrasive grits moves over the workpiece surface at a high velocity. Each grit acts as an individual cutter. The rake angle of these grits is usually negative. There are four main types of grinding wheel. These are aluminium oxide, silicon carbide, diamond, and cubic boron nitride. The grits in the wheel are held together by either a resin or vitreous bond. The size of the grits, the strength of the bond, and the spacing of the grits can be varied to suit particular applications. During the grinding operation, the wheel wears. This involves the grits wearing down to produce wear flats, and also fracture of the grits. As a result, the wheel must be trued to restore the wheel shape, and dressed to clean and sharpen the wheel.

## 1.3 Surface Grinding:

In surface grinding, the wheel head is stationary, and the work is usually held in a magnetic chuck on a reciprocating table. The table is moved vertically to control the depth of cut. Coolant is generally supplied from a stationary nozzle, which floods the wheel and the contact zone with fluid. These grinding machines are common fixtures in machine shops, and are also used for production runs.

## 1.4 Cylindrical grinding:

This process is similar to surface grinding, except the work surface is of circular cross-section. The work is held either in clamps, or between centres, and the grinding wheel is fed onto it. Again, coolant is supplied by a fixed nozzle.

## 1.5 Deep Cut Grinding:

Deep cut grinding is a stock removal process, although it can in certain circumstances produce finished components in a single pass, which require no further finishing operations. It is generally used in the surface grinding mode. It differs from this process in several ways. Firstly, there is no table traverse. Secondly, the feed rate is typically much lower than that for surface grinding, generally being of the order of mm/s, compared with m/s in conventional grinding. Thirdly, the depth of cut is considerably larger than that for surface grinding. In addition, the specific energy can be significantly higher for deep cut grinding, typical values for creep feed grinding ranging from J/mm$^3$ to 1000J/mm$^3$.

## 1.6 Grinding Temperatures:

One of the major problems associated with grinding is the generation of high temperatures, which can adversely affect the work and the wheel. Practically all the process energy is converted to heat, from the chip formation process, or from friction between the wear flats on the wheel and the work. A very small percentage of the process energy is converted into sound, or stored in the atomic lattice of the workpiece. Some of the remaining heat enters the wheel, some is removed by the chips and the grinding fluid, and the rest is conducted into the work. The heat entering the work may result in high temperatures in the contact zone, which can cause thermally induced damage in the workpiece surface. This is discussed in section 1.6.2. The specific melting energy of steel is between 6J/mm$^3$ – 9J/mm$^3$. The specific grinding energy for production grinding of steels is typically much higher, ranging from 20J/mm$^3$ – 60J/mm$^3$. The fact that the specific grinding energy is so much greater than the specific melting energy would suggest that much of the grinding energy is expended on mechanisms other than chip removal. One possibility is friction between the wear flats of the grits and the workpiece. This is supported by the fact that the ratio of tangential to normal forces in the grinding process is 0.3 - 0.5, which is characteristic of a sliding friction process. This ratio is between 2 – 3 for the turning process, where the process energy is liberated at the shear plane. The grits themselves are also subjected to periodic high temperatures, which can affect wheel wear and performance. High temperatures in the contact zone affect the wheel integrity, the work's dimensional accuracy, the metallurgical structure of the work, and the level and nature of residual stresses in the work.

### 1.6.1 Wheel:

During the grinding process, the grit contact time is approximately $10^{-4}$s. This value corresponds with a arc of cut length of 2mm, and a peripheral wheel velocity of 2m/s During this time, the grit initially slides over the work, then ploughs the work surface, and then cuts a chip. These operations cause a sharp rise in temperature in the grit, which is then cooled after it leaves the grinding contact zone. This process is repeated for every wheel revolution. This cycle aids grit fracture by thermal fatigue, and may also help grit separation. This results in new cutting faces. In some cases, high grit temperatures can induce chemical reaction between the grit and work, i.e. the grinding of ferrous materials with diamond. This, in part, explains why diamond wheels are not used to grind all metals. Despite being extremely hard, diamond is not suited to grinding ferrous materials. This is due to high rates of attritious wear by the reversion of diamond to graphite, and its dissolution by iron. This wear of diamond is rapid in the presence of ferrous materials unsaturated with carbon. Cubic Boron Nitride, on the other hand, while softer than diamond, is chemically stable at higher temperatures, and wears less when grinding ferrous materials.

### 1.6.2 Workpiece:

High temperatures in the work induce thermal expansion. This expansion causes an increase in the depth of cut, which in turn leads to loss of dimensional accuracy. The fact that the work expands in this fashion makes it difficult to predict the final form of the work. Indeed, the process may become unstable. If the depth of cut increases due to thermal expansion, this implies additional heat generation, which can lead to further thermal expansion.

The interest in grinding temperatures is not driven by curiosity. The grinding temperatures are of interest because they may affect the metallurgical structure of the workpiece. One of the most commonly ground metals is steel. Steel is a generic name for iron, carbon, and various other alloying elements. The phase diagram for iron-iron carbide (Fe-$Fe_3C$) is shown in figure 1.1. The diagram shows that, above a temperature of 723°C, the steel has a composition of austenite $\gamma$ and either ferrite $\alpha$ or carbide $Fe_3C$. The austenite has face-centred-cubic (FCC) structure. If the steel cools to temperature below the autenising temperature, the austenite decomposes to form ferrite and carbide. The ferrite has body-centred-cubic (BCC) structure. The austenite can accommodate carbon atoms interstitially. The austenite can store up to ten carbon atoms in this fashion. The ferrite with its BCC structure has smaller interstitial sites, and only one carbon atom per five hundred unit cells of ferrite, can be dissolved. The carbide, $Fe_3C$, is a hard phase, and serves to reinforce the ferrite phase. In addition,

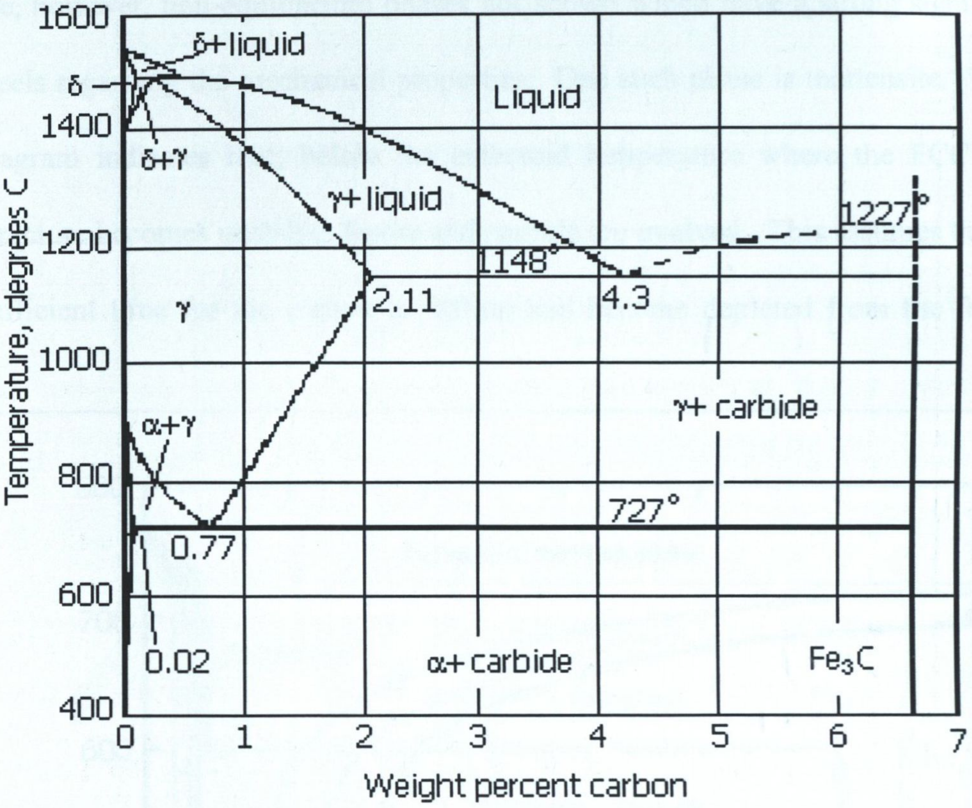

**Figure 1.1 – Phase diagram of steel [Van Vlack 1989]**

the BCC structure is less closely packed than the FCC structure, so the transformation of austenite to ferrite involves a volume increase of approximately 4%.

If the austenite is of eutectoid composition (~0.8% carbon) the formation of ferrite and carbide by slow cooling produces a lamellar mixture of the two phases. That is to say, the structure is composed of alternate layers of ferrite and carbide. This microstructure is called pearlite. The growth of the ferrite and carbide starts at the austenite grain boundaries. The lamelae grow inwards from the grain boundaries. If the cooling is slow, the carbon has time to diffuse a greater distance, and thicker layers are formed. This is known as coarse pearlite. On the other hand, if the cooling rate is more rapid, the diffusion distances are shorter, and fine pearlite is formed.

The phase diagram in figure 1.1 shows the equilibrium phases of Fe - $Fe_3C$. There are, however, non-equilibrium phases not shown which have a strong significance in steels regarding the mechanical properties. One such phase is martensite. The phase diagram indicates that, below the eutectoid temperature where the FCC austenite structure becomes unstable, ferrite and carbide are evolved. This assumes that there is sufficient time for the carbon to diffuse and become depleted from the ferrite, and

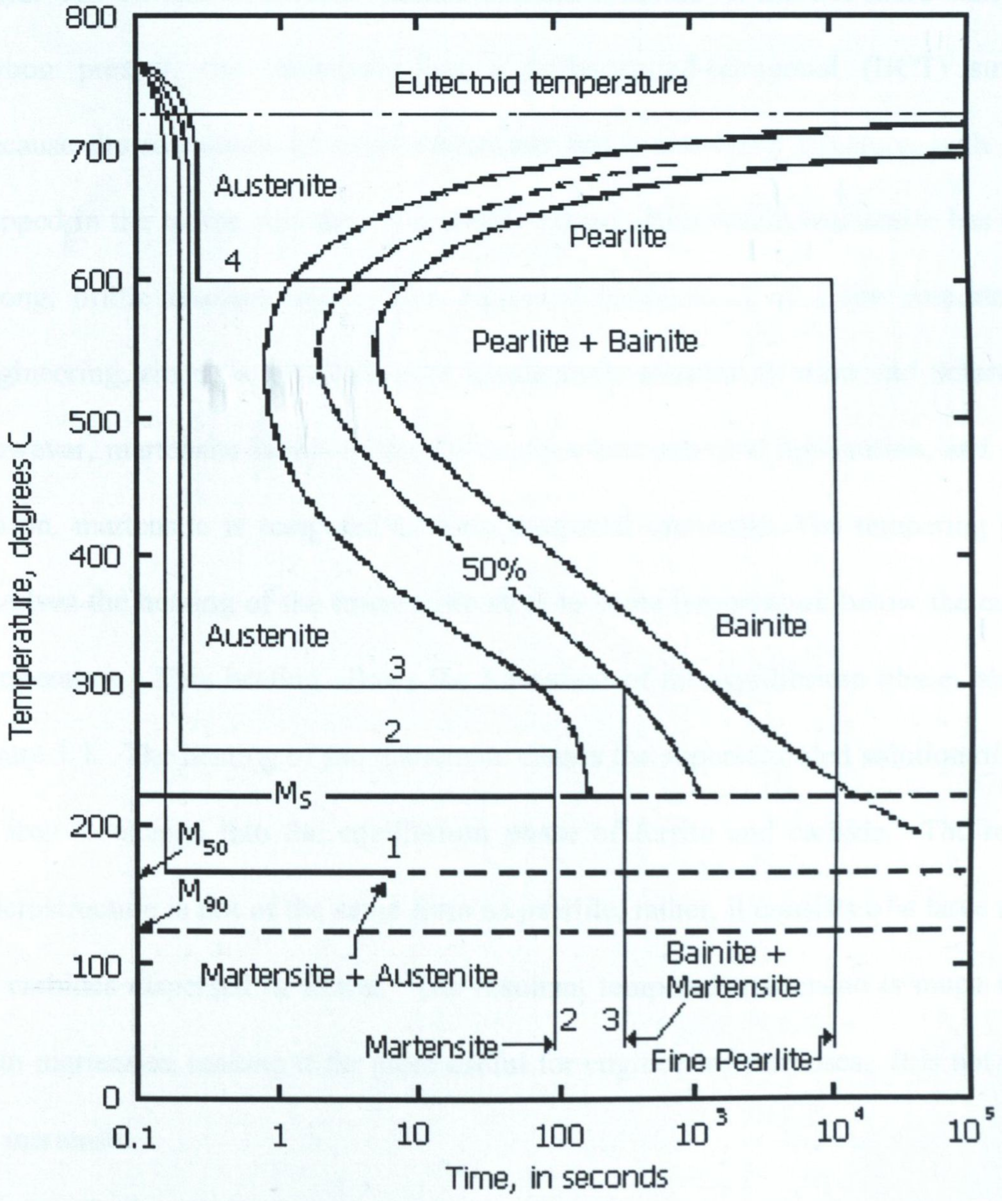

**Figure 1.2 – T-T-T diagram for a eutectoid steel [Van Vlack 1989]**

concentrate in the carbide phase. If there is insufficient time for this diffusion process to run its course, for example, if the austenite is quenched very rapidly, an intermediate phase of martensite is formed. This phase is not stable because, given an opportunity, martensite will proceed to form ferrite and carbide. Martensite forms above room temperature, but below the eutectoid temperature. With rapid cooling, the austenite changes spontaneously from a FCC to a BCC structure, in a manner which does not involve diffusion. The mechanism, not being a diffusion process, is very rapid. All the carbon present remains in solid solution. If there is more than 0.15% carbon present, the martensite has a body-centred-tetragonal (BCT) structure. Because the martensite of steels commonly has a non-cubic structure, with carbon trapped in the lattice, slip does not readily occur. As a result, martensite has a hard, strong, brittle characteristic. This enhanced hardness is of major importance in engineering, since the resultant steel is extremely resistant to wear and deformation. However, martensite is too brittle for nearly every potential application, and for this reason, martensite is tempered to form tempered martensite.The tempering process involves the heating of the martensitic steel to some temperature below the eutectoid temperature. This heating allows the formation of the equilibrium phases shown in figure 1.1. The heating of the martensite causes the supersaturated solution of carbon in iron to change into the equilibrium phase of ferrite and carbide. The resulting microstructure is not of the same form as pearlite, rather, it consists of a large number of carbides dispersed in ferrite. The resultant tempered martensite is much tougher than martensite, making it far more useful for engineering purposes. It is not as hard as martensite.

It is clear that the cooling rate of austenite is important, since it can lead to martensite formation. In fact, the manner in which the austenite is cooled (and possibly tempered) fully determines the micro-structure of the steel. Figure 1.2 shows a T-T-T (Time – Temperature – Transformation) diagram for a eutectoid steel (~0.79% carbon, ~ 0.76% manganese). The T-T-T diagram for a given steel illustrates the effect of different time-temperature paths of the micro-structure of the steel at room temperature. Figure 1.2 has four arbitrary paths marked. The first path shows a rapid quench to 160°C, followed by a twenty minute wait at the same temperature. The structure of the steel is half martensite, half austenite. The austenite will transform into bainite after time, with a volume change. Path two shows what is essentially a direct quench. The holding time at 250°C is not sufficiently long to allow the formation of bainite. The third path shows heat treatment leading to a microstructure with 50% bainite and 50% martensite. At the holding temperature of 300°C, the structure is half bainite, half austenite. The holding temperature for path four is 600°C, which is high enough to allow the formation of pearlite.

In high alloy steels, the tempering temperature can be important not only as far as the time it takes to allow the carbon to precipitate to form $Fe_3C$, but also in terms of the effect of precipitation of carbides formed by the alloying elements. At lower tempering temperatures, the rate of diffusion of heavy alloying elements is too slow to allow precipitation of alloy carbides. Carbon, being a lighter element can diffuse quickly, even at lower temperatures. This essentially means that, in a steel with a number of alloying elements, which can form carbides, the tempering temperature, if high enough, can cause the precipitation of appreciable amounts of alloy carbides. This results in a steel with a high resistance to tempering. Figure 1.3 illustrates the effect of tempering temperature on a steel with 0.35% carbon, with and without a carbide forming alloy. These steels are often used as tool steels, since they retain high hardness at the elevated temperature that can be experienced at tool/work interfaces.

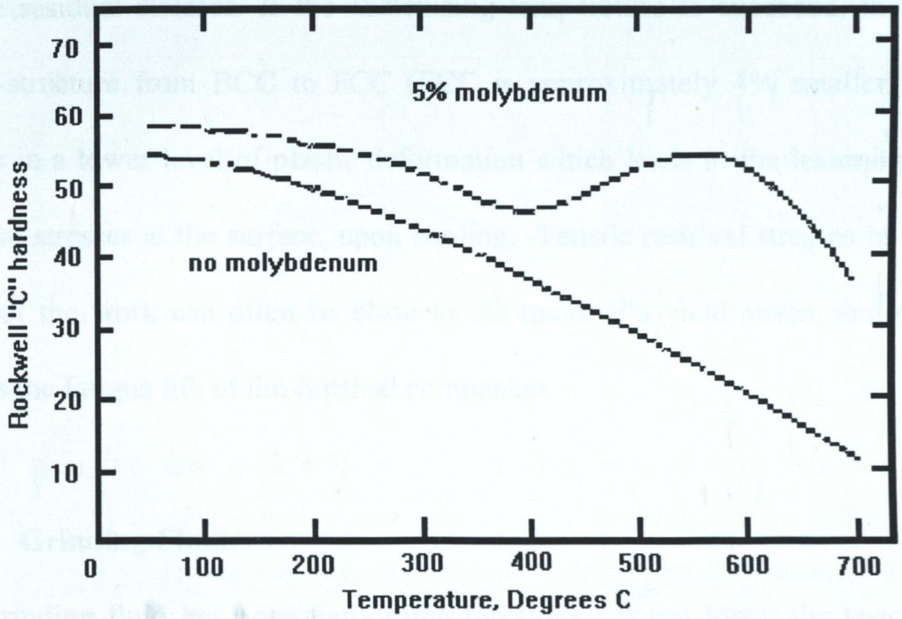

**Figure 1.3 – Tempering temperature hardness diagram [Van Vlack 1989]**

So, the metallurgical structure of the work near the surface can be affected adversely by high temperatures. The material may undergo a phase change if the austenising temperature is exceeded, the final micro-structure then depending on the rate of cooling, or, in the case of hardened steels, the surface of the work may be tempered. This is particularly the case when the material can potentially be tempered at a temperature below that generated during the grinding process. Equilibrium phase changes and tempering processes are dependent on both time and temperature. In the case of precipitation hardening materials, the surface hardness can also be affected if the work experiences elevated temperatures.

The net residual stress in a workpiece has three constituents. These are, the stress induced by mechanical plastic deformation, the stress induced by phase changes, and the stress induced by thermal plastic deformation. Mechanical plastic deformation induces compressive residual stresses, whereas thermal plastic deformation induces tensile residual stresses. If the austenising temperature is exceeded, the change in micro-structure from BCC to FCC (FCC is approximately 4% smaller than BCC) results in a lower level of plastic deformation which leads to the lessening of tensile residual stresses at the surface, upon cooling. Tensile residual stresses in the surface layer of the work can often be close to the material's yield stress, and can greatly reduce the fatigue life of the finished component.

### 1.6.3 Grinding Fluid:

The grinding fluid has potentially three functions. It can lower the specific cutting energy by reducing friction in the contact zone. It can react chemically with the work to allow easier cutting, and it can remove heat from the contact zone by convective cooling. In addition, it can flush generated wear particles out of the contact zone, and also from the wheel. In general, oil based grinding fluids reduce the specific energy more than water based fluids, but have lower convective cooling capabilities.

### 1.6.4 The Grinding Chips

The chips cut by the grinding wheel absorb some of the grinding energy. The upper limit for this energy can be found by measuring the specific melting energy of the workpiece material, and comparing it with the specific energy required to grind the work material. Since the chips are not part of the finished product, and, unlike the wheel and coolant, not required for further use, they are of little importance in affecting the quality of the finished workpiece.

## 1.7 The Objectives

The objective of this project was to identify problem areas in the grinding process, and formulate solutions. The areas considered were:

- The temperature distribution in form grinding. This involved examination of the effect of workpiece form on local temperature variations during the form grinding process
- The thermal induction of tensile residual stresses in grinding. This problem considered ideas on how to predict a critical temperature above which the workpiece residual stresses become tensile
- The temperature experienced by the ground plane in creep-feed grinding. The remaining workpiece surface in deep cut grinding was thought to experience a considerably lower temperature than that of the arc of cut. With a view to developing different methods of keeping the remaining workpiece surface cool, the problem of calculating ground plane temperatures was undertaken.
- The role of the cutting fluid in creep feed grinding. With a view to identifying the importance of a cutting fluid in creep feed grinding, an investigation focusing on drill flute grinding was carried out.

# Chapter 2

## Review of the Literature

### 2.1 Temperature Models for Conventional Grinding

In the study of grinding temperatures, the theory of moving heat sources developed by Jaeger [Jaeger 1942] has formed the foundation of many grinding temperature models. The objective of Jaeger's paper was to systematically characterise the temperature in a semi-infinite plane subjected to a moving heat source. He developed solutions for the transient temperatures for both band and square sources, and also the quasi steady-state solutions for these two cases. It is the quasi steady-state solutions which have found most application in the grinding temperature problem. In his general analysis, sources of uniform strength were considered. While this may model some operations, for example turning, the variable strength solution has been found more representative of the grinding process. Equation 2.1 illustrates the solution for a band source moving across a semi-infinite plane, in dimensionless form. $K_o$ is the modified Bessel function of the second kind of order zero, and $u$ is variable of integration. This is the most frequently used equation from Jaeger's seminal paper. Figure 2.1 illustrates the character of the uniform band source, moving across a semi-infinite plane with L=1 to L=10.

$$\frac{\theta \pi k V}{2qK} = \int_{X-L}^{X+L} e^{-u} K_o\left(|u|\right) du$$

**Equation 2.1**

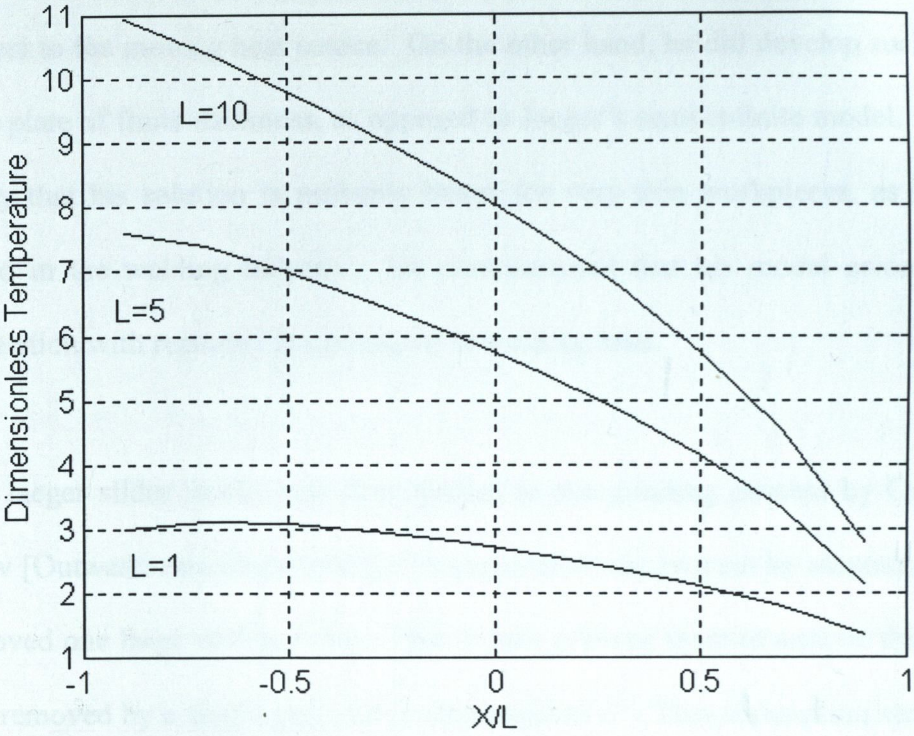

**Figure 2.1 – Jaeger uniform band source solution**

The dimensionless temperature in figure 2.1 is that defined in equation 2.1. Jaeger also noted that the solution is exact only if the source providing the heat input is a perfect insulator. This essentially means that for any real problem involving moving heat sources, not only must the temperature distribution be calculated, but also the energy partitioning between the source and the workpiece. The results of Jaeger's analysis also demonstrate that for large values of L, there is little difference between the solution for the square source and the band source.

Rosenthal [Rosenthal 1946] also examined the problem of temperatures generated by moving sources of heat. While he developed his solution with the specific problem of temperatures in welding processes in mind, it is equally applicable to other problems. His approach to the problem was somewhat different in formulation to that of Jaeger, Rosenthal calculating only the quasi steady-state solution. The quasi steady-state solution demonstrates the temperature solution when it becomes steady-state with respect to the moving heat source. On the other hand, he did develop such a solution for a plate of finite thickness, as opposed to Jaeger's semi-infinite model. This would imply that his solution is probably better for very thin workpieces, as likely to be found in the welding industry. He demonstrated that his model achieved a good correlation with recorded temperatures in welding tests.

The Jaeger slider model was first applied to the grinding process by Outwater and Shaw [Outwater and Shaw 1952]. They modelled the process by assuming the wheel removed one large uniform chip. This in turn allowed them to assume this large chip was removed by a single grit, with a rake angle of 0°. This assumption stemmed from the observation that the average rake angle of all the grits should be 0°. They further assumed that the angle of the shear plane heat source could be ignored, and thus they calculated a temperature distribution based directly on Jaeger's slider model. They did point out that energy partitioning occurs between heating of the workpiece, heating of the wheel, kinetic energy of the chips, heating of the chips, radiation to the surroundings, new surface generation, and residual energy remaining in the lattice of the workpiece and chips. Their analysis considered dry grinding, so there was no energy removed by a cutting fluid. The kinetic energy of the chips, the surface generation energy, and the residual lattice energy were shown to be negligible. The problem of energy partitioning between the chip and workpiece was solved, giving 35% of the process energy entering the workpiece. Some experimental measurements were performed, the authors noting that the recorded temperatures were not those experienced by the finished surface, rather those associated with the mean chip grit interface temperature. They predicted a maximum temperature of 1760°C on the shear plane, which would appear to be rather higher than more recent studies would suggest.

Hahn [Hahn 1956] introduced the grain-rubbing hypothesis. He identified three heat sources associated with the grain. These were the shear plane source, the wear flat source, and the grit-chip interference source. Contrary to Outwater & Shaw's work [Outwater and Shaw 1952] Hahn assumed that most of the energy entering the workpiece came via the wear flat source. He hypothesised that the heat generated at the shear plane would be convected away with the chip. Jaeger's analysis was then used to demonstrate that increasing the work speed resulted in lower temperatures. He also noted the tensile residual stresses would probably be reduced with a higher work speed

In a later paper [Mayer & Shaw 1957], the authors used a radiation technique to measure temperatures experienced by the ground plane during grinding trials. The apparatus consisted of a lead sulphide cell connected to an oscilloscope. The lead sulphide cell was positioned in such a fashion as to allow a sighting of the workpiece directly after grinding. The authors observed that the measured temperatures were about three times smaller than those computed using the model of Outwater &Shaw [Outwater and Shaw 1952]. They did, however, observe that the results were of the same character i.e. the measured and calculated temperatures varied proportionally with the specific grinding energy for a given wheel speed. In addition, they noted that the use of cutting fluid significantly reduced observed temperatures. While the cutting fluid type i.e. oil or water, seemed to make little difference to the observed temperatures, this was attributed to the fact that the lower specific grinding energy achievable with oil compensated for its poorer cooling performance relative to water.

Sato [Sato 1961] used the concept of an instantaneous heat source uniformly distributed over the apparent area of contact between the wheel and workpiece. In this fashion, he computed the average grinding temperature over the grinding zone. He also proposed that, for all dry cylindrical grinding, the proportion of heat entering the workpiece is about 84%.

Takazawa [Takazawa 1966] carried out an investigation concerning structural changes beneath the surface of ground materials as a result of grinding. Measurements of the subsurface temperatures were taken using a thermocouple/oscilloscope arrangement. He then used Jaeger's model to generate an approximate formula for the subsurface temperature produced by a moving band heat source. This is illustrated in equation 2.2

$$\frac{\theta\pi kV}{2Kq} = 3.1L^{0.53}e^{-0.69L^{-0.37}z}$$

**Equation 2.2**

He went on to correlate surface and subsurface hardness with computed temperature data, and to suggest some possible techniques to prevent change of surface structure during grinding. This work was also detailed in other publications [Takazawa 1964/72]

The conceptualisation of the nature of grinding temperatures changed in 1968 when Malkin [Malkin 1968] proposed that contact zone temperatures consisted of a background temperature, with an individual grain 'spike' temperature superimposed upon it. He reasoned that the temperature distribution locally around a grain was due not only to the grinding action of the grain concerned, but also to the grinding action of all the grains in the cutting zone. With this approach, Malkin outlined the mechanics of the energy/heat conversion in the wheel/work contact zone. He also illustrated that the analysis carried out by Outwater & Shaw [Outwater & Shaw 1952] was unrealistic as it neglected heat generation from grain wear flats rubbing the workpiece. In addition, the results indicated that Hahn had underestimated the temperatures resulting from a moving grain source, as the resultant temperature from the shear plane was considerably higher than that from the wear flat.

In 1969, DesRuisseaux & Zerkle [DesRuisseaux & Zerkle 1969] published a theoretical paper concerning their own analysis of the grinding process. They modelled the wheel/work contact as a band source on a semi-infinite plane. They noted Malkin's [Malkin 1968] assessment that temperatures in the arc of cut consisted of a background temperature with localised spike temperatures under the grinding wheel grits. The observation that while the spike temperatures under the grains may have repercussions for the wheel life, these spike temperatures may not necessarily affect the finished workpiece, was made. It was duly demonstrated using the approximation of Takazawa [Takazawa 1966] that the material between the grain and the remaining ground surface acts as a thermal insulator, and the grain spike temperature is not an important contributor to the workpiece temperature. The essence of the analysis demonstrated that the temperature field generated by the moving grain did not penetrate to the workpiece surface. In doing so, the band source model was validated as an effective way forward for theoretical grinding temperature evaluation.

Malkin [Malkin 1974] published the second of two related papers. The first paper considered energy partitioning, and will be discussed later. The second of these papers investigated surface temperatures and workpiece burn. He calculated the grinding zone temperature, and the local temperature under an abrasive grain. For the material considered, he measured the peak grinding zone temperature at burn, and used this to develop a relationship between the critical heat flux (for burn to occur), the workpiece velocity, and the depth of cut. He recognised that the results obtained were specifically applicable to dry straight surface grinding, although suggested they have possible application to cylindrical and internal grinding.

In a Keynote Paper for CIRP, Snoeys *et. al.* [Snoeys *et. al.* 1978] presented a comprehensive review of the state of the art to date, detailing thermal models in the literature, and highlighting areas in need of further consideration. One such area is the formation of thermally induced tensile residual stresses, and their negative influence on fatigue life of components. The importance of the transient temperature distribution, and the actual workpiece geometry were also highlighted.

In the first of two papers, Kopalinsky [Kopalinsky 1982] illustrated how the wear of grinding wheels could be explained by an increase in negative rake angles and a growth in wear flat areas on the grits, and how this allowed the increase in grinding forces with wheel wear to be explained. In the second paper, [Kopalinsky 1984] these results were used to develop a new model for the estimation of temperatures in grinding. The model, abandoning the band source theory, was based upon a distributed action by many grits. Rather than calculating the heat input to the contact zone from the process parameters, the effect of each individual grit was considered. Each grit was modelled as rectangular source, and using the results presented by Jaeger, the grinding zone temperature was calculated as a superposition of all the individual heat sources. The results of the analysis were then compared with Jaeger's band source model, and shown to be about 25% lower. This is accredited to the difference in approach taken, Kopalinsky's being essentially three dimensional, Jaeger's band source model being a two-dimensional solution. It was also noted that the increase in temperature with wheel wear can be attributed almost solely to increasingly negative rake angles, and associated wear flat growth. One interesting aspect of the model development is the potential to include the effect of a cutting fluid on the workpiece temperatures. The principle of superposition was used to calculate the overall temperature. The calculation region was the size of a wheel/work contact, with a scattering of individual heat sources moving through it. It could be possible, using superposition, to include convective cooling between the heat sources.

Lavine *et. al.* [Lavine & Jen 1991], working under Malkin, produced an interesting coupled model of temperatures developed in the grinding process. The model considered the heat fluxes entering the workpiece, the abrasive grits, and the grinding fluid. These individual analyses were coupled according to assumptions made concerning temperature compatabilities at the interface between the grits, cutting fluid, and workpiece. The workpiece background surface temperature was assumed to equal the fluid temperature rise, and the grain surface temperature was assumed to equal the sum of the workpiece background surface temperature and the workpiece under the grain surface temperature rise. This allowed a dimensionless coupled solution for the workpiece background surface temperature to be derived. The results obtained, for conventional grinding conditions, agreed well with experimental data obtained by Ohishi & Furukawa [Ohishi & Furukawa 1985]. For creep feed grinding conditions, the results agreed well when the coolant fluid was oil, but good agreement was not obtained when water was used. These discrepancies may possibly be explained by some of the assumptions made in the analysis. The heat source used for the evaluation of the heat transfer coefficient for the workpiece background surface temperature was assumed to be uniform. This assumption clearly breaks down for creep feed grinding where the heat source has a distinctly non-uniform distribution. For creep feed grinding, the power is distributed according to the normal infeed, which is a maximum at the front of the arc of cut, and zero at the back. In addition, the cutting fluid was modelled as a semi-infinite plane subjected to a moving heat source. While it is generally accepted that for conventional grinding, the grinding fluid has a low cooling ability in the arc of cut, it is thought (refs. below) that in the case of creep feed grinding, the grinding fluid has a considerably more significant effect on the arc of cut temperatures. The manner in which the cutting fluid works in creep feed grinding is not clear, but it has been demonstrated that it is considerably different to conventional grinding [chapter 7]. It is possible that the longer arc of cut in creep feed grinding allows more effective heat transfer between the wheel/workpiece and the cutting fluid. These points have been illustrated by Andrew *et. al.* [Andrew *et. al.* 1985], Werner *et. al.* [Werner *et. al.* 1980], and Salje [Salje 1984]. In chapter 3, the effect of cutting fluid on grinding temperatures is shown to be related directly to the non-dimensional Nusselt, Prandtl, and Reynolds numbers. Lavine [Lavine & Jen 1991] illustrated that the nondimensional temperature was a function of seven dimensionless parameters. The first three were based on material properties of the grain, fluid and workpiece. The fourth concerned the wheel and work speeds, the fifth being the ratio between the real and apparent area of contact. The last two parameters were the nondimensional contact lengths for the wheel and grains. The ratio between the real and apparent area of contact, and the nondimensional grain contact lengths are difficult to determine.

1995 saw the publication of work carried out by Rowe *et. al.* [Rowe *et. al.* 1995]. This work presented the results of an experimental investigation of heat transfer in grinding. Several important results were detailed. Firstly, it was shown that the uniform band source employed in Jaeger's analysis shows a different characteristic shape when compared with measured temperature signals. Both triangular and square law heat distribution were found to give better correlation with measurements, the square law being adopted for experimental partitioning calculations. In addition to this, it was demonstrated that the cutting action of the grains continued outside the geometric contact length, possibly due to elastic deflection of the grinding wheel. This lead to a semi-empirical method being developed for the calculation of an effective contact length. In addition, for a variety of ferrous materials, the maximum background temperature at which the onset of burn occurred was shown to be between $400^{o}$C-$500^{o}$C. Effective abrasive thermal properties were found by correlating experimental results with theoretical models.

## 2.2 Creep Feed Grinding Temperature Models

Creep feed grinding differs from conventional shallow cut grinding insofar as the depth of cut is much larger, the work velocity is much slower, and the specific energy can be considerably higher. There have been several different types of approach to evaluating temperatures in creep feed grinding, ranging from experimental to numerical to fully analytical.

Such an analytical approach was presented by Kuang-Hua *et. al*. [Kuang-Hua *et. al* 1994]. An approach similar to that of Lavine [Lavine & Jen 1991] was used to determine temperature distributions in workpiece, fluid, and grain. These expressions were not directly coupled; rather, a partitioning theory was applied to them individually. The results produced were compared with the experimental findings of Ohishi & Furukawa [Ohishi & Furukawa 1985]. They found excellent correlation with the experimental measurements. They did, however, use an effective contact ratio of 60%, compared to Lavine who used values ranging from 0.1% to 2%. This effective contact ratio was calculated from the volume porosity of the grinding wheel used. In a direct comparison with Lavine's model, the results of Kuang-Hua *et. al*. show a better general agreement with the character of the experimental data for both oil and water. They also conclude that the cutting fluid effectiveness can be increased by reducing the effective contact ratio i.e. using a more porous wheel, and note that despite it's poorer cooling ability, oil provides greater resistance to burn.

Ohishi & Furukawa [Ohishi & Furukawa 1985] modelled the creep feed grinding process using the finite element technique, and correlated their results with some experimental measurements. They indicated that once the maximum surface temperature rises above 100°C for water, and 300°C for oil, the temperature will rise sharply and burn will occur.

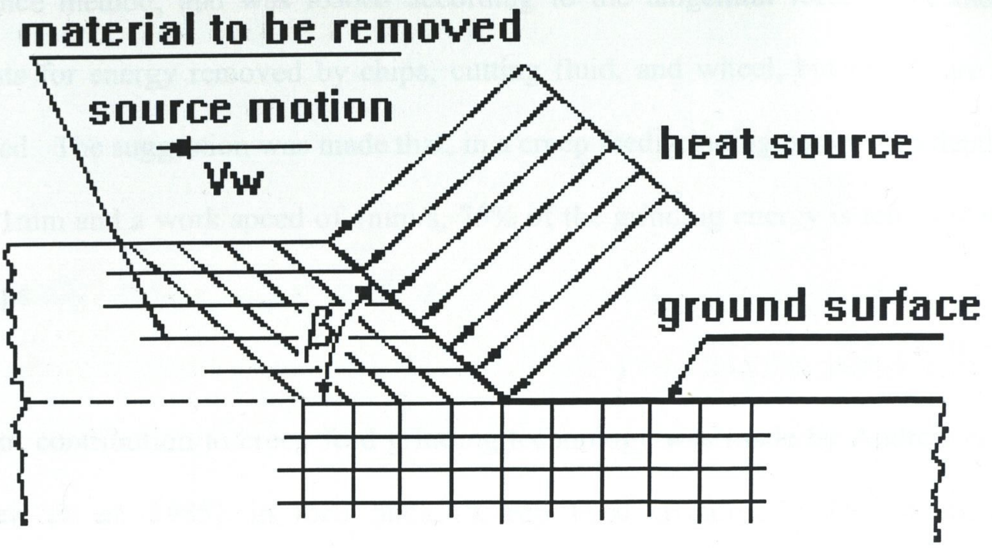

**Figure 2.2 – Finite element creep feed model**

Maris [Maris 1977, Snoeys *et. al.* 1978] also used the finite element technique to investigate temperatures developed in creep feed grinding. The model he used is illustrated in figure 2.2. He used a chord approximation for the arc of cut geometry. In addition, he assumed that the heat source was uniform. His conclusion, that for large angles of inclination of the moving heat source, the maximum temperature experienced by the ground plane is limited to 40% of the maximum surface temperature, is clearly dependant on the validity of the uniform loading. The maximum surface temperature for the uniform source occurs somewhere between the middle and back of the source. Snoeys *et. al.* [Snoeys *et. al.* 1978] showed the heat flux distribution to be triangular in nature. This would move the maximum surface temperature nearer to the top of the wheel/work contact, which would have the effect of reducing the maximum temperature experienced by the ground plane.

Werner *et. al.* [Werner *et. al.* 1980] also carried out some numerical analysis on the creep feed grinding process. The model was a combination of the finite element/finite difference method, and was loaded according to the tangential force. The model accounts for energy removed by chips, cutting fluid, and wheel, but details are not provided. The suggestion was made that, in a creep feed grinding pass with a depth of cut of 1mm and a work speed of 4mm/s, 75% of the grinding energy is removed with the chips.

A major contribution to creep feed grinding technology was made by Andrew *et. al.* [Andrew *et. al.* 1985], in their book, 'Creep Feed Grinding.' The monograph examined many aspects of the process, ranging from wheel dressing techniques to workpiece burn limitation. They also illustrated the versatility and application of the process, in a series of industrial case studies. These studies included applications such as flute grinding, turbine blade root grinding, and many more. The case studies also illustrated the use of different wheel types, from alumina to CBN to electroplated diamond.

Several other researchers involved with moving heat source theory have produced solutions for the problem of shear plane temperatures in metal cutting. While these solutions do not directly concern creep feed grinding, they do have possible application regarding the arc of cut temperature, if one is prepared to accept a chord approximation of the arc of cut geometry. Some of the less useful for grinding application amongst these, would include the efforts of Loewen & Shaw [Loewen & Shaw 1954], Leone [Leone 1954] and Weiner [Weiner 1954]. Two papers in particular lend themselves to a chord approximation model. Chao & Trigger [Chao & Trigger 1953] presented an analysis which allowed the temperature on an inclined slider moving across a semi-infinite plane to be calculated. They assumed a uniform band source heat flux, but a simple modification would allow a variety of source types to be used. In addition, using the methodology of Chao & Trigger, it is possible to change from a cartesian to polar co-ordinate system, and to compute the quasi steady-state temperature distribution from a circular arc heat source moving across a semi-infinite plane. This is illustrated in appendix 1. The flat source produces the highest maximum temperature, the inclined slider produces the lowest, and the circular arc maximum temperature lies between the two.

Hahn [Hahn 1951] also carried out an analysis of the temperature developed at the shear plane in metal cutting. His analysis differed somewhat in conception from that of Chao & Trigger. While Chao & Trigger considered an inclined slider moving at a velocity in the horizontal direction, Hahn considered a flat slider moving with a velocity in both the horizontal and vertical directions. This in turn meant that his solution differed somewhat from that of Chao & Trigger. It would seem that Chao & Trigger's model is probably more representative of the grinding situation than Hahn's model. Hahn's model, on the other hand, seems to be quite adequate for modelling the turning operation, with excellent correlation between theoretical and experimental results being obtained . Equation 2.3 illustrates Chao & Trigger's solution, and equation 2.4 shows Hahn's answer.

$$\Delta\theta = \frac{2\beta q}{\pi c \rho V} \int_{E-L}^{E+L} e^{-u\cos\phi} K_o\left(\left|u\right|\right) du$$

**Equation 2.3**

$$\Delta\theta = \frac{\beta q}{\pi c \rho V} \int_{E-L}^{E+L} e^{-u} K_o\left(\left|\frac{u}{\cos\phi}\right|\right) du$$

**Equation 2.4**

It can be seen that Chao & Trigger's solution differs from Hahn's not only in the way in which the heat source is modelled, but also by a factor of two. This is because Hahn found that, in case of shear plane temperatures in metal cutting, a heat source moving through an infinite solid better matched experimental results.

High efficiency deep grinding (HEDG) is a concept which followed on from the creep feed grinding process. This process uses higher wheel speeds, and higher workpiece feed rates. For example, in creep feed grinding, typical feed rates would be measured in cm/s, whereas in the HEDG process, feed rates would be of the order of mm/s. It takes advantage of the fact that, when using a CBN grinding wheel, a significantly lower percentage of the process power enters the workpiece. This is attributed to the higher conductivity of CBN, compared to conventional alumina. This allows grinding to take place at higher feed rates.

## 2.3 Temperature Models in Form Grinding

One particular area in industrial grinding where there is a distinct lack of information in the literature, is the area of temperatures experienced by the workpiece in form grinding. Form grinding concerns the use of a profiled wheel to grind surfaces which do not lie in the same plane. Generally, in form grinding the areas of main concern are sharp corners on the workpiece. Dickenson [Dickenson 1970] for example, showed an illustration of some threads which had been damaged by abusive thread grinding. The interesting aspect of this illustration is the location of the damage. The damaged region of the threads is confined to the area near the thread apex. The remainder of the threads appeared to be damage free.

There appear to be only two attempts to analytically examine the temperature developed at these geometric discontinuities which occur in form grinding. Maris [Maris 1977/78] developed a solution based on the Jaeger model for moving heat sources. His result is outlined as follows:

$T_{max}$ = maximum temperature in wedge = $(\pi/2\theta)$."temperature predicted by Jaeger's model"

This is to be used if only one side of the wedge is ground. If both sides of the wedge are ground simultaneously, then twice this value is to be used. The wedge used for his model is illustrated in figure 2.3. This model would imply that, in thread grinding with an included angle of 30°, the temperature at the tip of the wedge would be six times the value calculated by Jaeger's model. This would appear to be a rather large concentration factor, although it should be pointed out that this factor is applied to the flank temperatures. The flank temperature is related to the flat plane temperature according to the sine of half the included angle. This would give a concentration

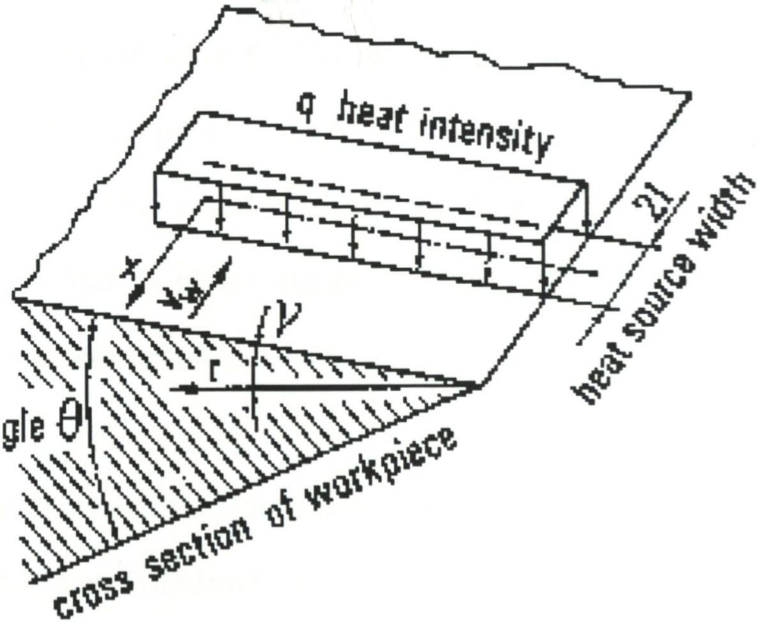

**Figure 2.3 – Wedge grinding model**

factor of 1.55 times the flat plane solution, for a given normal infeed. For an included angle of 60°, the concentration factor rises to 2.6, relative to the flat plane, for a given normal infeed. Further examination of Maris's solution shows that it has a singularity at $\theta = 0$. In addition, the assumption that the heat fluxes on both sides of the wedge are equal, is made. While this may be a reasonable assumption for thread, or thread-die grinding, it doesn't have application in the case of angle approach grinding, where the heat fluxes on each flank are generally not equal. In addition, the assumption that the heat source on each side of the wedge is semi-infinite may not be valid, particularly in thread grinding, where the thread height is of the same order of magnitude as the thread width.

The other analytical approach to this problem was presented by Khanzhin [Khanzhin 1971]. Khanzhin also used the Jaeger model as the basis of the analysis. The result of the analysis showed that the temperature at the tip of the wedge was equal to the Jaeger solution times a multiplication factor. This factor was found to be 1.5 for included angles between 0° and 60°. The manner in which this factor was obtained was not revealed. In a comparison with Maris's model detailed above, for the same problem as above, Khanzhin's model suggests the tip temperature to be 1.5 times the Jaeger solution, and Maris's model suggests a value 1.55 times the Jaeger solution. There is discrepancy between these models, worthy of further investigation.

Trmal [Trmal 1982] considered problems existing in form grinding, but not any of a thermal nature. Gordeev [Gordeev1976] suggested some methodologies for grinding with angular wheels. He did not address any thermal considerations. Salje *et. al.* [Salje & Damlos 1981] also considered some of the mechanical aspects of form grinding. One interesting point raised, concerned resultant axial forces appearing when asymmetrical forms are ground. The implication regarding any thermal analysis is that axial forces on the wheel/workpiece will result in a different heat input on the workpiece flanks, compared to that arrived at by calculation [Morgan *et. al.* 1998]. This is due to differing depths of cut on the flanks occurring during grinding, compared to what would be expected if the workpiece was symmetrical.

## 2.4 Energy Partition in the Arc of Cut

There are many different models for temperatures in the arc of cut in grinding. The more popular methods of calculation have been outlined in sections 2.1 & 2.2. There is one aspect common to any analytical effort involving grinding temperature evaluation, namely the partition of process energy in the arc of cut. The workpiece partition ratio is the percentage of the total process power which enters the workpiece. In terms of predicting the temperature in the arc of cut, the partition ratio can be regarded as a scaling factor. In essence, it adjusts the predicted temperature characteristic according to the applied power. If the applied power to the workpiece is halved, perhaps by switching from an alumina wheel to a CBN wheel, then the temperature at the workpiece surface will be halved. There have been a large number of proposed models, the first of these coming from Blok in 1937 [Blok 1937]. The approach was first to assume the wheel was a perfect insulator, with a percentage of the process energy entering the workpiece, and then to consider the workpiece as an insulator, with the remaining process energy entering the wheel. The average temperatures were then assumed equal, and the two expressions equated, yielding a formula for the partition ratio.

In their 1952 paper, Outwater & Shaw developed a partition ratio for the model devised to predict grinding temperatures. The technique devised by Blok [Blok 1937] was used in conjunction with Jaeger's slider model. The result for energy partitioning between the chip and workpiece for L>5 is shown in equation 2.5.

$$R = \frac{1}{1 + \frac{0.665 \cot \phi}{\sqrt{L}}}$$

**Equation 2.5**

Eshghy [Eshghy 1967] examined the energy partitioning for the abrasive cutoff operation. While this is a grinding operation, the thermal considerations are different. The heat flow is largely in the direction of the wheel feed which means the material affected by the heat is only instants from being ground away itself. This allows large stock removal rates, mainly due to the large percentage of heat removed by the chips.

In the first of two papers, Malkin [Malkin 1974] examined the energy partition between chip formation, plowing, and sliding. Sliding occurs during the initial grain contact with workpiece. During sliding, the grain merely rubs the workpiece surface. At some point later, the grain plows the workpiece. During plowing, the workpiece is plastically deformed, but no material is removed. After this stage, the grain enters the chip formation stage of the contact, where chips are formed, and removed, from the workpiece surface. An investigation of how much of each of these three energies entered the workpiece was then carried out. A conclusion was drawn, stating that nearly all the sliding and plowing energy entered the workpiece, and roughly 55% of the cutting energy also entered: this value was calculated using the technique presented by Outwater & Shaw [Outwater & Shaw 1952]. This paper did not address the broader issue concerning how much of the total process power was used in chip formation, plowing, and sliding.

There have been several other models in use over the past years. Hahn [Hahn 1956] proposed the following grain based model (equation 2.6):

$$R = \frac{1}{1 + \frac{k_g}{\sqrt{r_o v_s}\beta_w}}$$

**Equation 2.6**

Rowe et. al. [Rowe et. al. 1988] proposed a contact zone model, which required the heat conductivity of both the workpiece and the wheel. It should be noted that the bulk thermal properties of the wheel will be significantly different to the thermal properties of the grains. The heat conductivity was measured using steady state experiments. The model has the form shown in equation 2.7.

$$R = \frac{1}{1 + \left( \sqrt{\frac{v_s}{v_w}} \frac{\beta_s}{\beta_w} \right)}$$

**Equation 2.7**

Shaw [Shaw 1986] proposed two models for the energy partitioning in grinding. The first of these models considered dry grinding, the second included the effects of a coolant fluid. The dry grinding expression is given in equation 2.8. The observation that the area ratio was, on average, about 0.01, and the velocity ratio was about 100, was made. The product of these two ratios is unity, leading to a simpler expression, illustrated in equation 2.9.

$$R = \frac{1}{1 + \frac{\beta_s}{\beta_w}\sqrt{\frac{V_s}{V_w}\frac{A_{real}}{A_{apparent}}}}$$

**Equation 2.8**

$$R = \frac{1}{1 + \frac{\beta_s}{\beta_w}}$$

**Equation 2.9**

Using the same approach, an expression for energy partitioning with the effect of cooling included, was derived. This expression is given in equation 2.10.

$$R = \frac{1}{2 + \frac{\beta_s}{\beta_w}}$$

**Equation 2.10**

This expression is clearly useful only as a rough indication of the energy partitioning. It is specific to a water/steel combination of cutting fluid and work material.

The most recent energy partitioning model was presented in 1997, by Rowe *et. al.* [Rowe *et. al.* 1997]. This analysis stated clearly, for the first time, the nature of energy partitioning, and how it influences workpiece temperatures. It was noted that, while the important temperature for the workpiece is the background temperature, the background temperature occurs as a result of the grain action, and the energy transfer occurs at the grain/workpiece interface. The partitioning analysis made no assumptions about wheel/work interface temperatures. The partition solution was calculated from the observation that, at the points of energy transfer (i.e. at the grain/workpiece interfaces), the sum of the workpiece background temperature and the temperature directly beneath the grain, would be equal to the sum of the wheel background temperature and the grain-surface temperature rise. The effective thermal conductivity of C.B.N. was evaluated using an experimental grinding technique. In essence, the partition ratio was evaluated experimentally, and from the derived expression for this quantity (equation 2.11), the effective heat conductivity was calculated.

$$R_w = \left\{1 + 1.1\left(\frac{r_o}{l_e}\right)^{1/2}\left[\frac{\beta_g}{\beta_w}\right]f(\zeta)\right\}^{-1}\left(1 - \frac{e_{cc}}{e_c}\right)$$

**Equation 2.11**

The paper noted that the value of the chip specific energy is limited by its melting temperature. The value for ferrous materials is quoted as being about 6J/mm$^3$. The model was compared with experimental results, and the correlation was very satisfactory. The results were incorporated into a strategy for prevention of thermal damage in grinding.

## 2.5 The Role of Cutting Fluid in the Grinding Process

The cutting fluid in the grinding process performs several functions. It provides bulk cooling of the workpiece, lubrication between the wheel and workpiece, and a flushing function which removes debris from the wheel and interference zone [Malkin 1989]. The lubrication provided by the cutting fluid has the effect of reducing the specific grinding energy, which has a direct positive effect on the process power required. In conventional shallow cut grinding, the cutting fluid is thought to have little effect on grinding temperatures in the contact region, due to the small arc of cut length [Rowe *et. al.* 1997]. When boiling of the cutting fluid occurs, this effect becomes stronger, as the gaseous phase of the fluid forms an insulating layer between the wheel and workpiece. This further reduces the convective ability of the cutting fluid [Andrew *et. al.* 1985]. The onset of workpiece burn occurs at temperatures around 400°C – 500°C [Rowe *et. al.* 1995], although for a specific material, softening can occur at any temperature above the tempering temperature. Creep feed grinding, on the other hand, is thought to benefit considerably from the application of cutting fluid.

The first analytical attempt to investigate the role of a cutting fluid in the grinding process was presented by DesRuisseaux & Zerkle [DesRuisseaux & Zerkle 1970]. This analysis considered band sources moving across both a semi-infinite plane, and a rotating cylinder. The result, for the case of the semi-infinite plane, was of the same form as the Jaeger model, with an additional term superimposed accounting for energy removed by convective cooling. The authors presented results showing the influence of convective cooling on the surface temperatures of the geometries considered. A second paper by Lee *et. al.* [Lee *et. al.* 1971] presented the results of an experimental investigation of the heat transfer in cylindrical grinding. In this analysis, a workpiece was electrically heated, and the change in temperature resulting from fluid application was measured using embedded thermocouples. A new cutting fluid application system was designed which greatly reduced the bulk temperature rise of the workpiece.

The results of an experimental program about the cooling ability of cutting fluids were published in 1970 [Ueno *et. al.*]. This work was primarily concerned with the turning process, and the ability of cutting fluids to cool the tool/work interface. The technique involved using a notched bar which was electrically heated, and a thermocouple, to measure the convective heat transfer coefficient associated with various cutting fluids. Subsequently, tests were carried out using a cutting tool welded to a work piece. This arrangement was also electrically heated. The results presented highlighted some important aspects of convective cooling. The results indicated that water has a higher heat transfer coefficient than oil for a range of Reynolds numbers. Also noted was the fact that, despite water having higher heat transfer coefficients than oil, little difference in cooling ability was observed during the simulated turning experiments. The authors concluded that lower temperatures in the turning process could only be achieved by reducing the total cutting energy. The reason for this was attributed to the fact that, in the turning process, the region of heat generation is extremely small, and can be considered a point source. This is an interesting point, as it indicates indirectly that a larger area available for convective heat transfer would reduce temperatures in the cutting region. Such a case as this is to be found in creep feed grinding.

Osman & Malkin [Osman & Malkin 1972] carried out an investigation of the lubricating effect of grinding fluids in the grinding process. While not directly considering the cooling effect of the grinding fluids, it was noted that lubrication reduced the specific grinding energy, which is directly related to the grinding temperature. It was also noted that attritious wear of the abrasive grains was reduced with use of a grinding fluid.

1978 saw the publication of the first rigorous investigation into the role of cutting fluid in creep feed grinding [Powell & Howes 1978]. The investigation used an electrically heated mock workpiece to simulate the creep feed grinding process. The burnout flux of the heater element was used as a criterion to investigate the cooling ability of water based grinding fluids. The results indicated several important issues. Firstly, the penetration of the cutting fluid into the grinding wheel is important: higher penetrations result in higher burnout fluxes. A second point concerned the cutting fluid bulk temperature. A linear relationship between the cutting fluid bulk temperature and the burnout flux was demonstrated. This showed that the burnout flux decreased with rising cutting fluid temperature. The investigation used several different heater lengths, the longer heaters having a lower burnout flux. This suggested that the cooling ability of the cutting fluid decreased, as it flowed through the contact zone. In addition, it was shown that entrainment of the grinding fluid between the wheel and workpiece was an effective method of cutting fluid application in creep feed grinding. It was suggested that a mock workpiece be used in the wheel run-out zone to enhance this cutting fluid application technique. While the results were obtained for a mock grinding set up, the trends illustrated should be applicable to real grinding conditions. Stuart [Stuart 1977] went on to demonstrate that increasing the wheel speed increased the critical power flux in standard creep feed grinding tests. This was attributed to more cutting fluid flowing through the arc of cut. It was noted, however, that for the test material used, the benefit accrued from the increased cooling was outweighed by the increase in specific energy accompanying the wheel speed increase.

Andrew *et. al.* [Andrew *et. al.* 1985] suggested that the onset of workpiece burn coincided with the transition of the boiling mechanism from nucleate to film boiling. For water based cutting fluids, this would be somewhere around 150°C, and for oil, this would be somewhere above the boiling point, possibly around 400°C. This agrees in character with the results presented by Ohishi & Furukawa, who found experimentally that 100°C and 300°C were the critical temperatures for burn for water and oil respectively.

Ye & Pearce [Ye & Pearce 1984] released the results of research carried out comparing the benefits of oil versus water as a grinding fluid. It was noted in this work that profile wear on the wheel was less severe when oil was used as the grinding fluid. In addition, the authors experienced workpiece burn in the run-out region, which was credited to cutting fluid starvation in this region. This result lends credence to the assertion of Powell & Howes [Powell & Howes 1978] that a mock workpiece enhancing fluid entrainment in the grinding wheel is an effective method of cooling in the run-out zone.

Other efforts to characterise cutting fluid behaviour include those of Eda & Kishi [Eda & Kishi 1974] and Karaim [Karaim 1969]. Eda & Kishi investigated the effect of cutting fluid type and cutting fluid pressure on grinding temperature, residual stress level, surface finish, and geometric finish. The results of the analysis concluded that a very high cutting fluid pressure (>50Bar) was extremely effective in reducing surface temperature, and consequently residual stresses and workpiece deformation. In addition, the results indicated that for very high wheel speeds, where the air adjacent to the wheel develops a strong boundary layer, the high cutting fluid pressure was able to break down the boundary layer and provide effective cooling. Karaim carried out tests on cylindrical grinding machine which has cutting fluid provided through the pores of the grinding wheel. These results were compared with the results of similar experiments using standard cutting fluid application techniques. Empirical formulae were presented for both cases, relating the contact temperature to the depth of cut and the infeed rate. For the conditions considered, the application of cutting fluid through the pores of the wheels proved more effective. The results indicated that the contact zone temperature was a continuous function of the depth of cut, and the infeed rate. Details regarding cutting fluid velocity or pressure were not provided. The results of this paper may have indicated that cutting fluid application through the grinding wheel pores is more effective than standard application techniques. The most common method of cutting fluid application is via a nozzle, which delivers the fluid on to the wheel at the wheel/work interface. With this technique, some fluid is entrained in the pores of the wheel, and released in the contact zone under the influence of centrifugal forces. More of the fluid is hydrodynamically forced into the contact region by the wheel. The shoe application method involves forcing fluid into the pores of the wheel upstream from the contact zone, using a close fitting shoe. Another application method involves submersing the workpiece in a bath of cutting fluid, allowing the wheel to force the fluid through the contact zone. The results presented by Eda & Kishi would suggest that increasing the cutting fluid pressure using a standard nozzle or shoe would have the same effect as fluid application through the pores of the grinding wheel. This would appear to be a more easily implemented method of cutting fluid application. It would also be far more appropriate for denser wheels with lower porosities. These wheels would be prone to clogging by cutting fluid impurities over time.

Other research into cutting fluid effects in grinding have centred around analysing the cutting fluid velocity in the arc of cut. Saito *et. al.* [Saito *et. al.*1974] used a test rig similar to that of Powell & Howes to investigate the nature of the heat transfer coefficient in the contact region. The study examined the nature of air flow around, and through the pores, of the grinding wheel. A hot wire anemometer was used to measure the air velocity, and a thermocouple touching the heating element was used to measure the local heat transfer coefficient. The air flow around the wheel was characterised for varying wheel porosities. The results indicated that the local heat transfer coefficient was dependant on the air blowing out through the grinding wheel pores, and that it was neither symmetric nor uniform over the workpiece surface. While this work may be of some relevance to dry grinding, it does not readily translate to wet grinding. Several studies have been carried out investigating heat transfer in the arc of cut. However, rather than considering the convective cooling in terms of the nondimensional heat transfer parameters, i.e. the Nusselt, Prandtl, and Reynolds numbers, these studies focus on the convective heat transfer coefficient. In the case of water cooling, where boiling occurs at a temperature generally lower than the arc of cut temperature, this is fine. However, when oil is used as the cutting fluid, and tests are carried out to measure the heat transfer coefficient, the results are really specific to the test conditions only. However, if the results were presented in terms of the nondimensional heat transfer parameters, they would have a general application to conditions different to those of the test. This would be a more useful way to investigate the role of the cutting fluid, particularly for oil cooling, since it has a high boiling temperature > 350°C, and particularly for creep feed grinding which has an arc of cut long enough to allow the cutting fluid to effectively convect heat.

Schumack *et. al.* [Schumack *et. al.*1991] carried out an analysis of the fluid flow under a grinding wheel. Reynolds equation, with some modifications to suit the grinding process, was applied to the case of fluid flowing over a flat plane, and under a rotating smooth wheel. The assumptions of the model included: no account of the velocity boundary conditions at entry and exit from the contact zone; temperature effects assumed negligible; a two dimensional flow system. The researchers concluded that only a model based on the fully two or three dimensional Navier-Stokes equations would accurately predict fluid flow in the contact zone. Considering that the wheel porosity has been demonstrated as having a strong effect on the cutting fluid flow in the contact zone [Powell & Howes 1978] [Karaim 1969], it is not surprising that the smooth wheel model did not provide good agreement with experiment.

Two papers summarising a research project carried out at M.I.T. were published in the early nineties. Engineer *et. al.* [Engineer *et. al.* 1992], in the first of these papers, investigated experimentally the useful flow rate through the grinding zone. This was achieved using a test rig which separated and collected all the fluid that passed through the grinding zone. The results showed that the amount of the applied fluid which passed through the grinding zone depended mainly on the wheel bulk porosity and the nozzle position. The effect of nozzle type was not specified. Wheel dressing was noted to have only a secondary effect, attributed to the surface porosity change of the wheel. The depth of cut, and work speed were found to have a negligible influence on the amount of fluid flow through the grinding zone.

The second paper in this series presented an analytical model of fluid flow through the grinding zone [Malkin *et. al.* 1992]. The model included effects of nozzle position, wheel porosity, and also the re-entrainment of fluid on the workpiece into the grinding zone by the wheel. The results were in good agreement with the experimental findings of Engineer *et. al.* These two papers have shed light on a difficult aspect of cutting fluid application. It should be possible to use these efforts, in conjunction with heat transfer theory, to characterise the nature of effective cooling in grinding.

## 2.6 Residual Stresses in Grinding

Calculation of grinding temperatures has interested researchers for many years. This interest has not been fostered by mere curiosity, rather by a desire to correlate damage to the workpiece with the workpiece temperature. The workpiece damage is therefore the motivating reason for research into grinding temperatures. One particular type of grinding damage concerns residual stresses in the workpiece. These stresses can be either compressive or tensile in nature. Compressive stresses can be considered beneficial to the workpiece, as they serve to improve the fatigue life of components. Tensile residual stresses, serving to reduce fatigue life of components, are looked upon unfavourably. Compressive residual stresses are a result of plastic deformation of the workpiece by the grits of the grinding wheel [Snoeys *et. al.* 1978] [Torrance 1994]. The effect can be likened to shot peening. Tensile residual stresses are generated by plastic thermal deformation of the workpiece. Thermal plastic deformation occurs when the thermally generated stresses exceed the material's yield stress. The mechanism is outlined in chapter 4. There have been few papers published in the literature analysing residual stresses. This is probably due to the difficulty associated with analysing such non-linear behaviour.

An investigation into the residual stresses produced by metal cutting was published by Okushima *et. al.* in 1971 [Okushima *et. al.* 1971]. This analysis used the finite element technique to analyse the problem. The model included both a thermal and mechanical loading. The results of the numerical analysis indicated that the stresses induced by the mechanical loading were compressive in nature, if the horizontal force was zero, and tensile if it were not. The stresses induced by the thermal loading were tensile, and of far higher magnitude than the stresses resulting from the mechanical loading. The analysis concluded that, to reduce tensile residual stresses in cutting, a low cutting speed, large vertical ploughing force, and a low temperature are required.

Miskevich & Zotova [Miskevich & Zotova] investigated experimentally residual stresses resulting from diamond grinding of hardened steel. The test specimens were quenched after grinding, and subsequently annealed. The stresses measured were found to be compressive in nature. The tests did not include temperature measurements, so there is little to be gleaned, in general, from the analysis. It could be surmised, however, that the temperatures developed during the grinding of the test specimens were quite low, since the residual stresses were compressive in nature.

Saito & Kagiwada [Saito & Kagiwada 1974] examined the thermal stress distribution in the grits of a grinding wheel using a numerical technique. The analysis concluded that temperature rise of the grit, and the associated thermal stress, fade within one wheel revolution, and that the tensile stress in the grit is insufficient to cause fracture.

Hahn [Hahn 1976] examined form errors in cylindrical grinding. In a qualitative fashion, it was shown that the transient temperature on the workpiece can cause thermal stresses which can exceed the Von Mises yield criterion. The nature of this deformation was shown to be responsible for form error in the workpiece, and tensile residual stresses. It was suggested that low depths of cut, high work speeds, and sharp wheels are useful measures in the reduction of thermally induced residual stress. The higher work speeds lead to a significant reduction in workpiece surface temperature. This follows directly from Jaeger's model, outlined in equation 2.1, and figure 2.1 From figure 2.1, it can be seen directly that an increase in workspeed of 500% would reduce the maximum workpiece surface temperature by a factor of approximately 2.

Mishra *et. al.* [Mishra *et. al.* 1977] examined the problem of residual stresses in grinding using the finite element technique. The analysis included the effect of the mechanical loading and the thermal loading. The thermal load distribution was computed using the Jaeger slider model. The mechanical loading was modelled as a horizontal and vertical force component acting on the finite element mesh. The yield behaviour was assumed to be elastic-perfectly-plastic in nature. The load was moved along the mesh for a distance, and the remaining stress distribution was taken to be the residual stress. Development in finite element methods in recent years allow coupled thermo-mechanical models to be far more easily tackled, even allowing transient loading, negating the need for the difficult technique used by Mishra *et. al.* The research concluded that the contribution of the mechanical load resulted in compressive stresses, and that the thermal load resulted in tensile residual stresses. The magnitude of the tensile stresses was shown to be far greater than that of the compressive stresses, and the tensile stresses are, therefore, the dominant concern. The technique used in this analysis was very similar to that used by Okushima *et. al.*[Okushima *et. al.* 1971]. That research indicated that the mechanical load could result in tensile residual stresses. The mechanical loading in that case had a tangential to normal force ratio of about 0.4. The grinding model detailed above had a tangential to normal force ratio of 0.5. The force ratio for grinding is typically of the order 0.3 – 0.5. In turning however, this ratio is typically 2 – 3. This would suggest that the work of Okushima *et. al.* did not accurately represent the cutting process, and the work of Mishra *et. al.* would indicate a possible flaw in the modelling, considering the fact that mechanical loading has been practically demonstrated to induce compressive residual stresses [Snoeys *et. al.* 1978].

Despite the fact that compressive residual stresses are desirable in ground components, little research has been dedicated to characterising such stresses. This is not surprising since most research aims to expand knowledge on problem areas. There are, however, two interesting publications investigating compressive residual stresses. The first of these dates back to 1986 [Olver *et. al.*]. This research investigated the residual stress distribution resulting from a semi-infinite plane being indented by normal and tangential loads. The asperity contact with the plane was flat. The model used slip-line field theory as the basis for the modelling. Results from the analysis indicated that the residual stress on the surface of the contact could be tensile in nature. Torrance [Torrance 1994] modified this analysis to investigate residual stress distribution resulting from a hard wedge rubbing a soft surface. The analysis indicated that for most worn surfaces (i.e. surfaces which have been abraided by hard materials), the residual stress will be compressive in nature at the surface. The results of the model were compared with measured residual stresses from gently ground components, and were in reasonable agreement.

Brinksmeier [Brinksmeier & Tonshoff 1985] showed how residual stress measurement could be used to design the layout of machining processes.

# Chapter 3

# A Note on the Dimensional Technique

## 3.1 Introduction

The Baron Jean-Baptiste Fourier is generally regarded as the founder of the dimensional technique. In his work "Théorie analytique de la chaleur" Fourier stated "It should be noted that each physical quantity, known or unknown, possesses a dimension proper to itself and that the terms in an equation cannot be compared one with another unless they possess the same dimensional exponent."

It can further be stated that if magnitudes are to be operated upon, they must have the same dimensional formula, because only then do these operations have a physical significance. This point in turn illustrates the difference between ordinary algebra, and physical algebra. Ordinary algebra manipulates numbers. Physical algebra, on the other hand, considers each quantity to consist of a numeric and an associated unit. So, whereas with ordinary algebra a relationship is merely comparing numbers, in physical algebra a relationship is a comparison of magnitudes of similar quantities. A consequence of this is that arguments of mathematical functions, which are expressible as power series, must be pure numbers. If this were not the case, each term in the power series would have a different dimensional formula, making it physically invalid.

These physical quantities can have one of two types of associated unit: fundamental or derived. As the names suggest, derived units are developed from a declared set of fundamental units. In addition, the classification of units as fundamental or derived is not rigid, or bounded by natural laws. It is, to an extent, arbitrary, although fundamental units are generally recognised as being: mass, length, time, temperature, electric charge, and luminous intensity. In addition, some texts highlight the advantages of using the plane angle as a fundamental unit [Massey 1971] (measuring angles in degrees as opposed to radians, which are dimensionless), and others, demonstrating the direct relationship between force and mass, prefer to use force as a fundamental magnitude. In fact, if one considers the problem of the sphere falling through a viscous medium, the terminal velocity being required, then both force and mass can be declared fundamental units, since Newton's second law is not applicable when the sphere reaches terminal velocity, and there is no direct relationship between mass and force [Massey 1971 Huntley 1967].

All engineering mathematics is therefore founded on the following principle: For a given set of fundamental units, quantities of the same kind have the same dimensional formula, and any equation involving these quantities must be dimensionally homogeneous.

In essence, the Dimensional Technique is a study of the restrictions placed on the form of an algebraic function by the requirement of dimensional homogeneity. It indicates possible groupings of parameters that are supposed relevant to the phenomenon under investigation. It is, therefore, a method of processing information rather than providing it. It always supposes that the parameters of interest have been correctly identified. In general, only experiment, or numerical work will indicate if the dimensional analysis result is wrong.

## 3.2 The Pi Theorem:

The Pi theorem is a technique which allows logical processing of parameters of interest. It enables the result of an investigation to be presented in a general form. If a problem under investigation is thought to have N parameters of interest, and these N parameters contain M fundamental units, then the solution will contain N-M dimensionless Pi groups. The Pi theorem outlines a method of formulating these Pi groups. A recurring set of variables is chosen from the N parameters. The number of variables is equal to the number of fundamental units, M. The variables in the recurring set are not arbitrarily chosen. The recurring set must contain all of the fundamental units M. Each of the remaining parameters are, in turn, combined with the recurring set to form a dimensionless group. The Pi theorem does not necessarily yield the most concise solution. This technique can be illustrated using a problem which is of current relevance in engineering practice; that of the temperature developed during the grinding process. The solution to this problem will be developed in the following chapters, which further consider grinding temperatures.

## 3.3 Application of the Dimensional Technique

Figure 3.1 illustrates the situation under consideration. Essentially, a band heat source moves with a velocity across a semi-infinite plane. The assumptions in this model are identical to those assumed by Jaeger [Jaeger 1942] in his analytical analysis of the same problem. In dimensional analyses, it is necessary to identify the parameters of interest prior to beginning the analysis. The fundamental dimensions used for this

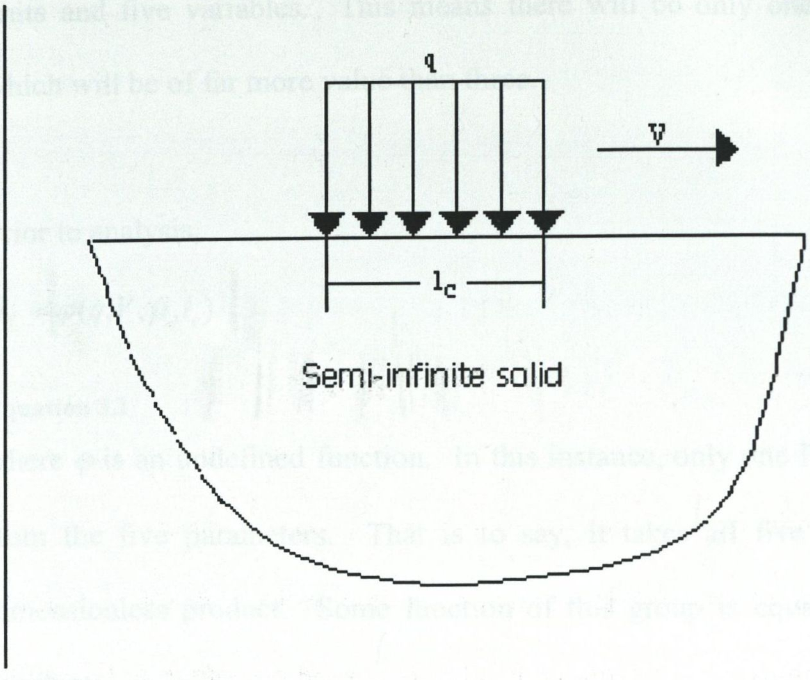

**Figure 3.1 – The semi infinite plane**

analysis were mass (M), length (L), time (T) and temperature (Θ). In this case, the relevant parameters and their fundamental dimensions are:

$q$ = the applied average heat flux $[MT^{-3}]$

$l_c$ = the arc of cut length$[L]$

$V$ = the work speed$[LT^{-1}]$

$\beta = (k\rho c)^{0.5}$ a material property$[MT^{-2.5}\Theta^{-1}]$

$\theta$ = maximum work temperature rise $[\Theta]$

It should be noted that $\beta$ is a compound parameter, representing the thermal properties of the workpiece. It is sometimes referred to as the "heat conductivity." Defining this parameter has a clear advantage. There are four fundamental units. If $\beta$ were broken into three separate properties, there would be seven variables, leading to three dimensionless groups. By recognising that these three variables collectively represent the workpiece thermal properties, one reduces the problem to that of four fundamental units and five variables. This means there will be only one dimensionless group, which will be of far more value than three.

Prior to analysis,

$$\theta_f = \varphi(q, V, \beta, l_c)$$

**Equation 3.1**

where $\varphi$ is an undefined function. In this instance, only one Pi group can be formed from the five parameters. That is to say, it takes all five parameters to form a dimensionless product. Some function of this group is equal to a nondimensional constant:

$$\varphi\left(\frac{(\theta \beta V^{0.5})}{q}(l_c^{\ 0.5})\right) = const$$

**Equation 3.2**

Rearranging this gives:

$$\theta_f = \varphi_1\left(\frac{q}{\beta}\sqrt{\frac{l_c}{V}}\right)$$

**Equation 3.3**

where again $\varphi_1$ is an undetermined function.

The expression developed above is of the same form as the Linear Jaeger model [Shaw 1996]. The only difference is that the function $\varphi_1$ is a constant of magnitude 1.414. The constant in this case is for the maximum surface temperature. The mean surface temperature is found by using a different constant. Thus, the dimensional analysis is equally valid for either the mean or peak temperature. Only the constant $\varphi_1$ is different.

units and five variables. This means there will be only one dimensionless group, which will be of far more value than three.

Prior to analysis,

$$\theta_f = \varphi(q, V, \beta, l_c)$$

**Equation 3.1**

where $\varphi$ is an undefined function. In this instance, only one Pi group can be formed from the five parameters. That is to say, it takes all five parameters to form a dimensionless product. Some function of this group is equal to a nondimensional constant:

$$\varphi\left(\frac{(\theta\beta V^{0.5})}{q}(l_c^{\ 0.5})\right) = const$$

**Equation 3.2**

Rearranging this gives:

$$\theta_f = \varphi_1\left(\frac{q}{\beta}\sqrt{\frac{l_c}{V}}\right)$$

**Equation 3.3**

where again $\varphi_1$ is an undetermined function.

The expression developed above is of the same form as the Linear Jaeger model [Shaw 1996]. The only difference is that the function $\varphi_1$ is a constant of magnitude 1.414. The constant in this case is for the maximum surface temperature. The mean surface temperature is found by using a different constant. Thus, the dimensional analysis is equally valid for either the mean or peak temperature. Only the constant $\varphi_1$ is different.

The above analysis has assumed an adiabatic surface, which would correspond with dry grinding. Most grinding is carried out using a coolant of some sort. Thus, it would be desirable to include the effect of coolant in the analysis. The coolant properties can be represented by the ratio of the convective to conductive heat transfer coefficients. This parameter has the following dimensional formula:

$$h/k = [L^{-1}]$$

**Equation 3.4**

The other parameters remain the same as for the previous example. Application of the Pi theorem reveals the following dimensional relationship:

$$\theta_f = \frac{q}{\beta}\sqrt{\frac{l_c}{V}}\phi\left(\frac{l_c h}{k}\right)$$

**Equation 3.5**

Again, $\varphi$ is an undefined function. The dimensionless group in the brackets is known as the Nusselt number. At this point, we know that the maximum surface temperature is directly proportional to the applied heat flux, inversely proportional to the heat conductivity, and proportional to the square root of the arc length over the velocity. The nature of the function $\varphi$ is unknown. This result is not, as it stands, particularly useful since the convective heat transfer coefficient *h* is not easily determinable from grinding tests. However, examination of the standard boundary layer equations [Incropera & DeWitt 1985] reveals rigorously that, for a specific geometry, the Nusselt number is related to the Prandtl and Reynolds numbers in the following way:

$$Nu = \phi(\Pr, \mathrm{Re})$$

**Equation 3.6**

This allows equation 3.5 to be written as:

$$\theta_f = \frac{q}{\beta}\sqrt{\frac{l_c}{V}}\phi(\Pr,\mathrm{Re})$$

**Equation 3.7**

which is valid for a specific geometry. It would seem reasonable to assume that the characteristic parameters defining the wheel/workpiece contact are the arc length of contact, and the mean wheel grit spacing, $x$. The geometry specific relationship between the Nusselt, Prandtl, and Reynolds numbers can also be derived using the dimensional technique. If the dimensional technique is used it is possible to include the geometry parameters previously identified. This would, in turn, yield the following general relationship for wet grinding:

$$\theta_f = \frac{q}{\beta}\sqrt{\frac{l_c}{V}}\phi\left(\Pr,\mathrm{Re},\frac{x}{l_c}\right)$$

**Equation 3.8**

Water and oil are the two most common types of coolant used in grinding practice. In the case of air cooling a further assumption can be made. The Prandtl number is almost constant, and can therefore be removed from the expression, giving:

$$\theta_f = \frac{q}{\beta}\sqrt{\frac{l_c}{\nu}}\phi\left(\mathrm{Re},\frac{x}{l_c}\right)$$

**Equation 3.9**

This may have a possible application in dry grinding or laser welding. For oil and water cooling however, the Prandtl number varies considerably with temperature, and cannot be removed from the bracketed expression.

Expression 3.8 can be compared with the analytical solution developed by DesRuisseaux & Zerkle [DesRuisseaux & Zerkle 1970] illustrating some clear advantages of deft application of the dimensional technique. Their solution for the

$$\frac{\pi k V}{2Kq}\theta(X,Z) = \int_{X-L}^{X+L} e^{-m} K_o\left(\left[Z^2 + m^2\right]^{\frac{1}{2}}\right) dm$$
$$- \ \pi H e^{HZ} \int_0^{\infty} \tau e^{H^2\tau^2} erfc\left(\frac{Z}{2\tau} + H\tau\right)\left[ erf\left(\frac{X+L}{2\tau} + \tau\right) - erf\left(\frac{X-L}{2\tau} + \tau\right)\right] d\tau$$

steady-state two-dimensional temperature distribution on a semi-infinite plane subjected to a moving heat source and surface cooling is:

**Equation 3.10**

The expression is mathematically complex, solvable only with the aid of computational techniques. It shares a common ambiguity with the dimensional solution, namely determination of the portion of the process power that actually enters the workpiece. There is another difficulty involved in implementation of this formula. This is determination of the convective heat transfer coefficient necessary to calculate the *H* term. It is not possible to measure the convective heat transfer coefficient during grinding trials, due to lack of determinability of the energy partitioning during actual grinding. That is to say, the amount of energy entering the coolant is not determinable. In order to measure the convective heat transfer coefficient, an experimental rig similar to that of Powell & Howes [Powell & Howes 1978] would be necessary. This rig uses a heating element to simulate heat generated in the grinding process, thereby allowing direct determination of the energy entering the coolant. The dimensional solution on the other hand, avoids this difficulty as the convective heat transfer coefficient does not explicitly appear in the solution. The Prandtl number, Reynolds number, and geometry factor can all be measured during an actual grinding test. The material properties of the Prandtl and Reynolds numbers can be evaluated at the film temperature, and the coolant velocity (for some common wheel types) can be found from Malkin *et. al.* [Malkin *et. al.* 1999], and Engineer *et. al.* [Engineer *et. al.*1992]. One further advantage of using the dimensional solution arises from the fact that any measurements taken would be taken during an actual grinding test, rather than from a simulated test, which will always be an approximation of reality.

As has been shown, the dimensional technique can be used, in combination with physical knowledge, to arrive at relatively simple solutions to complex problems, and to provide a basis for experimental rigs, or numerical modelling.

# Chapter 4

# Tensile Residual Stresses in Grinding

## 4.1 Introduction

The remaining surface layer of practically every ground component contains residual stresses. These stresses can be either tensile or compressive in nature. Compressive stresses are by far the more preferable of the two, acting against fatigue-type component failure. By corollary, tensile residual stresses are not desirable, as they can be close to the ground material's yield strength, aiding fatigue failure of the component. Compressive residual stresses are caused by the wheel grits leaving a plastically deformed layer on the surface of the ground component. The depth of this layer is limited to 5-10μm [Snoeys *et. al.* 1978]. Tensile residual stresses are associated with higher grinding temperatures. The surface layer of the workpiece is exposed to high temperatures, which cause thermal expansion. The top layer of the workpiece is constrained by the bulk material underneath, it being thermally unloaded. This causes the top layer to experience compressive stresses. If the thermal expansion is sufficiently large, then the compressive stresses in the top layer will exceed the yield stress of the material. When the thermal loading is removed, the top layer is elastically unloaded. Because the top layer has been plastically deformed, it does not return to it's original shape, and tensile residual stresses result. The process can be detailed, in principle, on a simplified single degree of freedom stress-strain diagram. Figure 4.1 shows the thermal loading cycle, and the associated stress-strain cycle. At $t_o$, the top layer and bulk material are in equilibrium, experiencing no

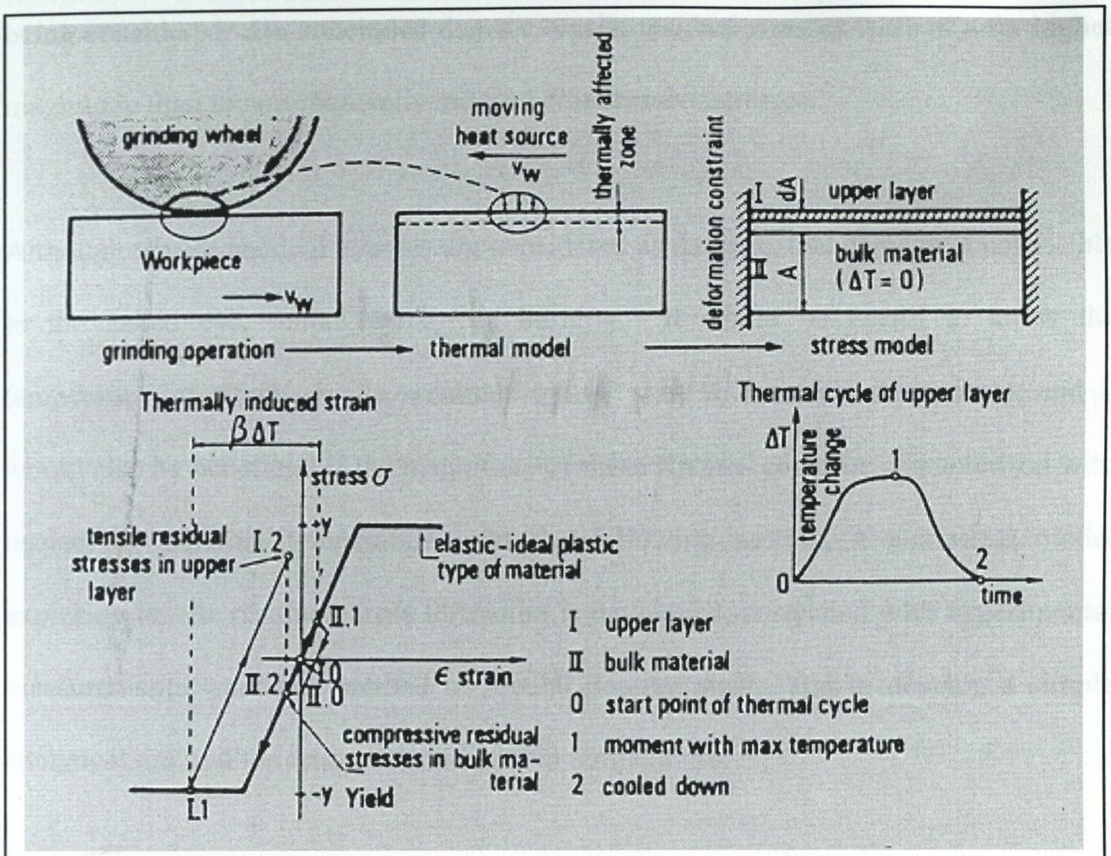

**Figure 4.1 – Tensile residual stress formation**

stress. At $t_1$, the top layer has yielded in compression, and the bulk material is tension, satisfying equilibrium. At $t_2$, the top layer has been elastically unloaded, and remains in tension, and the bulk material is now in compression. The magnitude of the compressive residual stress in the bulk material is considerably lower than the magnitude of the tensile residual stress in the top layer. This representation does not take account of directional effects, which may occur in grinding practice.

To date, no analytical models exist which allow tensile residual stresses to be calculated. This is due firstly to the transient nature of the thermal loading, and secondly to the coupled nature of the thermal and mechanical aspects of the problem. One prior attempt was made by Mishra [Mishra *et. al.*1977] to calculate residual stresses using the finite element technique. He did not specify what material was being considered. He concluded that the tensile residual stresses were of a far higher magnitude than the mechanically induced compressive stresses.

Although tensile residual stresses are considered as damage, this damage is not visible to the naked eye, unlike workpiece burning. It would be useful to know the temperature at which tensile residual stresses start to manifest themselves, and it would also be beneficial if the magnitude of these stresses could be characterised with respect to grinding temperature. In the following section, a numerical model exploring tensile residual stress formation is developed, correlated with experimental measurements, and then applied to several popular steels, and to develop a simple analytical method for estimating the critical temperature.

The approach taken in this work was thus semi-analytical. The finite element model was used to predict the critical temperature at which tensile residual stress formation began, and the magnitude of these stresses at higher temperatures. The dimensional technique was used to develop a characteristic relationship for the magnitude of the maximum tensile residual stress in the model between the critical temperature and the austenising temperature of the material. The model was validated with experimental measurements of residual stress and surface temperature, and subsequently used to examine other steels used in industry.

## 4.2 Theoretical Analysis

The first part of the analysis consisted of deriving a parametric model of the problem. As pointed out previously, it is necessary to identify the parameters of interest prior to application of the Buckingham Pi theorem. Examination of the literature suggests that the following parameters are likely to have a strong influence on thermally induced residual stresses: the maximum surface temperature, the coefficient of thermal expansion as a function of temperature, the modulus of elasticity as a function of temperature, and the yield stress, also as a function of temperature.

It is assumed that a band heat source moves with a velocity across a semi-infinite plane (figure 3.1), thus producing a temperature field in the workpiece. It is furthermore assumed that, after a certain time has elapsed, the temperature field is quasi-stationary. This means that an observer moving with the same velocity as the heat source would not observe any change in the workpiece temperature distribution. This is generally the case in shallow-cut grinding practice, where the grinding wheel is modelled as a moving band heat source [Shaw 1996]. This model is based, in principle, on the commonly used Jaeger model. The Jaeger based models have been shown to be capable of predicting grinding temperatures, and the purpose of the ensuing analysis is to correlate maximum surface temperatures with maximum tensile residual stresses. The fundamental dimensions used for this analysis were force (F), length (L), and temperature($\Theta$). For this case, the relevant parameters and their fundamental dimensions are:

$\theta$= maximum work temperature rise[$\Theta$]

$\alpha$(T)= coefficient of thermal expansion [$\Theta^{-1}$]

$E$(T)= modulus of elasticity[$FL^{-2}$]

$Y$(T)= yield stress[$FL^{-2}$]

$\sigma_r$= maximum residual tensile stress[$FL^{-2}$]

There are five variables, and three fundamental quantities. This means there will be two Pi groups. The Buckingham Pi theorem yields the following parameters:

$$\varphi\left(\frac{\theta.\alpha(T).E(T)}{Y(T)}, \frac{Y(T)}{\sigma_r}\right) = A$$

**Equation 4.1**

where A is a non-dimensional constant, and $\varphi$ is an unspecified function. This can be rewritten as:

$$\sigma_r = Y(T)\varphi_1\left(\frac{\theta.\alpha(T).E(T)}{Y(T)}\right)$$

**Equation 4.2**

Thus, the residual stress is a function of the yield stress at a particular temperature, and the dimensionless Pi group contained inside the brackets, and $\varphi_1$ is again an unspecified function.

## 4.3 Finite Element Modelling

The generation of thermally induced residual stresses was modelled using the finite element method. This was done using an indirectly coupled thermo-mechanical analysis. Essentially, a model representing a workpiece was subjected to a moving band heat source. The model was loaded with a heat flux at a particular point in time. The load was then time-incrementally moved along the model. After several increments, the temperature solution became quasi-stationary, and the loading was continued for a reasonable distance. For the last load case, a uniform temperature field representing ambient temperature was applied. This represented the cooling of the workpiece to room temperature after the thermal load was removed. The temperature distribution obtained at each time point was stored. Thus a series of temperature

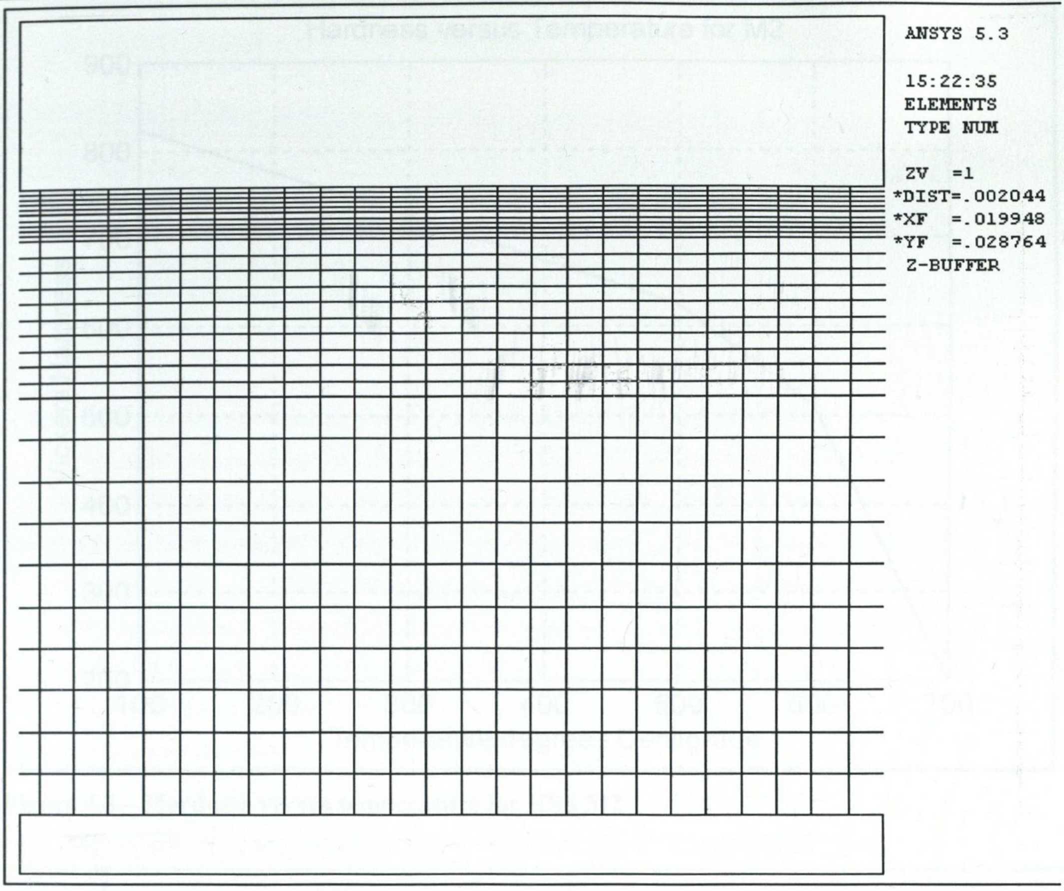

**Figure 4.2 – Finite element mesh**

distributions at incremental points in time were obtained. These temperature fields were applied as loads on an identical model meshed with structural elements. The residual stresses were then taken to be the stresses in the model when the thermal load cycle was completed.

The workpiece was modelled in two-dimensions, with plane-strain conditions prevailing. The finite element model was densely meshed in the region just below the surface. This is where the thermal gradient is highest, and also the region where plastic yielding will occur if the thermal stresses exceed the yield stress. Figure 4.2 illustrates this. The model depth in this figure is 3mm. The material used in the analysis was M2, a high-speed steel suitable for cutting tools. The material properties

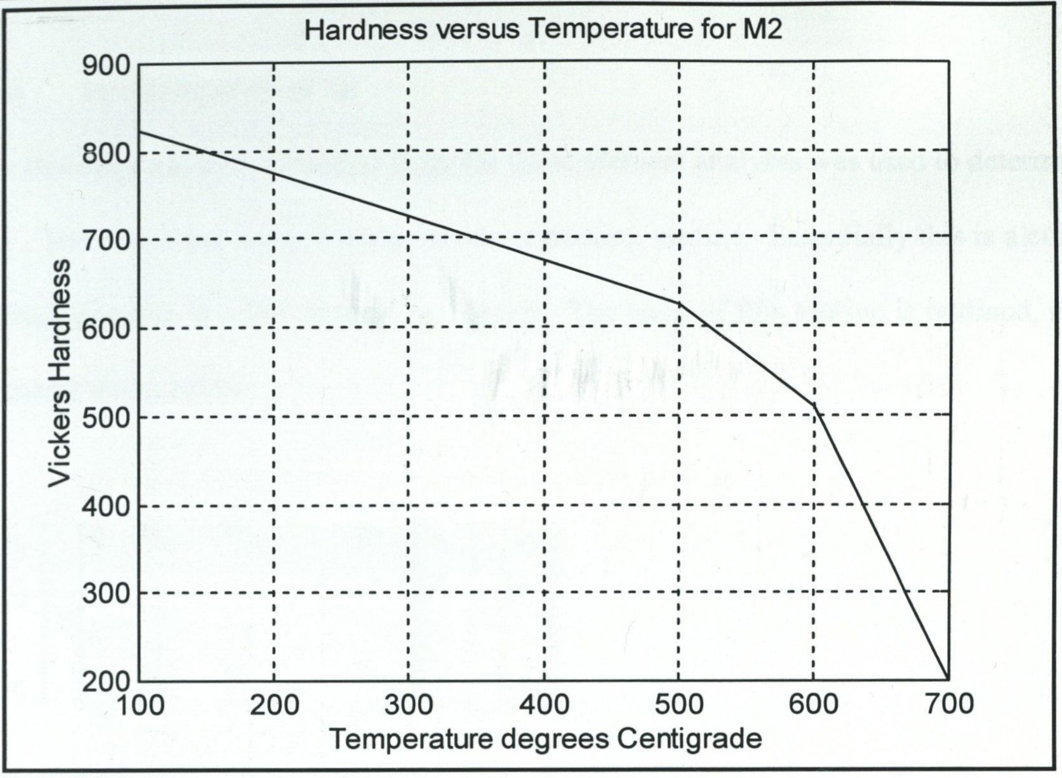

**Figure 4.3 – Hardness versus temperature for HSS M2**

are shown in table 4.4 (page 75). It is a hardened steel, with good hot hardness characteristics. Between 600°C and 700°C the hardness drops considerably. The yield stress values were calculated from hot hardness measurements. Figure 4.3 shows the variation of hardness with temperature. There was no information available regarding the Young's Modulus after yielding. However, because M2 has high hardness at low temperatures, it was assumed that the steel could accept little plastic strain at these temperatures. By corollary, when the temperature is higher, and the steel softer, the assumption was made that the steel could accept large amounts of plastic strain.

The yield behaviour was consequently modelled using a bilinear isotropic hardening law. In addition, the thermo-mechanical material properties were fully specified over the relevant temperature range.

## 4.4 Determination of $\varphi_1$

At this stage the data compiled from the finite element analyses was used to determine $\varphi_1$. This was done using a multi-variate regression routine. Essentially this is a curve fitting exercise in multi-dimensional space. The basis of this routine is outlined, in a general sense, below.

$$\begin{bmatrix} n_1 \\ n_2 \\ : \\ n_i \end{bmatrix} = \begin{bmatrix} 1 & Pi_{11} & Pi_{21} & \sim & Pi_{j1} \\ : & : & : & & : \\ : & : & : & & : \\ 1 & Pi_{1i} & Pi_{2i} & & Pi_{ji} \end{bmatrix} \begin{bmatrix} b_0 \\ b_1 \\ : \\ b_i \end{bmatrix} + \begin{bmatrix} e_1 \\ e_2 \\ : \\ e_i \end{bmatrix}$$

**Equation 4.3**

or

$$[N] = [Pi][B] + [E]$$

**Equation 4.4**

$N$ =vector of resultant data

$Pi$ =matrix of expected predictors

$E$ =vector of error terms

$B$ =vector of coefficients to be calculated

The vector containing the $b$ terms is calculated so that the error is minimised in a least squares sense. Thus the $b$ coefficients are given by:

$$[B] = [Pi'.Pi]^{-1}.[Pi'][N]$$

**Equation 4.5**

This gives a result of the following form:

$$n = b_0 + b_1 * Pi_1 + b_2 * Pi_2 + \ldots\ldots. b_n * Pi_n$$

**Equation 4.6**

The Pi matrix contains a set of predictors. These predictors can be the Pi groups derived earlier, or indeed, any combination of these Pi groups. A degree of serendipity may be required at this stage to determine any cross correlation between groups. In this case, it was found that an excellent correlation was achieved using a cubic function of the Pi group derived earlier in equation 4.2.

The choice of function is at the discretion of the analyst. In this particular case, it was required to find a function to fit data over a limited range. The cubic polynomial was chosen in this case because it allowed a fast, simple, and accurate fit for the numerical data.

The predictor matrix in this case takes the following form:

$$Pi = \begin{bmatrix} 1 & Pi_{11}^{1} & Pi_{12}^{2} & Pi_{13}^{3} \\ 1 & Pi_{21}^{1} & Pi_{22}^{2} & Pi_{23}^{3} \\ 1 & Pi_{31}^{1} & Pi_{32}^{2} & Pi_{33}^{3} \\ 1 & Pi_{41}^{1} & Pi_{42}^{2} & Pi_{43}^{3} \end{bmatrix}$$

An assurance criterion was used to assess the quality of the derived formula with the actual results. This measured the least squares deviation of the predicted concentration from the measured concentration. A value of unity indicates perfect correlation, whereas a value of zero indicates no correlation. This criterion is defined as:

$$AC=\frac{\left(\sum_{j=1}^{n}(\varphi_x)_j(\varphi_p)_j^{'}\right)^2}{\left(\sum_{j=1}^{n}(\varphi_x)_j(\varphi_x)_j^{'}\right)\left(\sum_{j=1}^{n}(\varphi_p)_j(\varphi_p)_j^{'}\right)}$$

**Equation 4.7**

$\varphi_x$= vector of measured parameters

$\varphi_p$= vector of predicted parameters

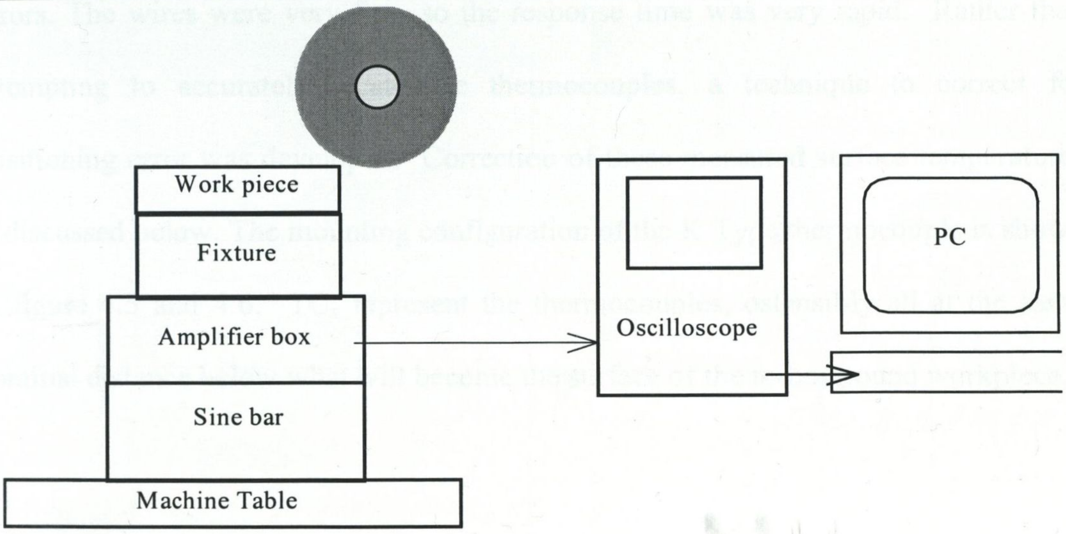

**Figure 4.4 – Experimental rig**

## 4.5 Experimental Method

This experimental section is abstracted from Walsh *et. al.* [Walsh *et. al.* 1998]. All the experimental tests were carried out by members of SIMR (The Swedish Institute for Metals Research). The residual stress measurements were measured from a workpiece ground in the following fashion. Essentially, a workpiece is fixed on a sine bar, as illustrated in figure 4.3. The sine bar allows the workpiece to be inclined at an angle relative to the datum. Thus, as the grinding wheel traverses the workpiece, the depth of cut increases according to the angle of inclination of the workpiece, a technique known as "wedge grinding".

The temperature measurements were made in the following fashion. It was decided to measure the temperature distribution in wedge grinding using three standard K type thermocouples. The main problem associated with this enterprise was the location of the three thermocouples at the same distance from the free surface. Since the thermal gradient close to the ground surface is usually very steep, the error associated with the location of the three thermocouples at different depths could result in substantial errors. The wires were very fine, so the response time was very rapid. Rather than attempting to accurately locate the thermocouples, a technique to correct for positioning error was developed. Correction of these measured surface temperatures is discussed below. The mounting configuration of the K Type thermocouple is shown in figure 4.5 and 4.6. $TC_x$ represent the thermocouples, ostensibly all at the same nominal distance below what will become the surface of the to-be-ground workpiece.

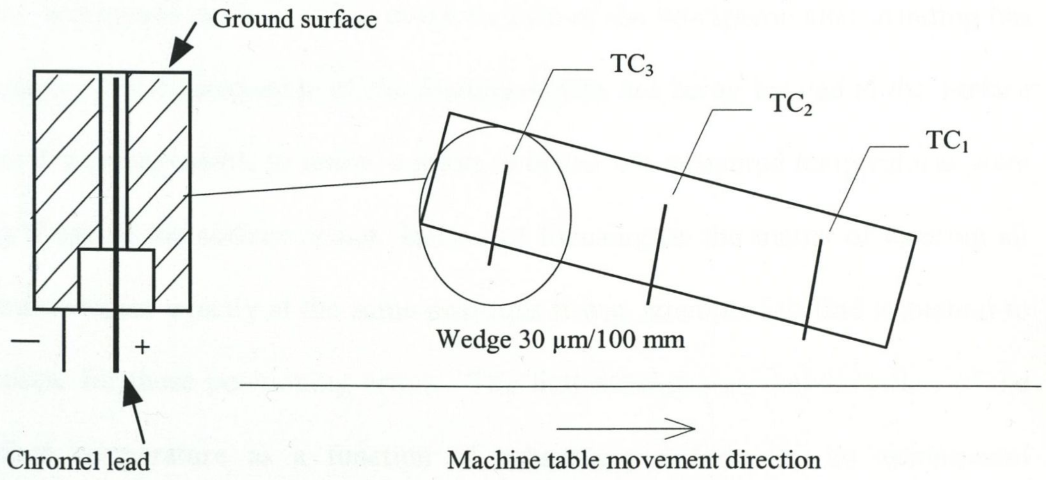

**Figure 4.5 – Thermocouple mounting arrangement**

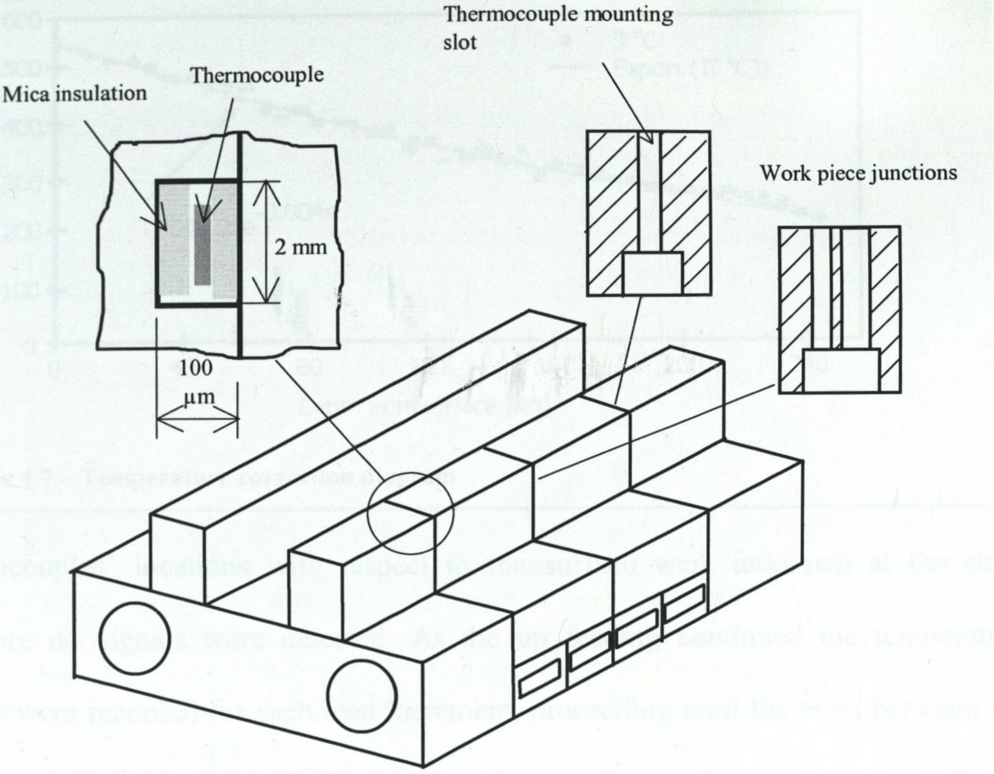

Figure 4.6 – Thermocouple mounting arrangement

## 4.6 Correction of the measured temperatures

Locating the standard K Type thermocouples at the work piece surface with the present fixture configuration proved to be difficult and time consuming. In all cases, the term 'workpiece surface' refers to the surface of the workpiece after grinding has taken place. The consequence of the thermocouples not being located at the surface was that it was impossible to know, a priori, whether the measured temperatures were actually those of the surface or not. Instead of focusing on the matter of locating all the thermocouples exactly at the same positions it was attempted to find a method to compensate for these positioning errors. The first attempt was determination of the subsurface temperature as a function of subsurface distance by an incremental material removal by using a 6 µm feed increment and a table speed of 4 m/min. The

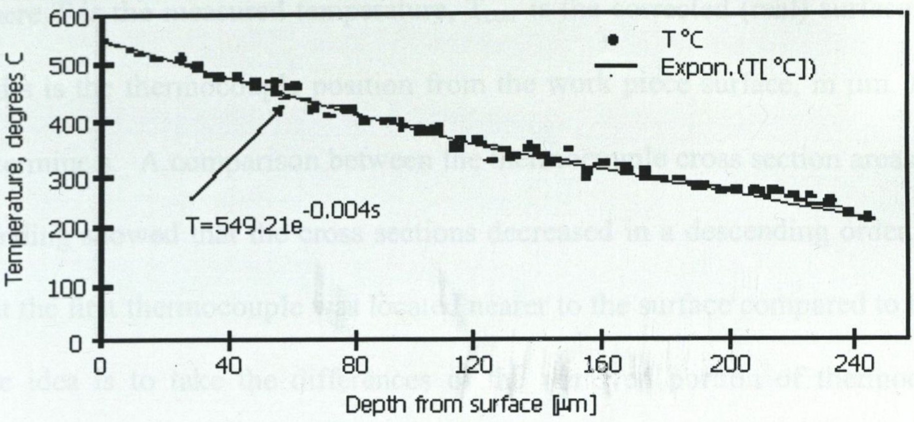

**Figure 4.7 – Temperature correction diagram**

thermocouples' locations with respect to the surface were unknown at the start, therefore no signals were detected. As the up feeding continued the temperature signals were recorded for each feed increment, proceeding until the bond between the thermocouple leads was broken. In order to keep the workpiece and the thermocouples temperature at a fixed ambiguous level, a holding time of 90 sec was introduced between each two successive steps. The result of these trials are shown in figure 4.7 where the recorded temperature is plotted as function of feed increment.

The temperature gradient is independent of the wheel depth of cut for a given material, which means that the curve is only offset up or down. The rate at which heat diffuses in a given material is an intrinsic material property. From this, a general form of equation 4.8 can be applied to the measured temperatures, yielding equation 4.9:

$$T = T_{corr} e^{-0.004s}$$

**Equation 4.8**

$$T_{corr} = Te^{0.004s}$$

**Equation 4.9**

where T is the measured temperature, $T_{corr}$ is the corrected (real) surface temperature and s is the thermocouple position from the work piece surface, in μm. It remains to determine s. A comparison between the thermocouple cross section areas after wedge grinding showed that the cross sections decreased in a descending order. This means that the first thermocouple was located nearer to the surface compared to the latter etc. The idea is to take the differences of the removed portion of thermocouples as a measure of the expected temperature level if there were no differences. This means that the correction would be unnecessary if the ground portion of thermocouples were equal. In this case, the second thermocouple was 25 mm lower than the first thermocouple, and the third thermocouple was 46 mm lower than the first thermocouple. Using these differences in the removed height differences of thermocouples the correction distance s was calculated, and applied with equation 4.9 to calculate the corrected temperature. This calculation is based on knowledge of the initial thermocouple height, and the amount of thermocouple ground during the tests. According to this the result of the above calculation is presented in table 4.1.

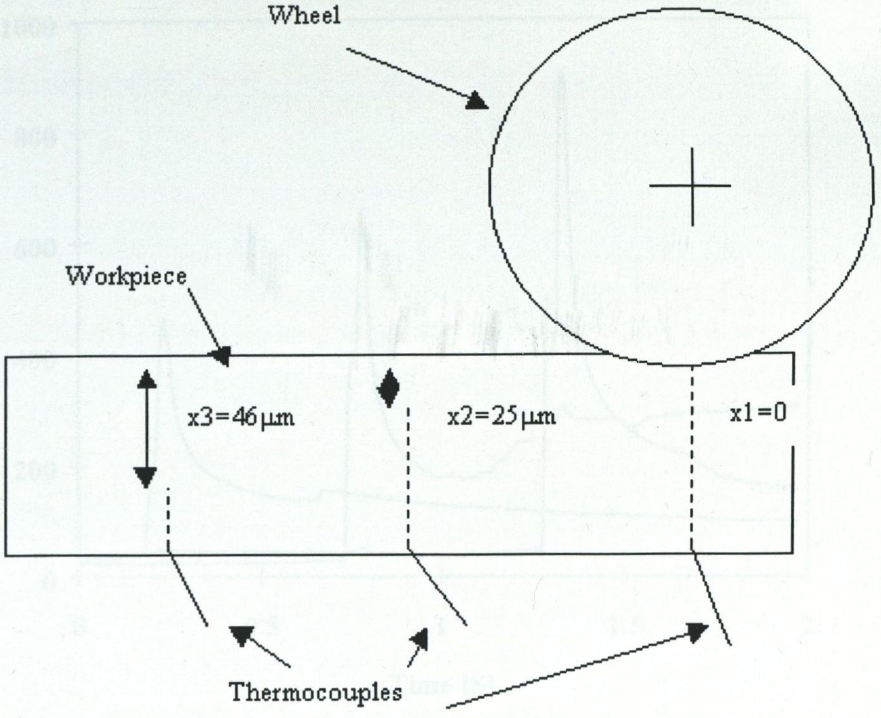

**Figure 4.8 – Relative thermocouple locations**

| $h_1$ [µm] | $h_2$ [µm] | $h_3$ [µm] | $L_1$ [µm] | $L_2$ [µm] | $L_3$ [µm] | $s_2$ [µm] | $s_3$ [µm] |
|---|---|---|---|---|---|---|---|
| 96 | 71 | 51 | 855 | 741 | 635 | 25 | 46 |

**Table 4.1**

where L is the remaining thermocouple cross section length and h is the thermocouple ground height. Using the uncorrected temperatures $T_2$ and $T_3$, the corresponding height differences $x_1$ and $x_2$ and equation 4.9, the corrected temperatures $T_{2corr}$ and $T_{3corr}$ were calculated. The original temperatures and those of corrected are presented in table 4.2. The value of x is used in microns in equation 4.9.

| Temperature [°C] | $T_1$ | $T_2$ | $T_3$ |
|---|---|---|---|
| Uncorrected | 480 | 615 | 759 |
| Corrected | 480 | 680 | 912 |

**Table 4.2**

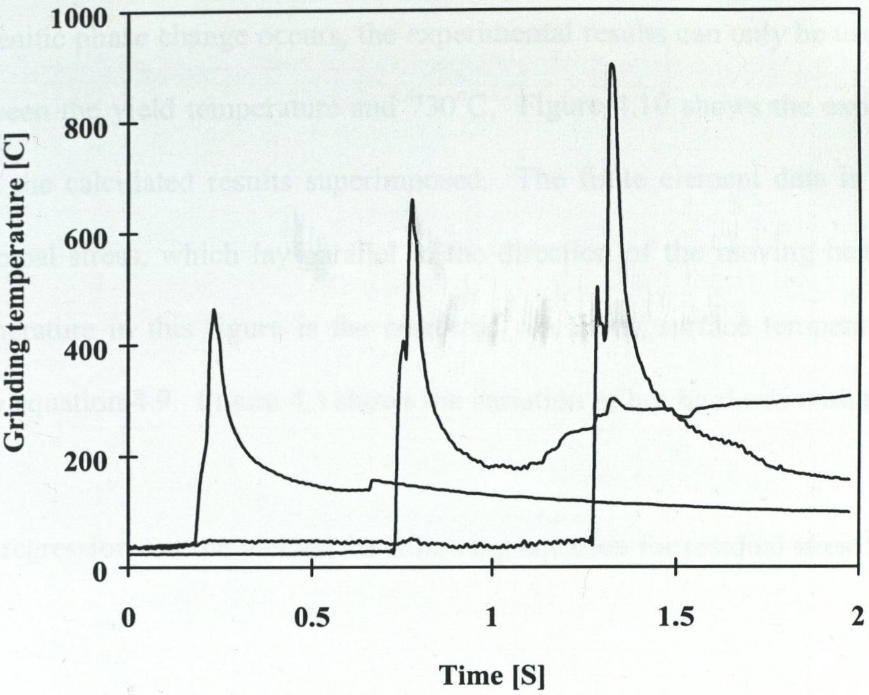

**Figure 4.9 – Temperature trace from wedge grinding pass**

Figure 4.9 shows a temperature trace for a wedge grinding pass.

The residual stress was measured using the x-ray diffraction technique. This technique is well documented in [Erko & Arotov 1996]. Essentially, the lattice spacing is measured using a laser coupled with an application of Braggs law. From this spacing the residual strains can be measured. These residual strains can be subsequently related to the residual stress in the material.

### 4.7 Results and Discussion

A simple hand calculation indicates that the thermal strain will not reach 1% until a temperature of about 600°C is reached. This was roughly found to be the case in the finite element model. Some experimental results were available, showing the level of residual stress measured as a function of grinding temperature. These results go as high as 950°C, which is above the austenising temperature of M2. Since the finite element calculations did not take any account of the volume change when the austenitic phase change occurs, the experimental results can only be used in the range between the yield temperature and 730°C. Figure 4.10 shows the experimental data with the calculated results superimposed. The finite element data is the maximum principal stress, which lay parallel to the direction of the moving heat source. The temperature in this figure is the corrected remaining surface temperature computed from equation 4.9. Figure 4.3 shows the variation of hot hardness with temperature.

The regression routine yielded the following equation for residual stress:

| $b_0$ | $b_1$ | $b_2$ | $b_3$ |
|---|---|---|---|
| -0.7611 | 0.2885 | 0.0791 | -0.0051 |

**Table 4.3**

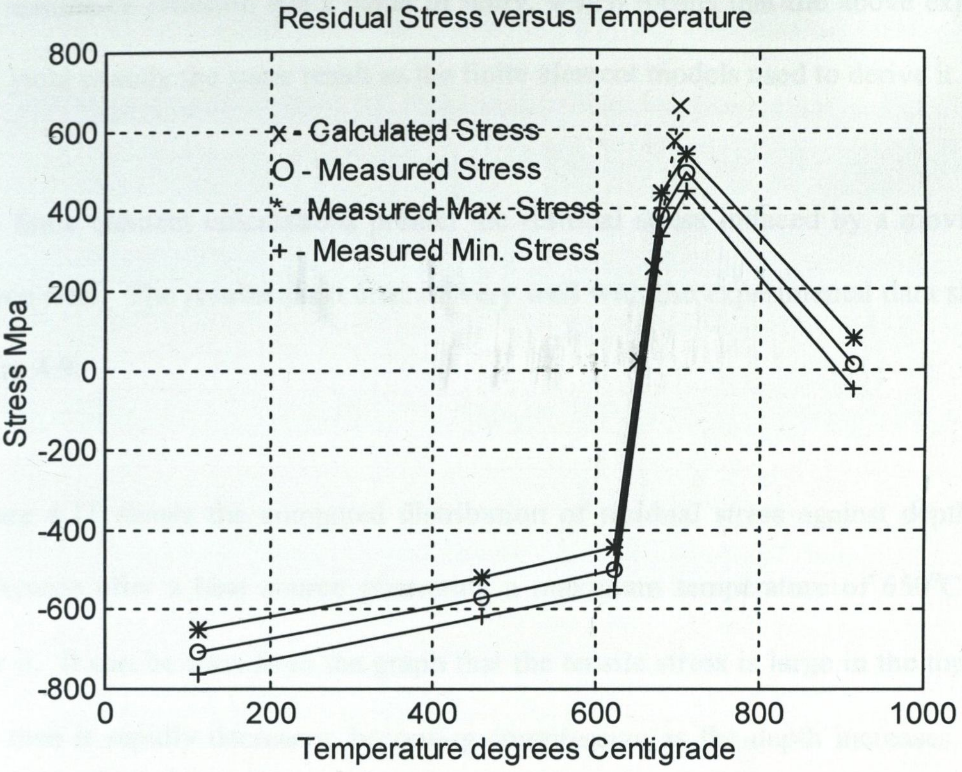

**Figure 4.10 – Measured and computed residual stresses**

$$\frac{\sigma_r}{Y(T)} = b_0 + b_1.Pi + b_3.Pi^2 + b_4.Pi^3$$

**Equation 4.10**

or

$$\sigma_r = Y(T).\left(b_0 + b_1.Pi + b_3.Pi^2 + b_4.Pi^3\right)$$

**Equation 4.11**

where

$$Pi = \frac{\theta.\alpha(T).E(T)}{Y(T)}$$

**Equation 4.12**

The assurance criterion yielded the following value for the regression calculation:

**Assurance Criterion** = 1

The assurance criterion has a value of unity, which means that the above expression will yield exactly the same result as the finite element models used to derive it.

The finite element calculations predict the residual stress induced by a moving heat source well. The results also correlate very well with the experimental data shown in figure 4.9.

Figure 4.11 shows the computed distribution of residual stress against depth in the workpiece after a heat source generating a maximum temperature of 650°C passed over it. It can be seen from the graph that the tensile stress is large in the top 30μm, and then it rapidly decreases, becoming compressive as the depth increases. These compressive stresses are of a far lower magnitude than the tensile stresses in the surface region.

The simple model proposed demonstrates a good correlation with actual grinding tests, despite the inherent assumptions. The model assumes a band source of infinite width, which is never the case in grinding practice. The austenitic phase change is not included in the model, since this constitutes a damage regime over and above tensile residual stress. In terms of actual grinding, the workpiece temperature would probably be lower near the edges of the workpiece, and resultant residual stresses of lower magnitude in these regions. It is, however, the maximum temperature and residual stress which is of importance, and the model seems to give good predictions in this respect. The actual grinding conditions during the tests are of secondary importance. The thrust of the testing centred around measuring a surface temperature,

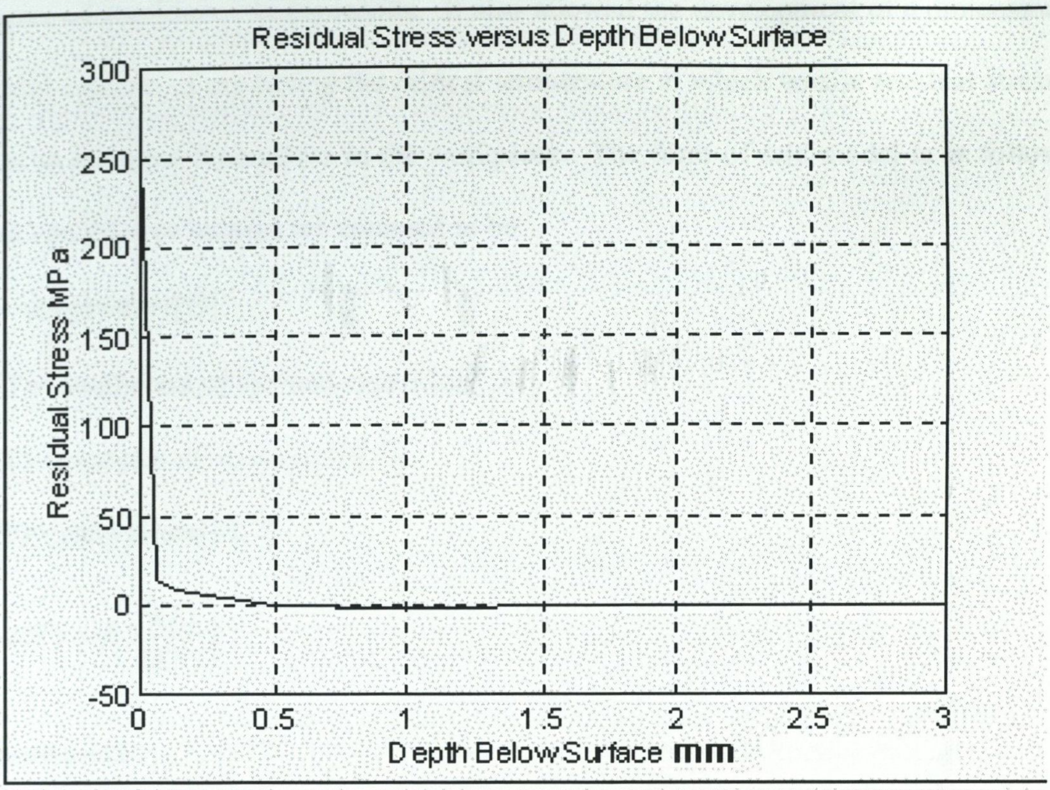

**Figure 4.11 – Residual stress versus depth**

(which has been generated by arbitrary grinding conditions), and correlating this with resultant residual stresses.

The technique used to generate equation 4.11 provides a reasonably straightforward method which allows a simple functional relationship between the tensile residual stress, the maximum surface temperature, and the materials mechanical properties. It is possible to use the same general relationship derived earlier to characterise more than one material. The primary difficulty with this is acquiring the material properties as a function of temperature.

## 4.8 Exploitation of Model

The finite element models accurately predicts the tensile residual stress formation, as a function of temperature. This allowed the model to be applied to other steels, with a degree of confidence in the results. It also allowed the development of a dimensional model capable of predicting the critical temperature at which tensile residual stresses start to manifest themselves in the workpiece. The form of said model is as follows. The variables of interest are assumed to be:

$\theta$= temperature[$\Theta$]

$\alpha$(T)= coefficient of thermal expansion[$\Theta^{-1}$]

$E$(T)= modulus of elasticity[$FL^{-2}$]

$Y$(T)= yield stress[$FL^{-2}$]

$$\theta.\alpha(T) = \phi\left(\frac{Y(T)}{E(T)}\right)$$

**Equation 4.13**

Y(T)/E(T) is the yield strain, allowing equation 4.13 to be written as:

$$\theta.\alpha(T) = \phi(\varepsilon)$$

**Equation 4.14**

The analysis was performed on seven steels in total. The material properties, and hot hardness data, for these materials are detailed below.

| **M2** | | **Temperature $^{o}$C** | |
|---|---|---|---|
| | **20** | **400** | **600** |
| **Density kg/m$^3$** | 8160 | 8060 | 8000 |
| **Youngs Modulus kN/mm$^2$** | 225 | 200 | 180 |
| **Thermal expansion ratio from 20 $^{o}$C 1/ $^{o}$C** | - | 12.1e-6 | 12.6e-6 |
| **Thermal conductivity W/mK** | 24 | 28 | 27 |
| **Specific heat J/kgK** | 420 | 510 | 600 |

**Table 4.4**

| **ASP2017** | | **Temperature °C** | |
|---|---|---|---|
| | **20** | **400** | **600** |
| **Density kg/m$^3$** | 7975 | 7870 | 7800 |
| **Youngs Modulus kN/mm$^2$** | 235 | 210 | 190 |
| **Thermal expansion ratio from 20 °C 1/°C** | - | 12.1e-6 | 12.7e-6 |
| **Thermal conductivity W/mK** | 24 | 27.5 | 29 |
| **Specific heat J/kgK** | 420 | 510 | 600 |

**Table 4.5**

| **ASP2023** | | **Temperature °C** | |
|---|---|---|---|
| | **20** | **400** | **600** |
| **Density kg/m$^3$** | 8050 | 7940 | 7875 |
| **Youngs Modulus kN/mm$^2$** | 230 | 205 | 184 |
| **Thermal expansion ratio from 20 °C 1/°C** | - | 12.1e-6 | 12.6e-6 |
| **Thermal conductivity W/mK** | 24 | 28 | 27 |
| **Specific heat J/kgK** | 420 | 510 | 600 |

**Table 4.6**

| **ASP2060** | | **Temperature °C** | |
|---|---|---|---|
| | **20** | **400** | **600** |
| **Density kg/m$^3$** | 7960 | 7860 | 7810 |
| **Youngs Modulus kN/mm$^2$** | 250 | 222 | 200 |
| **Thermal expansion ratio from 20 °C 1/°C** | - | 10.6e-6 | 11.1e-6 |
| **Thermal conductivity W/mK** | 24 | 28 | 27 |
| **Specific heat J/kgK** | 420 | 510 | 600 |

**Table 4.7**

| **QRO 90** | | **Temperature °C** | |
|---|---|---|---|
| | **20** | **400** | **800** |
| **Density kg/m$^3$** | 7800 | 7700 | 7550 |

| | | | |
|---|---|---|---|
| **Youngs Modulus kN/mm$^2$** | 202 | 175 | 130 |
| **Thermal expansion ratio from 20 °C 1/°C** | - | 12.6e-6 | 13.9e-6 |
| **Thermal conductivity W/mK** | 31 | 32 | 30 |
| **Specific heat J/kgK** | 410 | 510 | 600 |

**Table 4.8**

| **AISI D2** | | **Temperature °C** | |
|---|---|---|---|
| | **20** | **200** | **400** |
| **Density kg/m$^3$** | 7700 | 7650 | 7600 |
| **Youngs Modulus kN/mm$^2$** | 193 | 188 | 173 |
| **Thermal expansion ratio from 20 °C 1/°C** | - | 12.4e-6 | 13.4e-6 |
| **Thermal conductivity W/mK** | 20 | 21 | 23 |
| **Specific heat J/kgK** | 460 | 530 | 610 |

**Table 4.9**

| **EN31** | | **Temperature °C** | |
|---|---|---|---|
| | **100** | **400** | **600** |
| **Density kg/m$^3$** | 7810 | - | - |
| **Youngs Modulus kN/mm$^2$** | 210 | - | - |
| **Thermal expansion ratio from 20 °C 1/°C** | - | 14e-6 | 14.5e-6 |
| **Thermal conductivity W/mK** | 37 | 38 | 36 |
| **Specific heat J/kgK** | 481 | 507 | - |

**Table 4.10**

The following graphs show the results of the finite element calculations for the steels detailed above. In the case of EN31, some experimental data was available (the maximum principle residual stress), and is superimposed on the results from the numerical model.

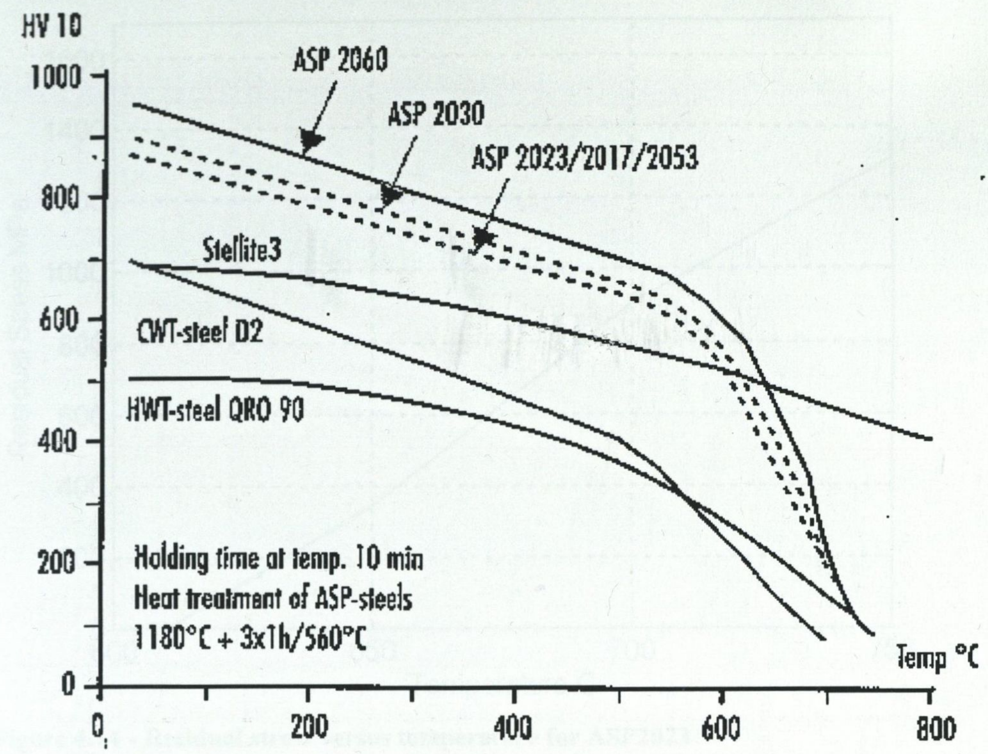

Figure 4.12 – Hardness versus temperature for various steels

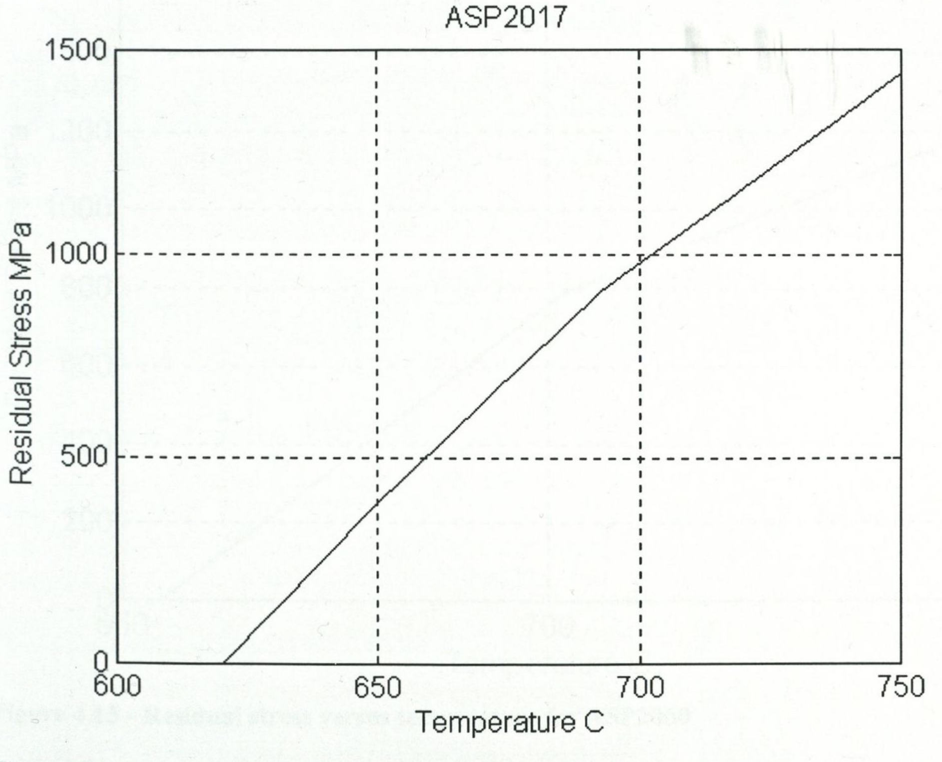

Figure 14.13 – Residual stress versus temperature for ASP2017

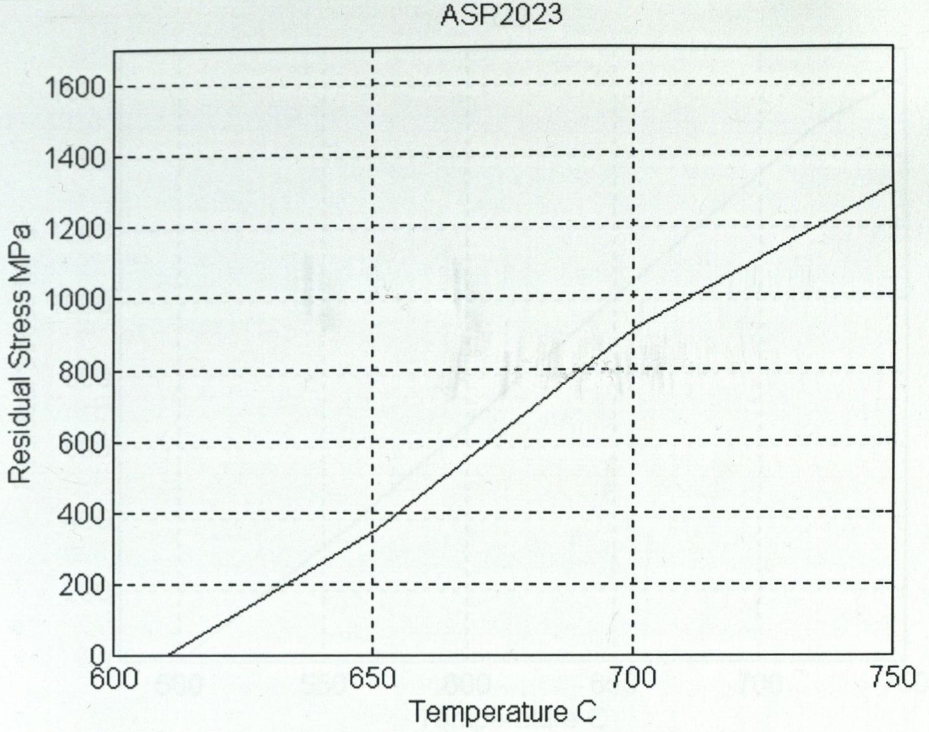

Figure 4.14 - Residual stress versus temperature for ASP2023

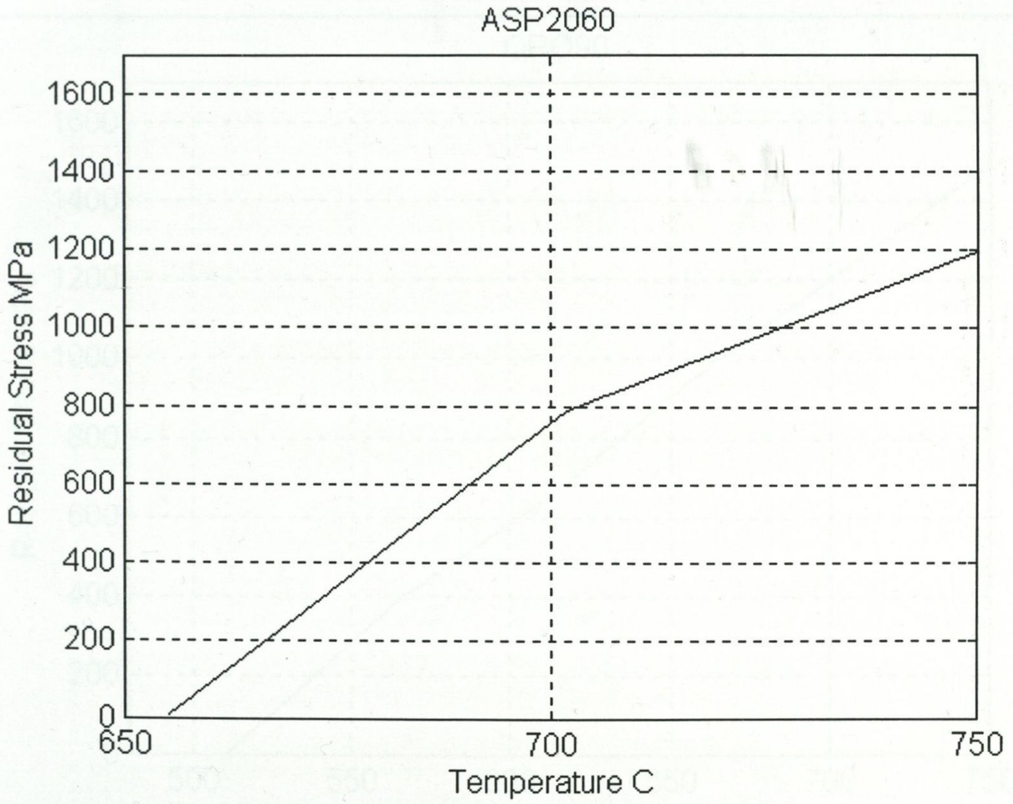

Figure 4.15 - Residual stress versus temperature for ASP2060

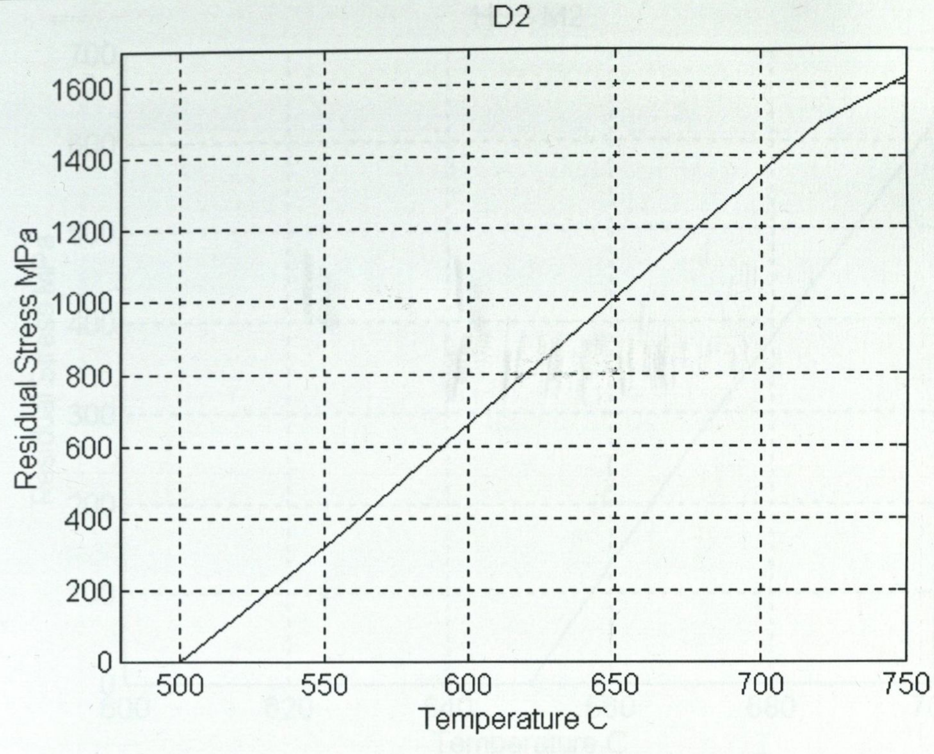

Figure 4.16 - Residual stress versus temperature for AISI D2

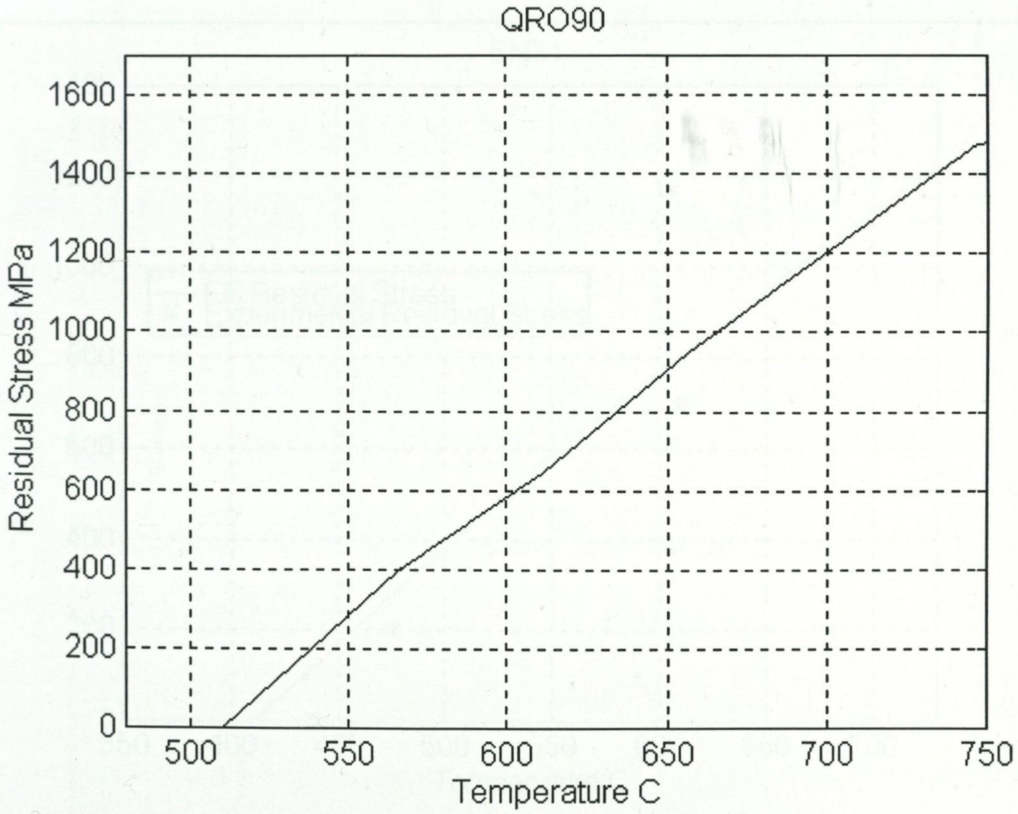

Figure 4.17 - Residual stress versus temperature for QRO90

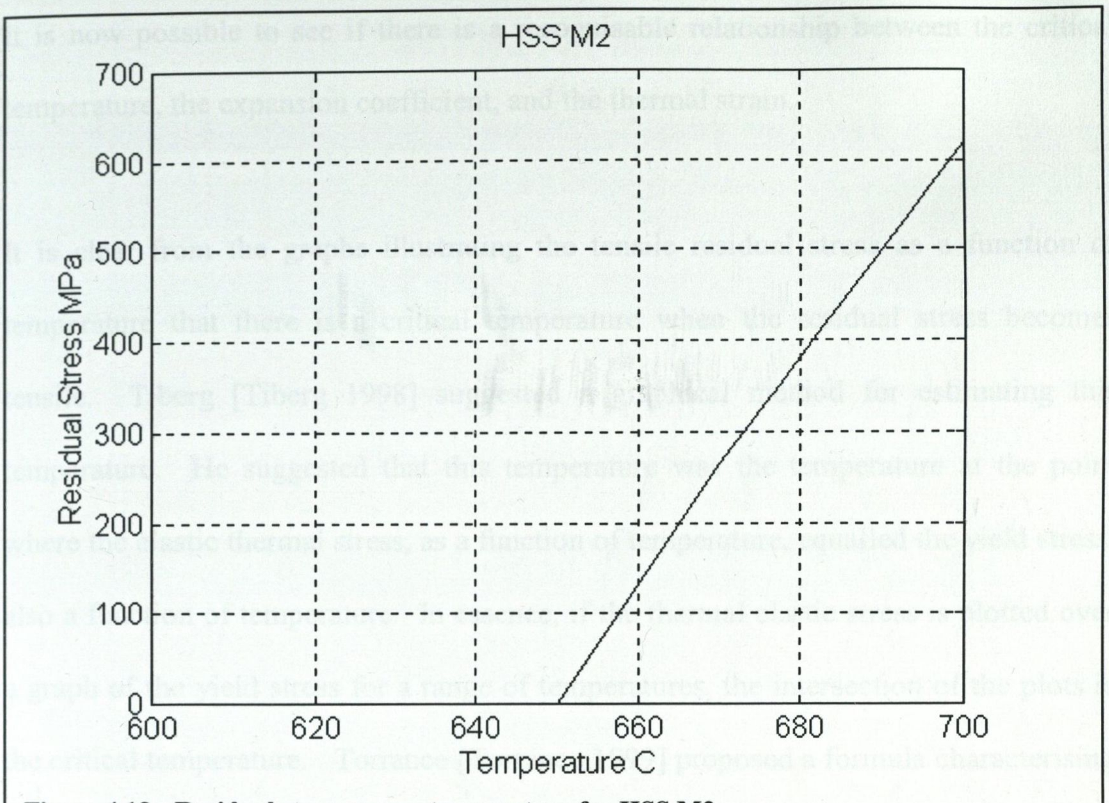

Figure 4.18 - Residual stress versus temperature for HSS M2

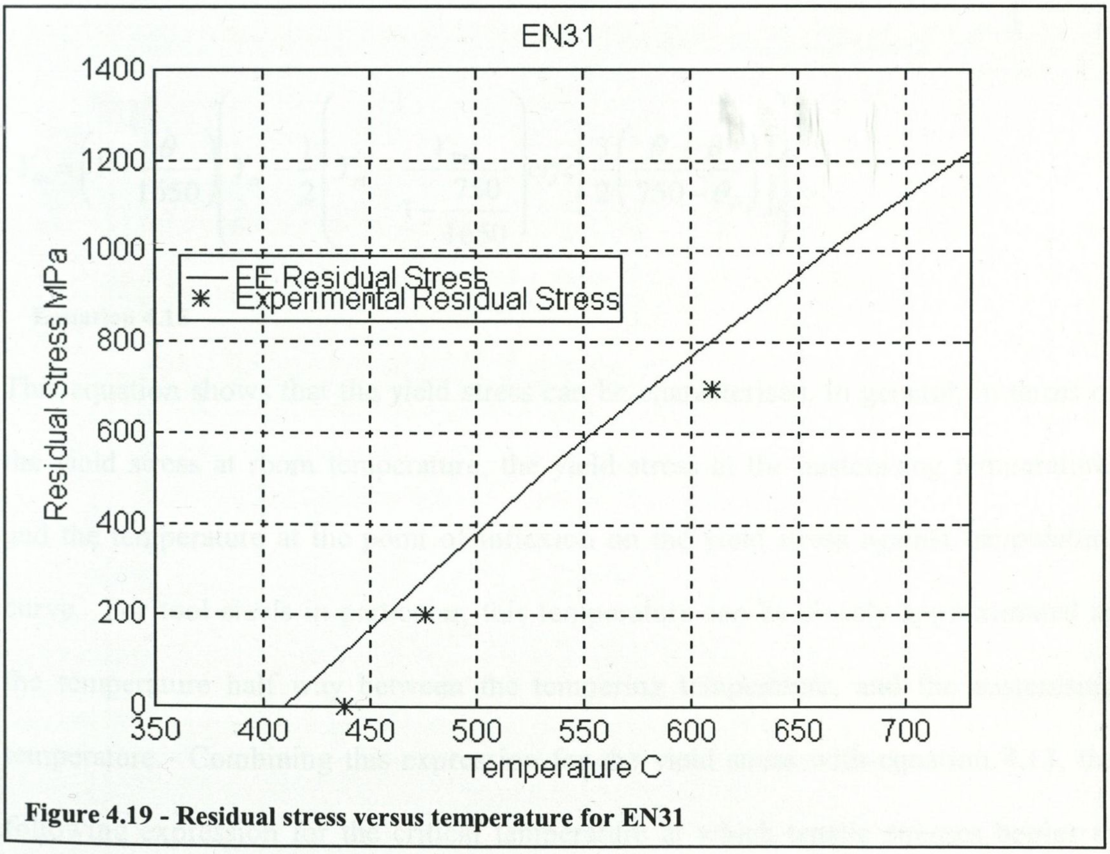

Figure 4.19 - Residual stress versus temperature for EN31

It is now possible to see if there is a recognisable relationship between the critical temperature, the expansion coefficient, and the thermal strain.

It is clear from the graphs illustrating the tensile residual stress as a function of temperature that there is a critical temperature when the residual stress becomes tensile. Tiberg [Tiberg 1998] suggested a graphical method for estimating this temperature. He suggested that this temperature was the temperature at the point where the elastic thermal stress, as a function of temperature, equalled the yield stress, also a function of temperature. In essence, if the thermal elastic stress is plotted over a graph of the yield stress for a range of temperatures, the intersection of the plots is the critical temperature. Torrance [Torrance 1999] proposed a formula characterising the manner in which the yield stress varies with temperature. This formula has the following form:

$$Y_\theta = \left(1 - \frac{\theta}{1650}\right)\left(Y_{rt} - \frac{1}{2}\left(Y_{rt} - \frac{Y_{700}}{1 - \dfrac{750}{1650}}\right) erfc\left[\frac{3}{2}\left(\frac{\theta_i - \theta}{750 - \theta_i}\right)\right]\right)$$

**Equation 4.15**

This equation shows that the yield stress can be characterised, in general, in terms of the yield stress at room temperature, the yield stress at the austenising temperature, and the temperature at the point of inflexion on the yield stress against temperature curve. For tool steels in particular, this temperature can be closely approximated as the temperature half way between the tempering temperature, and the austenising temperature. Combining this expression for the yield stress with equation 4.13, the following expression for the critical temperature at which tensile stresses begins to manifest themselves can be derived:

$$\theta_c = \left(\frac{1}{\alpha_i E}\right)\left(1-\frac{\theta}{1650}\right)\left(Y_{rt}-\frac{1}{2}\left(Y_{rt}-\frac{Y_{700}}{1-\frac{750}{1650}}\right)erfc\left[\frac{3}{2}\left(\frac{\theta_i-\theta_c}{750-\theta_i}\right)\right]\right)$$

**Equation 4.15**

This is an expression for the critical temperature θ<sub></sub>c, with the material properties evaluated at the inflexion temperature. It represents the intersection of the elastic stress and the yield stress as a function of temperature.

The following series of graphs illustrate the application of equation 4.15. The computed residual stress was taken to be the difference in the yield and elastic stress, for temperatures above the critical temperature.

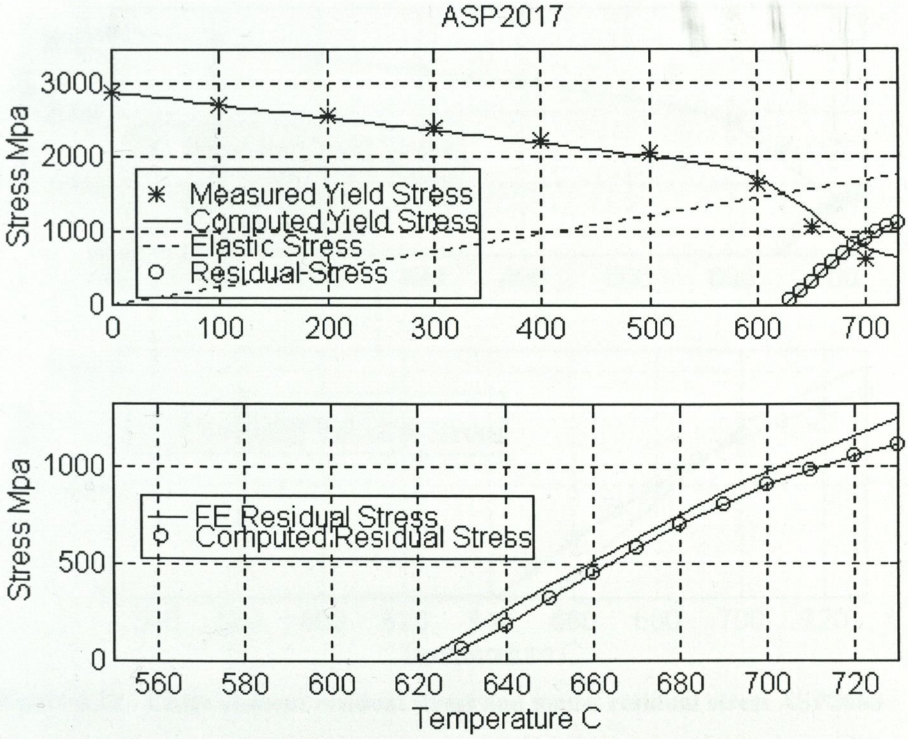

**Figure 4.20 – Finite element residual stress and model residual stress ASP2017**

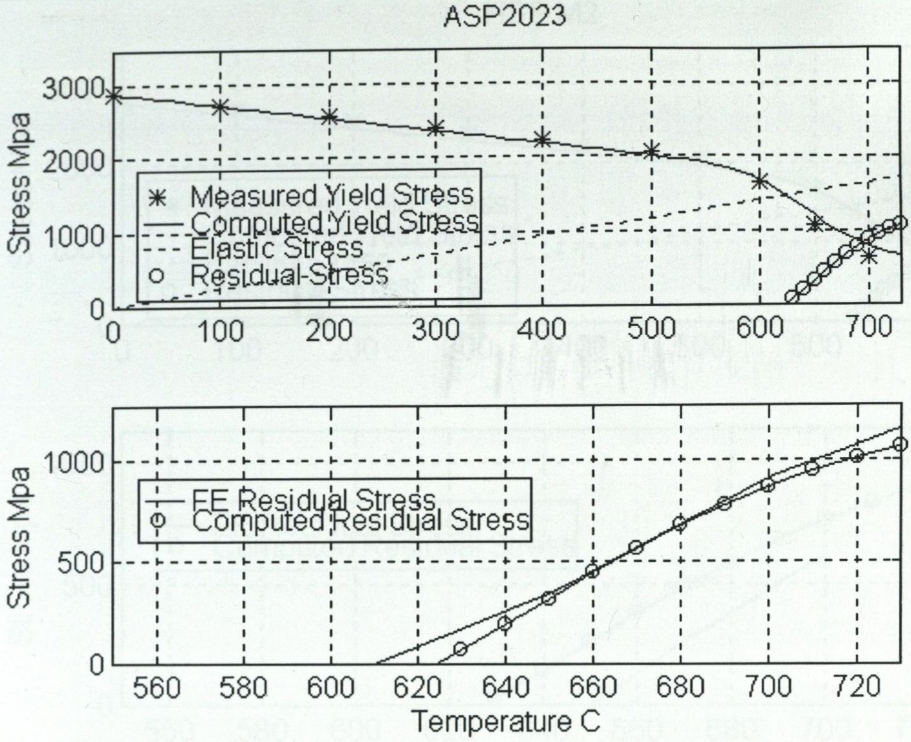

Figure 4.21 - Finite element residual stress and model residual stress ASP2023

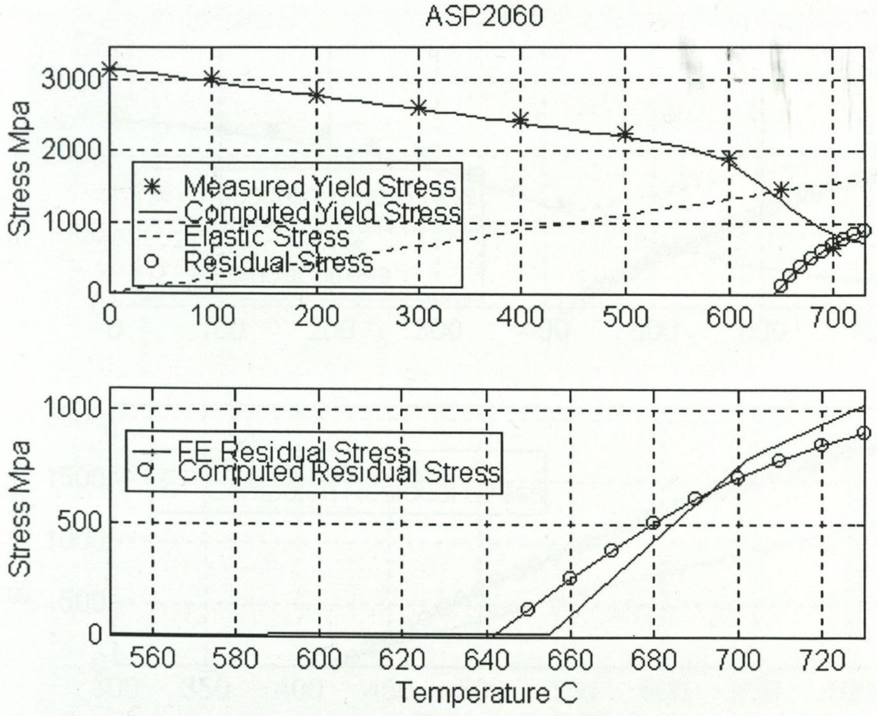

Figure 4.22 - Finite element residual stress and model residual stress ASP2060

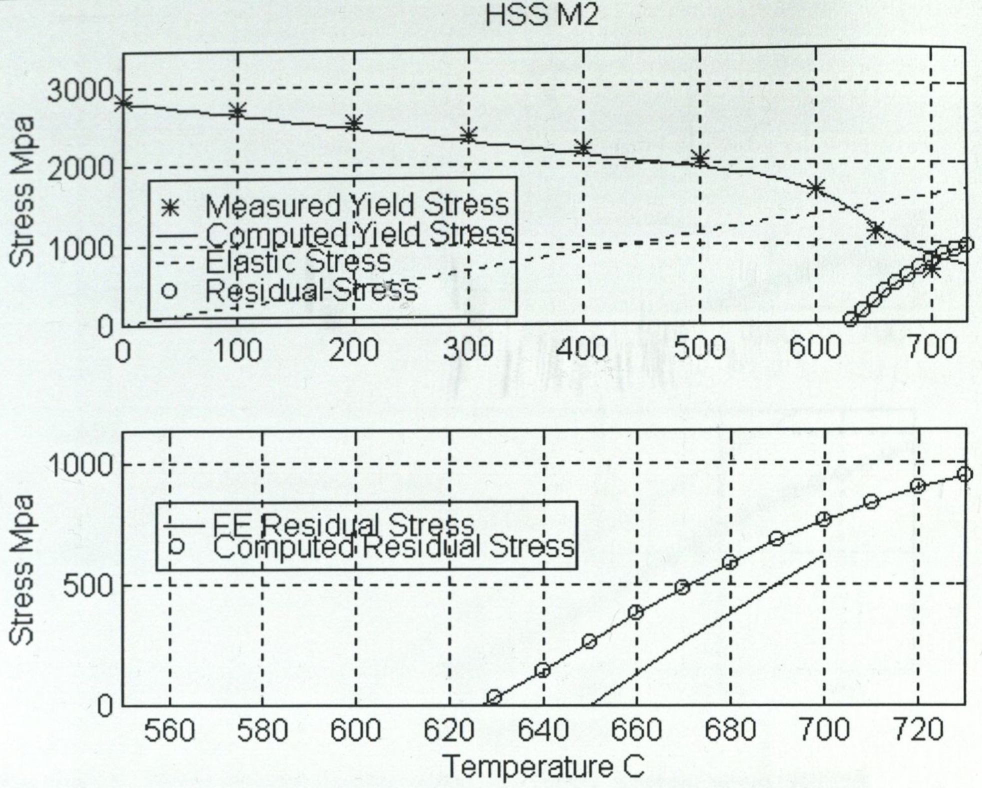

Figure 4.23 - Finite element residual stress and model residual stress HSS M2

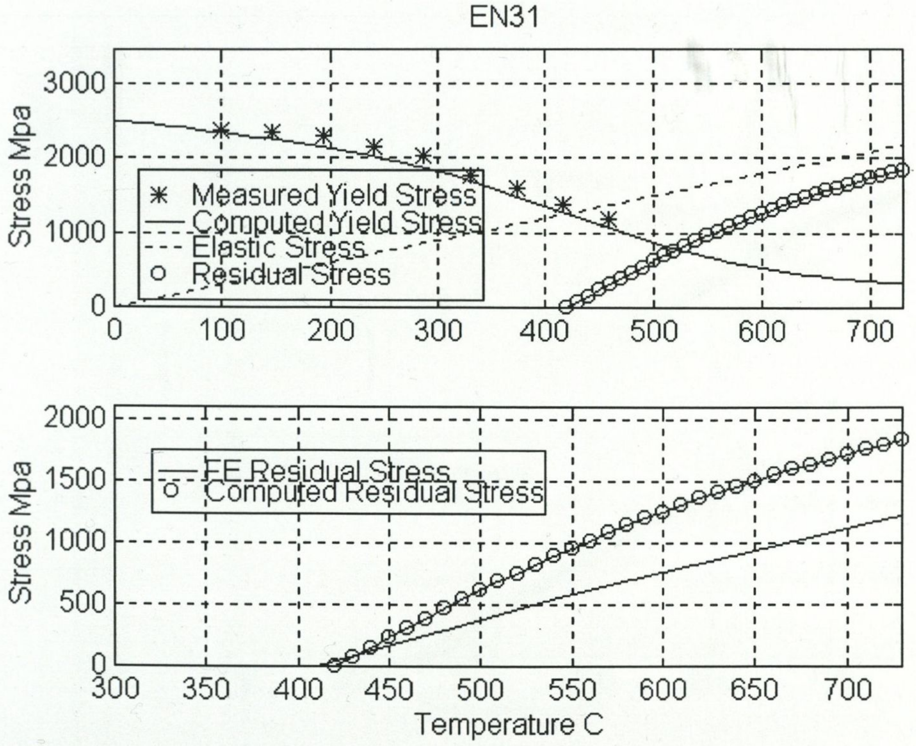

Figure 4.24 - Finite element residual stress and model residual stress EN31

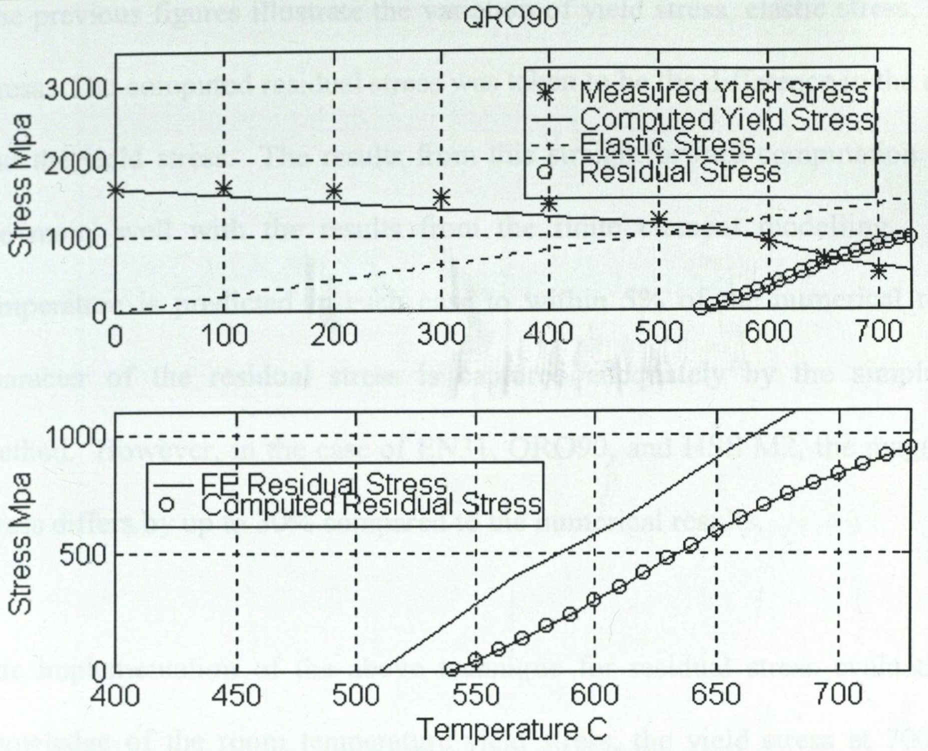

**Figure 4.25 - Finite element residual stress and model residual stress QRO90**

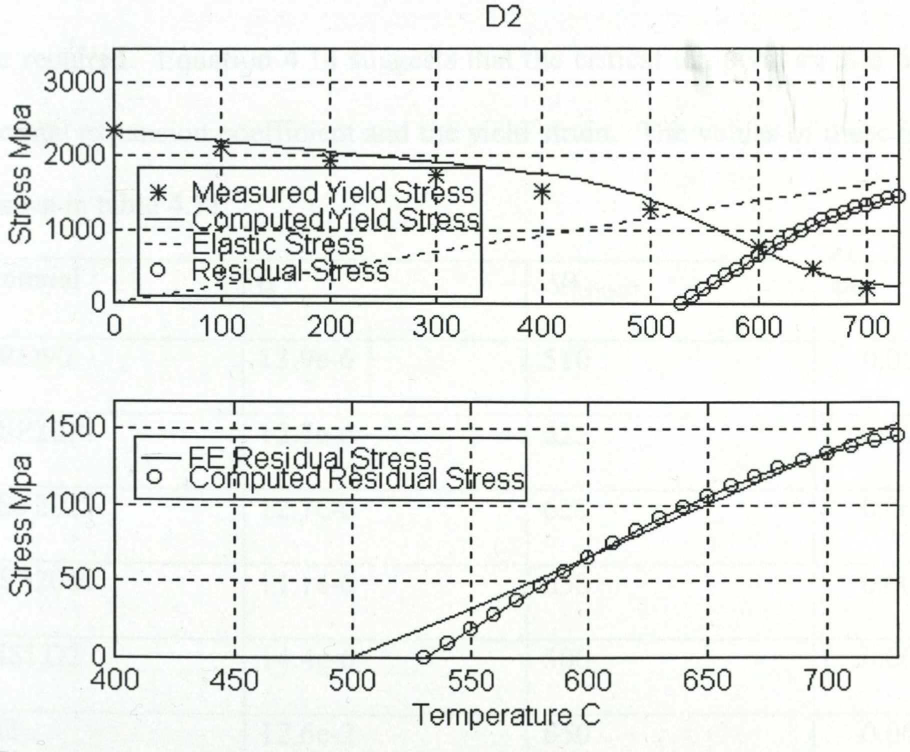

**Figure 4.26 - Finite element residual stress and model residual stress AISI D2**

The previous figures illustrate the variation of yield stress, elastic stress, and residual stress. The computed residual stress was taken to be the difference in the elastic stress and the yield stress. The results from this straightforward computation compare, in the main, well with the results from the finite element modelling. The critical temperature is predicted in each case to within 5% of the numerical results. The character of the residual stress is captured adequately by the simple difference method. However, in the case of EN31, QRO90, and HSS M2, the magnitude of the stress differs by up to 30% compared to the numerical results.

The implementation of the above technique for residual stress evaluation requires knowledge of the room temperature yield stress, the yield stress at 700°C, and the temperature at the inflection point of the yield stress versus temperature curve. All of the above can be obtained from a few hot hardness measurements. In addition, the elastic modulus and thermal expansion coefficient at the inflection point temperature are required. Equation 4.14 suggests that the critical temperature is a function of the thermal expansion coefficient and the yield strain. The values of these parameters are shown in table 4.11.

| Material | $\alpha$ | $\Delta\theta_{critical}$ | $\varphi\varepsilon$ |
|---|---|---|---|
| QRO90 | 13.9e-6 | 510 | 0.0071 |
| ASP2017 | 12.7e-6 | 625 | 0.0079 |
| ASP2023 | 12.7e-6 | 620 | 0.0079 |
| ASP2060 | 11.1e-6 | 650 | 0.0072 |
| AISI D2 | 14.4e-6 | 500 | 0.0072 |
| M2 | 12.6e-2 | 650 | 0.0082 |

**Table 4.11**

It can be seen that, for the materials considered, the product of the thermal expansion coefficient and the temperature rise (with the freezing point of water as a reference) at which tensile residual stresses appear in the workpiece is between 0.0071 and 0.0082. This would indicate a general criterion for estimating the temperature at which tensile residual stresses become discernible in a workpiece. However, this approximation is only likely to hold true for tool steels, due to the secondary hardening property which they exhibit. For low alloy steel, the value of the strain function, φε, is likely to be lower. The average value of φε, for the steels in table 4.10, is 0.0075. It is relatively easy to acquire the thermal expansion coefficient for many different steels. It is considerably easier than either actual grinding tests, or material property measurement for numerical analysis. Measuring the thermal expansion coefficient is a straightforward process, which would indicate a rough estimate of the critical temperature. Table 4.12 shows the coefficients to be used with equation 4.11 for each of the considered materials:

| Material | b0 | b1 | b2 | b3 | Assurance Criterion |
|---|---|---|---|---|---|
| QRO90 | -3.0931 | 2.6485 | -0.5064 | 0.0467 | 1 |
| ASP2017 | -0.1162 | -0.2530 | 0.2777 | -0.0798 | 1 |
| ASP2023 | 0.2113 | -0.6818 | 0.3942 | -0.0288 | 1 |
| ASP2060 | 0.3562 | -0.8046 | 0.4157 | -0.0302 | 1 |
| AISI D2 | -1.2725 | 0.9969 | -0.1141 | 0.0079 | 1 |
| HSS M2 | -0.7611 | 0.2885 | 0.0791 | -0.0051 | 1 |

**Table 4.12**

The application of equation 4.11 requires all units to be compatible. While all the graphs are presented with temperature in degrees Centigrade for convenience, the temperature in this analysis represents an absolute rather than a difference, and the fundamental unit of Kelvin must be used with equation 4.11. In addition, the equation is only valid between the critical temperature when tensile residual stresses form, and the austenising temperature.

# Chapter 5

# Temperature Concentration in Form Grinding

## 5.1 Introduction

In the past, most research in the area of grinding temperatures has considered only two basic geometries, namely the flat semi-infinite plane, and the cylinder. As a result, there exists in the literature techniques for estimating surface temperatures for geometries close to these cases. These analyses do not, however, cover all the geometries which are ground in industry. In fact, they neglect the entire area of form grinding. The purpose of this work was to attempt to produce a model to explain the effect of form on surface temperatures. In particular, a specific geometry was investigated. This was a V-form. The V-form can represent many common geometries found in form grinding. Specifically, a V-form could represent a thread in a thread grinding process, or a shoulder on a cylindrically ground workpiece.

As pointed out above, much work has been done previously on the basic geometries. This suggested that the Galileo principle might be used. This concept originated with Shaw [Shaw 1992]. It expounds the idea of seeking relative solutions as opposed to absolute solutions. The dimensional technique is admirably suited to such a task, yielding as it does, a solution which directly allows relative comparisons to be made. It indeed proved to be the way forward. In this work, the dimensional technique was used to develop a model, and finite element analysis was used to provide the numerical data to fit the derived model.

The approach taken in this work was thus similar to that used in the residual stress problem investigated in chapter 4. A dimensional analysis was combined with data taken from a finite element analysis to produce a formula capable of predicting the temperature concentration experienced by the workpiece at geometric discontinuities. This concentration factor could then be combined with existing thermal models to allow more efficient grinding to take place, after Walsh & Torrance [Walsh & Torrance 1999].

## 5.2 Theoretical Analysis

In essence, a dimensional analysis was applied firstly to a semi-infinite plane [Shaw 1996], and then to a generalised V-form. These models were then combined to provide a concentration factor highlighting the effect of the geometry.

### 5.2.1 Temperature on the Semi-infinite Plane

Figure 5.1 illustrates the situation under consideration. Essentially, a band heat source moves with a velocity across a semi-infinite plane. In dimensional analyses it is necessary to identify the parameters of interest prior to beginning the analysis. The fundamental dimensions used for this analysis were force (F), length(L), time(T) and temperature(Θ). In this case, the relevant parameters and their fundamental dimensions are:

$q$ = the applied heat flux $[FL^{-1}T^{-1}]$

$l_c$ = the arc of cut length$[L]$

$V_w$ = the work speed$[LT^{-1}]$

$\beta = (k\rho c)^{0.5}$ a material property$[FL^{-1}T^{-0.5}\Theta^{-1}]$

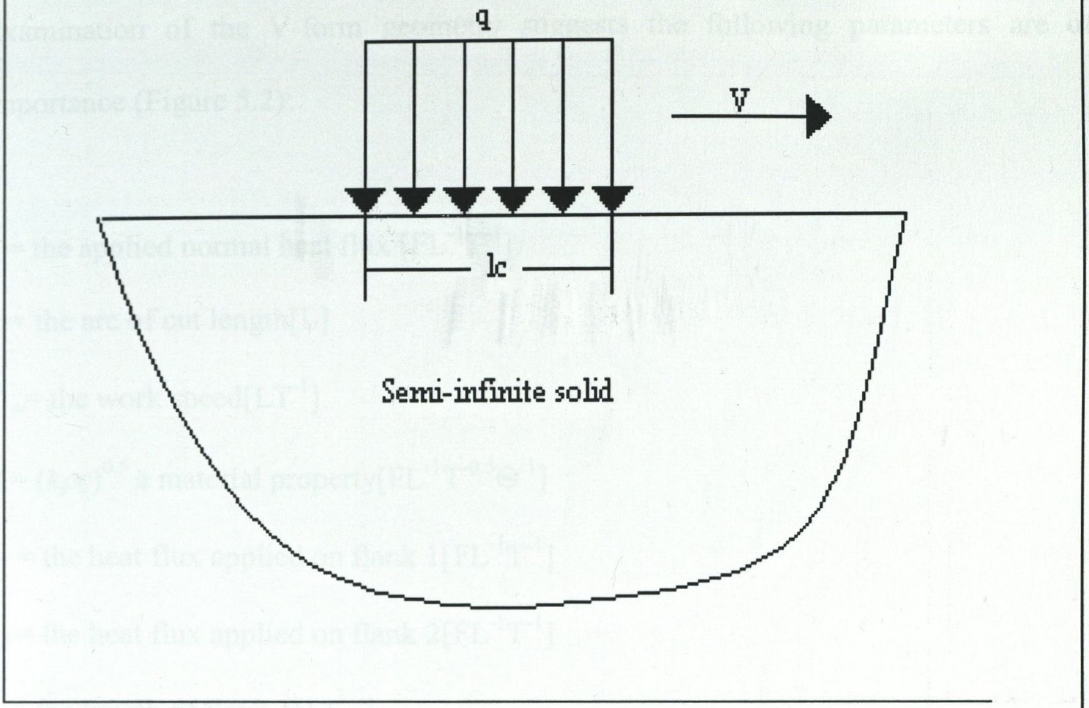

**Figure 5.1 – The semi-infinite plane**

$\theta_f$= maximum workpiece temperature rise[$\Theta$]

Prior to analysis,

$$\theta_f = \varphi(q, V, \beta, l_c)$$

**Equation 5.1**

giving equation 5.2 after application of the Buckingham Pi theorem

$$\theta_f = \varphi_1\left(\frac{q}{\beta}\sqrt{\frac{l_c}{V}}\right)$$

**Equation 5.2**

where again $\varphi_1$ is an undetermined function.

The expression developed above is of the same form as the linear Jaeger model [Shaw 1996]. As pointed out in chapter 3, the undetermined function is a constant.

## 5.3 Temperature on Peak of V-form Geometry

Examination of the V-form geometry suggests the following parameters are of importance (Figure 5.2):

$q$ = the applied normal heat flux $[FL^{-1}T^{-1}]$

$l_c$ = the arc of cut length$[L]$

$V_\omega$= the work speed$[LT^{-1}]$

$\beta = (k\rho c)^{0.5}$ a material property$[FL^{-1}T^{-0.5}\Theta^{-1}]$

$q_1$ = the heat flux applied on flank 1$[FL^{-1}T^{-1}]$

$q_2$ = the heat flux applied on flank 2$[FL^{-1}T^{-1}]$

$l_1$ = the length of flank 1$[L]$

$l_2$ = the length of flank 2$[L]$

$\alpha_1$ = the angle of incidence of flank 1$[A]$

$\alpha_2$ = the angle of incidence of flank 2$[A]$

$\alpha$ = the reference angle ($\pi/2$) $[A]$

$\theta_p$= maximum temperature rise at work apex$[\Theta]$

For this analysis, angles are assumed to have units of degrees (A). The reason for this is as follows. The included angles are obviously very important concerning the heat concentration, and can possibly feature explicitly in the analysis. This point is admirably illustrated by Massey [Massey 1971], when the problem of torque applied to a shaft is examined. If the radian unit is used, the angle can only feature implicitly in the solution, since the radian is itself dimensionless. As a result, it is better practice to assume the angles are measured in degrees. Since there are twelve parameters and five fundamental units, there will be seven Pi groups. These are as follows:

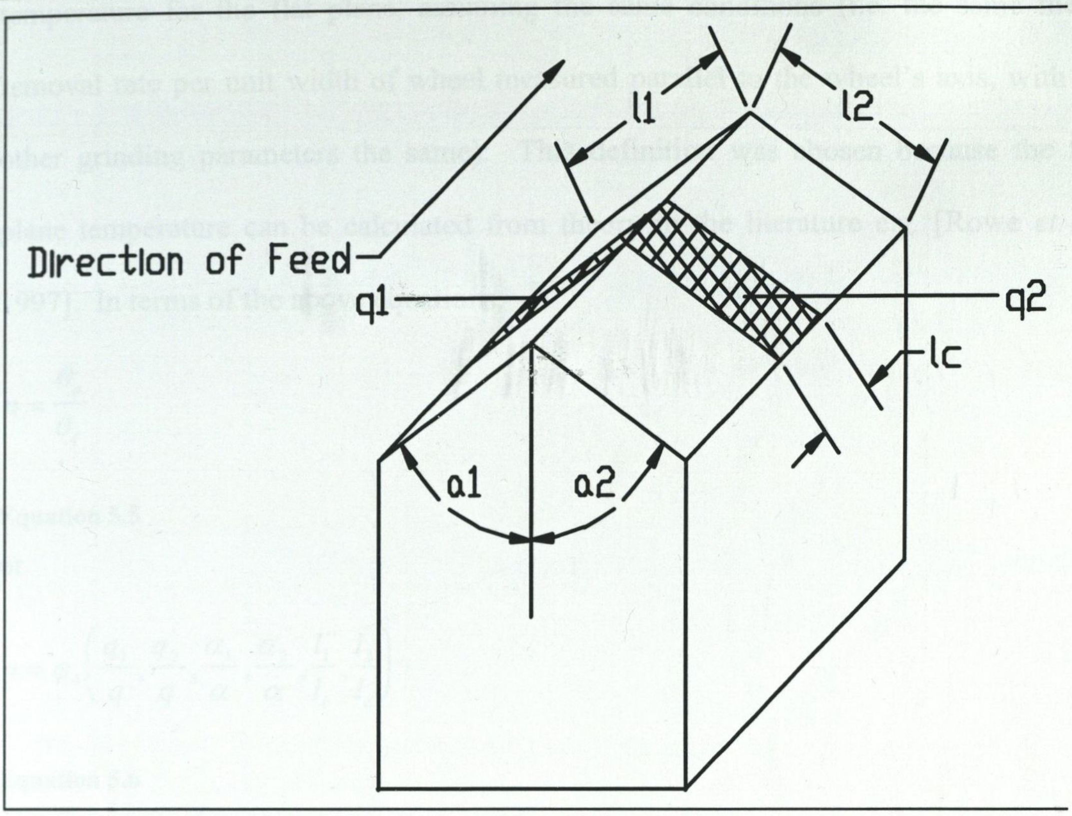

**Figure 5.2 – The V-form geometry**

$$\varphi_2\left(\frac{q_1}{q},\frac{q_2}{q},\frac{\alpha_1}{\alpha},\frac{\alpha_2}{\alpha},\frac{l_1}{l_c},\frac{l_2}{l_c},\frac{\beta}{q}\sqrt{\frac{V}{l_c}}\theta_p\right)=const$$

**Equation 5.3**

This can be rearranged to give the following expression:

$$\theta_p=\frac{q}{\beta}\sqrt{\frac{l_c}{V}}\varphi_3\left(\frac{q_1}{q},\frac{q_2}{q},\frac{\alpha_1}{\alpha},\frac{\alpha_2}{\alpha},\frac{l_1}{l_c},\frac{l_2}{l_c}\right)$$

**Equation 5.4**

### 5.3.1 The Concentration Factor

At this juncture, it is desirable to define a concentration factor. It was decided to make this equal to the peak temperature for the V-form, divided by the maximum temperature for the flat plane, assuming the same conditions (i.e. the same metal removal rate per unit width of wheel measured parallel to the wheel's axis, with all other grinding parameters the same). This definition was chosen because the flat plane temperature can be calculated from theory in the literature e.g. [Rowe *et. al.* 1997]. In terms of the above equations,

$$n = \frac{\theta_p}{\theta_f}$$

**Equation 5.5**

or

$$n = \varphi_4\left(\frac{q_1}{q}, \frac{q_2}{q}, \frac{\alpha_1}{\alpha}, \frac{\alpha_2}{\alpha}, \frac{l_1}{l_c}, \frac{l_2}{l_c}\right)$$

**Equation 5.6**

The above expression shows that the concentration factor is a function of six dimensionless Pi groups. Several points of interest arise from the analysis. Firstly, the concentration is independent of the material properties. Secondly, the distribution of the heat source (i.e. rectangular or triangular) is also an independent property. Thirdly, the speed of the workpiece is immaterial. In addition, it can be seen that the concentration is a function only of the workpiece geometry, the direction of the infeed, and the contact geometry. The direction of infeed is contained implicitly in the first two Pi groups. The variable $q$ represents the normally applied heat flux. The variables $q_1$ and $q_2$ represent the heat flux applied on flanks 1 and 2 respectively. These are factored according to the angle of infeed, and the angle of the flanks.

## 5.4 Finite Element Modelling

In order to use equation 5.6 in a meaningful way, determination of $\varphi_4$ was essential. This implied either a series of tests, or a series of finite element models. Finite element modelling was considered the better alternative. Fundamentally, each model was very similar. The included angles, and flank lengths were varied. Just over one hundred models were constructed. These models consisted of a one arc length segment of the workpiece, with a heat source applied in representation of the following nominal assumed grinding conditions:

| | |
|---|---|
| Arc length of cut: | 0.001m |
| Depth of cut: | 5µm |
| Grinding wheel diameter: | 0.2m |
| Specific Energy: | 50J/mm$^3$ |
| Partition ratio | 0.8 |
| Power to workpiece | 100W/mm$^2$ |

Figure 5.3 illustrates the model. It can be seen that the model represents only the top layer of the workpiece. This is because there is no appreciable heat penetration beyond this depth. In addition, there was a high density of elements in the depth modelled. This was to allow for the steep gradients in the temperature field. The parameter of interest in these models was the temperature at the peak of the apex, or the nadir of the V, depending on the magnitude of the included angle. One of the models was a flat plane. This was subsequently used as a benchmark for calculation of the concentration factor from equation 5.5. Thus a series of concentration factors for specific grinding conditions was compiled.

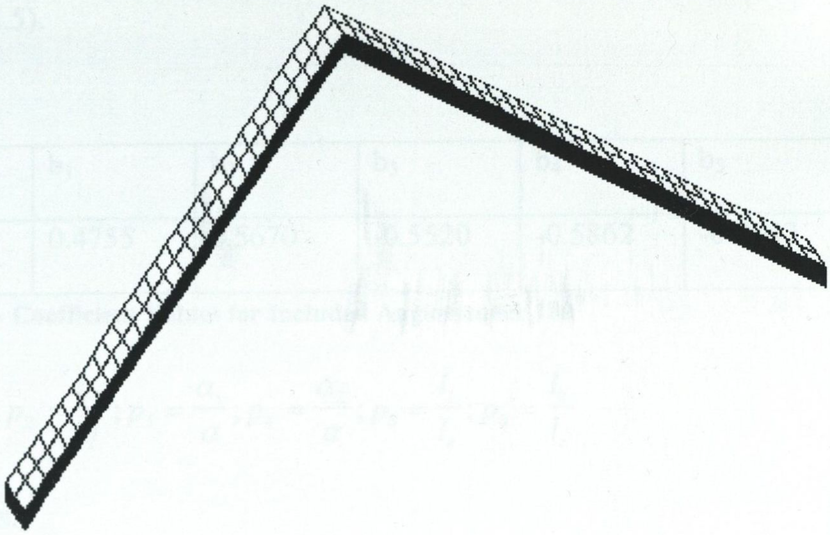

Figure 5.3 – The finite element model

## 5.5 Determination of $\varphi_4$

At this stage the data compiled from the Finite Element analyses was used to determine $\varphi_4$. This was done with the multi-variate regression routine, as used for the residual stress problem. The basis of this routine is outlined in chapter 4.

A degree of serendipity may be required at this stage to determine any cross correlation between groups. Here, the simple approach was found to be perfectly adequate: only the Pi groups developed earlier are used; each group is assumed to be raised to the power of one. This was done to prevent instability in the regression formula, and to keep the final predictive formula as simple as possible. Some accuracy may be sacrificed, but a linear fit can be achieved without any problem. The quality of the fit resulting from this simple approach could be improved if the results were separated into two parts: one for workpieces with included angles of greater than

$180^{\circ}$ (Figure 5.4), and one for workpieces with included angles of less than $180^{\circ}$ (Figure 5.5).

| $b_0$ | $b_1$ | $b_2$ | $b_3$ | $b_4$ | $b_5$ | $b_6$ |
|---|---|---|---|---|---|---|
| 1.2284 | 0.4755 | 0.5670 | -0.5520 | -0.5862 | -0.0043 | -0.0040 |

**Table 5.1 - Coefficient Values for Included Angles under $180^{\circ}$**

$$p_1 = \frac{q_1}{q}; p_2 = \frac{q_2}{q}; p_3 = \frac{\alpha_1}{\alpha}; p_4 = \frac{\alpha_2}{\alpha}; p_5 = \frac{l_1}{l_c}; p_6 = \frac{l_2}{l_c}$$

**Equation 5.9**

$$n = b_0 + b_1 p_1 + b_2 p_2 + b_3 p_3 + b_4 p_4 + b_5 p_5 + b_6 p_6$$

**Equation 5.9**

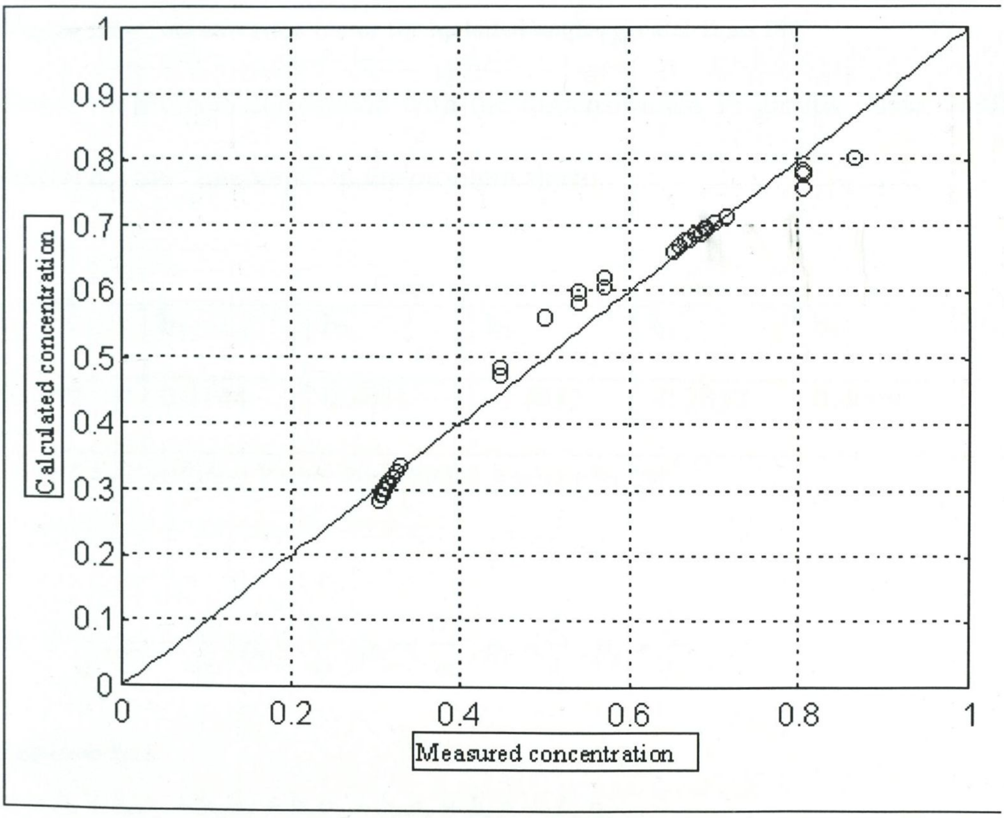

**Figure 5.4 - Concentration factor for included angles less than $180^{\circ}$**

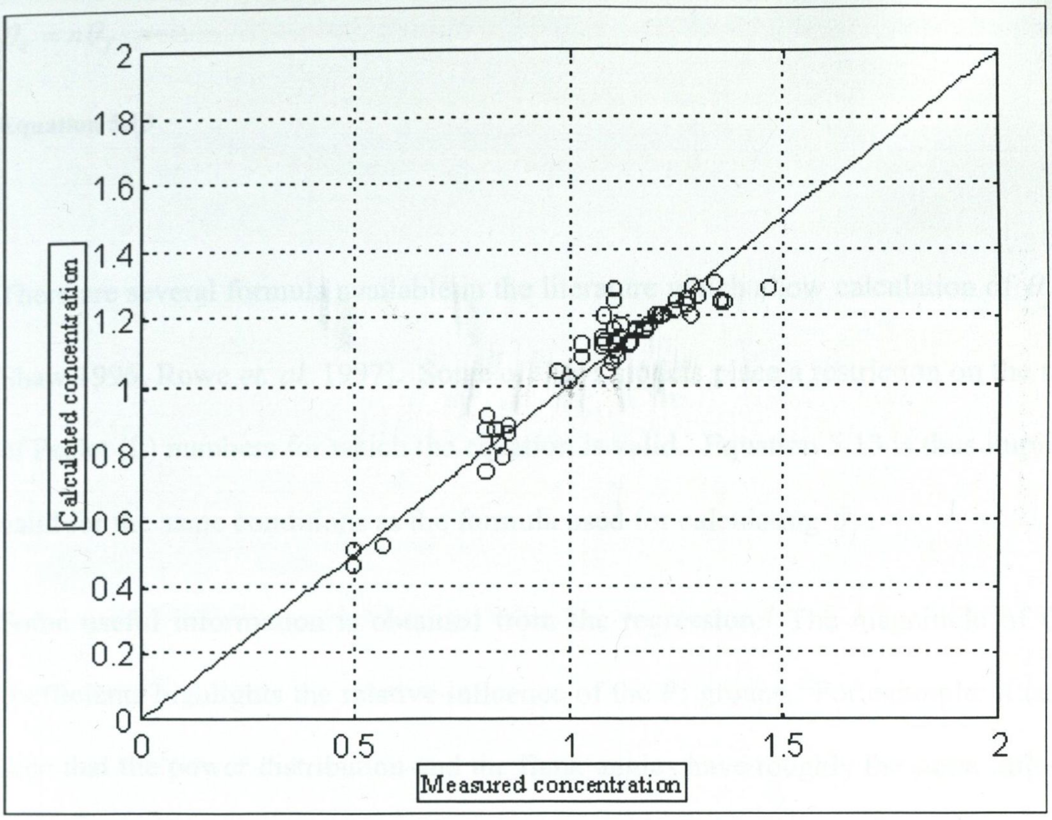

**Figure 5.5 - Concentration factor for included angles greater than 180°**

The *b* coefficients correspond with the dimensionless Pi groups. The coefficient $b_0$ represents the "intercept" in the problem space.

| $b_0$ | $b_1$ | $b_2$ | $b_3$ | $b_4$ | $b_5$ | $b_6$ |
|---|---|---|---|---|---|---|
| 0.6092 | 0.3144 | 0.3481 | -0.2032 | -0.2037 | 0.0009 | 0.0009 |

**Table 5.2 - Coefficient Values for Included Angles over 180°**

$$p_1 = \frac{q_1}{q}; p_2 = \frac{q_2}{q}; p_3 = \frac{\alpha_1}{\alpha}; p_4 = \frac{\alpha_2}{\alpha}; p_5 = \frac{l_1}{l_c}; p_6 = \frac{l_2}{l_c}$$

**Equation 5.11**

$$n = b_0 + b_1 p_1 + b_2 p_2 + b_3 p_3 + b_4 p_4 + b_5 p_5 + b_6 p_6$$

**Equation 5.12**

The maximum temperature at the geometric discontinuity is now given by:

$$\theta_d = n\theta_f$$

**Equation 5.13**

There are several formula available in the literature which allow calculation of $\theta_f$ [e.g Shaw 1996, Rowe *et. al.* 1997]. Some of these models place a restriction on the range of Peclet (L) numbers for which the equation is valid. Equation 5.13 is thus implicitly valid for the same conditions as the formula used for calculating $\theta_f$.

Some useful information is obtained from the regression. The magnitude of the *b* coefficients highlights the relative influence of the Pi groups. For example, it can be seen that the power distribution and the flank angles have roughly the same influence on the temperature concentration. The flank lengths on the other hand have considerably less of the influence the flank angles and power distribution have on the temperature concentration.

The assurance criterion introduced in chapter 4 was used to assess the quality of the derived formula with the actual results. This measured the least squares deviation of the predicted concentration from the measured concentration. A value of unity indicates perfect correlation, whereas a value of zero indicates no correlation.

The assurance criterion yielded the following values for the two general angles considered above:

| | **Included Angle over 180°** | **Included Angles of Under 180°** |
|---|---|---|
| **Assurance Criterion** | 0.9980 | 0.9970 |

**Table 5.3**

In both cases the fit is good, though the linearity of the results in figure 5.5 is not so good as it is in figure 5.4. This could doubtless be rectified by assuming a more complex functional relationship between the Pi groups, but only at the risk of de-stabilizing the regression routine result, and finishing with a more cumbersome formula for the concentration factor.

## 5.6 Discussion and Application of Results

The analysis that was carried out raised some interesting issues regarding the effect of form on the grinding temperatures experienced by the workpiece. The workpiece type investigated here was a general V-form. There is now a method for assessing the effects of any form on workpiece temperature. The dimensional analysis can be applied to any form, provided there is awareness of the influencing parameters. It should be clear from this analysis that the geometric parameters, and wheel infeed direction are likely to feature prominently in any result obtained. Indeed, the same base reference could be used, i.e. the linear Jaeger semi-infinite band source model.

Some further clarification is also necessary regarding the choice of grinding conditions for the base reference. The contact width of the wheel on the workpiece is immaterial. This is because the base model is essentially a two-dimensional solution. The band source in figure 5.1 stretches to infinity both into and out from the page. In addition, the flank lengths were shown to have a small influence on the temperature concentration. The depth of cut is the other important parameter to consider. The choice of this for the base reference is entirely arbitrary. One can choose either the equivalent depth of cut, defined as the depth of cut to give the same metal removal rate in both cases, or the depth of cut in the direction of infeed. In this work, the latter

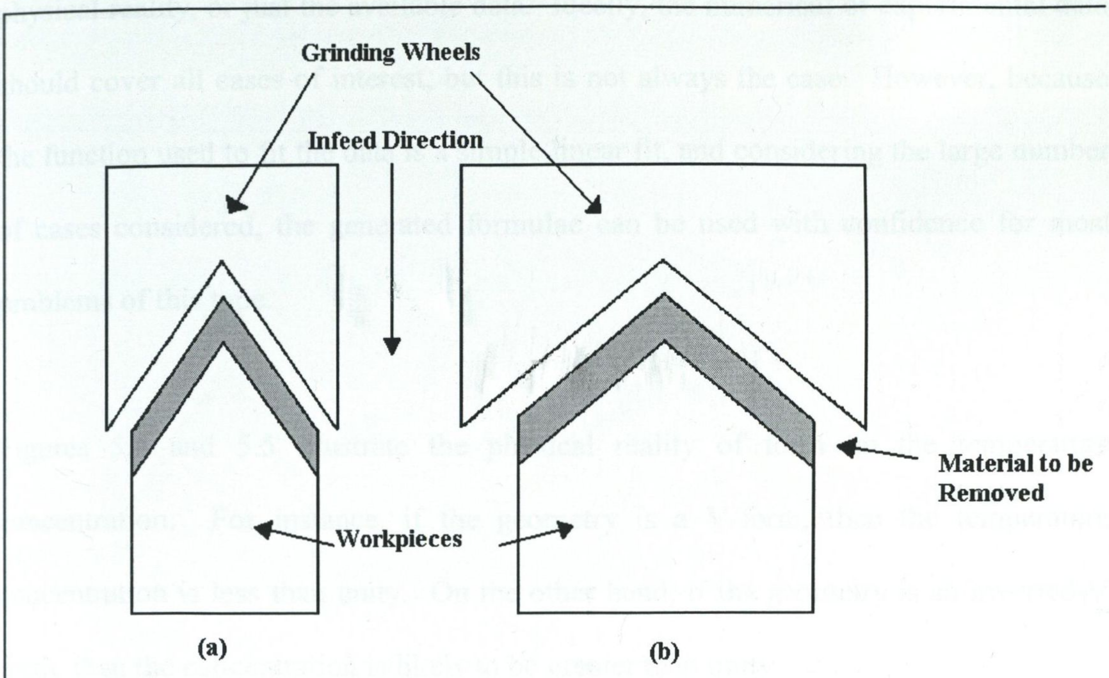

**Figure 5.6 – Material removal model**

was chosen, as it is considerably easier to implement. Figure 5.6 illustrates how this is so. In both cases the normal depth of cut is the same, but the metal removal rate is different. However, the same base reference can be used for both cases. It should be noted that both ways are satisfactory, but the coefficients in equation 5.10 and equation 5.15 will be different.

Application of equation 5.10 and equation 5.15 will require some caution however. The validity of the equations outside the envelope of cases covered by the finite element modelling is not immediately clear. The linear regression technique is intended as an interpolative tool, as opposed to an extrapolative tool. On the other hand, the dimensional technique is a generally applicable method. The crux of the issue is the choice of the undetermined function, and whether it actually represents the physical reality, or just the available data. Ideally, the numerical or experimental data should cover all cases of interest, but this is not always the case. However, because the function used to fit the data is a simple linear fit, and considering the large number of cases considered, the generated formulae can be used with confidence for most problems of this type.

Figures 5.4 and 5.5 illustrate the physical reality of form on the temperature concentration. For instance, if the geometry is a V-form, then the temperature concentration is less than unity. On the other hand, if the geometry is an inverted-V form, then the concentration is likely to be greater than unity.

The application of the concentration factor in a meaningful fashion requires a knowledge of the temperature experienced by a flat plane under similar grinding conditions. If a concentration factor greater than unity is predicted for the form being ground, grinding parameters could be adjusted to reduce the flat plane temperature to such a degree that the concentration at the geometric discontinuity did not cause workpiece burn, or tensile residual stresses. The following examples illustrate how the technique can be applied to two typical industrial cases.

### 5.6.1 Plunge Thread-Die Grinding

Figure 5.7 shows a plunge thread-die finish grinding operation.

The grinding conditions are assumed to be as follows:

| | |
|---|---|
| Workspeed: | 500mm/s |
| Normal depth of cut: | 0.0005mm |

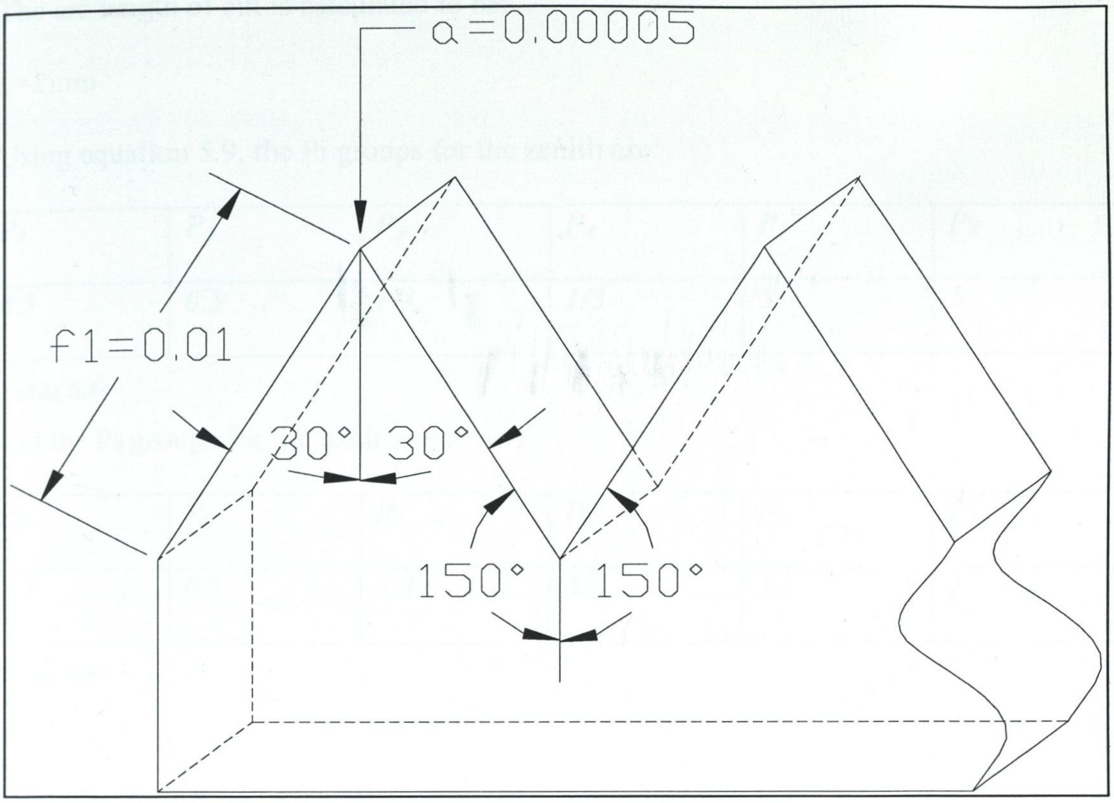

**Figure 5.7 – Thread die schematic**

| | |
|---|---|
| Partition Ratio: | 0.85 |
| Specific Energy: | $30J/mm^3$ |
| Wheel Diameter: | 200mm |

The power required for this operation is:

$P=63.75W/mm^2$

This power is factored according to the sine of the flank angle. This is to allow for the fact that the normal infeed on the flank is different to the infeed in the direction of the grinding wheel. Thus, for this example, the power on each flank is given by:

$P_{f1}=31.9\ W/mm^2$

$P_{f2}=31.9\ W/mm^2$

The arc length of cut is calculated to be:

$l_c$=2mm

Using equation 5.9, the Pi groups for the zenith are:

| $P_1$ | $P_2$ | $P_3$ | $P_4$ | $P_5$ | $P_6$ |
|---|---|---|---|---|---|
| 0.5 | 0.5 | 1/3 | 1/3 | 5 | 5 |

**Table 5.4**

and the Pi groups for the nadir are:

| $P_1$ | $P_2$ | $P_3$ | $P_4$ | $P_5$ | $P_6$ |
|---|---|---|---|---|---|
| 0.5 | 0.5 | 5/3 | 5/3 | 5 | 5 |

**Table 5.5**

Using the following representative material properties for steel:

$k$=33.52W/mK

$c$=494J/KgK

$\rho$=7870Kg/m$^3$

Equation 5.2 is used to calculate the maximum flat plane temperature.

$\theta_f$=499°C

The concentration factor at the zenith of the form is calculated from equation 5.10, and the concentration factor at the nadir is found using equation 5.12, the appropriate set of Pi groups being used for each case.

$n_z$=1.33

$n_n$=0.272

Thus the temperature experienced by the workpiece at these positions is:

$\theta_z$=664°C

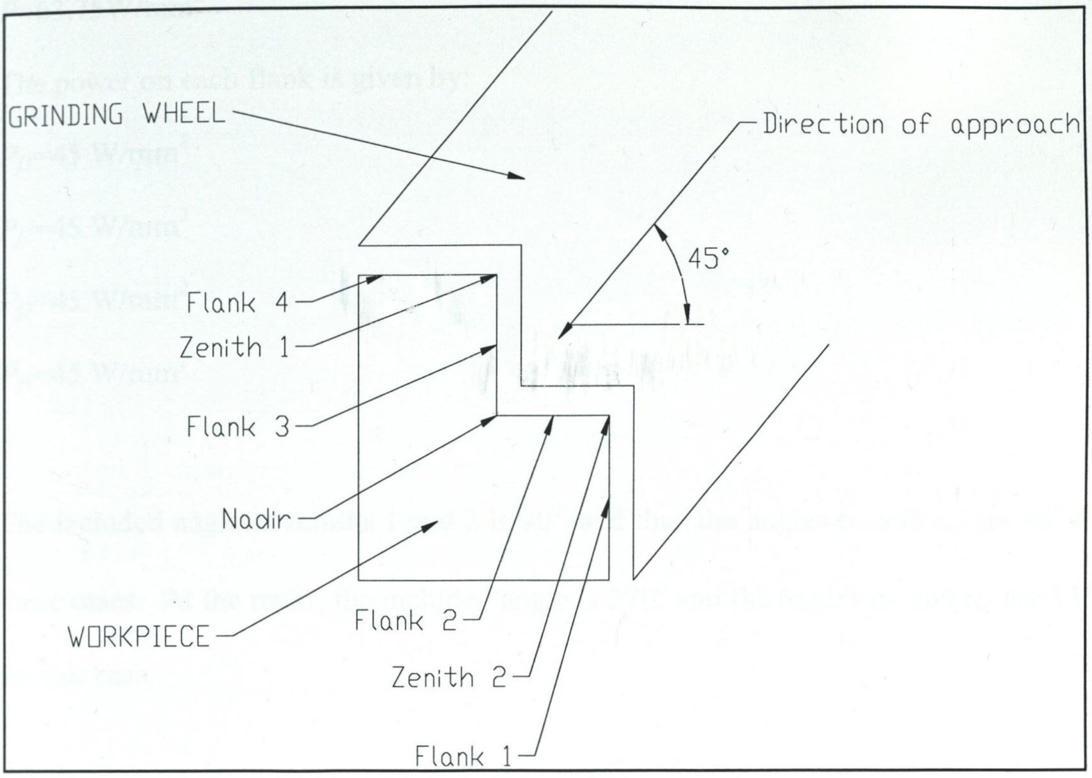

**Figure 5.8 – Angle approach grinding, 45°**

$\theta_n$=136°C

### 5.6.2 Angle Approach Grinding

A second example of the application of the analysis considers angle approach grinding. Figure 5.8 illustrates a representative case.

Workspeed: 500mm/s

Normal depth of cut: 0.0005mm

Partition Ratio: 0.85

Specific Energy: 30J/mm$^3$

Wheel Diameter: 200mm

The power required for this operation again is:

$P$=63.75W/mm$^2$

The power on each flank is given by:

$P_{f1}$=45 W/mm$^2$

$P_{f2}$=45 W/mm$^2$

$P_{f3}$=45 W/mm$^2$

$P_{f4}$=45 W/mm$^2$

The included angle at zeniths 1 and 2 is 90°, and thus the angles $\alpha_1$ and $\alpha_2$ are 45° for these cases. At the nadir, the included angle is 270° and the angles $\alpha_1$ and $\alpha_2$ are 135° for this case.

The arc length of cut is calculated to be:

$l_c$=2mm

The flank lengths are:

$l_{f1}$=0.02m

$l_{f2}$=0.02m

$l_{f3}$=0.02m

$l_{f4}$=0.02m

Using equation 5.9, the Pi groups for the zeniths are:

| $P_1$ | $P_2$ | $P_3$ | $P_4$ | $P_5$ | $P_6$ |
|---|---|---|---|---|---|
| 0.707 | 0.707 | 1/2 | 1/2 | 10 | 10 |

**Table 5.6**

and the Pi groups for the nadir are:

| $P_1$ | $P_2$ | $P_3$ | $P_4$ | $P_5$ | $P_6$ |
|---|---|---|---|---|---|
| 0.707 | 0.707 | 3/2 | 3/2 | 10 | 10 |

**Table 5.7**

Using the same material properties as for example 1 the maximum flat plane temperature is again estimated from equation 5.2:

$\theta_f$=499°C

The concentration factor at the zeniths of the form is calculated from equation 5.12, and the concentration factor at the nadir is found using equation 5.10, again using the appropriate set of Pi groups.

$n_{z1}$=1.31

$n_{z2}$=1.31

$n_n$=0.49

Thus the temperature experienced by the workpiece at these positions is:

$\theta_{z1}$=653°C

$\theta_{z2}$=653°C

$\theta_n$=242°C

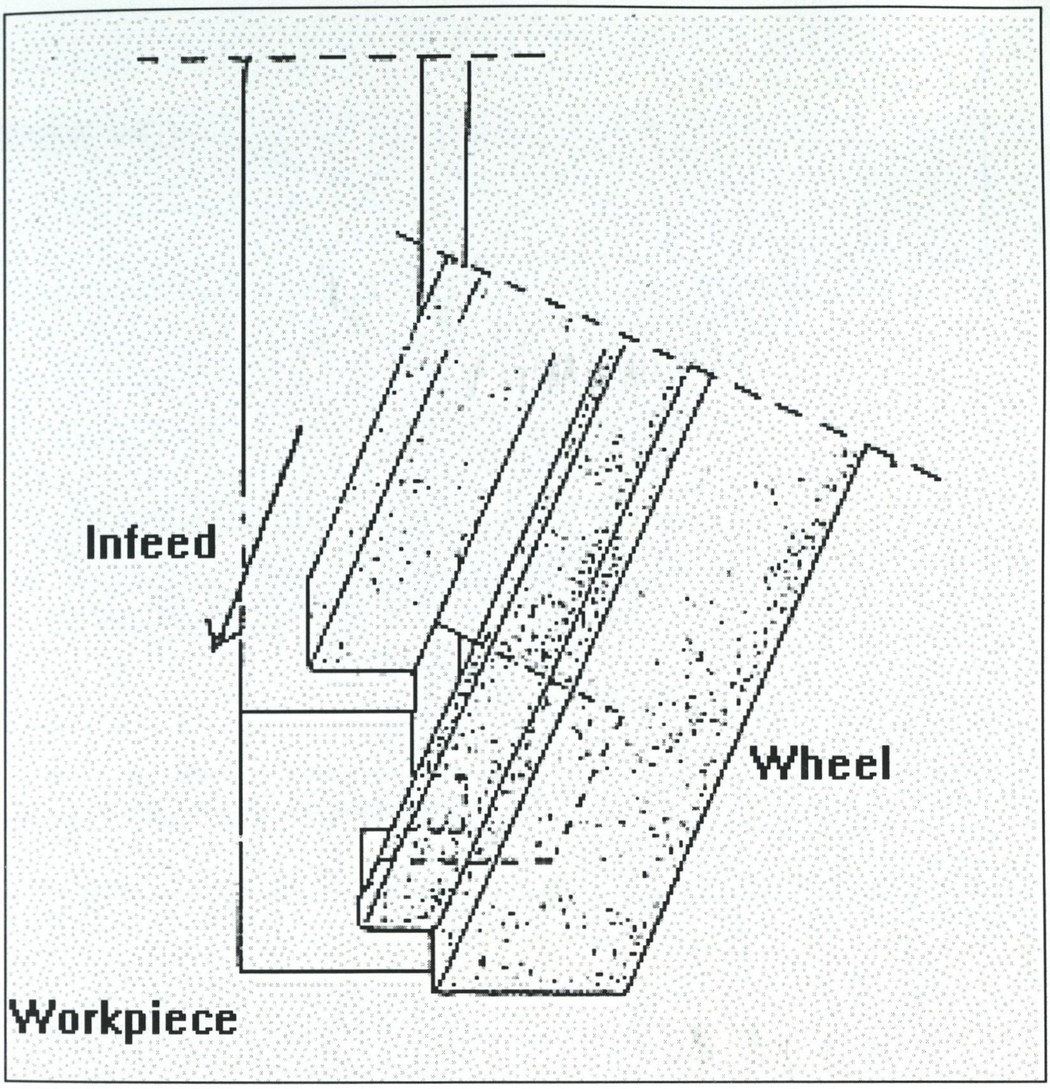

**Figure 5.9 – Angle approach form grinding**

A third example of the application of the analysis considers, again, angle approach grinding with a different angle of approach. Figure 5.9 illustrates a representative case, Figure 5.10 showing a schematic of one shoulder, with an approach angle of 30°.

| | |
|---|---|
| Workspeed: | 500mm/s |
| Normal depth of cut: | 0.0005mm |
| Partition Ratio: | 0.85 |
| Specific Energy: | 30J/mm$^3$ |

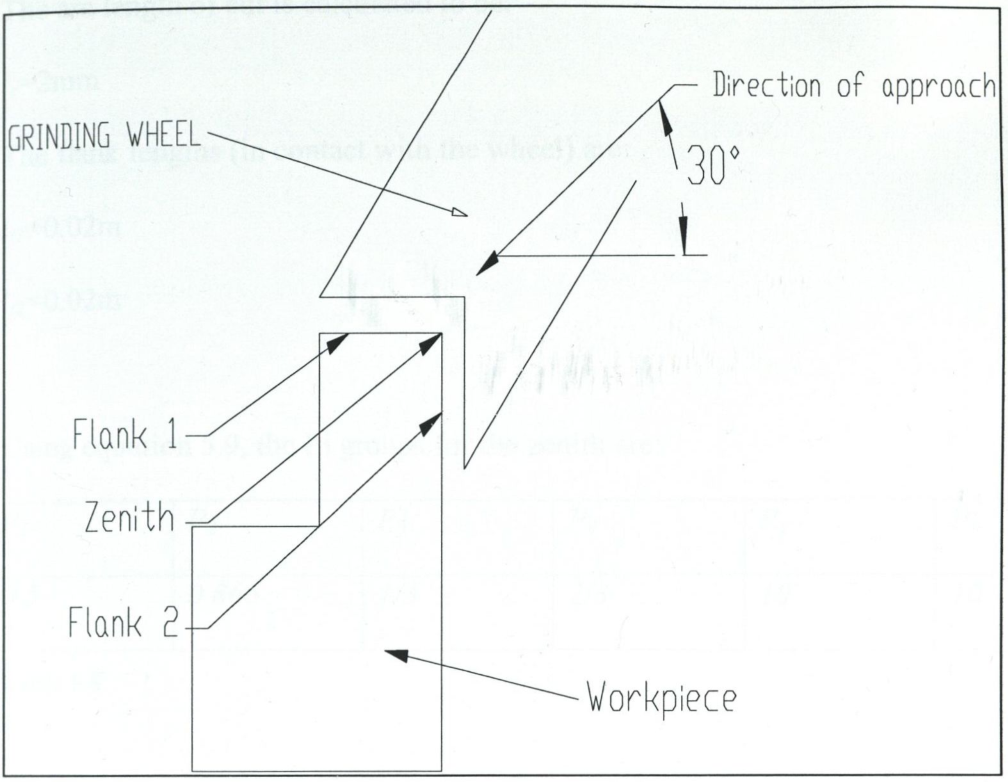

**Figure 5.10 – Angle approach grinding, 30°**

Wheel Diameter: 200mm

The power required for this operation again is:

$P$=63.75W/mm$^2$

The power on each flank is given by:

$P_{f1}$=31.86 W/mm$^2$

$P_{f2}$=55.2 W/mm$^2$

The included angle at the zenith is 90°, and thus the angles $\alpha_1$ and $\alpha_2$ are 45° for this case.

The arc length of cut is calculated to be:

$l_c$=2mm

The flank lengths (in contact with the wheel) are:

$l_{f1}$=0.02m

$l_{f2}$=0.02m

Using equation 5.9, the Pi groups for the zenith are:

| $P_1$ | $P_2$ | $P_3$ | $P_4$ | $P_5$ | $P_6$ |
|---|---|---|---|---|---|
| 0.5 | 0.866 | 1/3 | 2/3 | 10 | 10 |

**Table 5.8**

These groups are arrived at by rotating the workpiece/wheel configuration until the wheel is approaching the workpiece normally. This is illustrated in Figure 5.11.

Using the same material properties as for example 1 the maximum flat plane temperature is calculated from equation 5.2:

$\theta_f$=499°c

The concentration factor at the zenith of the form is calculated from equation 5.12

$n_z$=1.30

Thus the temperature experienced by the workpiece at these positions is:

$\theta_z$=649°c

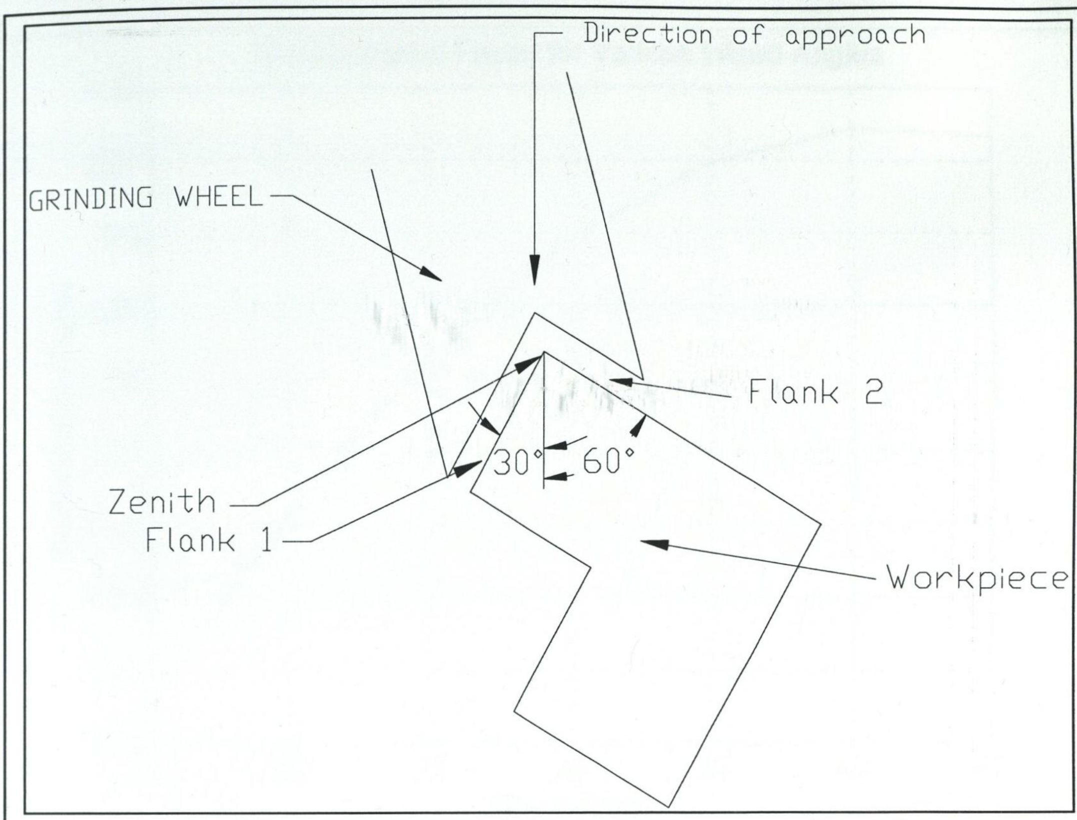

**Figure 5.11 – Angle approach grinding, 30° reoriented**

Figure 5.12 shows how the concentration factor varies at the zenith of the form in shoulder grinding, according to the approach angle of the grinding wheel. The same grinding conditions used for the examples are assumed.

## 5.7 Conclusions

The effect of geometric discontinuities has been examined. In particular, the V-form has been investigated, and a quantitative result for the temperature concentration has been obtained. A method for determining the effect of form on surface temperatures has been developed in such a way as to be applicable to any geometry and grinding conditions. The technique should be applicable to both surface and cylindrical grinding. The concentration factor should prove useful in industry, with a view to more reliable grinding. It has been demonstrated that inverted-V forms experience a

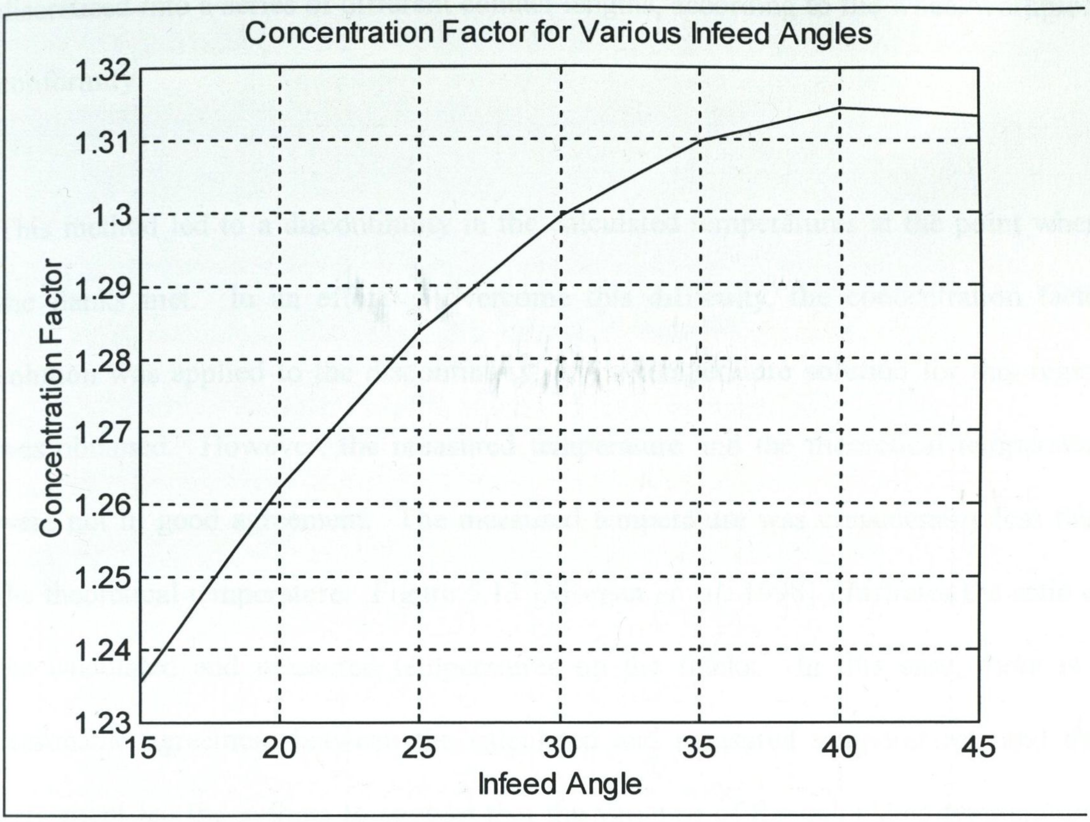

**Figure 5.12 – Concentration factor for various infeed angles**

concentration of greater than unity, and thus more care is needed when grinding these forms. The concentration factor varies in a favourable manner with increasing approach angles. It should also be noted that the specific energy is directly related to the approach angle, also varying in a favourable manner. This implies that the overall temperature calculation needs to take into account this variation.

## 5.8 The Effect of a Tip Radius on the Inverted V-Form

Subsequent to the previous analysis, some experimental temperature measurements for the grinding of an inverted V-form were published [Morgan *et. al.* 1998]. This work presented a theoretical analysis of form grinding temperatures. The technique was based on the finite difference technique, the contact region on each flank being discretised into a series of different contact lengths, according to the wheel/workpiece conformity.

This method led to a discontinuity in the calculated temperatures at the point where the flanks met. In an effort to overcome this difficulty, the concentration factor solution was applied to the discontinuity, and a temperature solution for this region was obtained. However, the measured temperature and the theoretical temperature were not in good agreement. The measured temperature was considerably less than the theoretical temperature. Figure 5.13 [Morgan *et. al.* 1998] illustrates the ratio of the calculated and measured temperatures on the flanks. In this case, there is a reasonable agreement between the calculated and measured temperatures, and this agreement led the authors to suggest that the variance of the calculated temperatures with respect to the experimental measurements was due, in part to the radius of 0.15mm imparted on the form as necessitated by the dressing roll on the wheel, and in part to the sampling width of the thermocouple which was 0.5mm. Figure 5.14 [Morgan *et. al.* 1998] illustrates the calculated/measured temperature ratio for the apex of the form.

The influence of the fillet radius was investigated in the same fashion as the sharp forms. It was found that, regardless of other factors such as arc length and flank angle, that once the radius was 0.15mm and greater, the temperature at the apex was the same as that of the flat plane under the same grinding conditions. This result indicated that, for most form grinding operations, the radius on the grinding wheel generated by the dressing roll effectively limits the maximum temperature of the form to the flat plane solution, with the normal infeed being the crucial parameter for the

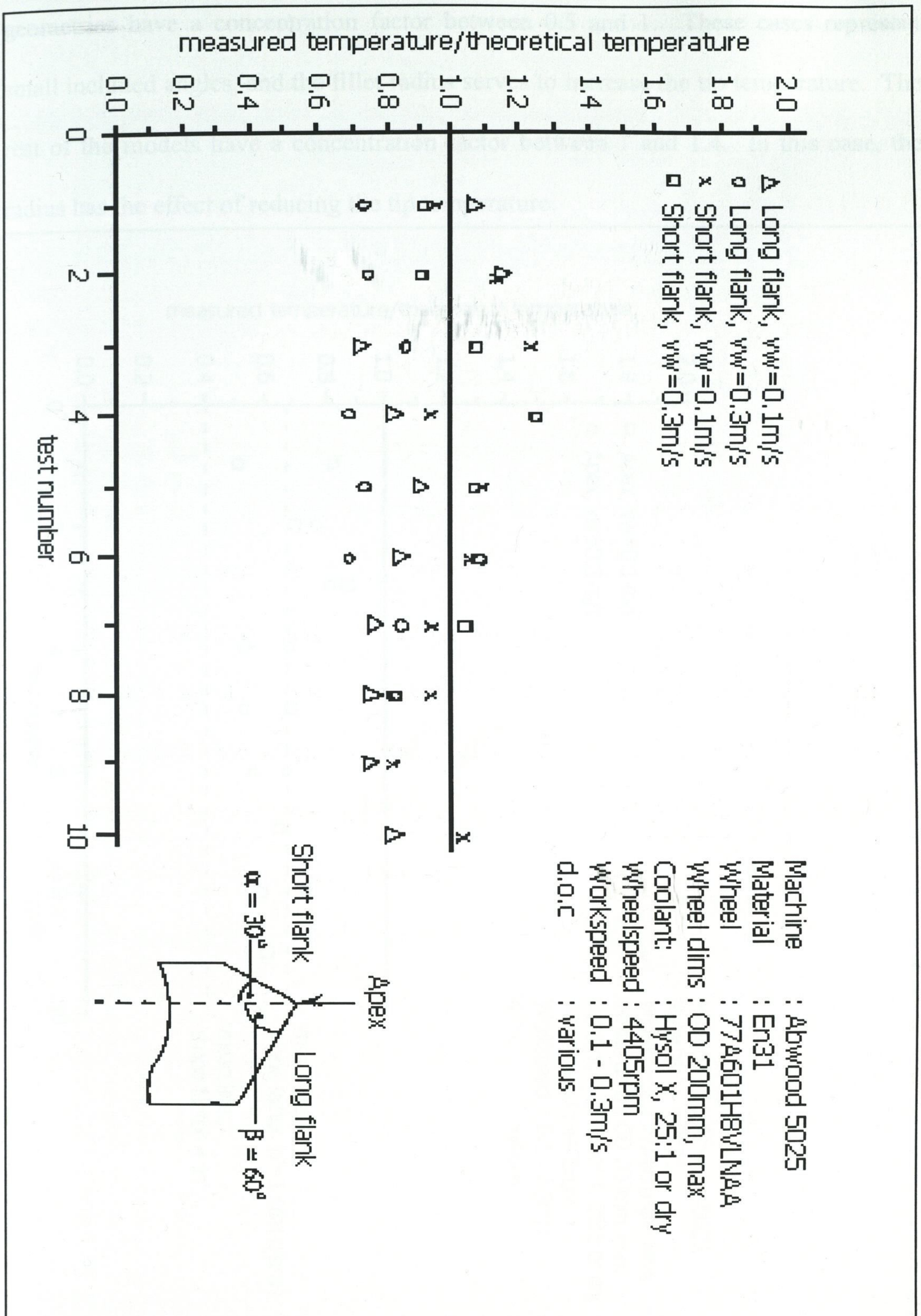

**Figure 5.13 – Flank temperatures in form grinding, from Morgan *et. al.* 1998**

heat flux evaluation. Figure 5.5 indicates that this phenomenon is likely to be beneficial for most of the geometries considered. Roughly 30% of the considered geometries have a concentration factor between 0.5 and 1. These cases represent small included angles, and the fillet radius serves to increase the tip temperature. The rest of the models have a concentration factor between 1 and 1.4. In this case, the radius has the effect of reducing the tip temperature.

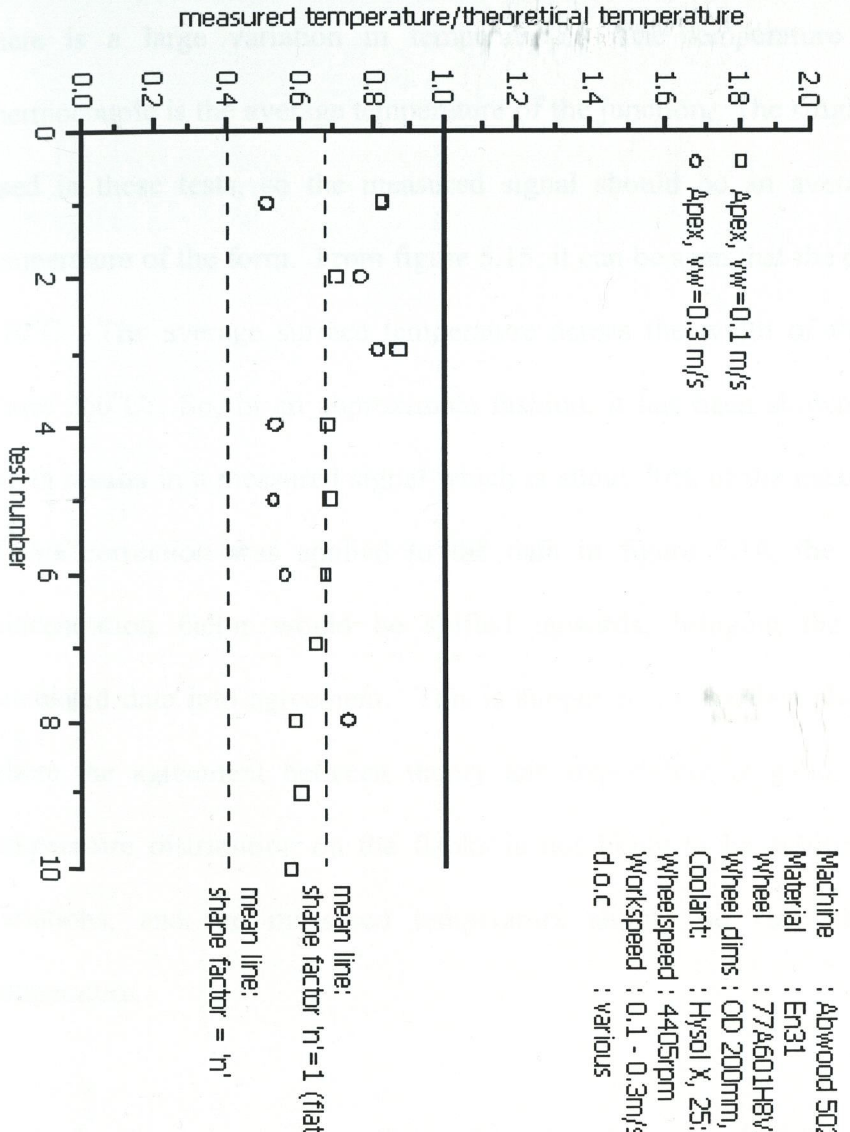

**Figure 5.14 - Apex temperatures in form grinding, from Morgan *et. al.* 1998**

The effect of the width of the thermocouple on the measured temperature was also investigated in a numerical model. Figure 5.15 shows the heat flux distribution for a form with a 0.1mm fillet radius. Figure 5.16 shows the resultant temperature distribution from the applied flux. This figure also illustrates the sampling width of the thermocouple. It can easily be seen that across the thermocouple sampling width there is a large variation in temperature. The temperature measured by the thermocouple is the average temperature of the junction. The single pole method was used in these tests, so the measured signal should be an average of the surface temperature of the form. From figure 5.15, it can be seen that the peak temperature is 370°C. The average surface temperature across the width of the thermocouple is about 260°C. So, in an approximate fashion, it has been shown that the sampling width results in a measured signal which is about 70% of the maximum temperature. If this correction was applied to the data in figure 5.14, the mean line for the concentration factor would be shifted upwards, bringing the experimental and calculated data into agreement. This is supported by the data shown in figure 5.13, where the agreement between theory and experiment is good. In this case, the temperature distribution on the flanks is not likely to be subjected to strong local variations, and the measured temperature should be very close to the actual temperature.

It can be seen clearly from figure 5.16 that the general V-form experiences very strong thermal gradients in the vicinity of the geometric discontinuity. The effect of the form radius imparted on the wheel by the dressing roll would seem to limit the value of the concentration factor to one. It should be noted that the tip of the inverted-V form can still be considerably hotter than the flanks, particularly when the included

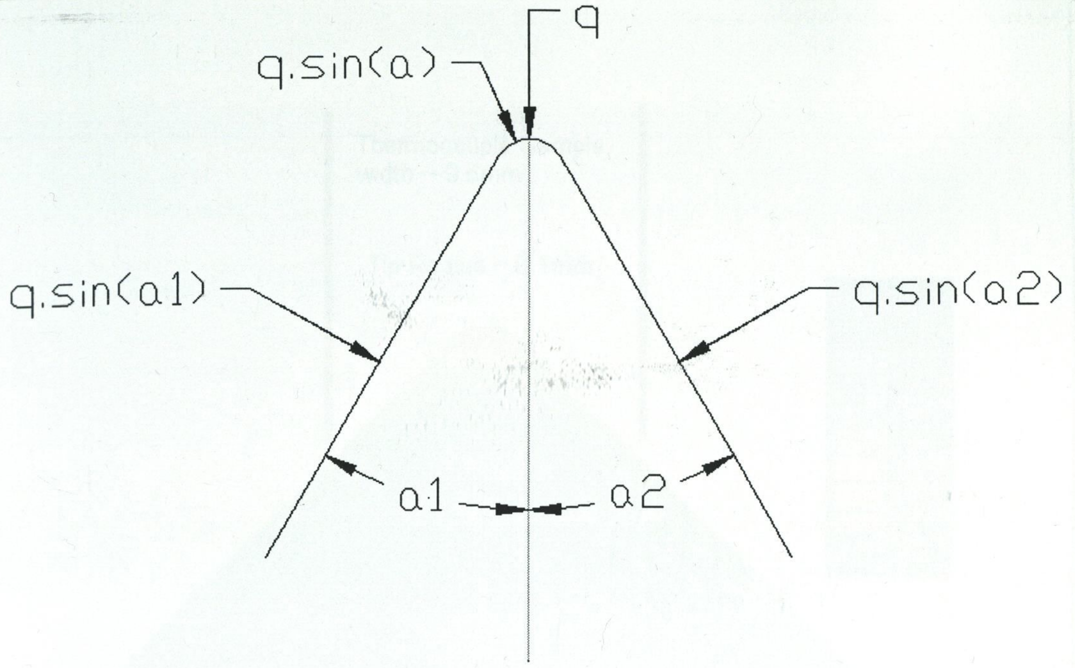

**Figure 5.15 – Fillet radius loading diagram**

angle is small. For example, if the included angle is 60°, then the tip temperature will still be about twice that of the flanks, as illustrated in figure 5.15.

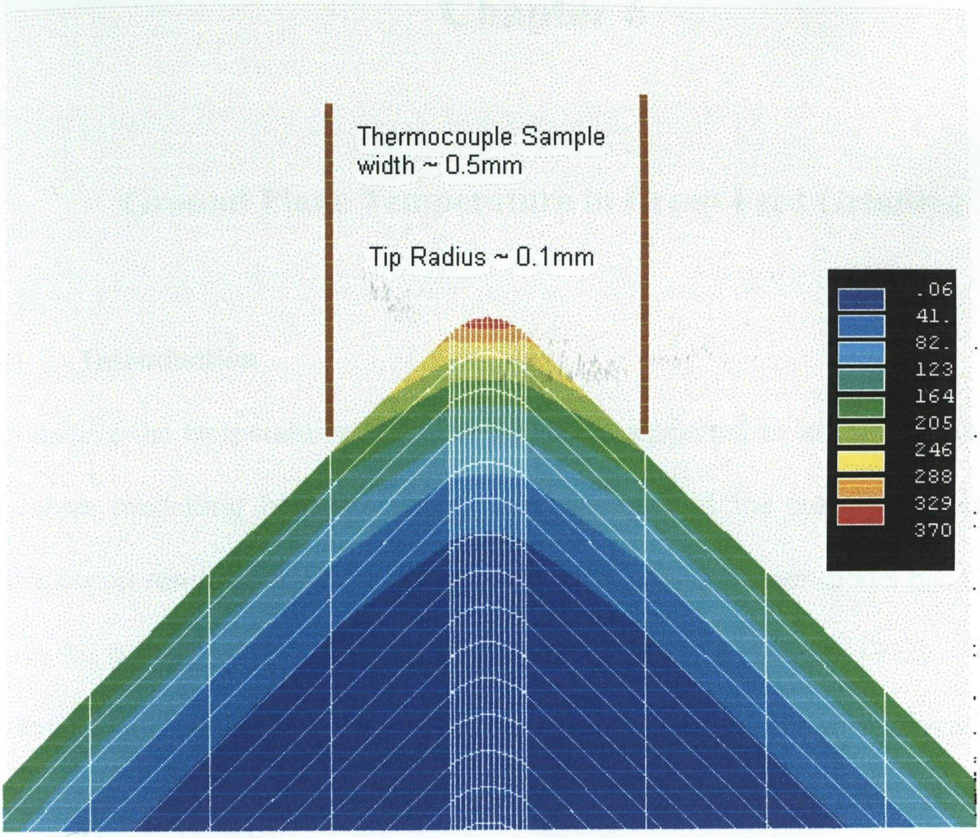

**Figure 5.16 – Thermocouple sample width over temperature distribution**

# Chapter 6

# Ground Plane Temperature in Creep Feed Grinding

## 6.1 Introduction

Modelling the temperatures that a workpiece is subjected to in the grinding process involves modelling both the energy partitioning, and the subsequent temperature distribution resulting from the energy input. The classic Jaeger model has formed the basis for many models predicting temperature distribution [Jaeger 1942]. The energy partitioning models generally make some assumptions about the average grain temperature being the same as the average workpiece temperature. One common aspect of these efforts has been that the end result is usually a model which estimates the temperature in the arc of cut, during a grinding cycle.

In creep feed grinding, however, it is not the temperature in the arc of cut that is of interest. Rather, the temperature that the remaining ground plane experiences, is of interest. In conventional shallow-cut grinding, the depth of cut is very small, typically of the order of microns. The maximum temperature in the arc of cut is a reasonable approximation of the maximum ground plane temperature. The creep feed grinding process, on the other hand, uses depths of cut of the order of millimetres. Figures 6.1 and 6.2 illustrate some typical creep feed grinding applications. Figure 6.1 shows a turbine blade. The root of the blade has a fir-tree form, which is achieved using a wheel dressed in the form of a fir tree. The form is ground in one pass, and the depth of cut is several millimetres. Figure 6.2 shows some components with slots which are ground using the creep feed technique. In each case, the remaining surface is a considerable distance from the arc of cut. The implication is that the ground plane temperature may be considerably lower than the arc of cut temperature. This point is supported by the manner in which heat is generated during the creep feed grinding process. It is accepted that the heat is applied proportionally, according to the normal infeed rate. This would preclude the use of the approximation developed by Takazawa [Takazawa 1966] for the temperature below the ground plane, as he only considered the square band source. Essentially, the highest heat input is applied where the depth of cut is greatest, and there is no heat applied at the trailing edge, which is the ground plane. This being the case, the dimensional technique was applied to the problem of the maximum temperature the ground plane experiences, and a series of finite element models were solved, allowing the development of a closed form solution to this problem.

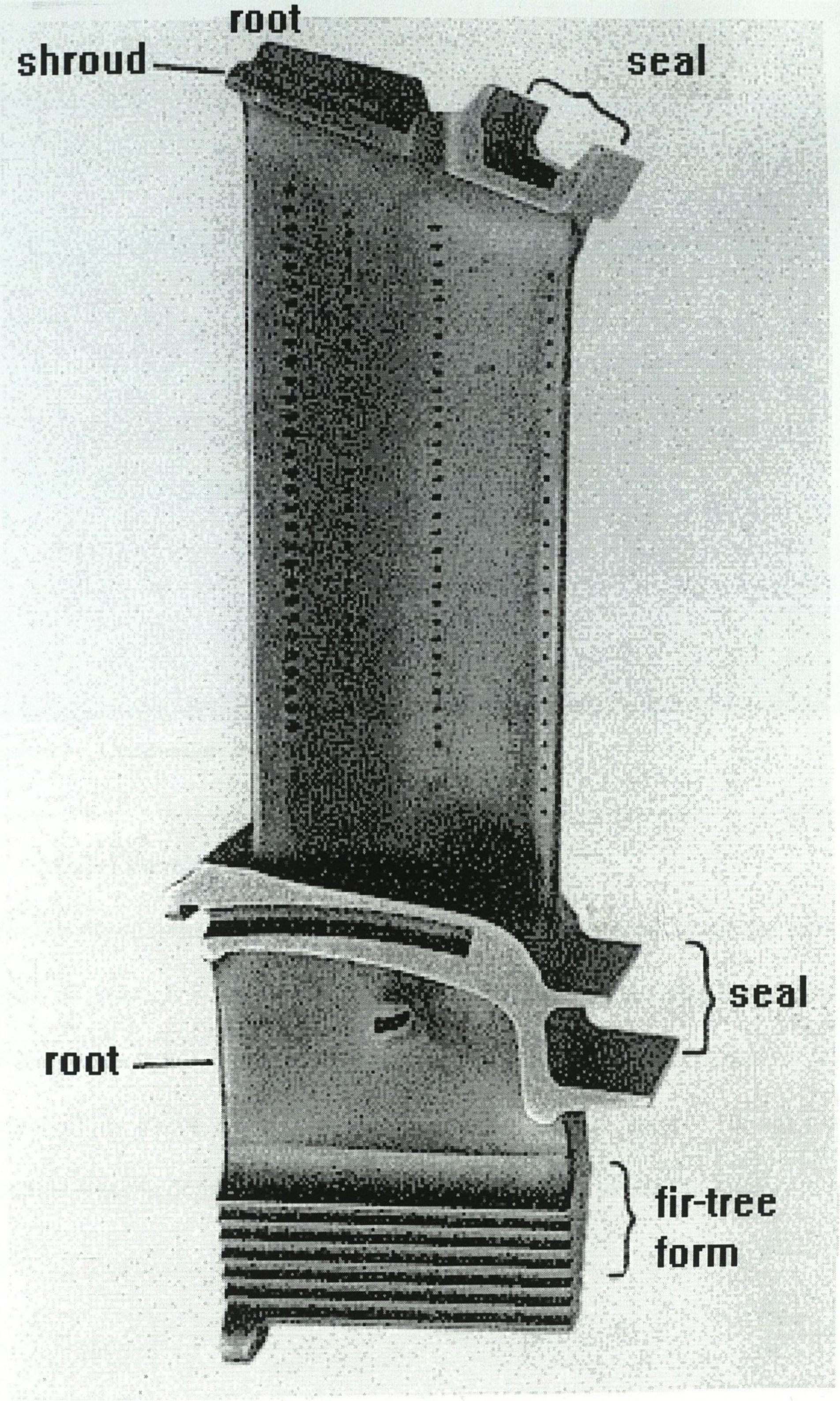

Figure 6.1 – Turbine blade

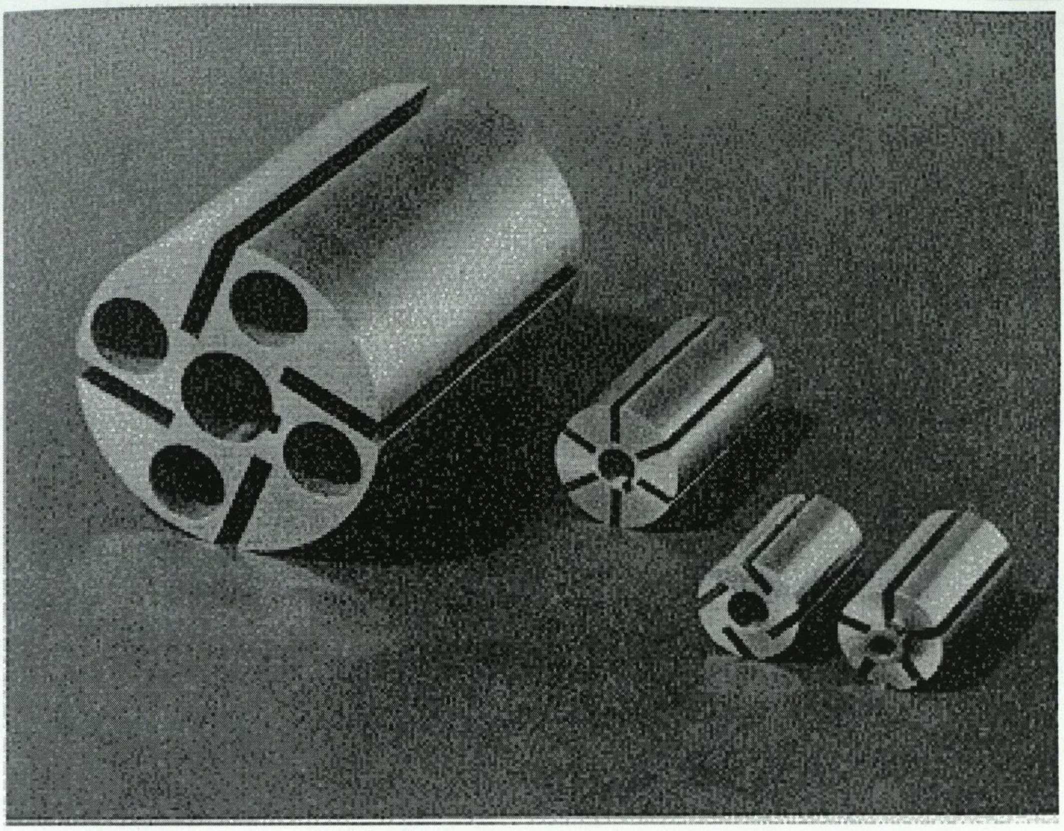

**Figure 6.2 – Components with slots**

## 6.2 Model Development

The initial development of the dimensionless model followed along the same lines as outlined in chapters 3 and 4. To facilitate the modelling, a chord approximation was used to represent the wheel/work contact geometry. This approximation is good for large diameter wheel, where contact geometry is almost linear. The only additional parameter was the depth of cut. A dimensional analysis yields the following result:

$d = [\mathrm{L}]$

$$\theta_m = \frac{q}{\beta}\sqrt{\frac{l_c}{V}}\varphi\left(\frac{d}{l_c}\right)$$

**Equation 6.1**

The parameter $d/l_c$ can be replaced by the chord angle:

While this dimensional solution (equation 6.4) contains an additional parameter more than equation 6.2, there are two clear advantages to this form. The first of these advantages is that the formulation is of the same form as the standard Jaeger [Jaeger 1942] model, and also conforms with the later efforts of DesRussieux & Zerkle [DesRussieux & Zerkle 1970], and Chao & Trigger [Chao & Trigger 1953]. This allows a direct comparison of results with those derived by the aforementioned, and allows presentation in a recognised style.

The second advantage concerns the finite element modelling, necessary to determine the function $\varphi_I$. Because the temperature is not an explicit function of the arc length of cut, rather a function of the non-dimensional length L, it is not necessary to explicitly vary the arc length in the finite element model, only the non-dimensional length. The finite element models developed to investigate this problem are quite complex, due to the fact that the removal of material must be modelled. The formulation for the temperature outlined above allows a great saving to be made in the modelling time, which was considerable.

## 6.3 The Finite Element Modelling

The finite element models were two-dimensional transient thermal analyses with element removal simulating the material removed by the grinding wheel in grinding practice. The two dimensional assumption means that convective cooling at the edges of the workpiece is neglected. This would, in practice, serve to lower workpiece temperatures locally, but it is unlikely that the maximum arc of cut temperature would be affected by such cooling. In essence, a heat source conforming to the maximum normal infeed was moved along a plane, until steady state conditions were achieved.

The elements behind the sliding heat source were removed, using the element kill option featured in the Ansys software.

Three different angles of inclination were considered: 7 °, 10 °, 15°. These were expected to give a reasonable representation of creep feed grinding operating regions. The models were constructed as illustrated in figure 6.3. The heat source was applied as a triangular function, the maximum heat input at the leading edge, reducing to zero at the trailing edge. This is an excellent representation of the normal infeed loading, given by sin($\gamma$), for values of $\gamma$ up to about 20 °. $\gamma$ is the angle made between the trailing edge of the wheel-work contact, the wheel centre, and some point in the wheel-work contact. In this region, sin($\gamma$) is virtually linear. The heat source was applied for a time representing an arbitrarily chosen velocity. The heat source was then removed, and applied on the next inclined plane, again for the same time. The elements associated with the preceding area were then deactivated. This process was continued along the length of the model, which was sufficiently long to allow steady state conditions to prevail. In the general course of events, this type of problem would be solved in a batch mode. This involves writing each successive load case into a load step file, and subsequently solving each load step file in a non-interactive fashion. Unfortunately, the Ansys software does not support element birth and death operations from load step files, necessitating an interactive solution of the models. This is a major drawback when many models require solution. In an effort to overcome this, an input file was created. An input file is a series of commands. The input file allowed a series of previously generated load cases to be applied and solved interactively, complete with the required element death, without requiring operator input. Essentially, this meant that an input file for each of the three considered angles was generated, and the load cases applied were modified between successive problems. This greatly reduced the modelling time, despite the initial time overhead involved setting up the input and load case files.

The following figures illustrate the character of the finite element results. The mesh is illustrated in figure 6.3. The parallelograms on the surface represent the material to be removed, the heat source being sequentially applied on the generated surfaces. Figure 6.4 demonstrates the loading type, i.e. triangular. The remaining finite element models show a specific solution for the first, last, and an intermediate load step (figures 6.5 6.6, 6.7).

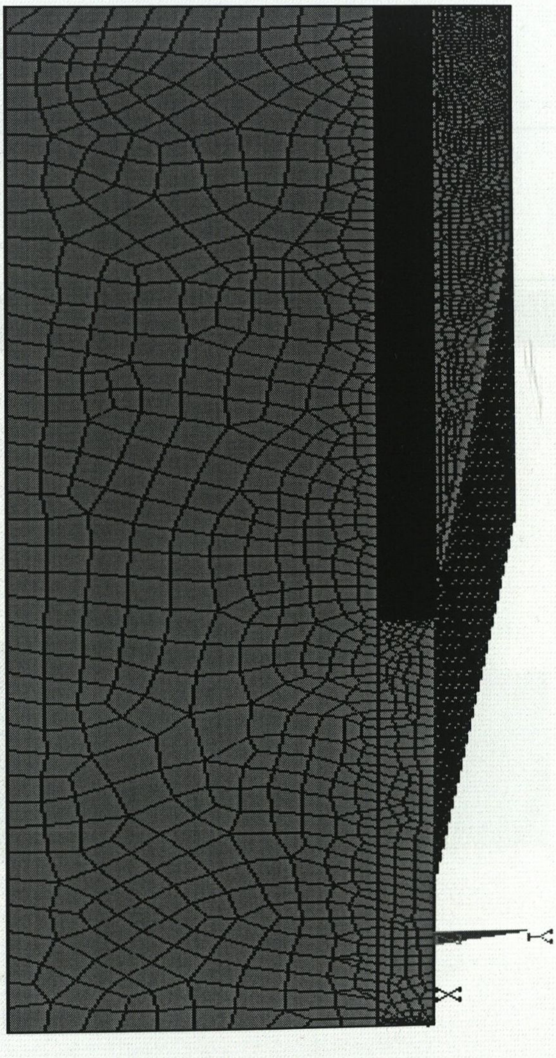

**Figure 6.3 – The finite element model for creep feed grinding**

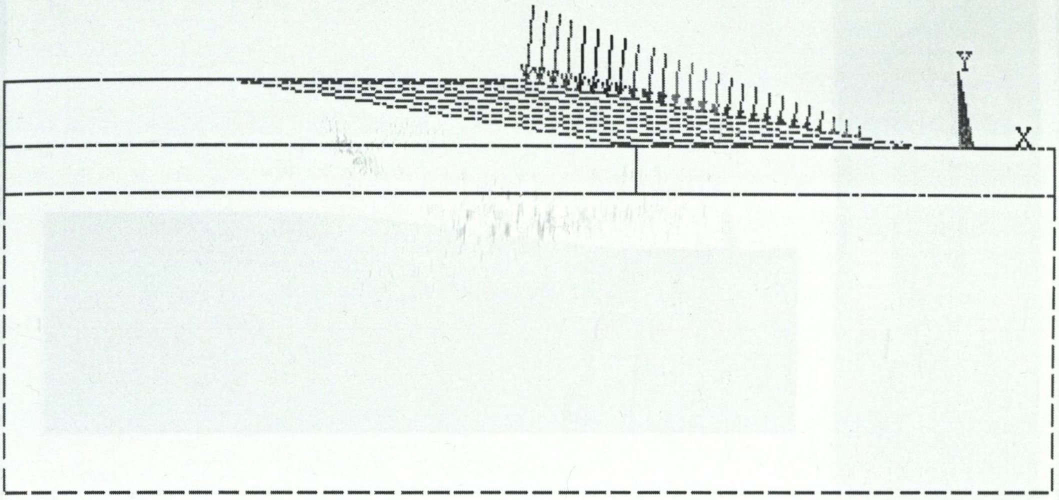

Figure 6.4 – Loading of finite element model

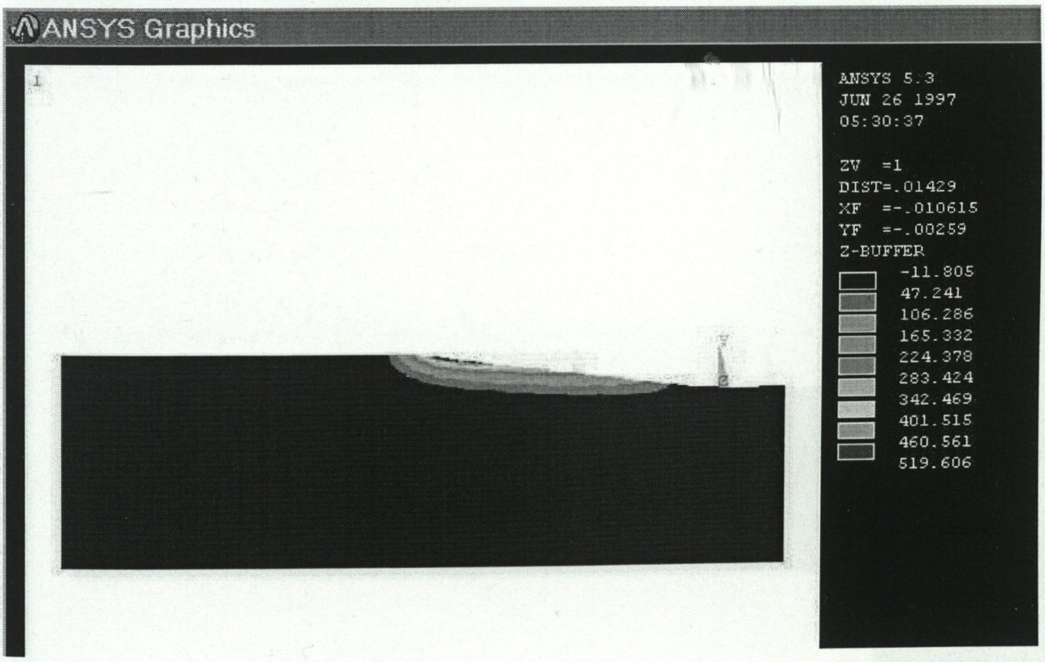

Figure 6.5 – Temperature at start of pass

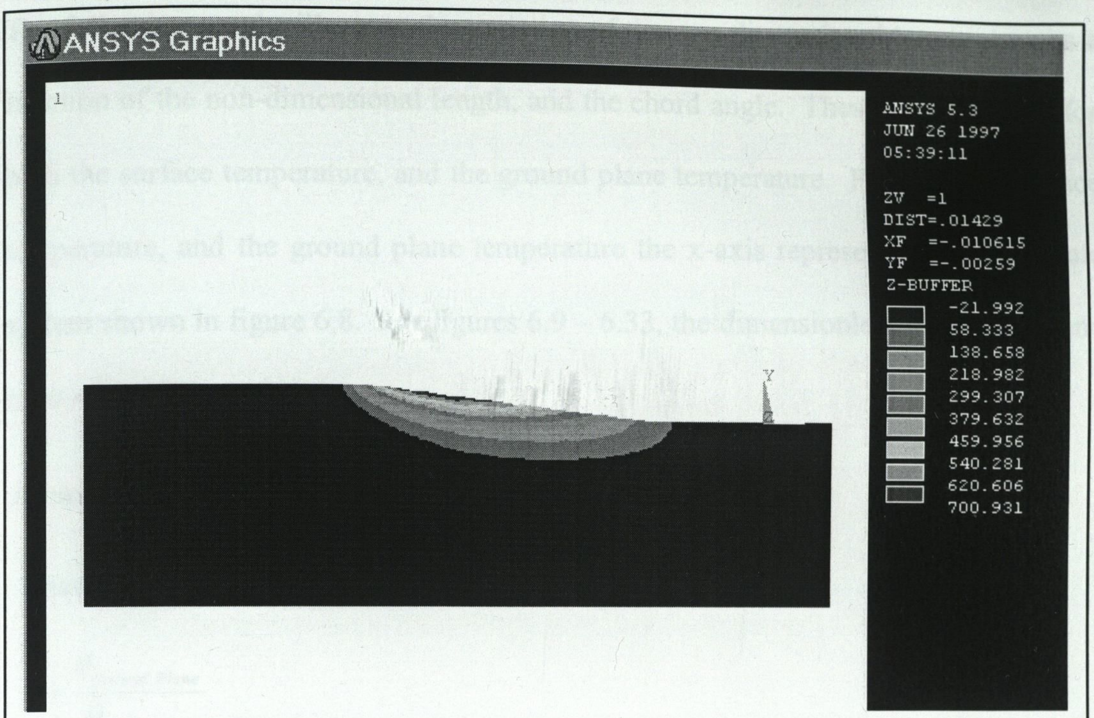

ANSYS 5.3
JUN 26 1997
05:39:11

ZV =1
DIST=.01429
XF =-.010615
YF =-.00259
Z-BUFFER
-21.992
58.333
138.658
218.982
299.307
379.632
459.956
540.281
620.606
700.931

Figure 6.6 – Temperature at middle of pass

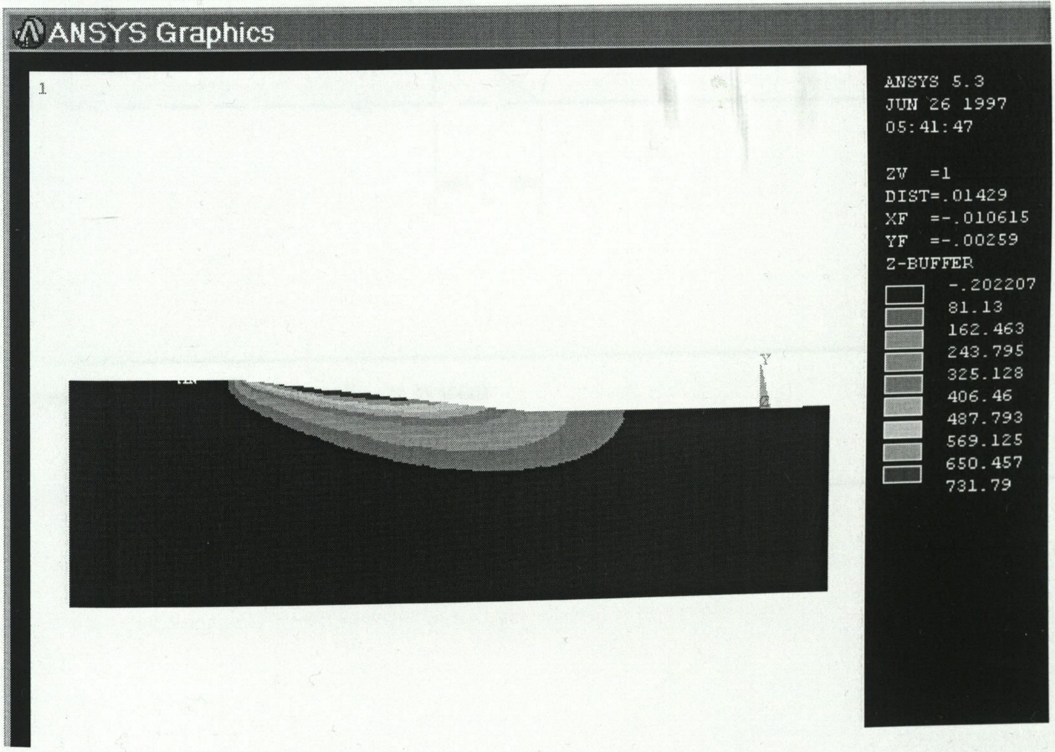

ANSYS 5.3
JUN 26 1997
05:41:47

ZV =1
DIST=.01429
XF =-.010615
YF =-.00259
Z-BUFFER
-.202207
81.13
162.463
243.795
325.128
406.46
487.793
569.125
650.457
731.79

Figure 6.7 – Steady state temperature

The following graphs illustrate the variation of the non-dimensional temperature as a function of the non-dimensional length, and the chord angle. These are illustrated for both the surface temperature, and the ground plane temperature. For both the surface temperature, and the ground plane temperature the x-axis represents the co-ordinate system shown in figure 6.8. For figures 6.9 – 6.33, the dimensionless temperature and ratio $r$ are defined as:

$$\textit{Dimensionless Temperature} = \frac{\theta \pi k V}{2qK}$$

**Equation 6.5**

$$r = \frac{\theta_{\textit{Ground Plane}}}{\theta_{\textit{Arc of Cut}}}$$

**Equation 6.6**

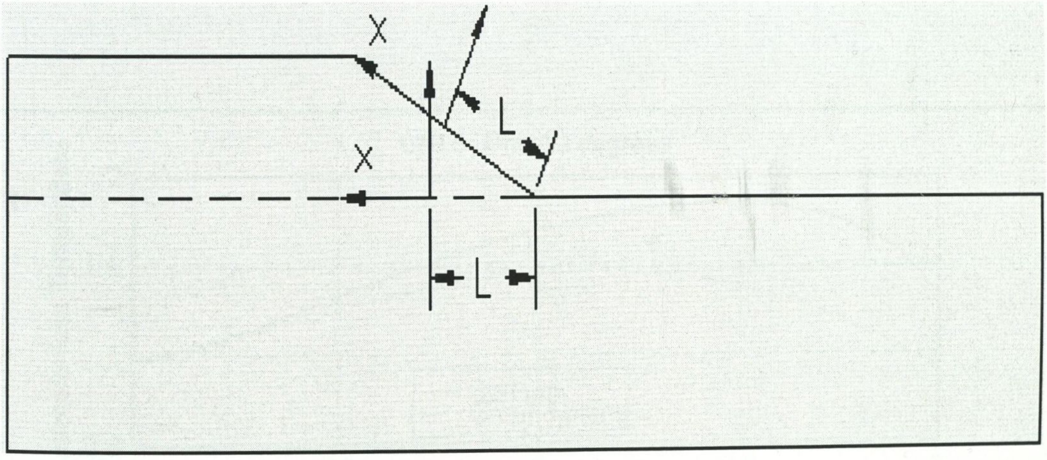

**Figure 6.8 – Reference co-ordinate system**

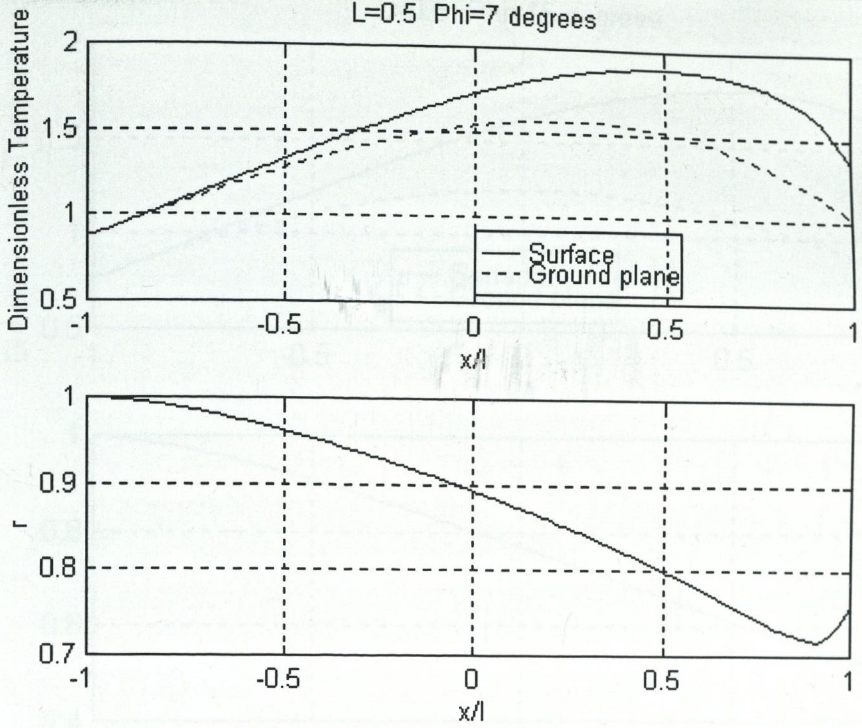

**Figure 6.9 – Temperature distribution, L=0.5, $\psi$=7°**

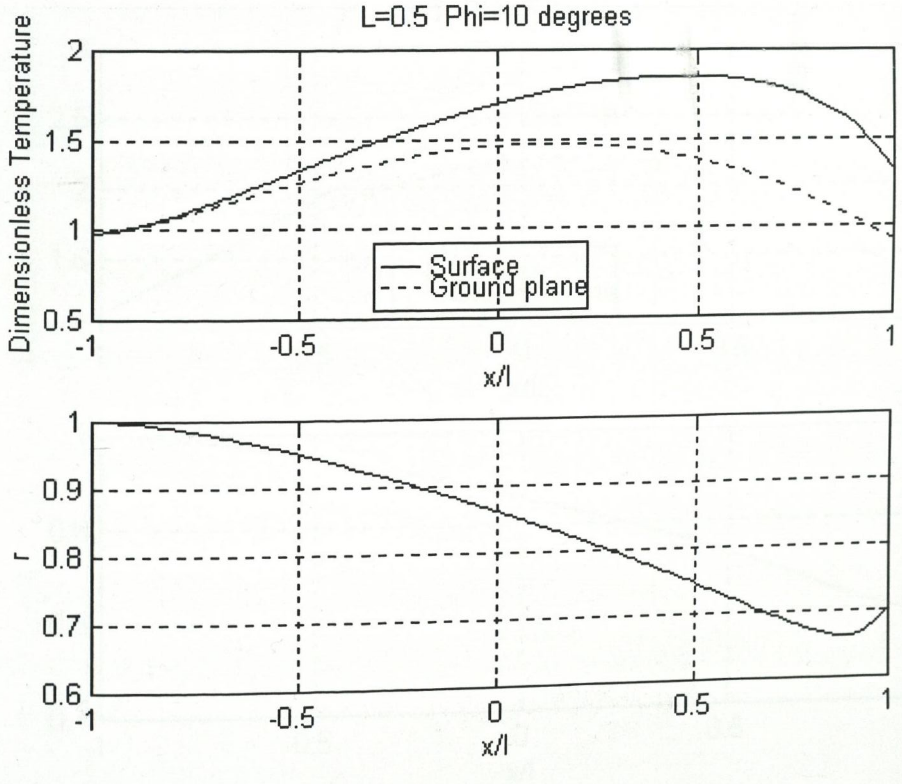

**Figure 6.10 – Temperature distribution, L=0.5, $\psi$=10°**

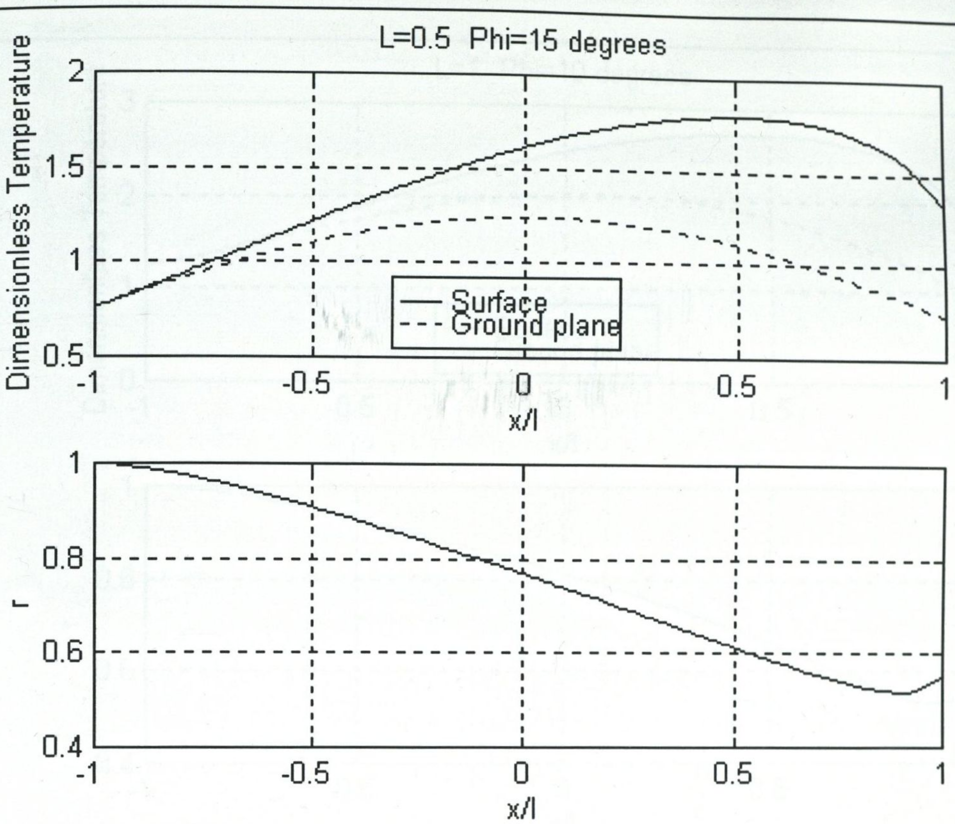

Figure 6.11 – Temperature distribution, L=0.5, ψ=15°

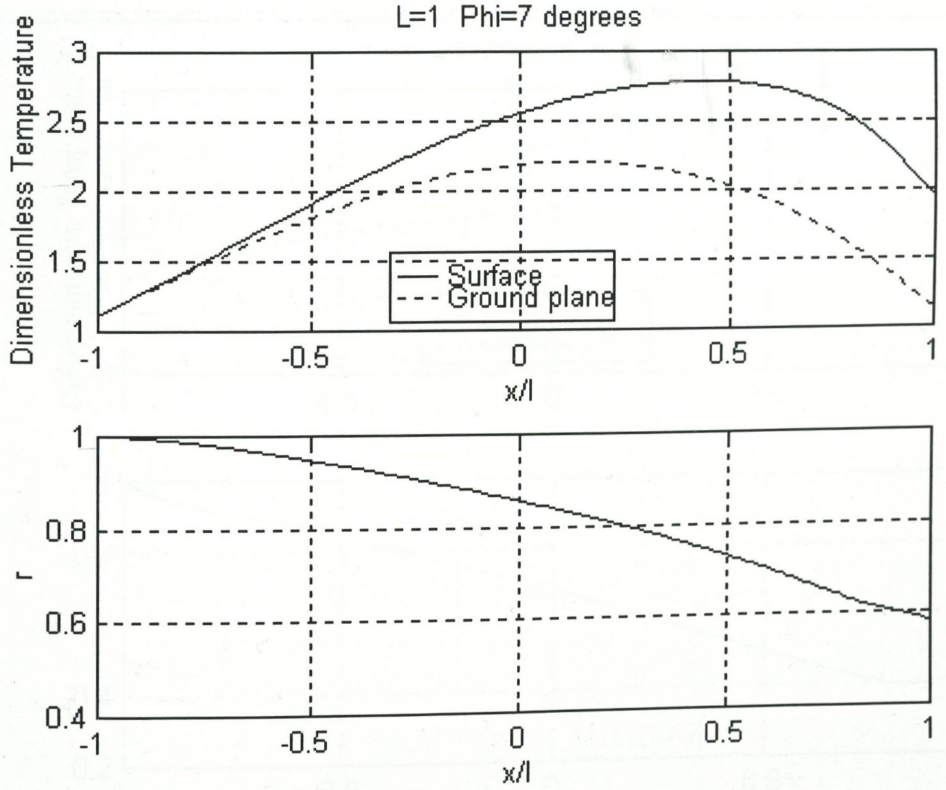

Figure 6.12 – Temperature distribution, L=1, ψ=7°

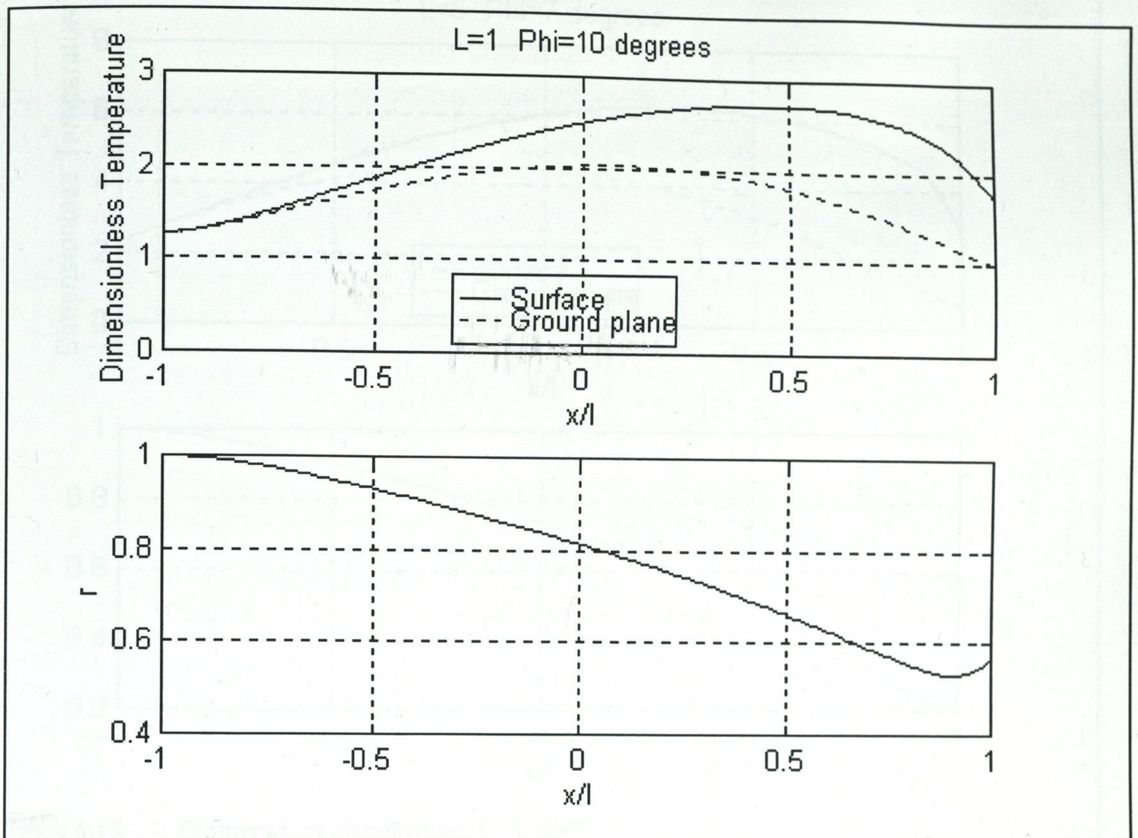

**Figure 6.13 – Temperature distribution, L=1, ψ=10°**

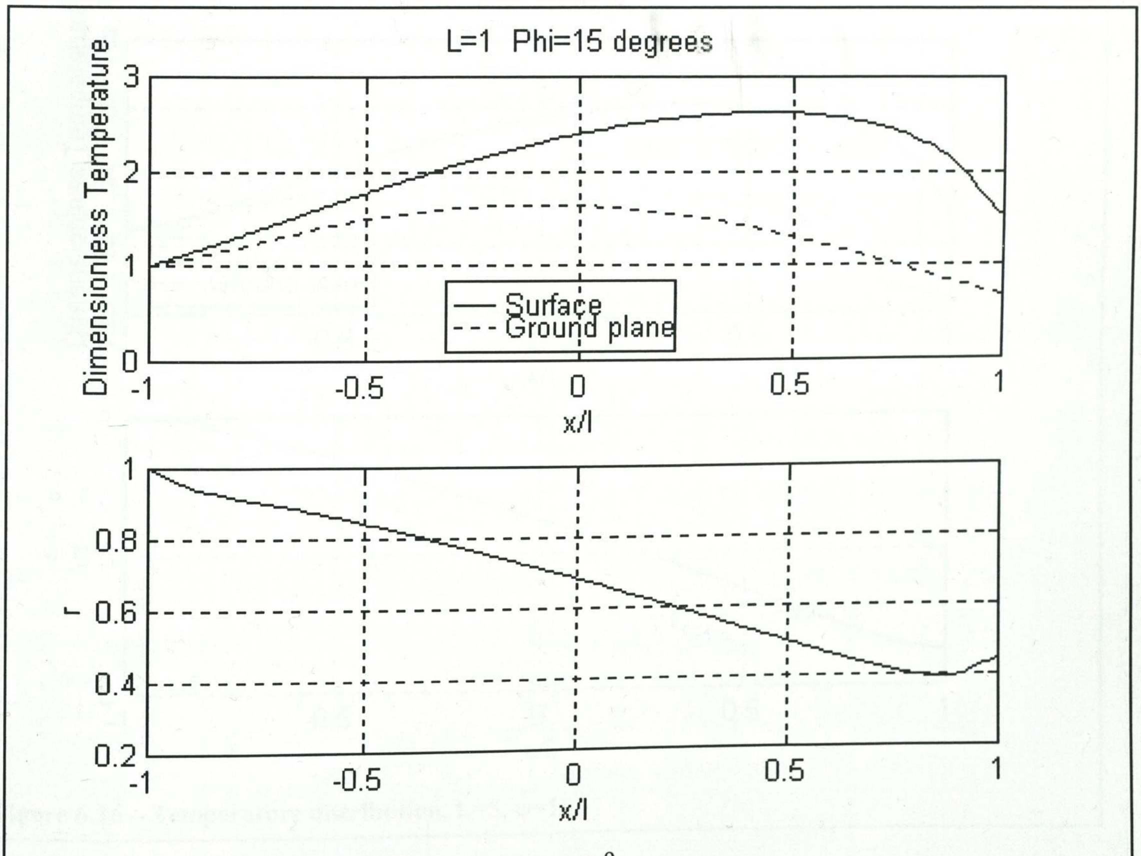

**Figure 6.14 – Temperature distribution, L=1, ψ=15°**

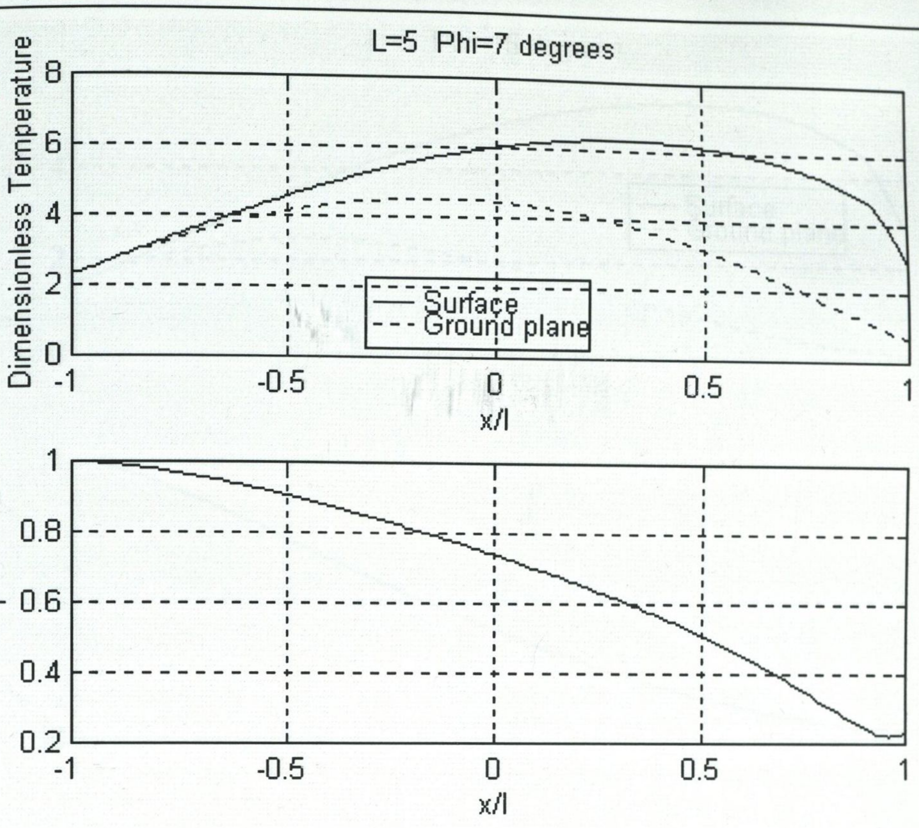

**Figure 6.15 - – Temperature distribution, L=5, $\psi=7^{o}$**

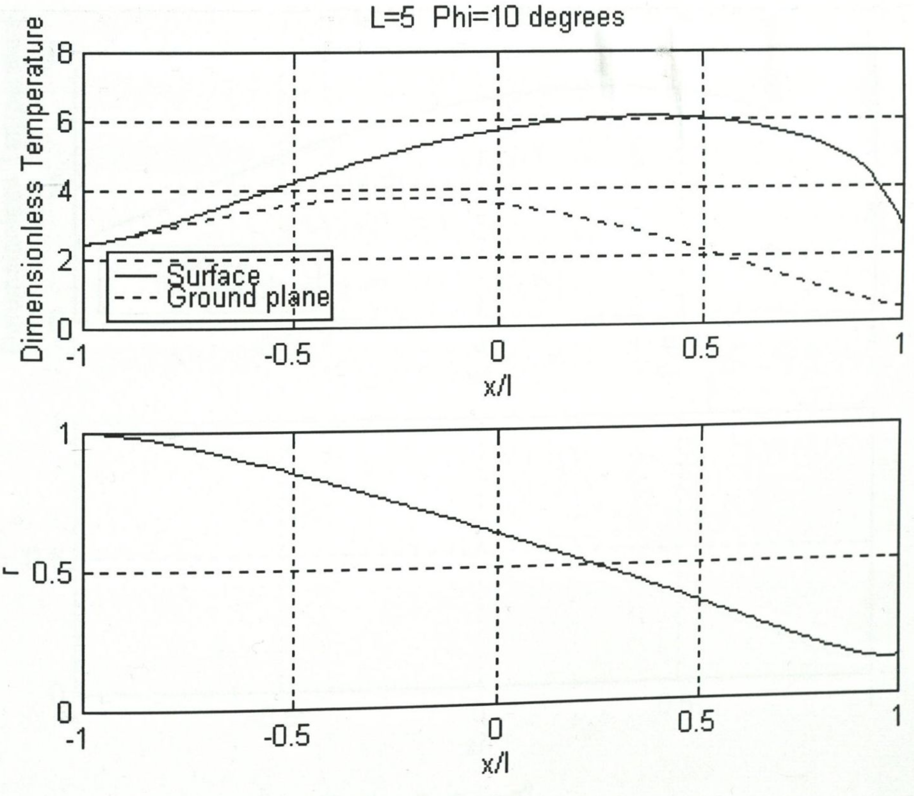

**Figure 6.16 – Temperature distribution, L=5, $\psi=10^{o}$**

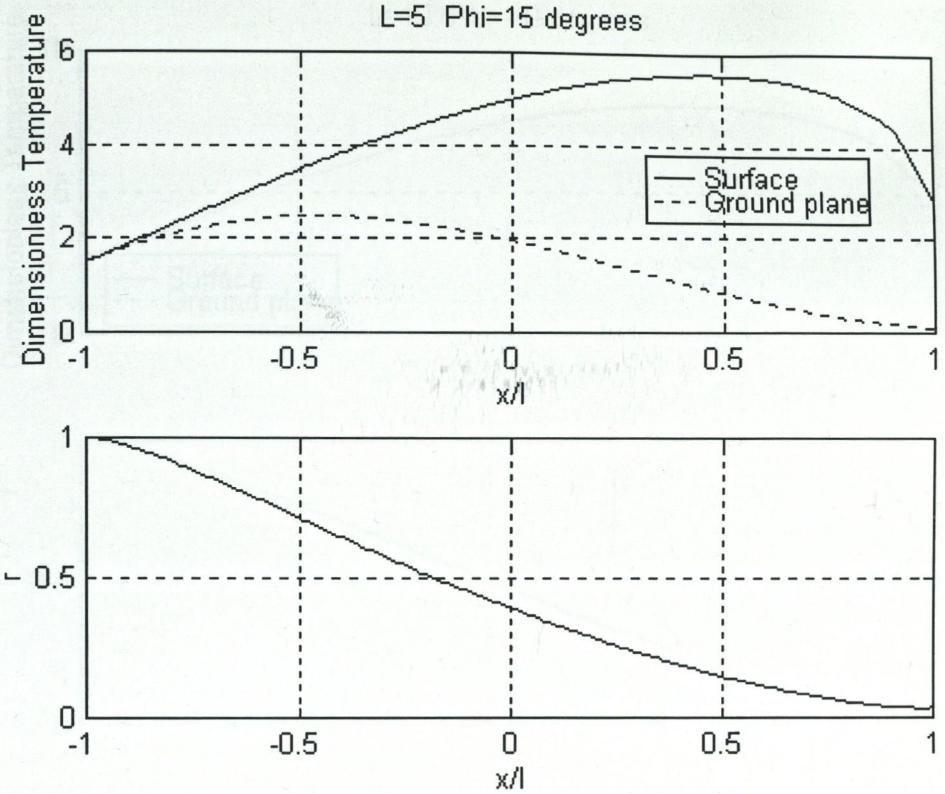

**Figure 6.17 – Temperature distribution, L=5, ψ=15°**

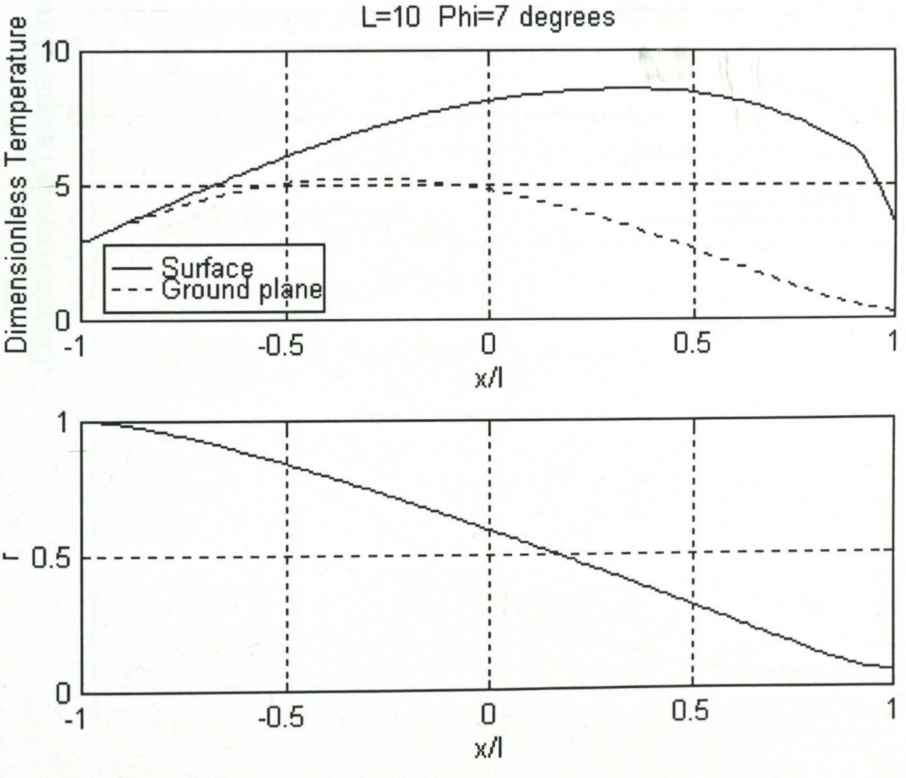

**Figure 6.18 – Temperature distribution, L=5, ψ=7°**

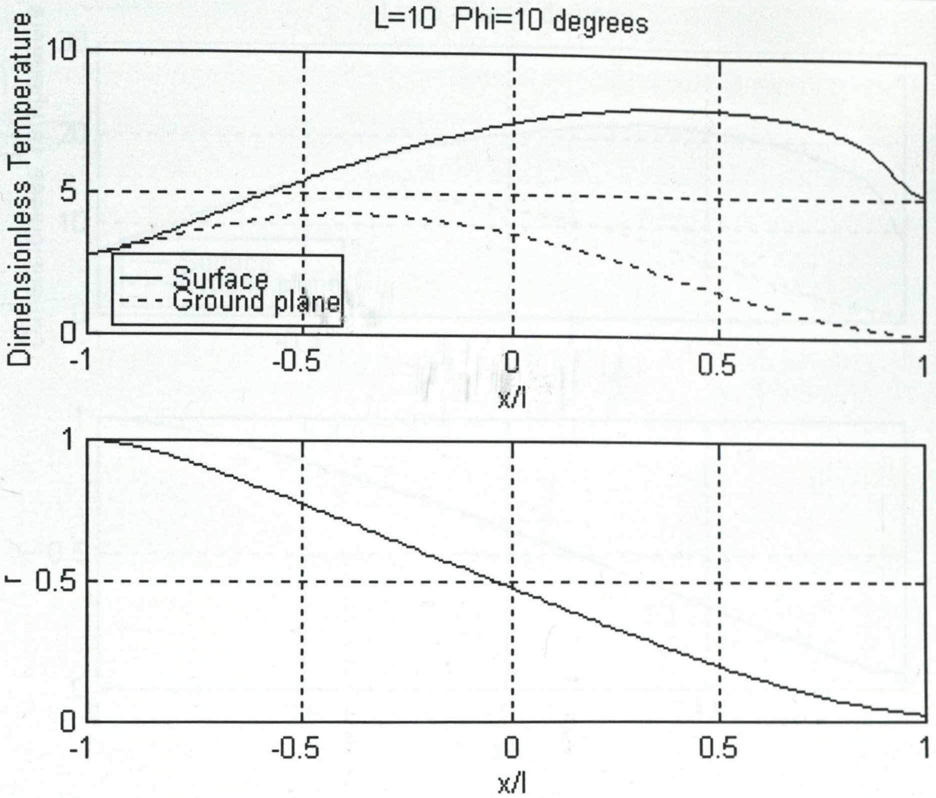

Figure 6.19 – Temperature distribution, L=10, ψ=10°

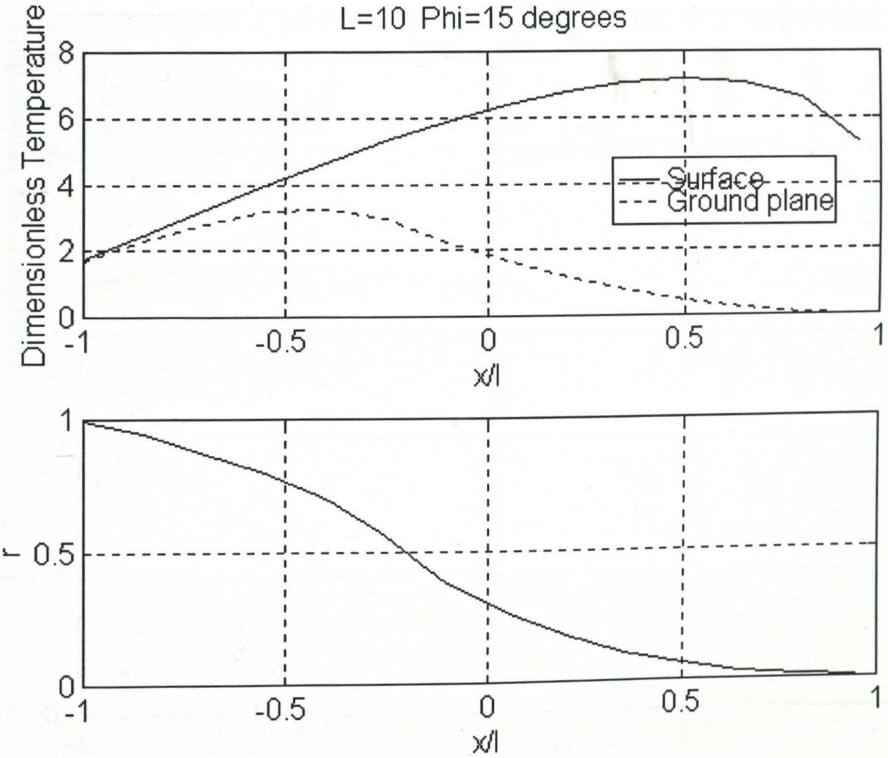

Figure 6.20 – Temperature distribution, L=10, ψ=15°

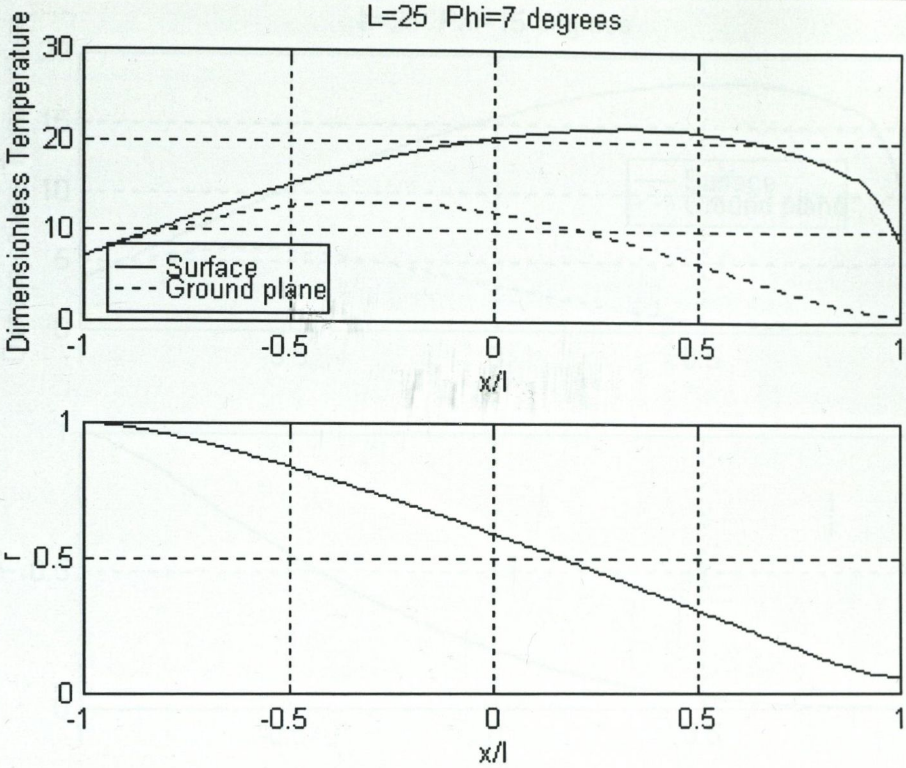

**Figure 6.21 – Temperature distribution, L=25, ψ=7°**

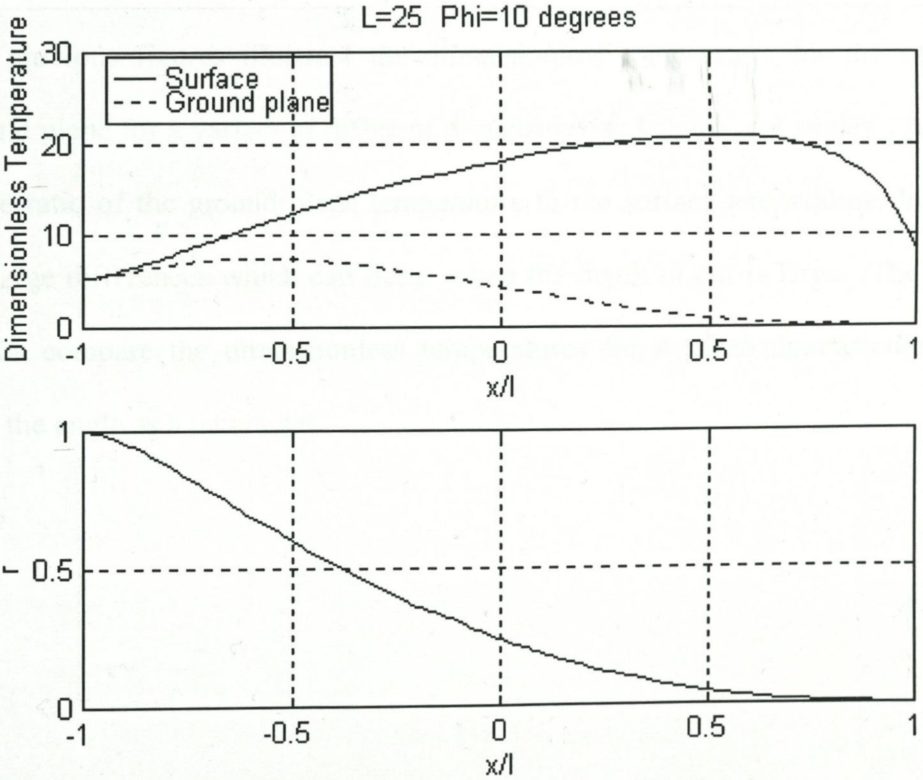

**Figure 6.22 – Temperature distribution, L=25, ψ=10°**

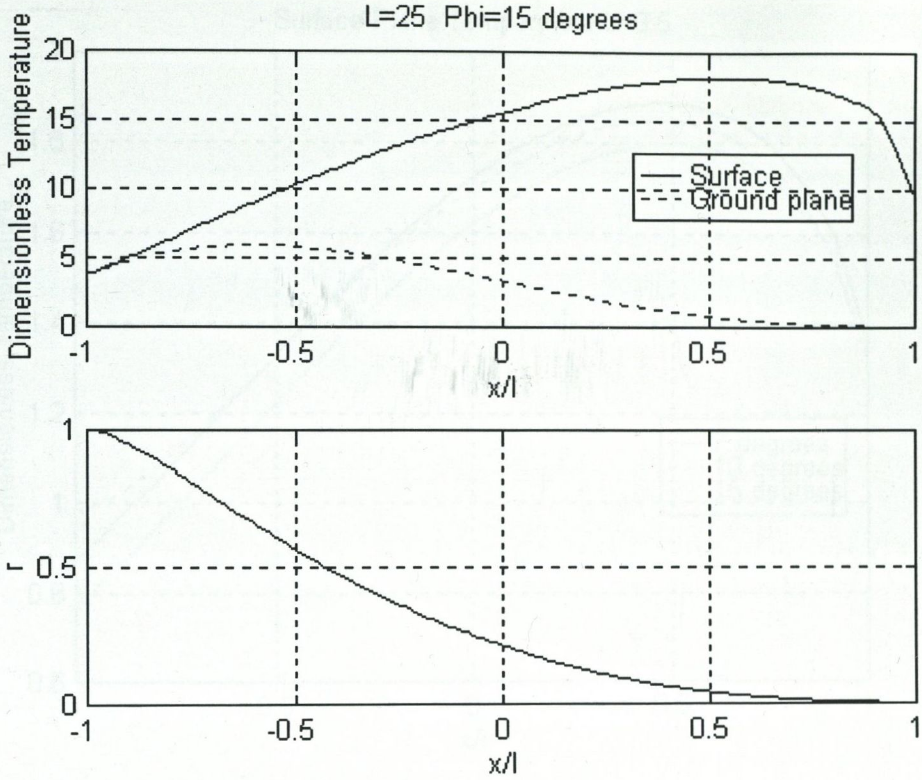

Figure 6.23 – Temperature distribution, L=25, $\psi$=15°

The previous figures illustrate the dimensionless temperature for the surface and ground plane for a variety of different dimensionless lengths and angles. Also shown is the ratio of the ground plane temperature to the surface temperature, highlighting the large differences which can occur when the depth of cut is large. The following graphs compare the dimensionless temperatures for a given dimensionless length, with the angle as a parameter.

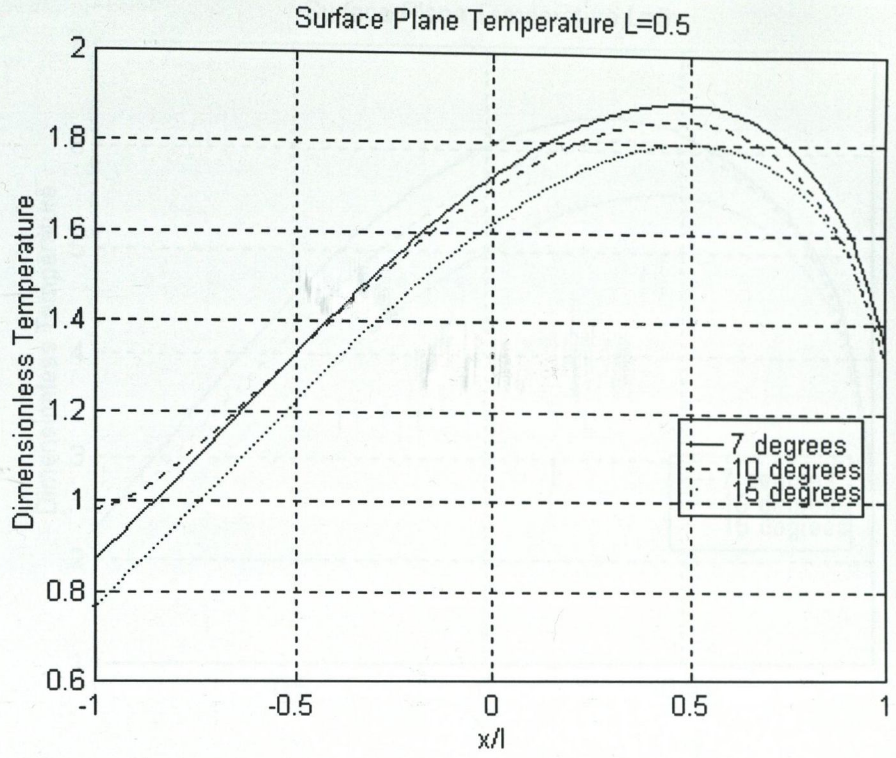

Figure 6.24 – Surface temperature, various angles, L=0.5

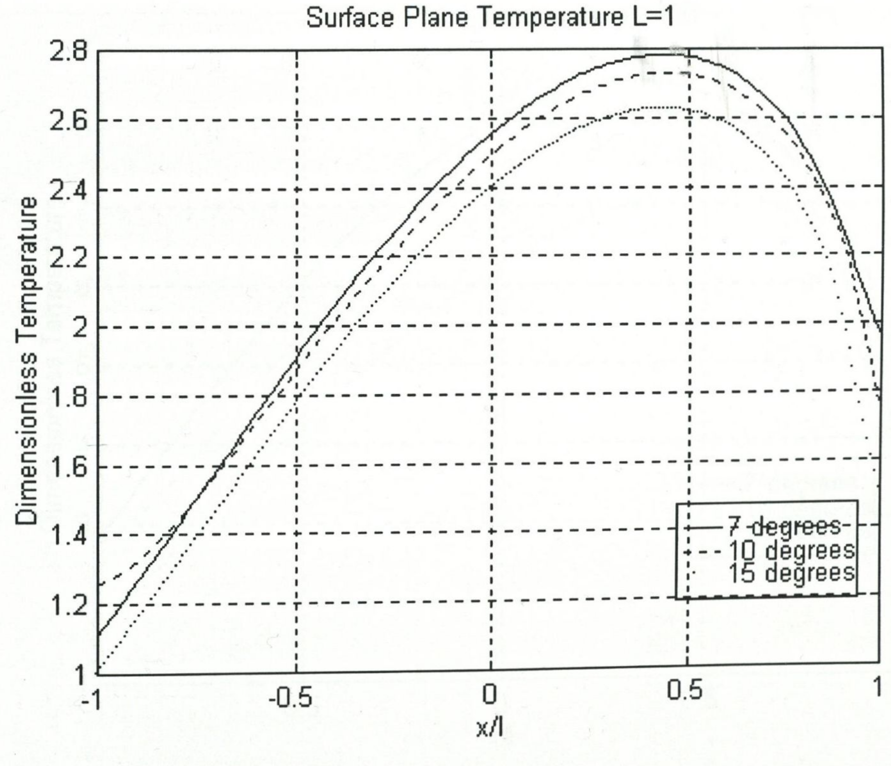

Figure 6.25 – Surface temperature, various angles, L=1

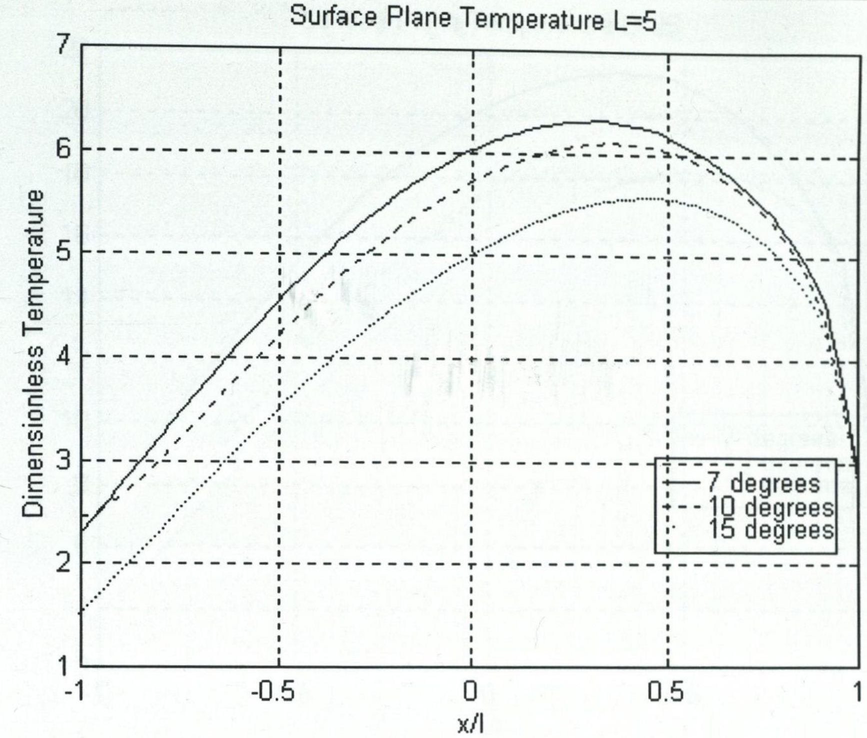

Figure 6.26 – Surface temperature, various angles, L=5

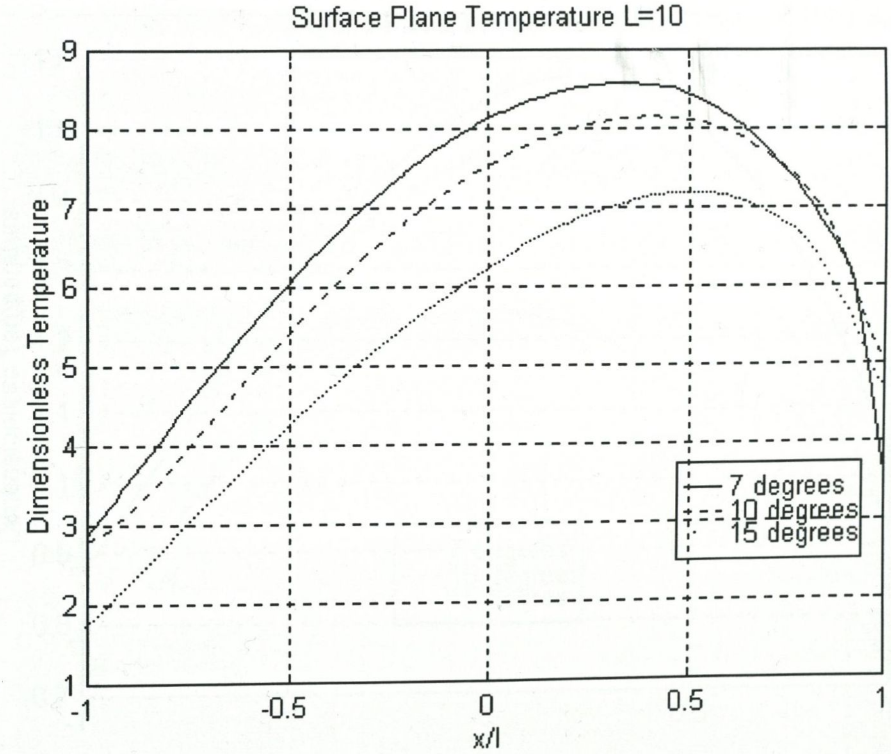

Figure 6.27 – Surface temperature, various angles, L=10

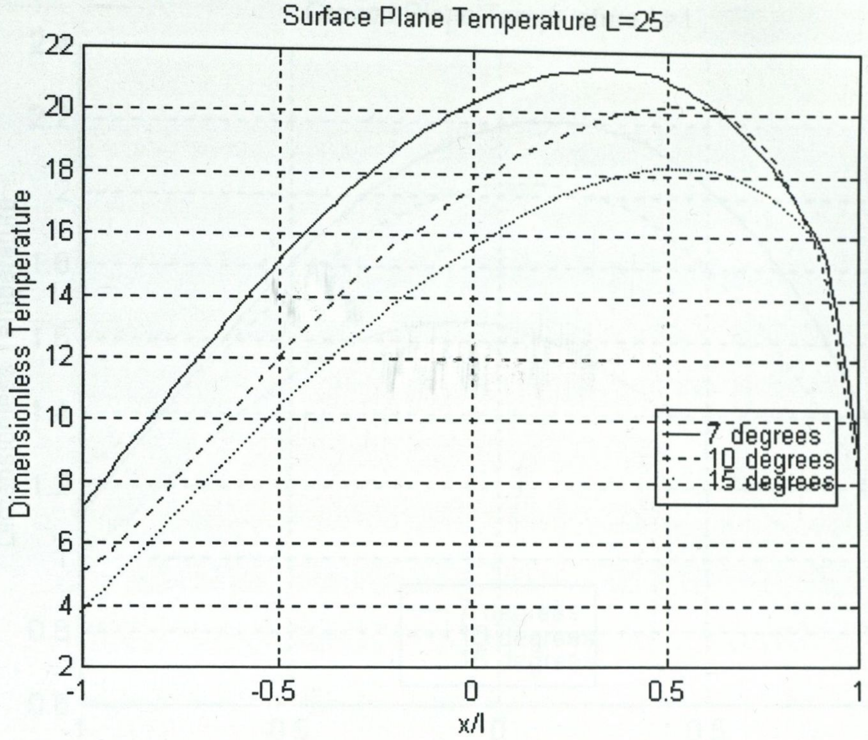

**Figure 6.28 – Surface temperature, various angles, L=25**

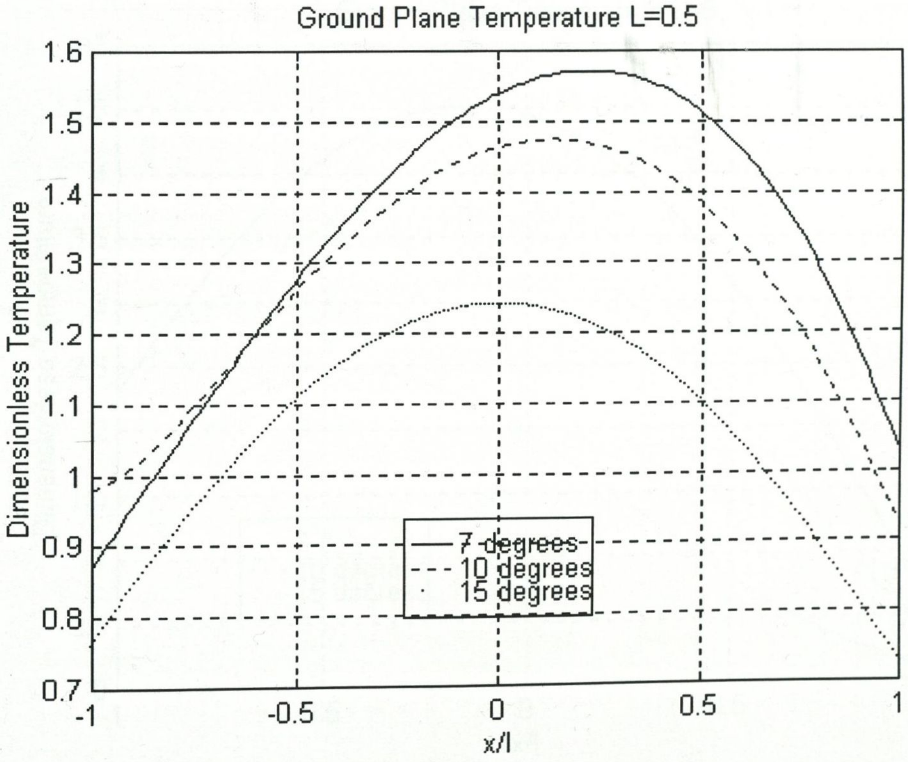

**Figure 6.29 – Ground plane temperature, various angles, L=0.5**

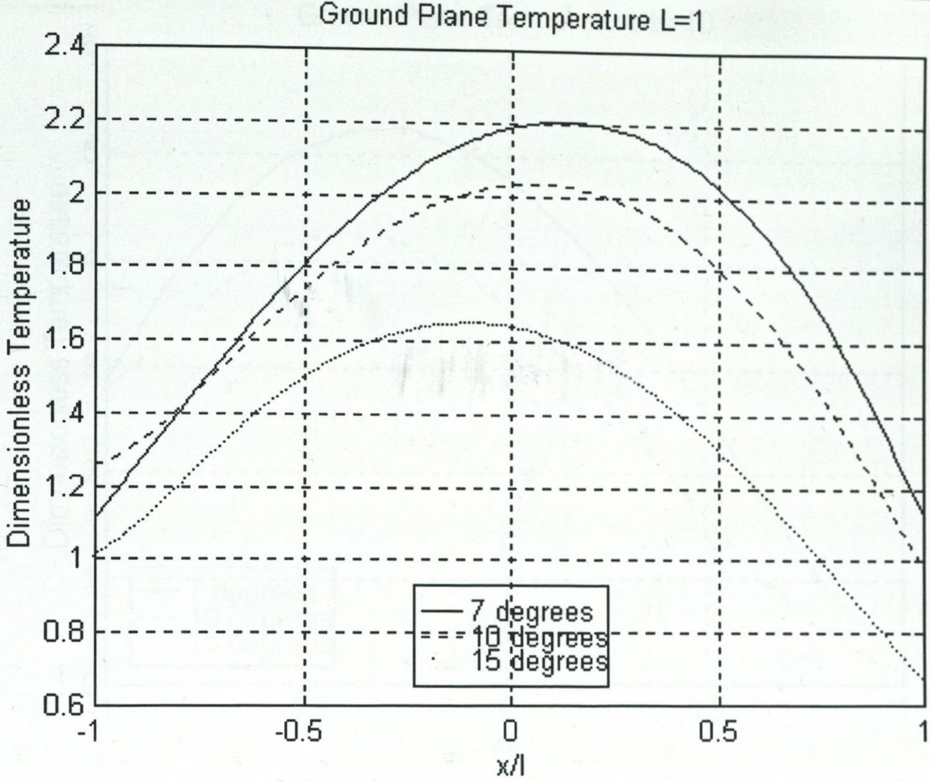

Figure 6.30 – Ground plane temperature, various angles, L=1

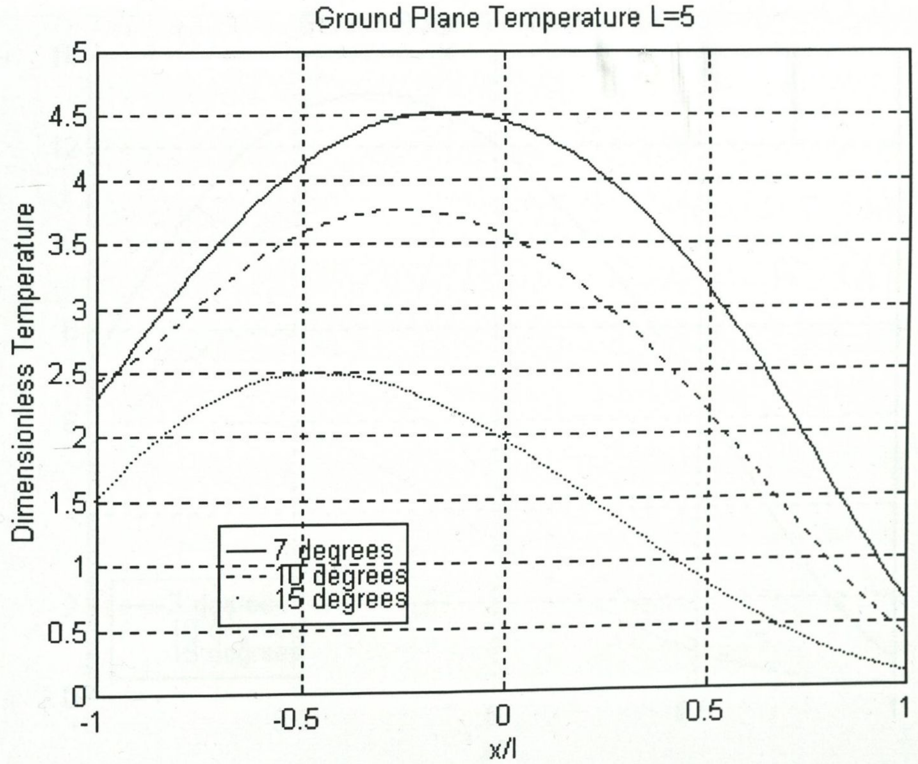

Figure 6.31 – Ground plane temperature, various angles, L=5

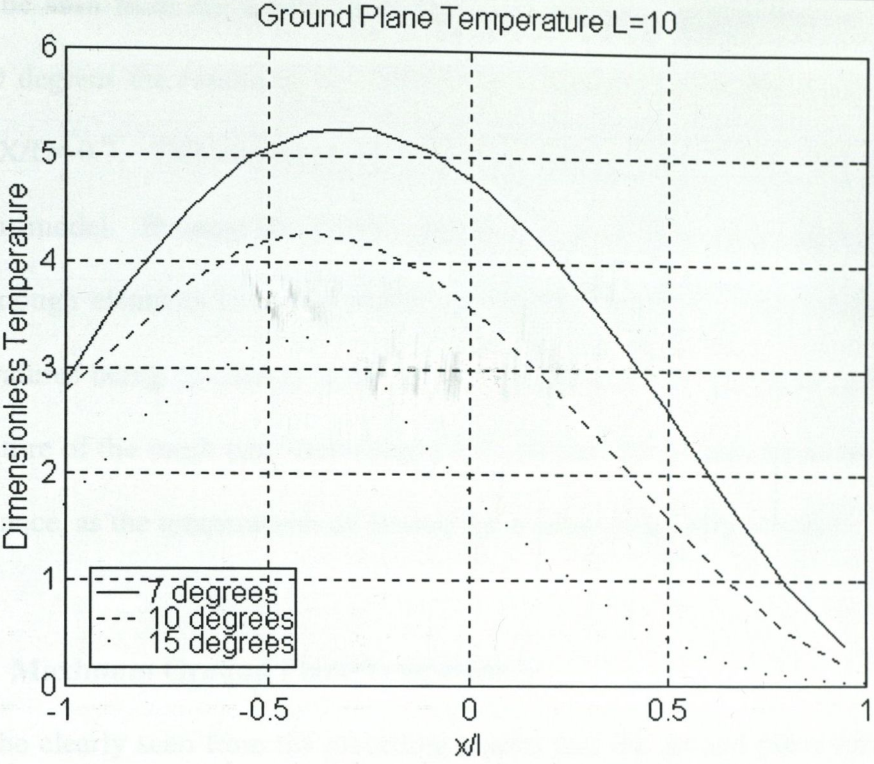

Figure 6.32 – Ground plane temperature, various angles, L=10

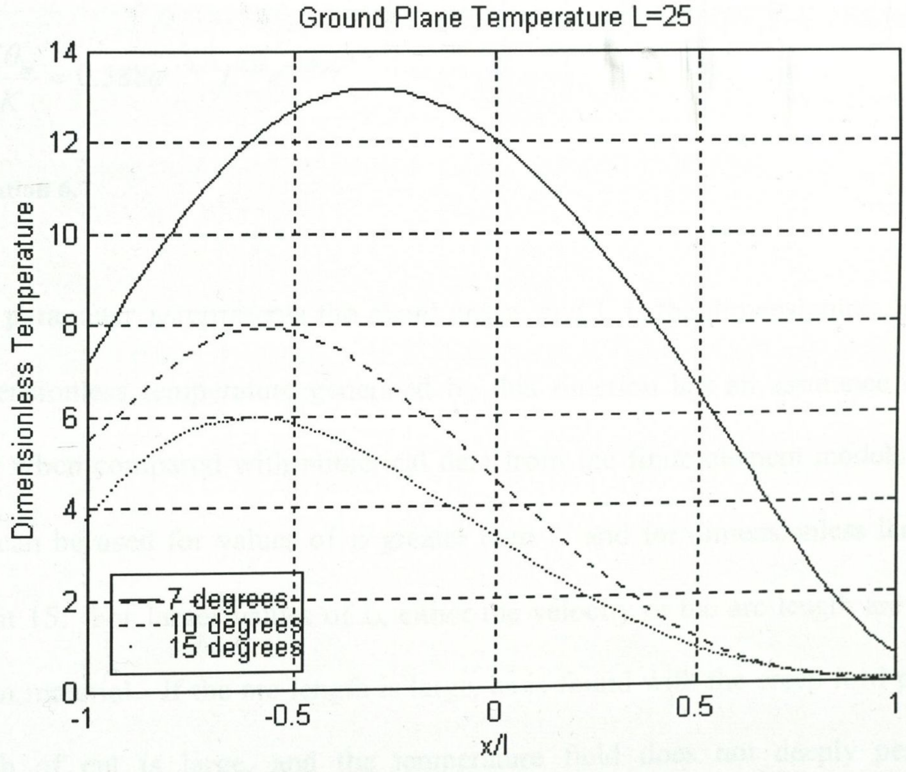

Figure 6.33 – Ground plane temperature, various angles, L=25

It can be seen from the results presented in the previous graphs that for the case of phi=10 degrees the results do not follow the expected trend in the region X/L=-1 to about X/L=-0.7. This can be attributed to the mesh density in this area of the finite element model. Because the angle is small, it is difficult to mesh the corner region with enough elements to accommodate the thermal gradient. This results in higher temperatures being calculated in this part of the model. The problem can be seen in the picture of the mesh type used (figure 6.3). It was not considered to be an issue of importance, as the temperatures of interest lie in other areas of the model.

## 6.4 Maximum Ground Plane Temperature

It can be clearly seen from the preceding graphs that the ground plane temperature is significantly different from the temperature the surface experiences. The maximum surface temperature on the ground plane was combined with the functional form of the solution, outlined in equation 6.4, in the following manner.

$$\frac{\pi k V \theta_m}{2qK} = 0.388\psi^{-0.45} L^{0.36} e^{-0.9\psi L^{-0.55}}$$

**Equation 6.7**

The parameter $\psi$ represents the chord angle, and L is the dimensionless length. The dimensionless temperature generated by this function has an assurance criterion of 0.99 when compared with numerical data from the finite element models. Equation 6.7 can be used for values of $\psi$ greater than $7^{\circ}$ and for dimensionless lengths up to about 15. For larger values of L, either the velocity or the arc length are large for a given material. If the arc length is large, as is found with the creep feed process, the depth of cut is large, and the temperature field does not deeply penetrate the workpiece material, allowing most of the applied heat to be removed with the chips.

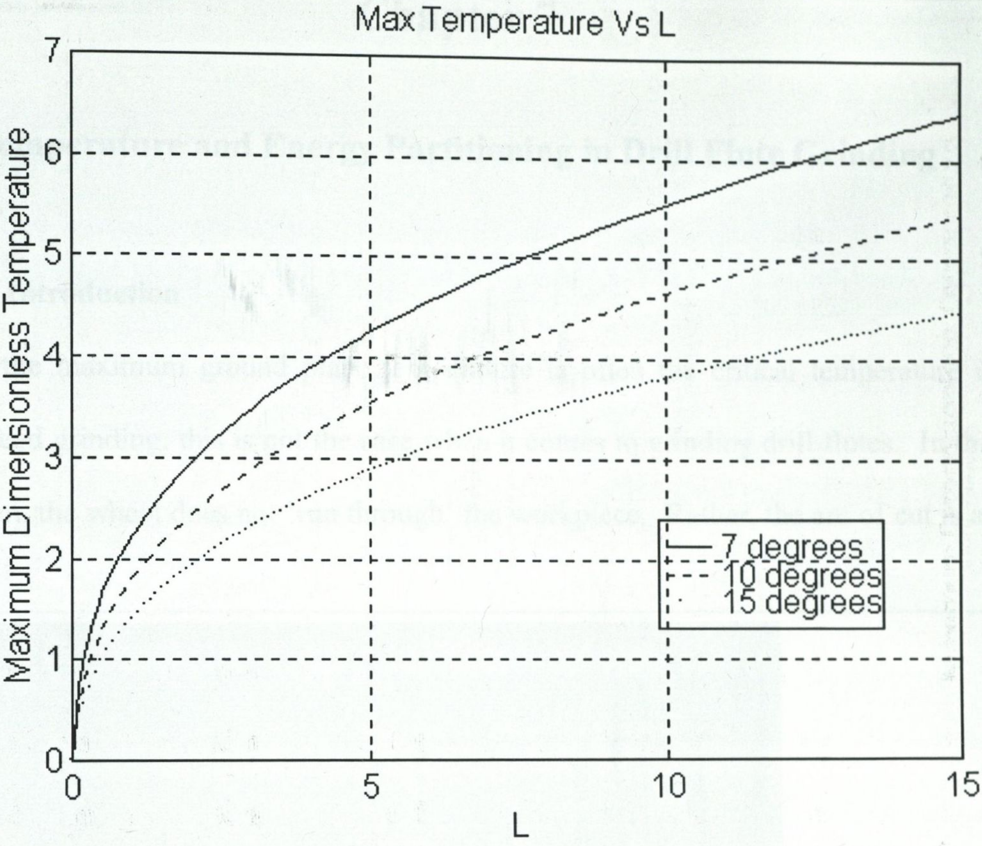

**Figure 6.34 – Maximum ground plane temperature versus L**

If the velocity is large, the temperature field is very shallow, and hence the ground plane remains relatively unaffected. Equation 6.7 can be plotted, as shown in figure 6.34, the dimensionless temperature against the dimensionless length, with the angle as a parameter. The angle units are the dimensionless radians.

# Chapter 7

# Temperature and Energy Partitioning in Drill Flute Grinding

## 7.1 Introduction

While the maximum ground plane temperature is often the critical temperature in creep feed grinding, this is not the case when it comes to grinding drill flutes. In this situation, the wheel does not 'run through' the workpiece. Rather, the arc of cut is an integral part of the finished workpiece, as shown in figure 7.1. The temperature in the arc of cut is, therefore, of primary importance in drill flute grinding.

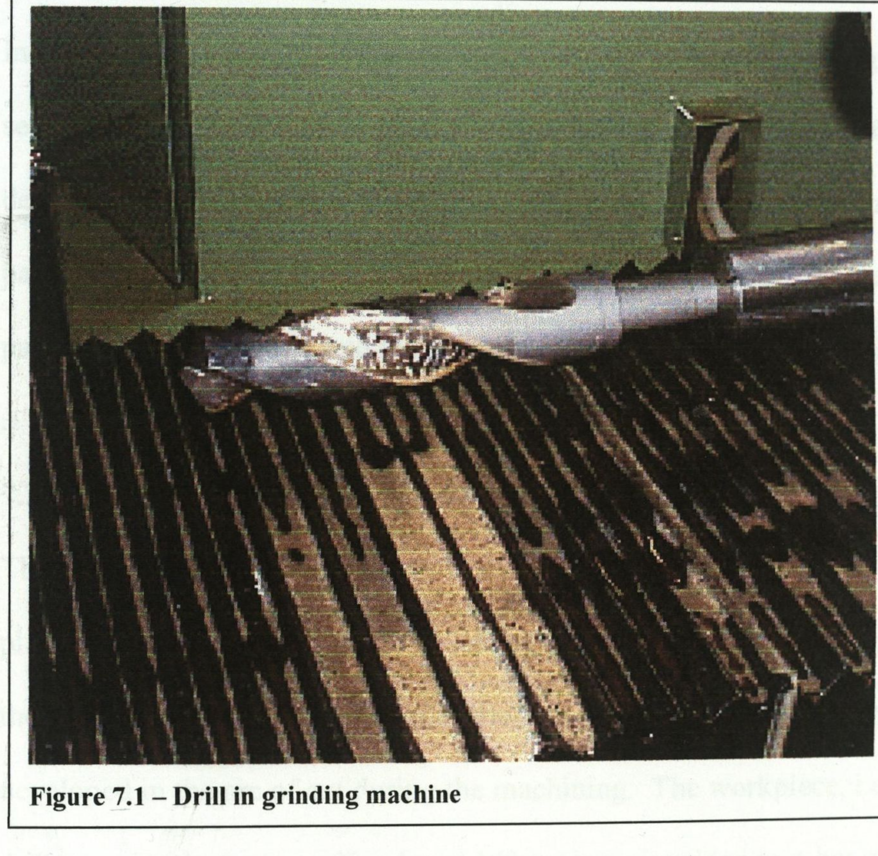

**Figure 7.1 – Drill in grinding machine**

Another factor of great interest in drill flute grinding, and creep feed grinding in general, is the effect of the cutting fluid. While it is accepted that, in the case of conventional shallow cut grinding, the cutting fluid has little effect on the temperature in the arc of cut, it is thought that it plays a far more significant role in creep feed grinding. This is supposed to be a direct consequence of the larger arc of cut. Hassell [Hassel 1979] found that higher critical power fluxes for burn were obtained with neat oil compared with water during the creep feed grinding of M42 tool steel. He obtained critical fluxes of 16-20 W/mm$^2$ with oil, and 5-6 W/mm$^2$ with water. That the oil had higher critical power fluxes was probably due to effective cooling in the arc of cut.

In this section, some experimental measurements were taken during the grinding of a series of drill flutes, a finite element model of the thermal aspect of the grinding was developed, and the information from both was combined with an existing energy partitioning model. The actual temperatures in the arc of cut were measured, the partition ratio evaluated, and the convective heat transfer coefficient evaluated.

## 7.2 The Experimental Procedure

The experimental measurements were carried out on the shop floor in the Dormer plant in Worksop, Sheffield. The objectives of these measurements were to identify the process power involved in the grinding process, and to measure the temperature developed in the arc of cut during the machining. The workpiece, i.e. the unmachined drill, consisted of a bar of hardened M2 tool steel welded to a bar of EN9 steel. The M2 was the drill proper, and the EN9 was the drill shank. The EN9 was the steel under investigation, since this steel was the part of the drill which had the form of the wheel/work contact. The drill blank was modified to allow a thermocouple to be placed in the path of the grinding wheel. During the test, the grinding wheel would grind through the thermocouple, allowing a temperature signal to be recorded. The thermocouple itself was positioned to allow the maximum temperatures in the arc of cut to be recorded. This position was located using finite element techniques, outlined in section 7.4, and approximately corresponds to a point one third of the arc-of-cut length from the top of the arc of cut. These maximum temperatures occur near the front of the arc of cut, as demonstrated in chapter 6. Figure 7.2 shows the modified drill blank, complete with thermocouple.

The machining parameters for the tests are outlined below:

| | |
|---|---|
| Wheel type: | TSGR-16-RB34<br>400x40mm |
| Cutting fluid: | Neat oil |
| Machine: | Karl Haux<br>Siemens control<br>80kW maximum power |

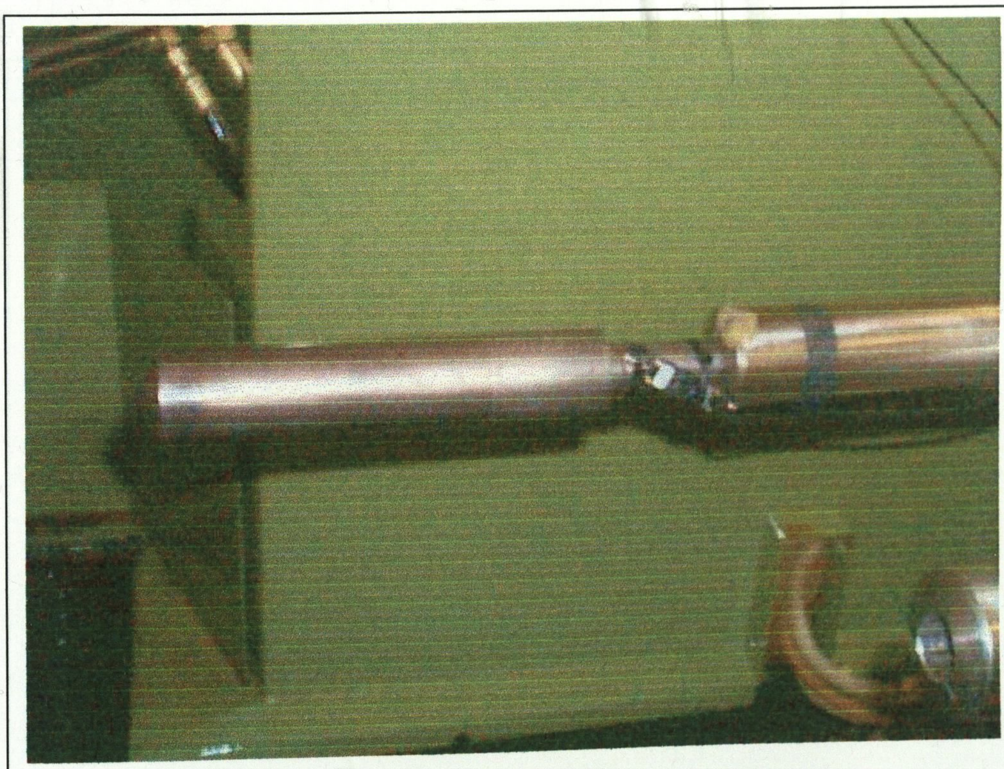

Figure 7.2 – Modified drill blank in grinding machine

| | |
|---|---|
| Wheel speed: | 2950rpm |
| Nominal Work speed | Pass 1 – 300mm/min |
| (see table 7.1) | Pass 2 – 370mm/min |
| Workpiece: | M2/En9 |
| | Diameter – 48mm |
| | Total length – 219mm |
| Dressing Interval: | Each flute |
| | Single point |
| | 0.04mm removed per pass |
| Displacement transducer: | Ultrasonic |
| Thermocouple: | Type J standard (Iron-Constantan) |
| | Diameter 1mm |
| | Double pole method |

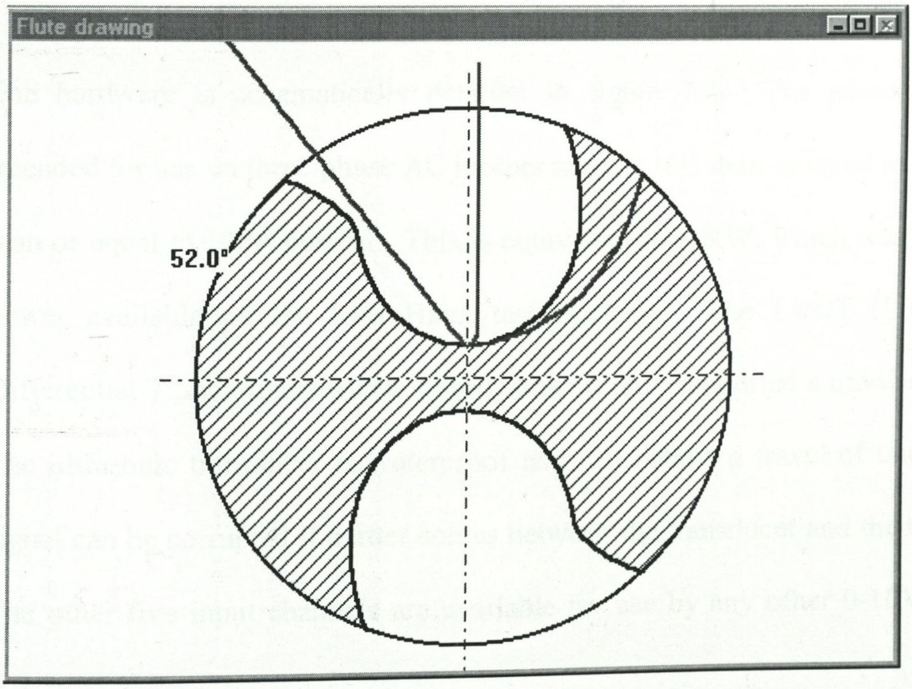

**Figure 7.3 – Drill flute profile**

The drill flute profile is illustrated in figure 7.3. This was generated using proprietary software developed by Dormer. This software was also used in the construction of the finite element model.

Data Acquisition:

The data acquisition was carried out using the Field Instrumentation System, developed by SAINT-GOBAIN ABRASIVES. The Field Instrumentation System (FIS) offers a way to view, record, and analyse grinding power and machine slide positions with respect to time. The hardware is contained in a carrying case, and is easily connected to any grinding machine. It does not require calibration on the part of the user. The associated software is a Microsoft Windows based program. It features data collection, review, and analysis which can assist in acquiring and identifying the critical aspects of a grinding process, for example, the grinding power and infeed rates with respect to time. The FIS is intended as an analytical tool for use in testing and optimising abrasive processes in use at manufacturing sites.

The hardware is schematically detailed in figure 7.4. The power transducer is intended for use on three-phase AC motors rated at less than or equal to 480V and less than or equal to 100A current. This is equivalent to 80kW, which was the maximum power available on the Karl Haux test machine. The LVDT (Linear Variable Differential Transformer) was not used, since it only supported a travel of two inches. The ultrasonic transducer is waterproof and can handle a travel of one meter. The signal can be corrupted if matter comes between the transducer and the target surface. The other five input channels are available for use by any other 0-10V transducers,

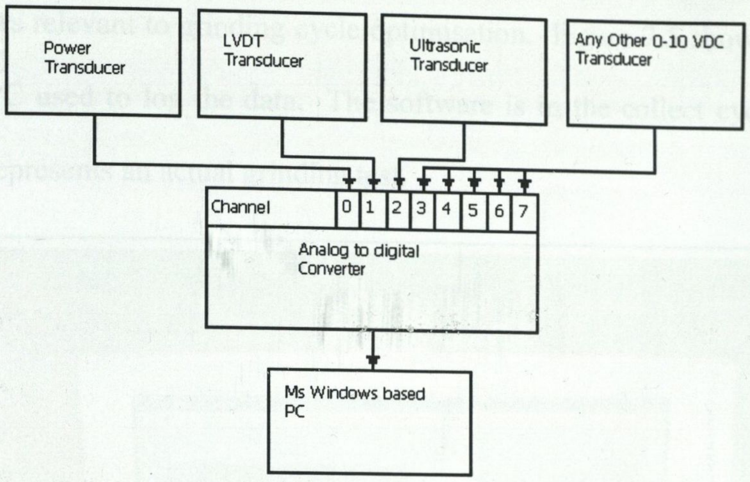

**Figure 7.4 – FIS hardware schematic**

which may possibly include another power transducer, or a dynamometer. In this case a standard J-type thermocouple with amplifier was connected.

The software has two primary functions; data collection and data reviewing. The program structure is detailed in figure 7.6. The Account Data is where test information is stored, i.e. testing objectives, machine information etc. The Operations Data section is for recording wheel and work speeds and dimensions, dressing and cutting fluid information. The Instrument Data section is where the hardware setup is specified in the software. This involves selecting the relevant hardware devices, and the voltage range and amperage range set on the power transducer. Set-up is a real time display of the signals from the channels that are currently enabled in the Instrument Data section. This allows the transducers to be checked, ensuring they are correctly set and yielding the required information. The Collect Data area is similar to the Set-up section. In addition to the Set-up features, it saves the logged data to disk for later analysis. The other main section of the software is the review section, which allows the logged data to be analysed. This analysis can include identification of material removal rates, specific power, machine stiffness, and several other parameters relevant to grinding cycle optimisation. Figure 7.5 shows a picture of the lap-top PC used to log the data. The software is in the collect cycle, so the screen display represents an actual grinding test.

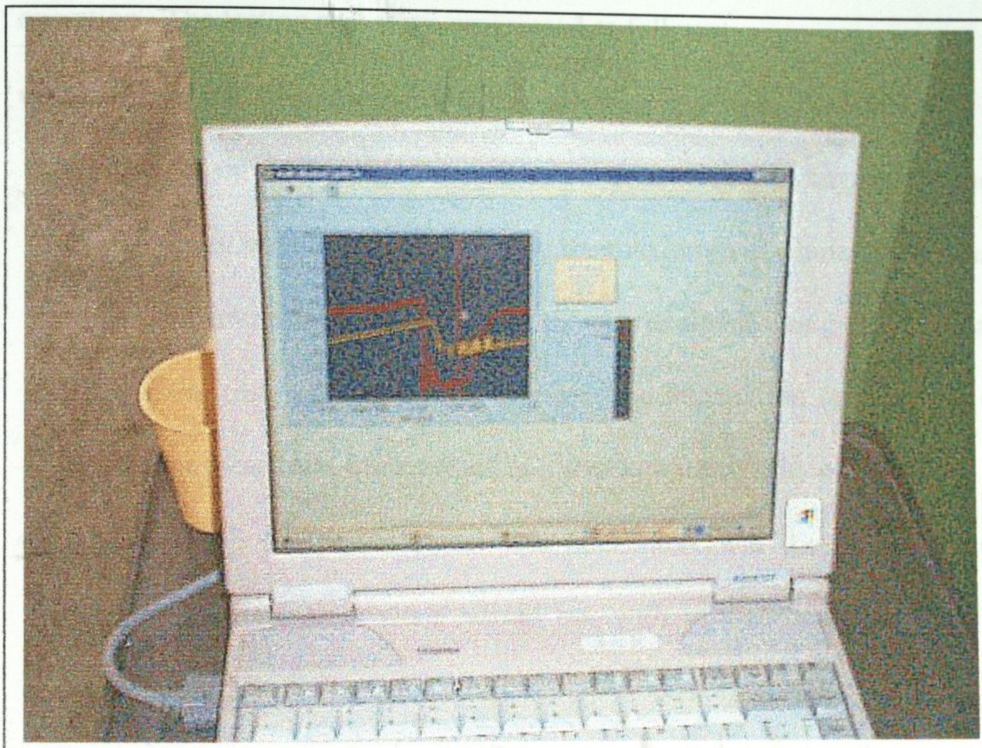

Figure 7.5 – Laptop during data acquisition

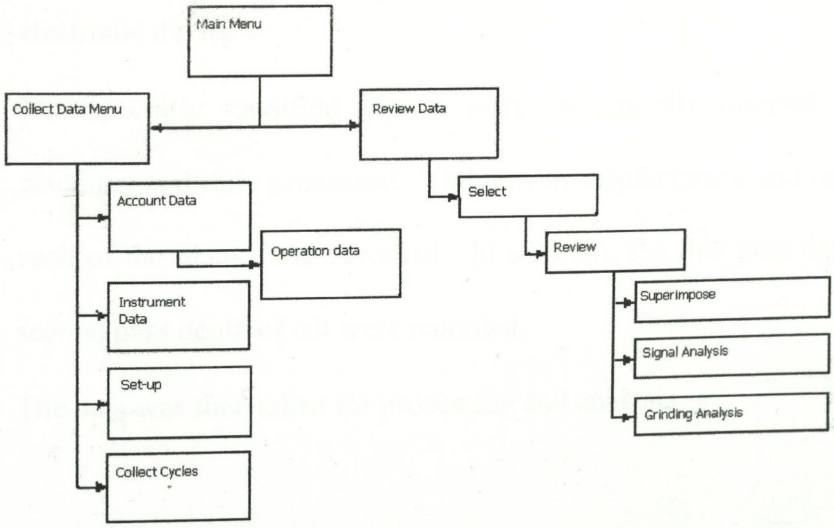

Figure 7.6 – FIS software schematic

The Test Procedure:

The power transducer voltage clips were connected to the grinding wheel drive motor power lines. Following this, the ultrasonic transducer was positioned to allow the displacement to be recorded. The grinding machine itself was then prepared for operation. The testing procedure progressed as follows:

- A drill blank was inserted into the grinding machine. The grinding cycle was carried out on the blank, turning it into a drill. The grinding power and machine displacement were recorded. Because the maximum machine power was the same as the maximum measurable power, the power signal was going to be attenuated. This initial test was carried out to allow the attenuation factor to be computed. Several of these tests were carried out to ensure uniformity of result.
- Subsequently, the power signal was attenuated, and the above procedure was repeated. These tests were carried out with unmodified blanks, allowing the attenuation factor to be calculated.
- There were ten blanks modified to allow thermocouple insertion. These thermocouples were glued in place with a non-silicone heat-transfer compound. The compound is more commonly used to glue heat sinks to heat-generating electronic devices.
- The specially modified blanks were sequentially inserted into the grinding machine, and duly processed. The power, displacement and temperature data for each of the blanks was recorded. In addition, the first pass depth of cut, and the second pass depth of cut were recorded.
- The data was then taken for processing and analysis.

## 7.3 The Test Results

The test results essentially consisted of the power attenuation data, and ten data sets for the power and temperature. For the attenuation factor, five tests were carried out with no signal attenuation, and five tests were carried out with the signal attenuated. This allowed a good estimate of the attenuation factor to be made. This data is shown in figure 7.7.

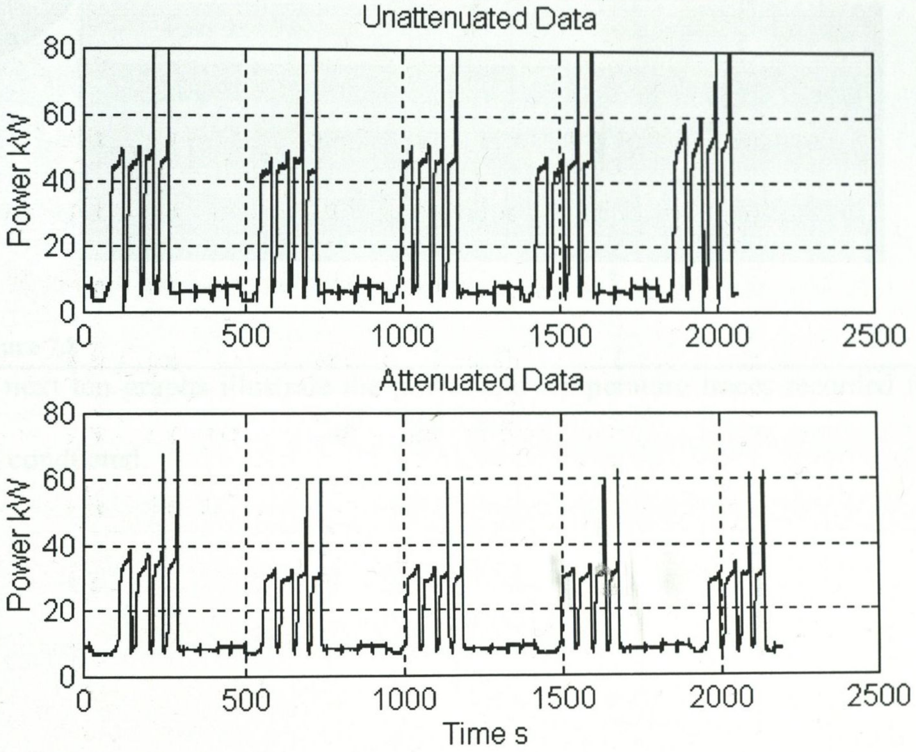

**Figure 7.7 – Calibration data**

Figure 7.7 shows power data for ten drill blanks, five with attenuated power data, and five without. Each drill blank has four distinct power traces. This is because the grinding wheel makes four passes at the blank. The first pass is a stock removal pass for the first flute. The second pass is a stock removal pass for the other flute. The next two passes are the finishing passes for both flutes. It can be seen easily that there is a sharp rise in the grinding power at the end of the finishing passes. This is because at the end of the second pass, the wheel is required to remove more material. A 2-D representation of this is shown in figure 7.8.

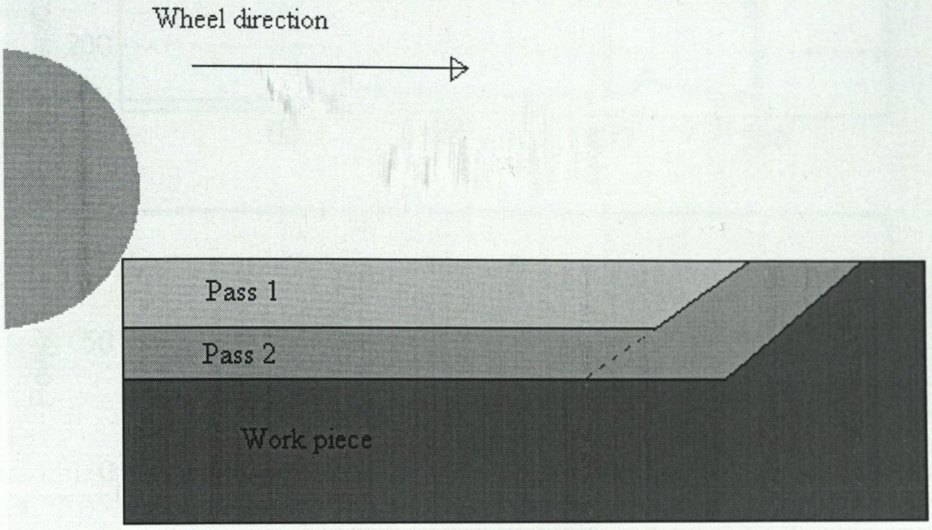

**Figure 7.8**

The next ten graphs illustrate the power and temperature traces recorded for the ten tests conducted.

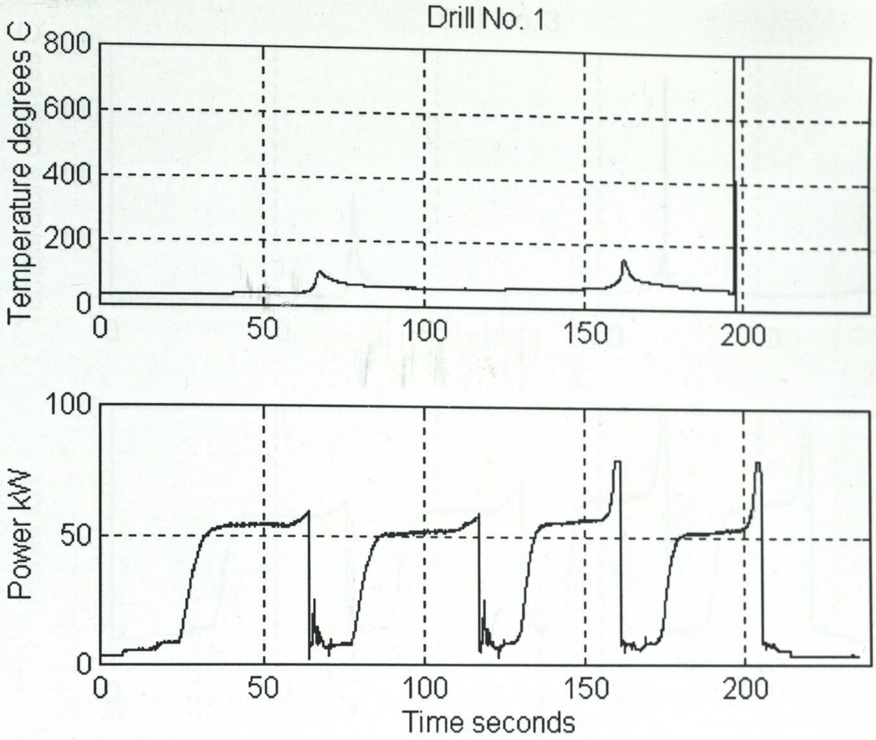

Figure 7.9 – Power and temperature data: Drill no. 1

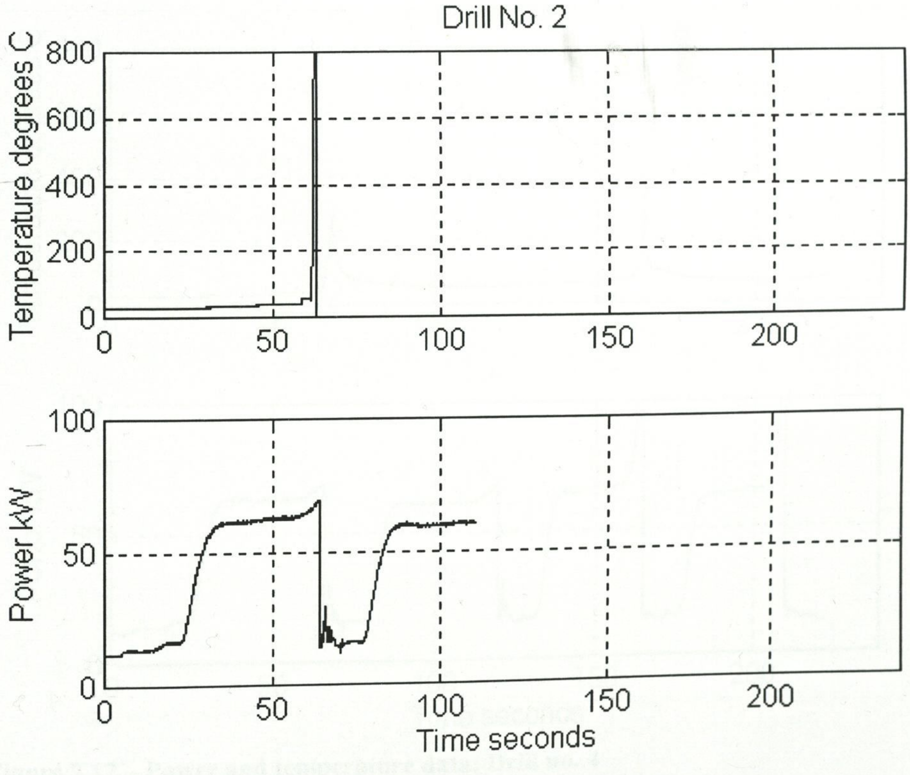

Figure 7.10 – Power and temperature data: Drill no. 2

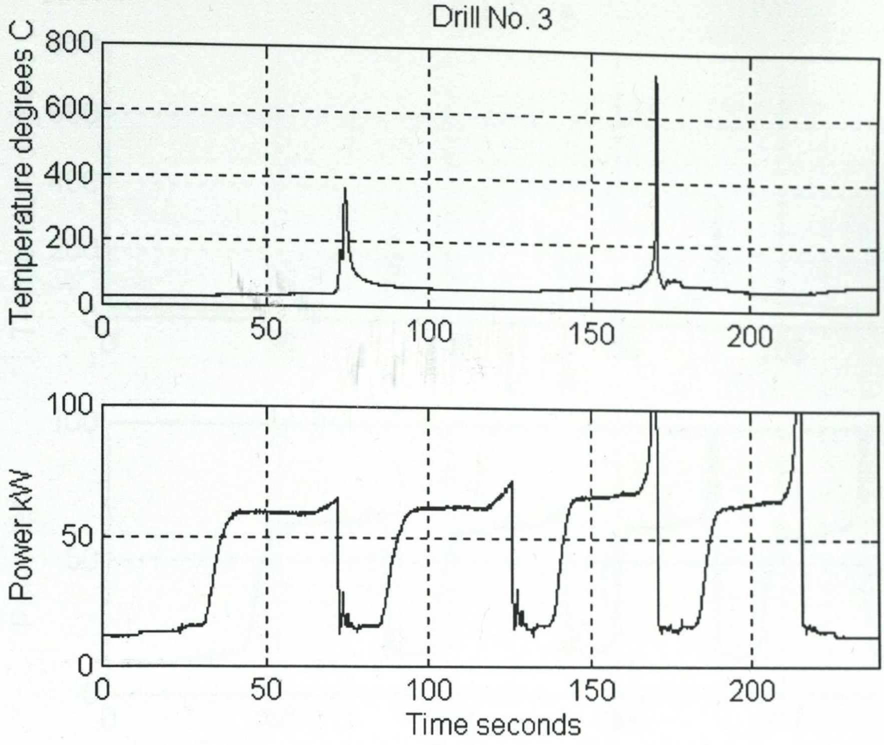

Figure 7.11 – Power and temperature data: Drill no. 3

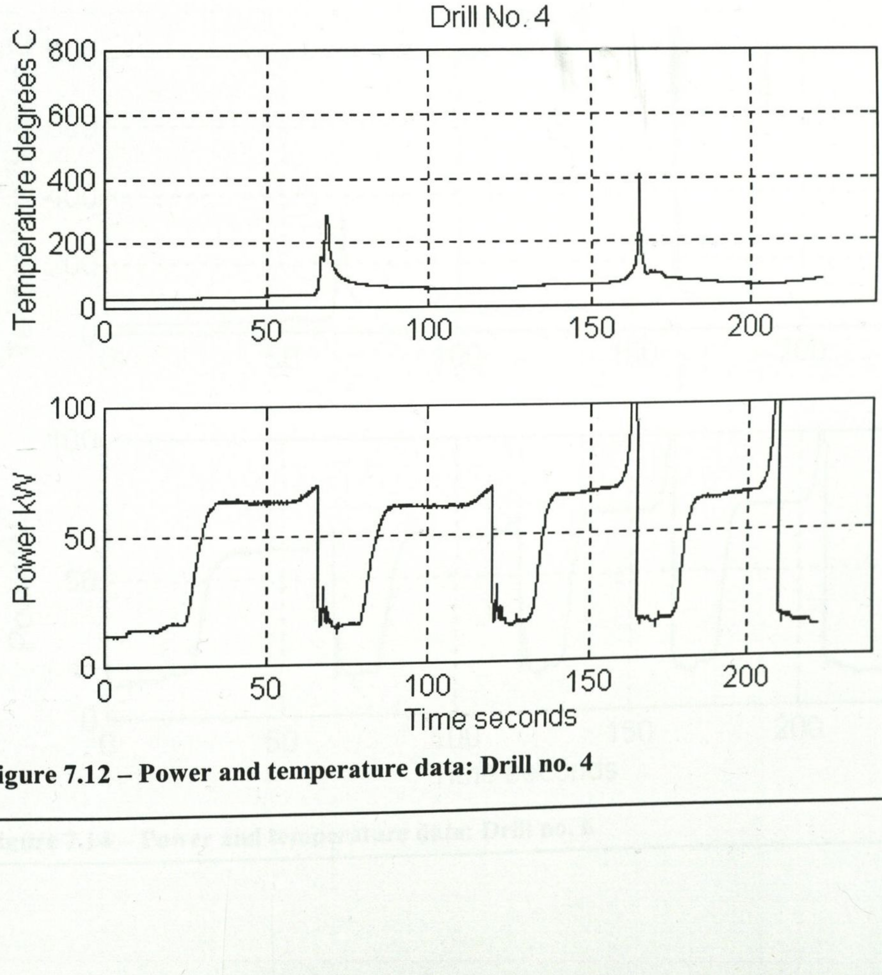

Figure 7.12 – Power and temperature data: Drill no. 4

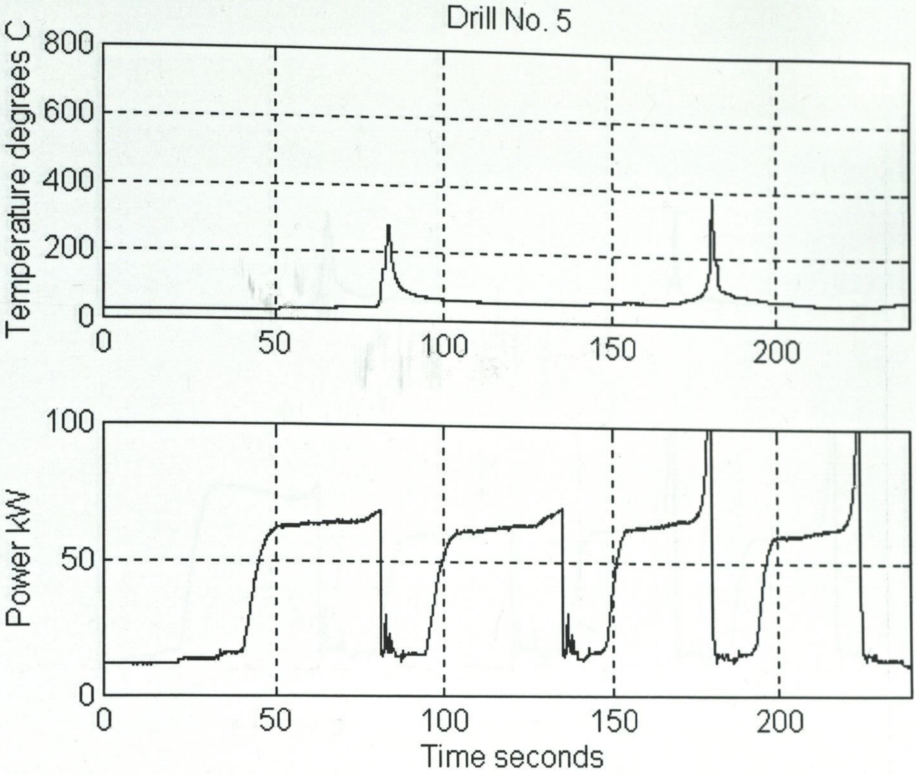

Figure 7.13 – Power and temperature data: Drill no. 5

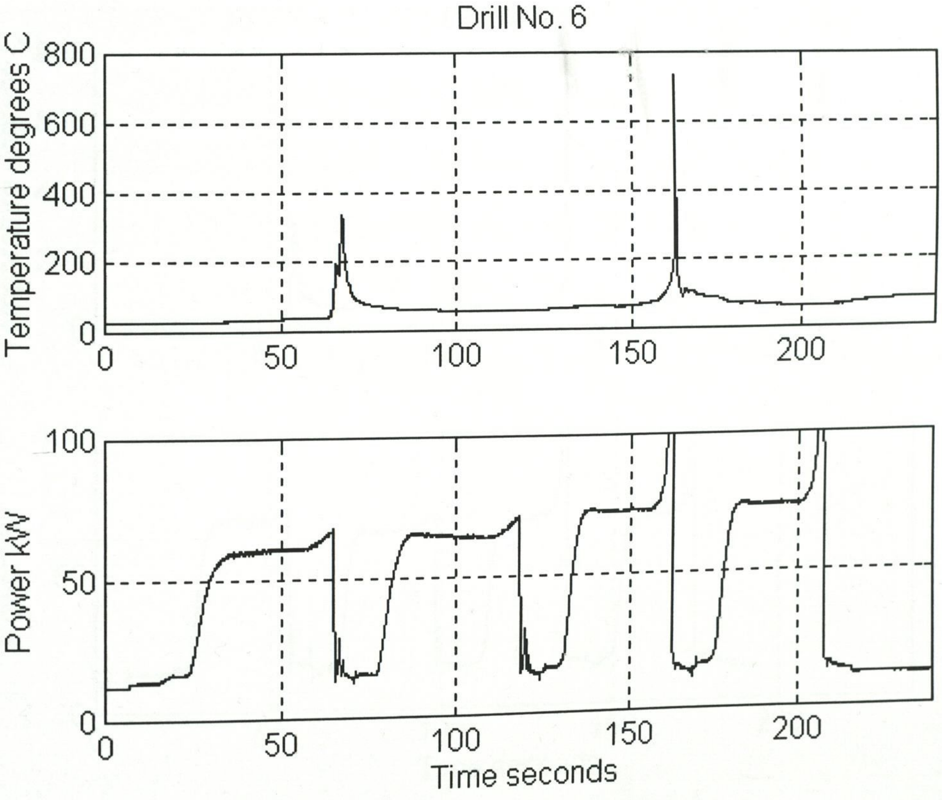

Figure 7.14 – Power and temperature data: Drill no. 6

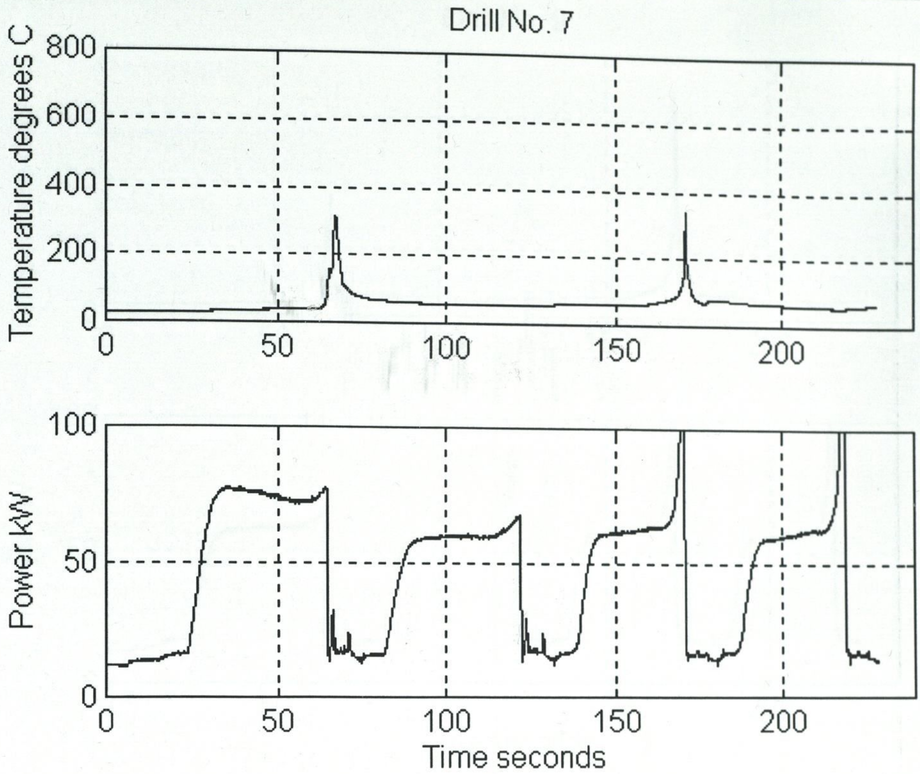

Figure 7.15 – Power and temperature data: Drill no. 7

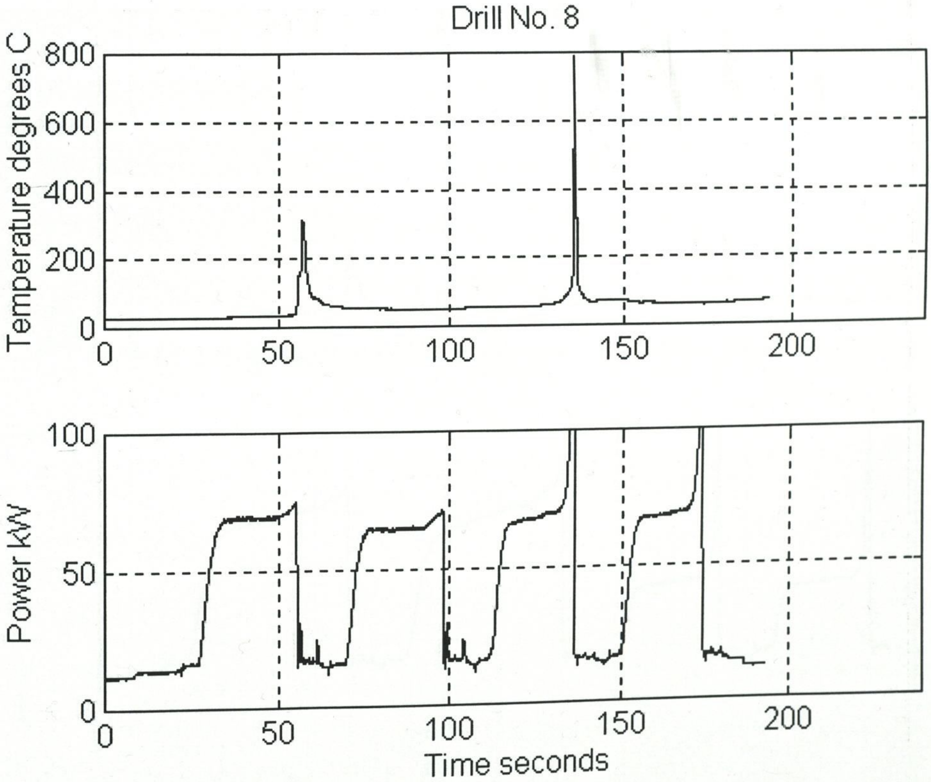

Figure 7.16 – Power and temperature data: Drill no. 8

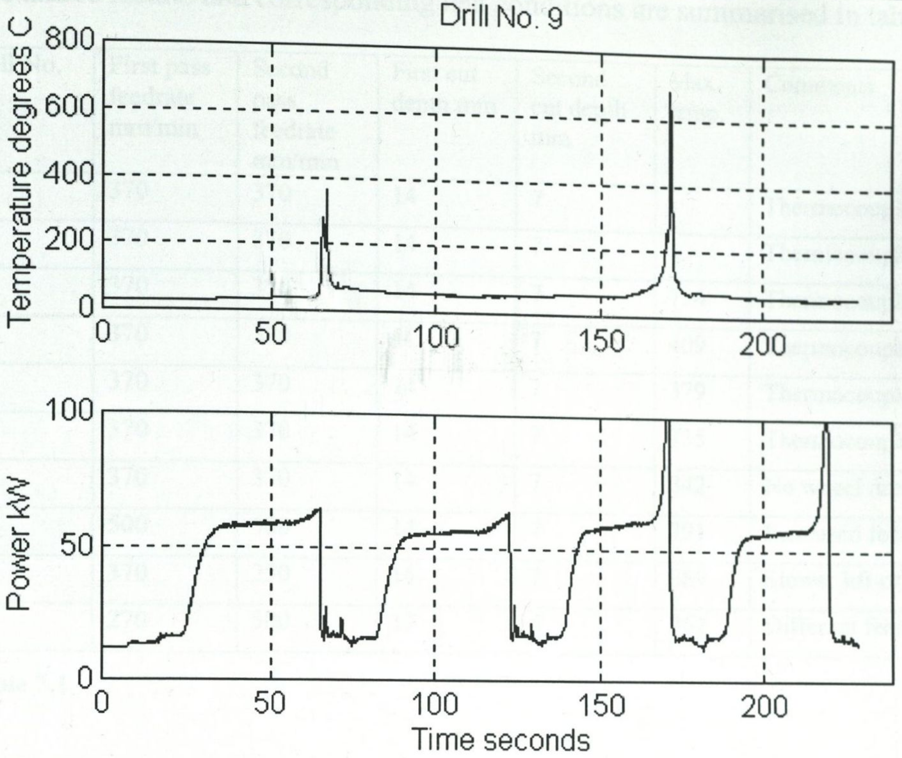

**Figure 7.17 – Power and temperature data: Drill no. 9**

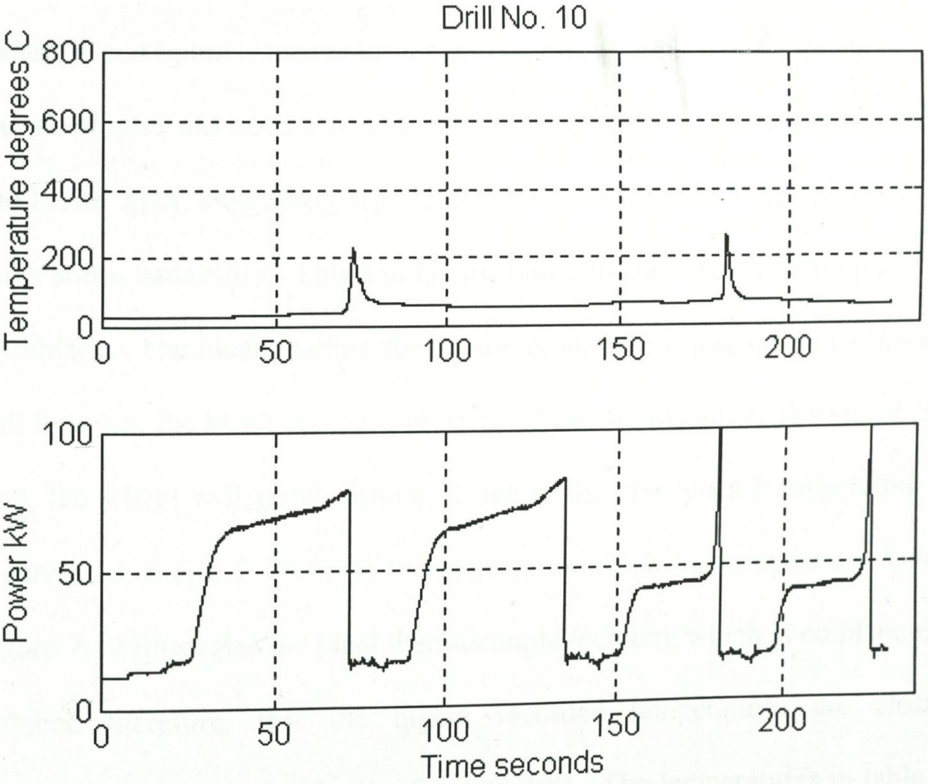

**Figure 7.18 – Power and temperature data: Drill no. 10**

The above results and corresponding test conditions are summarised in table 7.1.

| Drill No. | First pass feedrate mm/min | Second pass feedrate mm/min | First cut depth mm | Second cut depth mm | Max. temp. | Comments |
|---|---|---|---|---|---|---|
| 1 | 370 | 370 | 14 | 7 | - | Thermocouple broke |
| 2 | 370 | 370 | 14 | 7 | - | Thermocouple broke |
| 3 | 370 | 370 | 14 | 7 | 734 | Thermocouple worked |
| 4 | 370 | 370 | 14 | 7 | 409 | Thermocouple worked |
| 5 | 370 | 370 | 14 | 7 | 379 | Thermocouple worked |
| 6 | 370 | 370 | 14 | 7 | 735 | Thermocouple worked |
| 7 | 370 | 370 | 14 | 7 | 342 | No wheel dress |
| 8 | 500 | 500 | 14 | 7 | 791 | Increased feedrates |
| 9 | 370 | 250 | 14 | 7 | 689 | Slower lift-off |
| 10 | 270 | 500 | 17 | 4 | 262 | Different feedrates |

**Table 7.1**

In total, eight successful temperature measurements were taken. The previous series of graphs detail the temperature/power versus time characteristics for each ground drill. The first temperature maximum corresponds with the stock removal pass. The second maximum temperature corresponds with the finishing pass. The thermocouples did not survive the first couple of tests. Drill 8 subsequently cracked and broke apart, suggesting high tensile residual stresses. The recorded temperatures show some variability. This can be attributed to the thermocouple positioning in the drill blank. The ideal position for the thermocouple is just where the finished surface will lie when the blank has been ground. If the thermocouple is situated ahead of this face, the wheel will grind through it before the steady-state temperature is reached. Figures 6.5, 6.6, 6.7 illustrate the manner in which the temperature field develops. Figure 7.19 illustrates the ideal thermocouple location, which is on plane B. It can be deduced therefore, that the higher recorded temperatures are closest to the temperatures experienced by the finished drill. The temperatures in table 7.1 are the

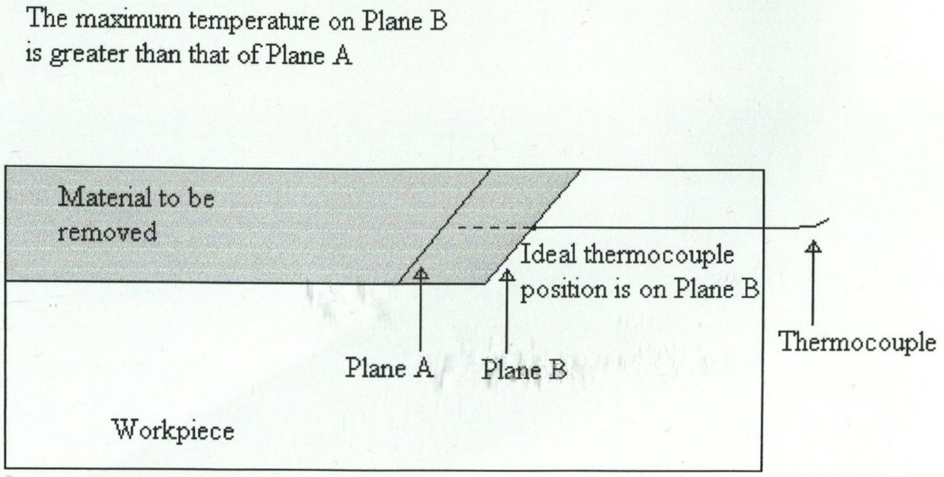

**Figure 7.19 – Thermocouple positioning**

maximum temperatures recorded during the testing. Figure 7.20 shows some of the ground drills, with the thermocouple position highlighted. The ground thermocouples can be seen near the end of the flute.

Some further information was available from the testing. From the recorded spindle

**Figure 7.20 – Ground drills showing thermocouple positions**

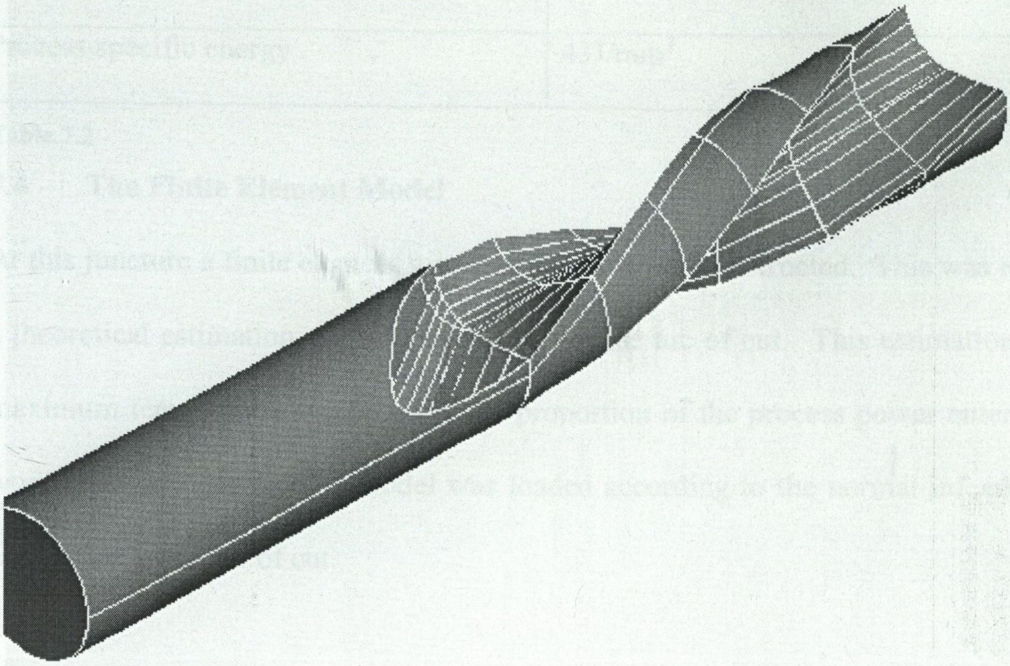

**Figure 7.21 – Solid model of drill flute**

power, and the time data, the total process work could be calculated. A solid model of the drill flute (illustrated in figure 7.21) yielded the ground volume of metal. Combining the information, the process specific energy was calculated.

In order to calculate the specific energy from the test data, the idle power was subtracted from the power data. The average power was then calculated. The grinding time was measured. The ground volume was calculated from a solid model, which was essentially an extrusion of the profile in figure 7.3, subtracted from a cylinder of the same dimension as the drill blank. This information is shown in table 7.2.

| | |
|---|---|
| Idle power | 5kW |
| Mean grinding power | 50.7kW |
| Grinding time | 148s |

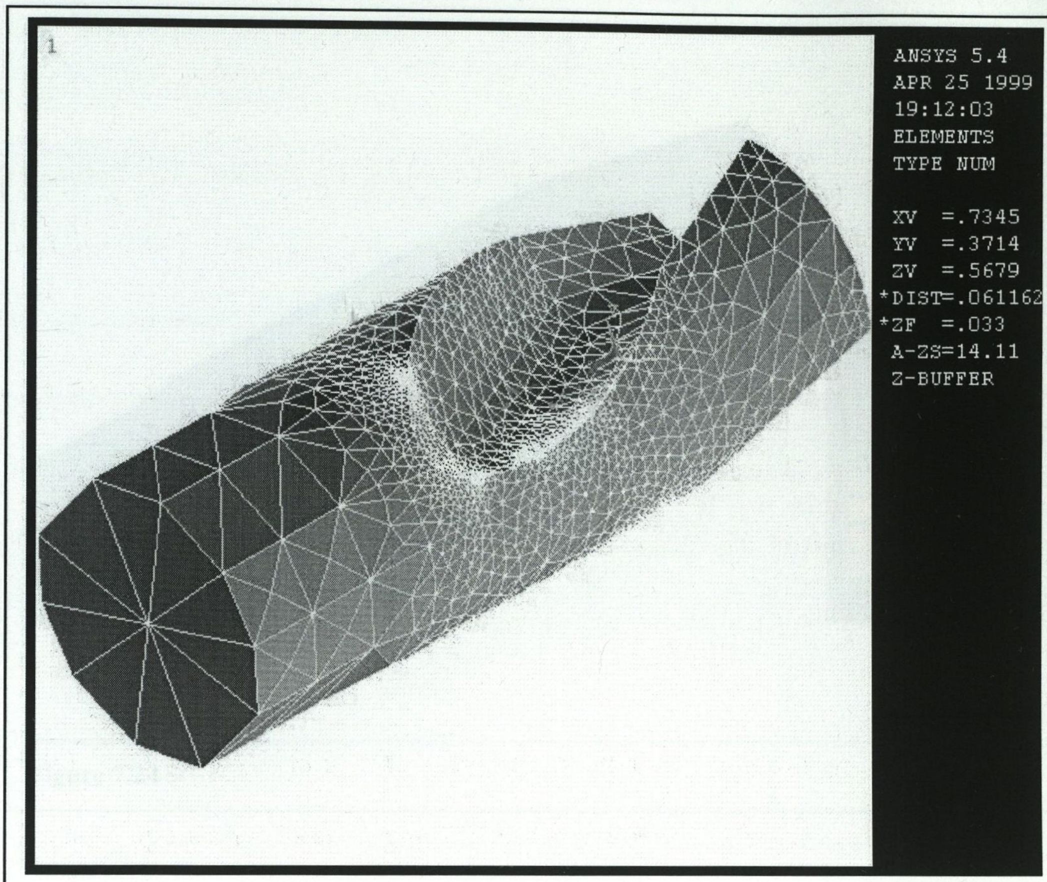

**Figure 7.23 – Drill finite element model**

If the energy partition to the workpiece is assumed to be 13%, then the maximum temperature in the arc of cut is found to be 730°C. This temperature involved one further assumption; the temperature field in the arc of cut for the second pass reaches a steady-state distribution. The finite element models used in chapter 6 to calculate the ground plane temperature demonstrated that the distance required for the temperature distribution to become steady-state is about 5mm. The graphs illustrating the power usage by the grinding wheel indicate that the remaining material to be ground in the runout zone in the second pass is about 6-7mm thick. Because of the complex geometry of the drill, it was not possible to model the material removal as it was in the ideal cases examined in chapter 6. This meant that any applied heat flux in the finite element model would generate not the steady state solution, but the transient distribution expected during initial engagement of the grinding wheel. Because the

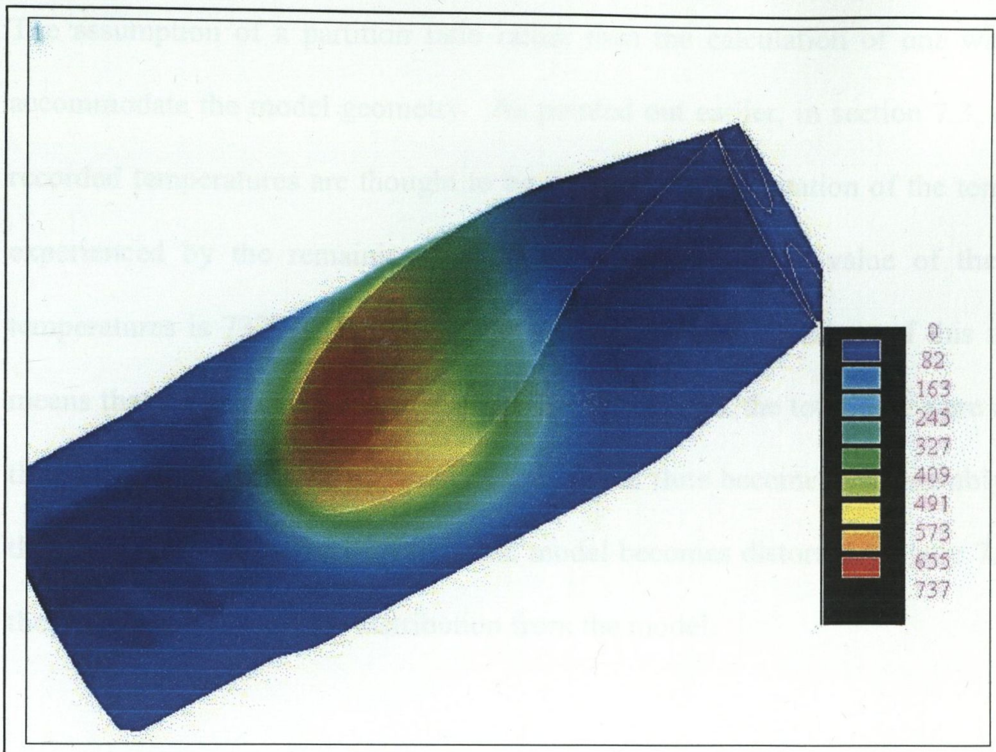

**Figure 7.24**

temperature distribution in the flute grinding reaches steady-state, and because the temperature and applied heat flux are directly proportional, it was possible to scale the applied heat flux in the drill flute model according to the difference in the initial transient temperature and the steady-state temperature in the inclined plane models from chapter 6. Essentially, when the grinding wheel initially engages the workpiece, the workpiece is cold, and a temperature rise associated with the applied heat flux is experienced. As the wheel progresses through the workpiece, a thermal field is generated ahead of the arc of cut, which preheats the workpiece. When the steady state condition is achieved, the temperature in the arc of cut is higher than it was during the initial engagement of the wheel. The results from chapter 6 were used to estimate the ratio of the initial to steady state temperatures. From the models most closely representing the geometry of the flute grinding, ie $\psi=15^{\circ}$ L=17, a factor of 1.56 was identified.

The assumption of a partition ratio rather than the calculation of one was done to accommodate the model geometry. As pointed out earlier, in section 7.3, the higher recorded temperatures are thought to be the better representation of the temperatures experienced by the remaining drill material. An average value of these higher temperatures is 737°C. In the drill model, a surface temperature of this magnitude means that the opposite drill flute remains unheated. If the total heat were applied to the model without energy partition, the opposite flute becomes considerably hot, and thus the temperature distribution in the model becomes distorted. Figure 7.24 shows the calculated temperature distribution from the model.

## 7.5 The Role of the Cutting fluid

The other interesting factor in the drill grinding process is the energy absorbed by the cutting fluid. While it is accepted that the cutting fluid has little effect in reducing the arc of cut temperatures in conventional grinding, this is clearly not the case in deep cut grinding. The energy partitioning equation developed for conventional grinding

$$R_w = \left\{1 + 1.1\left(\frac{r_o}{l_e}\right)^{1/2}\left[\frac{\beta_g}{\beta_w}\right] f(\zeta)\right\}^{-1}\left(1 - \frac{e_{cc}}{e_c}\right)$$

**Equation 7.1**

by Rowe *et. al.*[Rowe *et. al.* 1998] is shown in equation 7.1.

This neglects the effect of cutting fluid. A simple modification can be made to include this factor.

$$R_w = \left\{1 + 1.1\left(\frac{r_o}{l_e}\right)^{1/2}\left[\frac{\beta_g}{\beta_w}\right] f(\zeta)\right\}^{-1}\left(1 - \frac{e_{cc}}{e_c} - R_{cutting\ fluid}\right)$$

**Equation 7.2**

The function f(ζ) is a function of the grain geometry and diffusivity. These are detailed in equations 7.3 and 7.4.

$$\zeta = \left( \frac{\gamma^2 K_g l_e}{r_o^2 V_s} \right)^{1/2}$$

**Equation 7.3**

$$f(\zeta) = \frac{\zeta^3}{1+\zeta^2 - \left(2/\pi^{1/2}\right)\zeta - \exp(\zeta)^2 \, erfc(\zeta)}$$

**Equation 7.4**

Using the material properties, and geometry details outlined in table 7.3, the proportion of energy entering the cutting fluid, and wheel can be calculated.

| | |
|---|---|
| $r_o$ | 15μm |
| $l_e$ | 0.055m |
| $k_g$ | 36W/mK |
| $\rho_g$ | 3910kg/m$^3$ |
| $c_g$ | 765J/kgK |
| $k_w$ | 46W/mK |
| $\rho_w$ | 7830kg/m$^3$ |
| $c_w$ | 616J/kgK |
| $e_c$ | 43J/mm$^3$ |
| $e_{cc}$ | 6J/mm$^3$ |
| $\gamma=\tan(\theta)$ | 1 |
| $V_s$ | 63m/s |
| $k_{oil}$ | 51W/mK |

**Table 7.3**

The energy division in the drill flute grinding process is shown in table 7.4.

| | |
|---|---|
| $R_{cutting\ fluid}$ | 71% |
| $R_{chip}$ | 14% |
| $R_{work}$ | 13% |
| $R_{wheel}$ | 2% |

**Table 7.4**

The chip partition value is likely to be an over estimate, since the specific energy value used is the melting energy. It can be seen from the analysis that the cutting fluid plays a very significant role in reducing the temperatures in the grinding of drill flutes, and creep feed grinding in general. The work partition value would be in the region of 78% without the use of cutting fluid. This would correspond, with the same grinding conditions, to a maximum work temperature of around 4400°C.

The angle of the wheel/work contact is about 15°. The dimensionless length is 17. From the graphs presented in chapter 6, the dimensionless surface temperature would be in the region of about 17. From the grinding conditions outlined earlier, using the partition ratio for the work of 13%, the expected temperature would be about 574°C. This value is 79% of the average maximum recorded temperature. So, while the results presented in chapter 6 were not intended to be applied to such a case as drill flute grinding, they do provide a reasonable conservative estimate of the likely maximum temperature. The grinding conditions for the drill flute varies significantly from those assumed in the inclined slider models. For example, the slider models assume a semi-infinite plane with a band source of infinite length, whereas the drill has a geometry requiring non-uniform loading. The original Jaeger model for a band source moving across a flat plane would yield a maximum temperature of about

1022°C, if the maximum heat flux is used, and a temperature 511°C if the average temperature is used, again using a partition ratio of 13%. It would appear that the inclined slider model yields a closer value of the maximum temperature compared with the original Jaeger model. The most important parameter in creep feed grinding appears to be the cutting fluid. This is because the cutting fluid removes a very large percentage of the process power. In direct comparison with conventional grinding, it is clear to the observer that in deep cut grinding, the cutting fluid can be used to control workpiece temperatures, and hence the quality of the finished workpiece. It would be of great industrial advantage to characterise the Nusselt number for the type of fluid flow found in the arc of cut in creep feed grinding. If the Nusselt number could be related to the Reynolds and Prandtl numbers in the arc of cut, as indicated in section 3.3, a powerful method of controlling energy partitioning, and hence grinding temperatures, would be available.

For this particular case, it is possible to estimate the mean convective heat transfer coefficient. The area of the wheel/work contact was found to be $\sim 0.001995\ \text{m}^2$ from the numerical model. The mean grinding power was 50.7kW, of which 71% was removed by the cutting fluid. The average maximum recorded temperature was 730°C. Using Newton's Law of Cooling, this would give a rough estimate of the convective heat transfer coefficient as $24.8\text{kW/m}^2\text{K}$. This calculation is very much a rough estimate, since mean power and total area have been used in conjunction with a local temperature. It does, however, illustrate the order of magnitude of the average heat transfer coefficient. From the information available it is possible to estimate the value of the Nusselt number, ($l_c$=5.5cm, $k_{oil}$=51W/mK) but not to relate it to the Reynolds and Prandtl numbers. Using the data in table 7.3, the average Nusselt number should be about 27.

# Chapter 8

## Concluding Discussion and Exploitation of Results

## 8.1 Discussion of Results

### 8.1.1 Tensile Residual Stresses in Ground Components

The problem of determining the critical temperature, when tensile residual stresses appear in the workpiece, has been tackled. The analysis included some finite element modelling, correlation of numerical data with experimental data, and some analytical work. The finite element models were shown to predict both the critical temperature, and the magnitude of the tensile residual stresses developed during grinding tests of two industrial steels, to a high degree of accuracy. The finite element models, having been validated, were then used to investigate several other steels. At this point, a combined model, based on the yield strength and elastic stress as functions of temperature, was developed. For all the steels considered, the critical temperature was predicted to within 6% of that found by the rather more complicated finite element models.

Despite the great complexity of the problem of residual stress generation in workpieces resulting from transient thermal loading, a very simple method based on the yield strength at a temperature, and the thermal elastic stress for an elevated temperature, has been found. With very little effort, in terms of computation and experimental testing, it is now possible to calculate with confidence, the critical temperature at which residual stresses become tensile. The information required for this calculation can be acquired from a series of hot hardness tests, and a knowledge of the material's elastic modulus and thermal expansion coefficient at the inflexion point temperature of the hot hardness curve.

The value of this technique to industrial engineers is limitless. Many industrial grinding machines have in-process control, with the grinding power being monitored, and related to grinding temperatures using a suitable model, i.e. [Rowe *et. al.* 1997]. The industrial engineer is eager, initially, to hear that the residual stresses in the manufactured components are not tensile, and upon hearing that they are, he is eager to hear that they are very low. However, with explicit knowledge of a critical temperature, the engineer can modify the in-process control to maintain grinding temperatures below the critical temperature. This would involve adjusting wheel/work speeds and feeds to advantage.

In addition, the technique is not limited to use in grinding temperature calculations. The method is equally applicable to other machining processes, for example, turning and milling. The graphical technique can also be used to determine the maximum tensile mechanical load a component in tension can withstand without yield, in a hot environment.

### 8.1.2 Temperatures in Form Grinding

Chapter 5 investigated temperatures in components, with geometric discontinuities, subjected to a form grinding operation. Form grinding is a grinding technique which applies as much to deep cut grinding as it does to conventional shallow cut grinding. In fact, a large percentage of deep cut grinding operations involve the use of a formed wheel. A concentration factor for temperatures at corners in form grinding operations was developed using the dimensional technique. This analysis demonstrated that the concentration factor was a function of six dimensionless parameters, representing the grinding geometry and the form geometry. The nature of the interaction of these dimensionless groups was investigated using a finite element analysis and found to be a linear combination of said groups. The concentration factor, for included angles less than 180°, was found to lie mainly between 1 and 1.3. In a direct comparison with the work of Maris [Maris 1977/78] and Khanzhin [Khanzhin 1971], the results are far more conservative. For example, Maris suggests that for an included angle of 30°, with uniform heating on both sides of the wedge (figure 2.3), the concentration factor would be 6. This factor is applied to the flank temperatures, which would give a value of the concentration factor, relative to the flat plane used in chapter 5, of 1.55. Khanzhin suggests a value of 1.5 for all included angles less than 60°, and the analysis presented in chapter 5 would suggest a value in the region of 1.28, variable to some extent, depending on the flank and arc lengths. For an included angle of 60°, Maris would suggest a concentration factor of 2.6. The analysis in chapter 5 allowed some versatility in application, as it accounted for differing heat fluxes on the flanks of the general V-form, or wedge.

Subsequent work published by Morgan *et. al.* [Morgan *et. al.* 1988] suggested that the temperature concentration at sharp corners on forms was not as severe as analysis would suggest. It appeared that even a small radius at the sharp corners had a beneficial effect on the developed temperatures. This effect was investigated using the finite element method, and it was found that, for corner radii in excess of 0.15mm, the temperature at the corner was the same as that calculated using the standard flat plane solution. It should be noted that while the concentration factor has, for all intents and purposes, a value of unity, it does not change the fact that, for the example quoted in the previous paragraph, the tip temperature will be about twice the temperature on the flanks.

The temperature measurement technique used by Morgan *et. al* was shown to measure temperatures somewhat lower than the tip temperature under investigation, due to the sampling width of the thermocouple. This observation showed that the results presented by Morgan *et. al* for the apex temperatures could be corrected in such a manner as to improve their correlation with the theoretical calculations. In figure 5.14, the mean line for the measured over theoretical temperature, for n=1, is about 0.72. The illustrative figure, 5.16, suggests that the measured temperature is about 70% of the peak temperature, which would shift the mean line, for n=1, to 1.03. This is in good agreement with the numerical results, and in keeping with the trend demonstrated in figure 5.13.

The fact that the fillet radius on the form leads to a concentration factor of unity for forms with included angles under $180^o$, would suggest that the same is true for forms with included angles over $180^o$. This implies that for form grinding in general, geometric discontinuities of any type will experience higher temperatures, and the process parameters should be calculated accordingly.

### 8.1.3 Ground Plane Temperature in Grinding

It is clear that the important temperature in the grinding process is that temperature which is experienced by the remaining workpiece, rather than the material which is removed. In chapter 6, the temperature experienced by the workpiece was investigated for a variety of different conditions.

A dimensionless model was developed, which allowed a concise series of numerical models to be developed. The numerical models used a chord approximation for the wheel/work contact geometry, and the material removal was simulated by deactivating elements at appropriate times. The chord approximation should be used with care. Because the temperature profile beneath the arc of contact falls away according to the error function, the chord approximation model will predict lower temperatures than a circular arc model would. The chord approximation model is, therefore, most suited to problems involving large diameter wheels, and relatively small depths of cut. A triangular heat source was used to load the models, in accordance with the heat distribution found in deep cut grinding. The results of the analysis indicated that the ground plane temperatures can be considerably lower than the arc of cut temperatures. In addition, it was found that, when the dimensionless length was large (L> 25), the ground plane was essentially unaffected by the temperature in the arc of cut. For the creep feed grinding process, this means that the heat in the workpiece has insufficient time to penetrate through the workpiece to the ground plane, before it is removed by the grinding wheel. The work material acts as an insulator. The triangular heat source distribution also means that the maximum surface temperature corresponds with the front part of the wheel/work contact, where the depth of cut is large.

Maris [Maris 1977/78] looked at this problem in a similar fashion. However, he used a uniform heat distribution to load the models, which clearly is not representative of the physicality of the creep feed grinding operation. This can be observed by comparing the surface temperature characteristic in figures 6.9-6.23 loaded triangularly, with figures 2.1 and A.2, which were loaded with a uniform source. Maris suggested that the maximum ground plane temperature was limited to 40% of the maximum surface temperature for large angles of inclination. The results shown in figures 6.9-6.23 show that the maximum ground plane temperature is 84% of the maximum surface temperature for $L=0.5$, $\phi=7^{\circ}$. At the other end of the spectrum, with $L=25$, $\phi=15^{\circ}$, the maximum ground plane temperature is 30% of the maximum surface temperature.

The results from this analysis were then combined with the dimensionless model (equation 6.4), allowing the development of an expression for the maximum ground plane temperature for a variety of chord angles, and dimensionless lengths. This expression can be used, given knowledge of the average applied heat flux and the workpiece partition ratio, to estimate the temperature experienced by the remaining ground plane.

### 8.1.4 Temperature and Energy Partitioning in Drill Flute Grinding

Much speculation exists concerning the role of the cutting fluid in deep cut grinding. In chapter 8, an industrial drill flute grinding process was characterised, and an approximate figure for the convective heat transfer coefficient was found for the process.

The cutting fluid application system was extremely straightforward. The drill blank was machined in a bath of neat oil, providing lubrication and cooling. The cutting fluid was forced through the arc of cut by the hydrodynamic action of the wheel. This action is similar to that found in journal bearings, the space between the wheel and workpiece being filled with cutting fluid. The rotating wheel absorbs oil when it is immersed in the fluid. This fluid is released in the arc of cut under the influence of centrifugal force. Temperatures in the arc of cut were measured using thermocouples inserted in specially modified blanks. Process power and infeed rates were also measured.

The data logged from the tests was processed as outlined in chapter 8, utilising numerical modelling, and existing partitioning theory. The important point arising from the analysis was the value of the cutting fluid partition ratio, and, following from this, the value of the workpiece partition ratio. The cutting fluid partition ratio was found to be in the region of 71%, the workpiece absorbing 13% of the process power. The swarf removed 14% of the process power, about the same amount of power as the workpiece absorbed. The convective heat transfer coefficient worked out at approximately 24W/mm$^2$K. The cutting fluid clearly makes an extremely important contribution to the arc of cut temperature. Without cutting fluid, the model would estimate the temperature to be in the region of 4400°C; in practice, the workpiece would have melted before this temperature was reached.

The examination of the drill flute grinding process has highlighted the need to make a fundamental study of the role of the cutting fluid in deep cut grinding. It would appear to be the one remaining area in grinding technology which has not been systematically studied. There have been studies carried out investigating creep feed cutting fluid application, and how the critical heat flux for burn varies with different cutting fluid application methods. However, it would be of great benefit if the effect of the cutting fluid on grinding temperatures could be directly related to the grinding conditions, and the cutting fluid pressure.

## 8.2 Exploitation of Results

The following two case studies illustrate the manner in which the results of the foregoing chapters can be used to optimise grinding practice. The first of these studies examines a finish form grinding operation, and the second tackles a deep cut grinding problem.

### 8.2.1 Case Study 1

An EN31 steel form with an included angle of 90°C is to be finish-ground using a form-dressed vitrified alumina wheel of diameter 400mm. The dressing of the wheel necessitates a fillet radius of 0.15mm being imparted to the form. The normal infeed of the wheel is 5μm. The specific grinding energy is 30J/mm$^3$, and the approach angle is 45°. Identify a suitable work surface speed, such that the residual stress in the surface layer is compressive after grinding.

The temperature at which the residual stress state of the surface of the ground component changes from compressive to tensile can be identified from figure 4.34, or from equation 4.15, using table 4.10, and the following additional material properties:

Room temperature yield strength = 2500Mpa

700°C yield strength = 300Mpa

Inflection point temperature = 450°C

This critical temperature is 420°C.

The arc of cut length, $2l$, can be found from the following equation:

$$2l \approx 2\sqrt{dD}$$

**Equation 8.1**

This gives the arc length of contact $2l = 2.8\text{mm}$

This is shallow cut grinding, which means that the cutting fluid application has a negligible effect on grinding temperatures in the arc of cut.

The workpiece partition ratio can thus be calculated from equation 7.1, using the following wheel/work material properties:

| | |
|---|---|
| $r_o$ | 15μm |
| $l_e$ | 2.8mm |
| $k_g$ | 36W/mK |
| $\rho_g$ | 3910kg/m$^3$ |
| $c_g$ | 765J/kgK |
| $k_w$ | 37W/mK |
| $\rho_w$ | 7810kg/m$^3$ |
| $c_w$ | 481J/kgK |
| $e_c$ | 43J/mm$^3$ |
| $e_{cc}$ | 6J/mm$^3$ |
| $\gamma=\tan(\theta)$ | 1 |
| $V_s$ | 63m/s |

**Table 8.1**

This gives the workpiece partition ratio a value of 71%.

In chapter 5 it was demonstrated that the maximum temperature in a right-angle form would be found at the corner. The dressing roll on the wheel introduced a small fillet radius of 0.15mm. This implies that the temperature at the tip radius can be calculated using the Jaeger slider solution, with the heat flux calculated according to the normal infeed.

The maximum surface temperature resulting from a uniform moving heat source is given by:

$$\theta_m = \frac{2q}{K}\sqrt{\frac{2kl}{\pi V}}$$

**Equation 8.2**

The difference between the maximum temperature rise for uniform and triangular sources is negligible. The average heat flux to the workpiece, $q$, is given by:

$$q = RwS.E.V\cos(\psi)$$

**Equation 8.3**

where ψ is the mean infeed angle, l/r (the contact length being 2l), and S.E. the specific grinding energy, which gives

$$\theta_m = \frac{2RwS.E.\sin(\psi)}{K}\sqrt{\frac{2klV}{\pi}}$$

**Equation 8.4**

Solving for $V$, all other parameters being determined:

$$V \leq \left(\frac{\theta_m K}{2RwS.E.\sin(\psi)}\right)^2 \frac{\pi}{2kl}$$

**Equation 8.5**

To avoid tensile residual stresses, $V$ must be less than 0.3m/s

### 8.2.2 Case Study 2

A series of parallel slots 7mm deep are to be ground from a fully hardened M2 workpiece. The CBN wheel is 400mm in diameter, and the specific grinding energy is 70J/mm$^3$. The workpiece is immersed in a bath of neat oil during grinding. Determine a workpiece feed rate which will ensure a compressive surface state on the finished component.

The critical temperature can be found by referencing figure 4.23, or by using table 4.10, and the following additional material properties:

Room temperature yield strength = 2800Mpa

700°C yield strength = 650Mpa

Inflection point temperature = 650°C

This temperature is 630°C

The cutting fluid delivery system in this problem is the same as the Dormer set up, outlined in chapter 7. The arc of cut in this case is found to be 5.2cm. The expected temperature rise is 630°C, so the convective heat transfer coefficient should be approximately the same ~ 34W/Kmm$^2$. The chord angle is 15°, from the contact geometry.

The maximum ground plane temperature can be calculated from equation 6.7. The average heat flux can be calculated from equation 8.3. Combining these two equations, the following expression for the ground plane temperature is found:

$$\theta_m = \frac{0.776 S.E.\sin(\psi) Rwk}{\pi K}\psi^{-0.45}L^{0.36}e^{-0.9\psi L^{-0.55}}$$

**Equation 8.6**

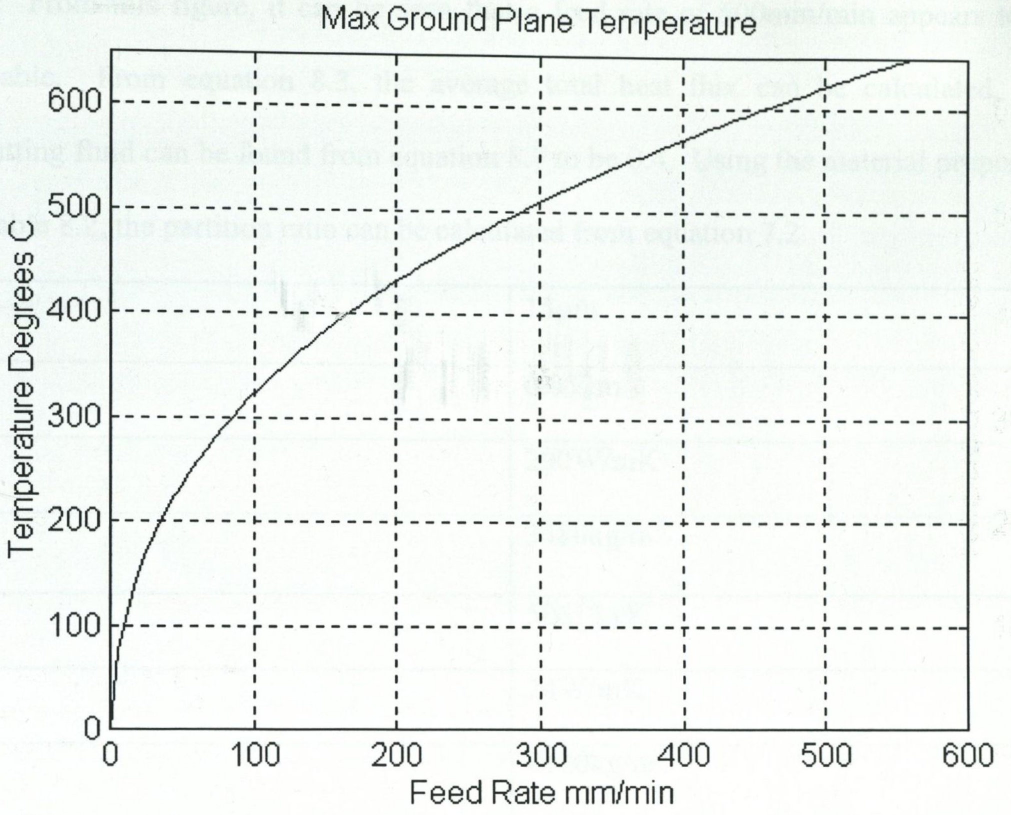

**Figure 8.1 – Ground plane temperature versus feed rate**

In this case, the value of the partition ratio is not directly determinable, since:

$$R_{coolant} = \frac{q_{coolant}}{q_{total}}$$

**Equation 8.7**

and the total heat flux is not known until the feed rate is known. This problem must be iteratively solved. This involves choosing a likely value for the partition ratio, solving for a suitable feed rate, evaluating the total heat flux, calculating the partition ratio with this heat flux, and comparing this value with the assumed value. This process is repeated until convergence.

It is not possible to solve for a feed rate from equation 8.7, due to the complexity of the function. It is a simple matter, however, to plot the function for a variety of feed rates, and this is shown in figure 8.1. The workpiece partition ratio is assumed to be

0.2. From this figure, it can be seen that a feed rate of 500mm/min appears to be suitable. From equation 8.3, the average total heat flux can be calculated, and Rcutting fluid can be found from equation 8.7 to be 0.4. Using the material properties in table 8.2, the partition ratio can be calculated from equation 7.2.

| | |
|---|---|
| $r_o$ | 15μm |
| $l_e$ | 0.052m |
| $k_g$ | 290W/mK |
| $\rho_g$ | 3480kg/m$^3$ |
| $c_g$ | 506J/kgK |
| $k_w$ | 24W/mK |
| $\rho_w$ | 8120kg/m$^3$ |
| $c_w$ | 420J/kgK |
| $e_c$ | 53J/mm$^3$ |
| $e_{cc}$ | 6J/mm$^3$ |
| $\gamma=\tan(\theta)$ | 1 |
| $V_s$ | 63m/s |

**Table 8.2**

This computes as Rw = 0.22, compared with the assumed value of 0.2. This is satisfactory.

To avoid tensile residual stress, the feed rate should be less than 500mm/min. This corresponds to a dimensionless length, L=15, which validates the use of equation 6.7

| | |
|---|---|
| Ground volume | $175e3mm^3$ |
| Process specific energy | $43J/mm^3$ |

**Table 7.2**

## 7.4 The Finite Element Model

At this juncture a finite element model of the drill was constructed. This was to allow a theoretical estimation of the temperatures in the arc of cut. This estimation of the maximum temperature would allow the proportion of the process power entering the work to be identified. The model was loaded according to the normal infeed rate at each point in the arc of cut.

Because the normal infeed rate varies in both the direction of infeed and the direction perpendicuar, the heat application was applied to the finite element model using a discrete version of the following formula:

$$q = f\cos(\theta)\cos(\psi)S.E.$$

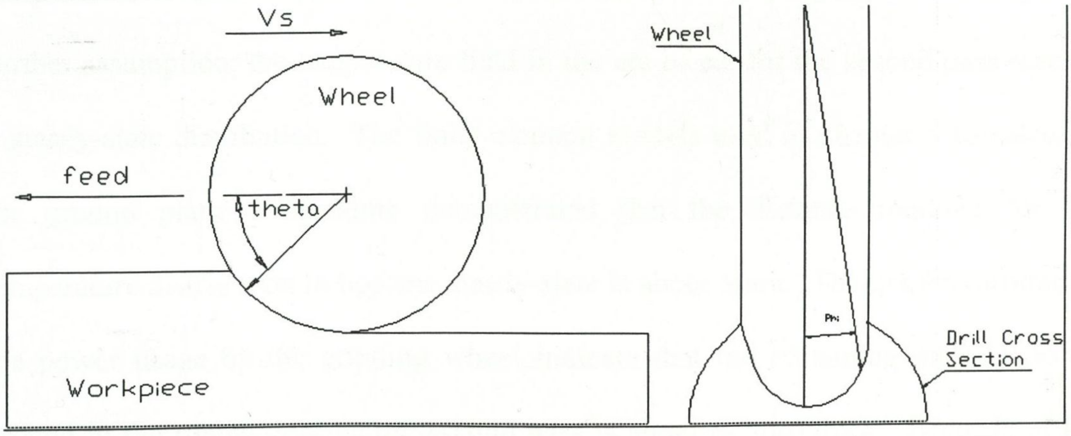

**Figure 7.22 – Loading diagram for the finite element model**

The heat application in the model is a function of the wheel shape and diameter. Figure 7.22 shows the loading diagram. Figure 7.23 shows the finite element mesh.

# Appendix 1

## Steady-State Temperature due to a Circular-Arc Source Moving Over a Semi-Infinite Plane

In 1953, Chao & Trigger [Chao & Trigger 1953] presented a temperature distribution solution for an inclined heat source moving across a semi-infinite plane. In this appendix, the same methodology is used to develop, in an analogous fashion, the temperature distribution in a semi-infinite plane resulting from a circular-arc heat source moving across it. Figure A.1 illustrates the essence of the analysis. The co-ordinate axis X and Y are fixed in space with the origin located at the centre of the arc, at time T=0, when grinding commences. The arc represents the grinding wheel/work contact. The grinding wheel has a radius R'. The axes $\zeta$ and $\eta$ move in the direction of grinding with the same velocity as the grinding wheel feed. This co-ordinate system is also represented in polar terms by R and $\phi$. Three positions of the heat source are shown in figure A.1; T=0, T', and T respectively. The objective of the analysis is to find the temperature rise at point P(R, $\phi$) due to the continuous heating of the moving source, at time T seconds after heating starts. The quasi steady state temperature distribution can then be found by investigating the limiting case when T tends to infinity. At some arbitrary instant, T' (0<T'<T) the temperature rise at point P due to an instantaneous line source of strength:

$$\frac{qds'dT'}{c\rho}$$

**Equation A.1**

located at point ds' of the source, (T-T') seconds later is:

$$d\theta = 2\left[\frac{qds'dT'}{c\rho(4\pi k)}\right]\frac{1}{T-T'}\exp\left[-\frac{r^2}{4k(T-T')}\right]$$

**Equation A.2**

This expression can be found in Carslaw & Jaeger [Carslaw & Jaeger 1959]. This expression assumes an adiabatic work surface, which means that a partition theory needs to be applied to evaluate a correct value of $q$, and constant material properties. From figure A.1, it can be seen that $r^2$ is given by:

$$r \; = a^2 + b^2$$

**Equation A.3**

From the geometry shown in the figure,

$$a = X - VcT' - R'\sin\phi'$$
$$b = Y - R'\cos\phi'$$

**Equation A.4**

and X and Y can be represented by:

$$X = VcT + R\sin\phi$$
$$Y = R\cos\phi$$

**Equation A.5**

This in turn allows $r^2$ to be expressed as:

$$r^2 = \left(R\sin\phi - R'\sin\phi' + Vc(T-T')\right)^2 + \left(R\cos\phi - R'\cos\phi'\right)^2$$

**Equation A.6**

Substituting equation A.6 into equation A.2, and simplifying gives:

$$d\theta = \frac{qds'dT'}{2\pi K}\frac{1}{T-T'}\exp-\left[\begin{array}{l}\dfrac{\left(R\sin\phi - R'\sin\phi'\right)^2 + \left(R\cos\phi - R'\cos\phi'\right)^2}{4k(T-T')}\\ +\dfrac{Vc}{2k}\left(R\sin\phi - R'\sin\phi'\right)\\ +\dfrac{Vc^2}{4k}(T-T')\end{array}\right]\frac{dT'}{(T-T')}$$

**Equation A7**

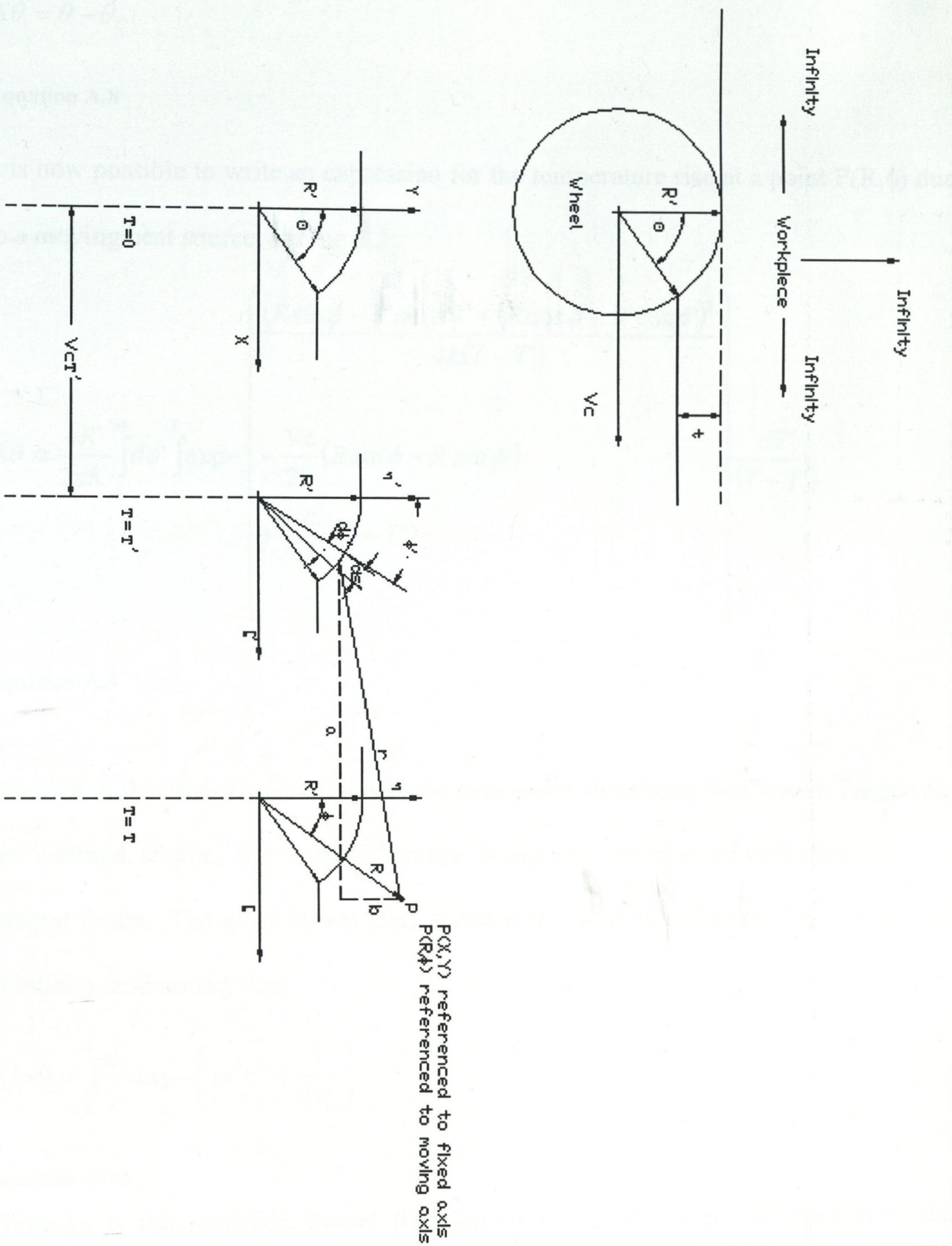

**Figure A1 – Moving circular-arc heat source**

The final temperature at point P(R,ϕ) is found by integrating the line source between 0 and Θ, and between 0 and T. Noting the following two relationships:

$$ds' = R'd\phi'$$

$$\Delta\theta = \theta - \theta_0$$

**Equation A.8**

it is now possible to write an expression for the temperature rise at a point P(R,$\phi$) due to a moving heat source, at time T.

$$\Delta\theta = \frac{qR'}{2\pi K}\int_0^{\Theta} d\phi' \int_0^{T} \exp-\left[\begin{array}{l} \dfrac{(R\sin\phi - R'\sin\phi')^2 + (R\cos\phi - R'\cos\phi')^2}{4k(T-T')} \\ + \dfrac{\mathrm{Vc}}{2\mathrm{k}}(R\sin\phi - R'\sin\phi') \\ + \dfrac{\mathrm{Vc}^2}{4\mathrm{k}}(T-T') \end{array}\right] \frac{dT'}{(T-T')}$$

**Equation A.9**

Equation A.9 is directly analogous to the expression developed by Chao & Trigger for the inclined source, the only difference being the position co-ordinates, and the integral limits. The quasi steady state solution is found by taking the limit as T tends to infinity, and noting that:

$$k_0(m) = \int_0^{\infty} \frac{dz}{z} \exp-\left(m^2z^2 + \frac{1}{4z^2}\right)$$

**Equation A.10**

where $k_0$ is the modified Bessel function of the second kind, of order zero, the temperature rise at a point P(R,$\phi$) is found to be:

$$\Delta\theta = \frac{qR'}{\pi K}\int_0^{\Theta} k_0\left\{\frac{Vc}{2k}\left[(R\sin\phi - R'\sin\phi')^2 + (R\cos\phi - R'\cos\phi')^2\right]^{\frac{1}{2}}\right\}\exp-\left[\frac{Vc}{2k}(R\sin\phi - R'\sin\phi')\right]d\phi$$

**Equation A.11**

Since equation A.11 was developed with the creep feed grinding process in mind, it is worth making one further modification to allow the heat input to applied according to the normal infeed. This is easily accomplished by replacing $q$ with $q.\sin(\phi')$, and moving the sine function inside the integral, shown in equation A.12. The temperature in the arc of cut can be calculated by setting R equal to R', the radius of the heat source.

$$\Delta\theta = \frac{qR'}{\pi K}\int_{0}^{\Theta}\sin\phi'\left[\begin{matrix} k_0\left\{\dfrac{Vc}{2k}\left[(R\sin\phi - R'\sin\phi')^2 + (R\cos\phi - R'\cos\phi')^2\right]^{\frac{1}{2}}\right\} \\ \exp-\left[\dfrac{Vc}{2k}(R\sin\phi - R'\sin\phi')\right] \end{matrix}\right]d\phi'$$

**Equation A.12**

In figure A.2, a comparison of the three different sources, i.e. flat, inclined, and circular, is shown. The material properties and other parameters are the same for all three source types. The lengths of each source are the same. For the flat and inclined source, the non-dimensional length L is 20. Defining a similar parameter for the circular source:

$$S = \frac{Vc.s}{K}$$

**Equation A.13**

where s is the length of the arc source. The value of S was also 20. The angle of the inclined source was the effective chord angle of the circular source, calculated from equation A.14.

$$\phi = 2\sqrt{\frac{t}{d}}$$

**Equation A.14**

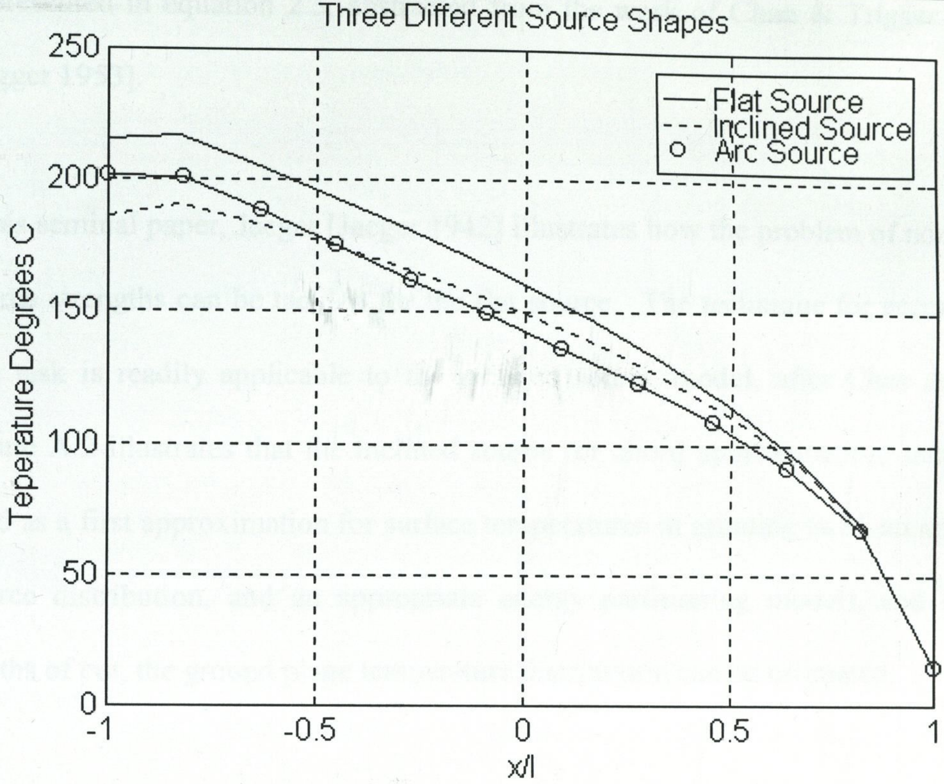

**Figure A.2 – Comparison of three different source shapes**

Figure A.2 illustrates, in a comparative fashion, the manner in which each of the three sources develop temperature in the contact plane. The temperature solution generated by the circular source solution was mapped onto the axis used for the other two solutions. The lengths of all the sources were identical, and the solution points were proportionally the same. In this example a uniform temperature distribution was used, purely for ease of comparison. The results of the calculations were presented in explicit form rather than the more standard dimensionless form, because equation A.12 does not readily lend itself to comparison in dimensionless form.

The equation for calculating the moving flat source temperature distribution is detailed in equation 2.1. The relevant equation for calculation of the inclined source is presented in equation 2.3, abstracted from the work of Chao & Trigger [Chao & Trigger 1953].

In his seminal paper, Jaeger [Jaeger 1942] illustrates how the problem of non-uniform source strengths can be tackled for the flat source. The technique for accomplishing this task is readily applicable to the inclined source model, after Chao & Trigger. Figure A.2 illustrates that the inclined source (or chord approximation) may well be used as a first approximation for surface temperatures in grinding (with an appropriate source distribution, and an appropriate energy partitioning model), and for small depths of cut, the ground plane temperature distribution can be estimated.

# Appendix 2

## List of References

**Andrew, C., Howes, T., Pearce, T.** *Creep Feed Grinding* Holt Rinehart & Winston 1985

**Blok, H.** *Theoretical Study of Temperature Rise at Surface of Actual Contact Under Oiliness Lubricating Conditions* Inst. Mech. Eng. 2, 222 1937

**Bokuchava, G.W.** *Cutting temperatures in grinding* Russian Eng. J. Vol. 43 No. 11 1963

**Brinksmeier, E., Tonshoff, H.K.** *X-ray stress measurement – A tool for the stury and layout of machining processes* CIRP Annals Vol. 34/1 p485-494 1984

**Chao, B.T., Trigger, K.J.** *The significance of the thermal number in metal machining* Trans ASME Paper No. 52-SA-58 January 1953

**DesRuisseaux, N.R, Zerkle, R.D.** *Thermal Analysis of the Grinding Process* Trans. ASME (Journal of Engineering for Industry) 1969. Paper No. 69-WA/Prod-2 Journal of Engineering for Industry

**DesRuisseaux, N.R, Zerkle, R.D.** *Temperature in Semi-infinite Bodies Subjected to Moving Heat Sources and Surface Cooling.* Trans. ASME (Journal of Engineering for Industry) **70** 1970 p.456 Paper No. 70-HT-J

**Dickenson, G.R.** *The influence of machining of the performance of ultra high strength steels* Trans ASME Paper No. GT-72, 1970

**Eda, H., Kishi, K.** *Improvement of grinding process for difficult-to-grind materials by acting the jet infusion of grinding fluids* Annals of the CIRP Vol. 1 665-670 1974

**Engineer, F., Guo, C., Malkin, S.** *Experimental measurement of fluid flow through the grinding zone* Trans. ASME (Journal of engineering for industry) Vol. 114 p61-73 February 1992

**Erko, A.I., & Arotov, V.V.** *Diffraction x-ray optics* Institute of Physics Publication, University of Bristol 1996

**Eshghy, S.** *Thermal aspects of the abrasive cut-off operation. Part 1-Theoratical analysis* Trans. ASME Paper No. 66-WA/prod-21 1966

**Eshghy, S.** *Thermal aspects of the abrasive cut-off operation. Part 1-Partition functions and optimum cut-off* Trans. ASME Paper No. 67-WA/prod-10 1967

**Gordeev A.V.** *Grinding with angular wheels* Machines and Tooling Vol. 47 No. 6 34-35 1976

**Hahn, R.S.** *On the loss of surface integrity and surface form due to thermoplastic stress in plunge grinding operations* Annals of the CIRP Vol. 25 1976

**Hahn, R.S.** *On the temperature developed at the shear plane in the metal cutting process* Proc. 1st US Nat Cong of Appl Mech 661-666 1951

**Hahn, R.S.** *The Relation between Grinding Conditions and Thermal Damage in the Workpiece.* Trans ASME, **78**, 807-812 1956.

**Hassell, B.** *A grinding fluid comparison* MAI Dissertation Trinity College Dublin 1979

**Huntley, Herbert Edwin** *Dimensional analysis* New York : Dover, 1967

**Incropera, F.P., DeWitt, D.P.** *Introduction to heat transfer* John Wiley and Sons Inc. 1985

**Jaeger, J.C.** *Moving Source of Heat and Temperatures at Sliding Contacts* Proc. R. Soc. New South Wales **76**, 203. 1942

**Kahnzhin, N.N.** *Temperature calculations for grinding operations* Machines and Tooling Vol. XLII No. 8 1971

**Karaim, I.P.** *Influence of cooling method on grinding zone temperature* Machines and Tooling Vol. XL No.6 1969

**Kopalinsky,, Eleonora M.** *A New Approach to Calculating the Workpiece Temperature Distributions in Grinding.* Wear, **94**, 295-322, (1984)

**Kopalinsky, Eleonora M.** *Modelling of Material Removal and Rubbing Processes in grinding as a Basis for Realistic Determination of Workpiece temperature Distributions.* Wear, **81**, 115-134, (1982)

**Korolev, V.V.** *Temperature distribution calculations during abrasive machining* Machines and Tooling Vol. 42 No. 4

**Kuang-Hua., F. Huang, J.** *Thermal analysis of creep feed grinding* J. of Matter Process Technology Vol. 43 109-124 1994

**Lavine, A.S., Jen, T.-C.** *Thermal aspects of grinding: Heat transfer to workpiece, wheel, and fluid* Trans. ASME (Journal of Heat Transfer) Vol. 113 May 1991

**Lee, D.G., Zerkle, R.D., DesRuisseaux, N.R.** *An experimental study of thermal aspects of cylindrical plunge grinding* Trans. ASME Paper No. 71-WA/prod-4 1971

**Leone, W.C.** *Distribution of shear zone heat in metal cutting* Trans ASME Paper No. 53-S-7 p121-125 January 1954

**Loewen, E.G., Shaw, M.C.** *On the analysis of cutting tool temperatures* Trans ASME Paper No. 53-S-15 p217-231 February 1954

**Malkin, S.** *Grinding Technology* Ellis Horwood Ltd. 1989

**Malkin, S.** *Analysis of fluid flow through the grinding zone* Trans ASME (Journal of Engineering for Industry) Vol. 114 Nov. 1992

**Malkin, S.** *Thermal aspects of grinding. Part 1: Energy partition* Trans ASME Paper No. 73-WA prod-1 1973

**Malkin, S.** *Thermal aspects of grinding. Part 2: Surface temperatures and workpiece burn* Trans ASME Paper No. 73-WA prod-2 1973

**Malkin, S.** *Thermal Aspects of the Grinding Process* PhD Dissertation MIT 1968

**Malkin, S., Guo, C.** *Analysis of fluid flow through the grinding zone* Trans ASME (Journal of Engineering for Industry) Vol. 104 427-434 1992

**Maris, M.** *Thermische aspekten van de oppervlakte-integriteit bij het slijpen* PhD Dissertation 1977 Kath. Univ. Leuven

**Massey, B.S.** *Units, Dimensional Analysis and Physical Similarity* Van Nostrand Reinhold Company, 1971

**Mayer, J.E. Shaw, M.C.** *Grinding temperatures* Jour. ASLE January 1957

**Mishra, A., Rao, U.R.K., Natarajan, R.** *An analytical approach to the calculation of residual stresses in grinding* Proceedings, International conference on production engineering, Inst. Mech. Engrs. (India) p40-50 1978

**Morgan, M.N., Lin, Z.X., Rowe, W.B.** *Temperatures in angle approach form grinding* Proceedings of the International Seminar on Improving Machine Tool Performance, San Sebastian, Spain 411-422 1998

**Ohishi, S., Furukawa, Y.** *Analysis of workpiece temperature and grinding burn in creep feed grinding* Bull JSME Vol. 28 No. 242 391-411 1985

**Okushima, K., Kakino, Y.** *The residual stress produced by metal cutting* Annals of the CIRP Vol. 20 1971

**Olver, A.V., Spikes, H.A., Bower, A.F., Johnson, K.L.** *The residual stress distrbution in a plastically deformed model asperity* Wear 107 151-174 1986

**Osman, M., Malkin, S.** *Lubrication by grinding fluids at normal and high wheel speeds* Jour. ASLE Vol. 15 No. 4 p261-268 1972

**Outwater, J.O., Shaw, M.C.** *Surface temperatures in grinding* Trans ASME January Paper No. 51-SA-10 p73-86 1952

**Peters, J., Maris, N.F.WO., Snoeys, R.** *Thermally induced Damage in Grinding.* Annals of the CIRP, **27/2**, 1978, p.571

**Powell, J.W., Howes, T.D.** *A study of the heat flux at which burn occurs in creep feed grinding* Proc. 19th Int. MTDR Conf. (Manchester) 629-636 1978

**Rosenthal, D.** *The theory of moving sources of heat and its application to metal treatments* Trans. ASME (Journal of Heat Transfer) Vol. 68 849-866 1946

**Rowe, W.B., Morgan, M.N..** *Experimental Investigation of Heat Transfer in Grinding.* Annals of the CIRP Vol. 1 p133-144 1995

**Rowe, W.B., Black, S.C.E., Mills, B., Morgan, M.N., Qi, H.S.** *Grinding Temperatures and Energy Partitioning.* Proc. R. Soc. Lond. A **453**, 1083-1104 (1997)

**Saito, K., Kagiwada, T.** *Transient distribution of temperature and thermal stress in a grain due to a pulsating heat source* Bull. Japan Soc. of Prec. Engg Vol. 8 No. 3 Sept 1974

**Salj□, E.** *Creep feed grinding* Proceedings of the fifth international conference on production engineering JSPE Tokyo p63-74 1984

**Salj□, E., Damlos, H., Teiwes, H.** *Problems in profile grinding – Angular plunge grinding and surface grinding* Annals of the CIRP Vol. 30 p219-222 1981

**Sato, K.** *Grinding temperatures* Bull of Jap. Soc. of Grinding Eng. No. 1 p31-33 1960

**Schumack, M.R., Chung Jin-Bok Schultz, W.W., Kannatey-Asibu, E.** *Analysis of fluid flow under a grinding wheel* Trans ASME (Journal of Engineering for Industry) Vol. 113 p190-203 May 1991

**Shaw, M.C.** *Principles of Abrasive Processing*. Clarendon Press, Oxford (1996)

**Shaw, M.C.** *The Galileo Principle*, Annals of the CIRP 1992

**Snoeys, R., Maris, M., Peters, J** *Thermally induced damage in grinding* Annals of the CIRP Vol. II p571-581 1978

**Stuart, T.V.** *High speed creep feed grinding* PhD Dissertation University of Bristol 1977

**Takazawa, K.** *Effects of grinding variables on surface structure of hardened steel* Bull JSPE Vol. 2 No1. p688-692 1966

**Takazawa, K.** *The Ratio of Heat Entering the Work to Total Grinding Heat - Theoretical Analyses on the Grinding Temperature* (2nd report). Jour. Japan Soc. Precision Engineering, **30** 12 p914 1964

**Takazawa, K.** *Theory and Measuring method of the Temperature Distribution in Ground Surface Layer - Theoretical Analyses on the Grinding Temperature* (1st report). Jour. Japan Soc. Precision Engineering, **30** 11 p851 1964

**Takazawa, K.** *Thermal aspects of the grinding operation* Industrial diamond review April 143-149 1972

**Tiberg,J.** *Private communication* October 1998

**Torrance, A.A.** *Private communication* June 1999

**Torrance, A.A.** *The calculation of residual stresses in worn surfaces* Proc. Instn. Mech. Engrs. Vol. 208 113-119 1994

**Trmal, G.J.** *Form grinding – Problems and solutions* Proc. of the 3rd polytechnic symposium on manufacturing engineering Wolverhampton 237-245 1982

**Ueno, T., Ishibashi, A., Katsuki, A.** *Experiments on the cooling ability of cutting fluids* Bull. J.S.P.E. Vol. 13 No. 59 p729-735 1970

**Van Vlack L.H.** *Elements of Materials Science and Engineering* Adison-Wesley 1989

**Walsh, D., Izadi, H., Torrance, A.A.** *A semi-analytic approach to evaluating residual stress on the surface of components subjected to a moving heat source* Proceedings of the International Seminar on Improving Machine Tool Performance, San Sebastian, Spain 875-885 1998

**Walsh, D., Torrance, A.A.** *Influence of form on surface temperatures in form grinding* Proc. I.Mech.E. 213 Part C 601-611 1999

**Weiner, J.H.** *Shear-plane temperature distribution in orthogonal cutting* Trans ASME Paper No. 54-A-65 p1331-1341 November 1955

**Werner, P.G., Younis, M.A., Schlingensiepen, R.** *Creep feed – An effective method to reduce work surface temperatures in high efficiency grinding processes* Proc. 8th North American metal working research conference Soc. Manu. Engineers 312-319 1980

**Ye, N.E., Pearce, T.R.A.** *A comparison of oil and water as grinding fluids in the creep feed grinding process* Proc. I.Mech.E. Vol. 14 No. 198B 229-237 1984